Investigating the Effects of Hypoxia on the Sphingolipid System and Adiponectin in Adipocytes and Perivascular Adipose Tissue

Saleh Ali Saleh Almarshad

Pharm.D., MSc

Thesis submitted in fulfilment of the requirements for the degree of Doctor of Philosophy

September 2025

School of Cardiovascular and Metabolic Health,
College of Medical, Veterinary and Life Sciences
University of Glasgow

Abstract

Perivascular adipose tissue (PVAT) exerts important paracrine control over vascular tone, but how acute hypoxia impacts upon PVAT signalling and vascular reactivity remains incompletely understood. Hypoxia is central to adipose pathophysiology because as the volume of adipose depots expand, limited oxygen diffusion and inadequate angiogenesis create localised hypoxia that drives metabolic stress, inflammation, and altered secretion of adipokines and bioactive lipid mediators. Together with impaired perfusion responses in obesity, these changes indicate that the regulatory role of PVAT may change and hypoxia may be central to this. To address this, I combined wire myography with molecular and biochemical measurements in rat thoracic aorta and mesenteric arteries, 3T3-L1 adipocytes, and ex vivo PVAT depots exposed to normoxia and hypoxia.

Functionally, pre-exposure to hypoxia altered subsequent contractile responses to phenylephrine and relaxant responses to cromakalim in a manner dependent on vessel type, PVAT status, and endothelium; when hypoxia was applied acutely during sustained phenylephrine-induced tone, thoracic aorta relaxed robustly even without endothelium, and relaxation was significantly augmented by PVAT, supporting an endothelium-independent component mediated by PVAT-derived factors.

Adiponectin is an abundant adipocyte-derived hormone with insulin-sensitising and anti-inflammatory actions and has recognised roles in vascular homeostasis. Therefore, adiponectin content and release were measured in 3T3-L1 adipocytes and in thoracic and mesenteric PVAT to determine if acute hypoxia alters PVAT-derived adiponectin and whether these changes could account for hypoxia-induced vascular relaxation. Adiponectin studies showed that short-term hypoxia reduced adiponectin protein and Adipoq mRNA in 3T3-L1 adipocytes and lowered adiponectin in thoracic but not mesenteric PVAT; under normoxic conditions, thoracic PVAT exhibited higher basal adiponectin protein content than mesenteric PVAT, and a trend toward increased release during hypoxia. Pharmacological manipulation revealed that, with PVAT present, neither β_3-adrenoceptor agonist nor AdipoR1 blockade altered hypoxic relaxation; in PVAT-removed endothelium-intact rings, β_3-agonism (CL-316,243) attenuated relaxation, indicating an inhibitory endothelial β_3 pathway unmasked by PVAT removal. An exploratory

adipokine array indicated broader hypoxia-induced reductions in several factors secreted from thoracic PVAT.

Sphingosine-1-phosphate is a PVAT-derived bioactive lipid produced by SphK1 that regulates vascular tone and plays key roles in cardiovascular and immune function. Hence, after observing that acute hypoxia induces relaxation with PVAT present, S1P was investigated as a candidate mediator linking hypoxia to vessel responses. SphK/S1P experiments demonstrated that hypoxia selectively and transiently increased SphK1 mRNA and SphK1 phosphorylation in adipocytes, while a short exposure to gas hypoxia did not change SphK1 protein or tissue S1P in PVAT. Thoracic PVAT released less S1P under hypoxia. Inhibition of SphK1 with PF543 reduced S1P release under normoxia and further decreased it under hypoxia, consistent with SphK1-driven S1P export from PVAT. Conversely, mesenteric PVAT showed no effect of PF543 or hypoxia on SphK1 or S1P release. Thus, the hypoxic reduction in S1P release was depot specific. Exogenous S1P or selective $S1P_2$ activation (CYM 5478) reduced hypoxic relaxation only when PVAT was absent, suggesting that S1P/$S1P_2$ can limit relaxation of the vessel wall but this is masked by PVAT factors when PVAT is present.

Collectively, these data show that acute hypoxia induces a PVAT-enhanced, largely endothelium-independent vasorelaxation while rapidly altering adiponectin and S1P signals. When PVAT is present, adiponectin and $ß_3$ agonism are not the dominant acute mediators of hypoxic relaxation, and S1P/$S1P_2$ opposes relaxation primarily when PVAT support is removed. These findings refine the mechanistic understanding of PVAT to vessel crosstalk under hypoxic stress and point to PVAT factors as key acute effectors.

Table of Contents

List of Tables

List of Figures

Acknowledgement

In the name of Allah, the Beneficent and Merciful, I begin with praise to Allah, acknowledging the countless blessings that made the completion of this endeavour possible.

I wish to express my profound gratitude to my supervisors, Prof Simon Kennedy and Dr Kenneth Watterson, whose scientific guidance, expertise, and insight were instrumental to the direction and success of this research. Their unwavering encouragement and optimism continually motivated me to persevere. I also acknowledge with thanks the generous support and funding provided by Qassim University.

I am grateful to the many colleagues at the University of Glasgow whose support over the years has been invaluable. I owe particular thanks to members of the Kennedy Group for their help in numerous ways, especially Dr Ibrahim Aljaezi. I am also indebted to the laboratory technician, John McAbney, for his expert guidance and unfailing assistance with the wire myography work.

Throughout my academic journey, I have been sustained by the love and support of my family and friends. I owe an immeasurable debt of thanks to my parents, my late father, Ali, and my mother, Hailah, and to my brother and sisters, whose steadfast, unconditional support sustained me throughout this work. To my wife and our daughter, thank you for your patience, sacrifices, and constant encouragement; this achievement is as much yours as it is mine. I remain profoundly indebted to my parents for a kindness and compassion that began before I was born and has never waned. I dedicate this work to the cherished memory of my late father, Ali, and to my beloved mother, Hailah.

Author's Declaration

I hereby declare that the work presented in this thesis has been carried out by me unless otherwise stated. It is entirely of my own composition and has not in whole or in part been submitted for any other degree. This project was conducted under the supervision of Prof. Simon Kennedy and Dr. Kenneth Watterson in Prof. Simon's laboratory, School of Cardiovascular and Metabolic Health, College of Medical, Veterinary and Life Sciences, University of Glasgow, Glasgow, United Kingdom.

Saleh Ali S Almarshad

September 2025

Abbreviations/Definitions

3T3-F442A	Mouse preadipocyte fibroblast cell line (3T3-F442A)
3T3-L1	Mouse 3T3-L1 preadipocyte/adipocyte cell line
$[Ca^{2+}]_i$	Intracellular calcium concentration
ABC	ATP-binding cassette (transporter superfamily)
ACE	Angiotensin-converting enzyme
ACh	Acetylcholine
Adipoq	Adiponectin gene
AdipoR1	Adiponectin receptor 1
AdipoR1B	Adiponectin receptor-1 blocking peptide
AdipoR2	Adiponectin receptor 2
ARs	Adrenergic receptors
ADRFs	Adventitia-derived relaxing factors
Akt	Protein kinase B (PKB/Akt)
AMPK	AMP-activated protein kinase
Ang II	Angiotensin II
ANOVA	Analysis of variance
ANP	Atrial natriuretic peptide
ANT2	Adenine nucleotide translocase 2
AP-1	Activator protein-1 (transcription factor)
AP-2	Activator protein-2 (transcription factor)
APPL	APPL adaptor protein family (e.g., APPL1)
$ApoE^{-/-}$	Apolipoprotein E knockout (mouse)
ApoM	Apolipoprotein M
ARNT	Aryl hydrocarbon receptor nuclear translocator (HIF-1ß)
AT	Adipose tissue
AT1a	Angiotensin II type-1a receptor
AT1R	Angiotensin II type-1 receptor
AT2	Angiotensin II type-2 receptor
ATCC	American Type Culture Collection
AWERB	Animal Welfare and Ethical Review Body
BAT	Brown adipose tissue
BCA	Bicinchoninic acid
BK	Bradykinin
BK_{Ca}	Large-conductance Ca^{2+}-activated K^+ channel (KCa1.1)
BMI	Body mass index
BSA	Bovine serum albumin
C/EBP	CCAAT/enhancer-binding protein
CCL2	C–C motif chemokine ligand 2 (MCP-1)
CBS	Cystathionine-ß-synthase
CD36	Cluster of differentiation 36 (fatty acid translocase)
cAMP	Cyclic adenosine monophosphate
cDNA	Complementary DNA
cGMP	Cyclic guanosine monophosphate
CHOP	C/EBP homologous protein (DDIT3)
CIHH	Chronic intermittent hypobaric hypoxia
CIB1	Calcium- and integrin-binding protein 1
CK	Cromakalim
CM	Conditioned medium
$CoCl_2$	Cobalt chloride
COX	Cyclo-oxygenase (PTGS)
CRF	Central Research Facility
CVS	Cardiovascular system

db/db	Leptin receptor–deficient (diabetic mouse)
DMEM	Dulbecco's Modified Eagle's Medium
DMS	N,N-Dimethylsphingosine (SphK inhibitor)
DMSO	Dimethyl sulfoxide
DNase I	Deoxyribonuclease I
DTT	Dithiothreitol
E+	Endothelium-intact
E–	Endothelium-denuded
E2F	E2F transcription factor family
EDCFs	Endothelium-derived contracting factors
EDHF	Endothelium-derived hyperpolarising factor
EDTA	Ethylenediaminetetraacetic acid
eEF1A	Eukaryotic elongation factor 1A
EFS	Electrical field stimulation
EGF	Epidermal growth factor
EGTA	Ethylene glycol-bis (ß-aminoethyl ether)-N,N,N′,N′-tetra acetic acid
ELISA	Enzyme-linked immunosorbent assay
ECs	Endothelial cells
ER	Endoplasmic reticulum
ERK1/2	Extracellular signal-regulated kinases 1 and 2
FAK	Focal adhesion kinase
FAM	Fluorescein amidite
FCS	Foetal calf serum
FATP-1	Fatty acid transport protein 1 (SLC27A1)
FHL2	Four-and-a-half LIM domain protein 2
FLS	Fibroblast-like synoviocytes
FTY720	Fingolimod
FTY720-P	Fingolimod-phosphate
G12/13	Heterotrimeric G-protein α12/α13 family
GAPDH	Glyceraldehyde-3-phosphate dehydrogenase
Gi	G-protein αi subunit (inhibitory)
Gq	G-protein αq subunit
GPCRs	G-protein-coupled receptors
GSK-3ß	Glycogen synthase kinase-3ß
GSSG	Oxidised glutathione
H_2O_2	Hydrogen peroxide
H_2S	Hydrogen sulphide
HCC	Human corpus cavernosum
HDL	High-density lipoprotein
HFD	High-fat diet
HepG2	Human hepatocellular carcinoma cell line
HIF	Hypoxia-inducible factor(s)
HIF-1α	Hypoxia-inducible factor-1 alpha
HIF-1ß	Hypoxia-inducible factor-1 beta (ARNT)
HIF-2α	Hypoxia-inducible factor-2 alpha
HOMA-IR	Homeostatic Model Assessment of Insulin Resistance
HREs	Hypoxia-response elements
HRP	Horseradish peroxidase
Hsp90	Heat-shock protein 90
HUVECs	Human umbilical vein endothelial cells
IBMX	3-Isobutyl-1-methylxanthine
iNOS	Inducible nitric oxide synthase
IGFBP-1	Insulin-like growth factor-binding protein-1
IL-1ß	Interleukin-1ß
IL-6	Interleukin-6

IL-8	Interleukin-8 (CXCL8)
IL-10	Interleukin-10
IP3	Inositol 1,4,5-trisphosphate
IRE1	Inositol-requiring enzyme 1 (ERN1)
I/R	Ischaemia–reperfusion
IRS-1	Insulin receptor substrate-1
JNK	c-Jun N-terminal kinase
JTE-013	$S1P_2$ receptor antagonist
K^+	Potassium ion
K_{ATP}	ATP-sensitive potassium channel
K_{Ca}	Ca^{2+}-activated potassium channel
K_{Cl}	Potassium chloride
Kir	Inward-rectifier potassium channel
Kir6.x	Kir6.x subunits of KATP channels
KPSS	High-potassium physiological salt solution
Kv	Voltage-gated potassium channel
L-NMMA	NG-monomethyl-L-arginine (NOS inhibitor)
LC–MS/MS	Liquid chromatography–tandem mass spectrometry
LDH	Lactate dehydrogenase
LDL	Low-density lipoprotein
LDS	Lithium dodecyl sulphate
LIF	Leukaemia inhibitory factor
LMO2	LIM domain only protein 2
LPPs	Lipid phosphate phosphatases
LPS	Lipopolysaccharide
MAPKs	Mitogen-activated protein kinases
MCP-1	Monocyte chemoattractant protein-1 (CCL2)
MEGJs	Myoendothelial gap junctions
MFSD2B	Major facilitator superfamily domain-containing protein 2B (S1P exporter)
MFS	Major facilitator superfamily
MG132	Proteasome inhibitor MG-132
miR-	MicroRNA- (e.g., MicroRNA-124, MicroRNA-3677)
MLC	Myosin light chain
MLCK	Myosin light chain kinase
mRNA	Messenger RNA
NADH	Nicotinamide adenine dinucleotide
NADPH	Nicotinamide adenine dinucleotide phosphate
NCS	Newborn calf serum
NE	Norepinephrine
NO	Nitric oxide
NOS	Nitric oxide synthase
NP-40	Nonidet P-40 (non-ionic detergent)
O_2^-	Superoxide anion
OCT3	Organic cation transporter 3
OD	Optical density
PA	Phosphatidic acid
PAF	Platelet-activating factor
PAI-1	Plasminogen activator inhibitor-1 (SERPINE1)
PASMC	Pulmonary artery smooth muscle cell
PBS	Phosphate-buffered saline
PCR	Polymerase chain reaction
PDGF-BB	Platelet-derived growth factor-BB
PE	Phenylephrine
PECAM-1	Platelet endothelial cell adhesion molecule-1 (CD31)
PF543	Selective sphingosine kinase-1 (SphK1) inhibitor

PGI_2	Prostacyclin
PHB2	Prohibitin 2
PHD	Prolyl-hydroxylase domain (HIF prolyl hydroxylase)
PI3K	Phosphoinositide 3-kinase
PI3K/Akt	PI3K–Akt signalling pathway
PLGF	Placental growth factor
PLC	Phospholipase C
PO_2	Partial pressure of oxygen
PPARα or γ	Peroxisome proliferator-activated receptor-α or γ
PS	Phosphatidylserine
PSS	Physiological salt solution
PVAT	Perivascular adipose tissue
PVAT(+)	PVAT intact
PVAT(–)	PVAT removed
PVCFs	PVAT-derived contracting factors
PVRFs	PVAT-derived relaxing factors
qPCR	Quantitative real-time PCR
RA	Rheumatoid arthritis
RA-FLS	Rheumatoid-arthritis fibroblast-like synoviocytes
RAS	Renin–angiotensin system
RhoA	Ras homolog family member A
RIPA	Radio-immunoprecipitation assay
RLT	RNeasy lysis buffer
ROCK	Rho-associated coiled-coil-containing protein kinase
RPE	RPE wash buffer
ROS	Reactive oxygen species
RT-PCR	Reverse-transcription PCR
RW1	RW1 wash buffer
S1P	Sphingosine-1-phosphate
$S1P_{1/3}$	S1P receptors 1 and 3
$S1P_{1-5}$	S1P receptors 1–5
S1PP	Sphingosine-1-phosphate phosphatases (e.g., SGPP1/2)
S1PRs	Sphingosine-1-phosphate receptors (family)
SCD	Stearoyl-CoA desaturase
SD	Sprague–Dawley (rat strain)
SGBS	Simpson–Golabi–Behmel syndrome (human adipocyte model)
sGC	Soluble guanylate cyclase
SGPP1	Sphingosine-1-phosphate phosphatase-1
SERCA	Sarcoplasmic/endoplasmic reticulum Ca^{2+}-ATPase
SNP	Sodium nitroprusside
SOCE	Store-operated calcium entry
SPNS2	Spinster homologue 2 (S1P transporter)
SphK	Sphingosine kinase (family)
SphK1	Sphingosine kinase-1
SphK2	Sphingosine kinase-2
SPL	Sphingosine-1-phosphate lyase
SPT	Serine palmitoyltransferase
SUR	Sulfonylurea receptor (K_{ATP} channel regulatory subunit)
SVF	Stromal vascular fraction
T2DM	Type 2 diabetes mellitus
TAG	Triacylglycerol
TBS	Tris-buffered saline
TBP	TATA-box binding protein
TBST	Tris-buffered saline with Tween-20
TEA	Tetraethylammonium

TEMED	N,N,N′,N′-Tetramethylethylenediamine
TGF-β	Transforming growth factor-β
TLR4	Toll-like receptor 4
TNF-α	Tumour necrosis factor-α
TRAF2	TNF receptor-associated factor 2
U46619	Thromboxane A_2 receptor agonist (TXA_2 analogue)
UCP1	Uncoupling protein-1
UPR	Unfolded protein response
VEGF	Vascular endothelial growth factor
VHL	von Hippel–Lindau protein
VSMCs	Vascular smooth muscle cells
WAT	White adipose tissue
WHO	World Health Organization
WKY	Wistar Kyoto (rat strain)
$β_3$-AR	$β_3$-Adrenergic receptor
CYM 5478	Selective $S1P_2$ receptor agonist
CA-074ME	Cell-permeable cathepsin-B inhibitor

Conference abstracts.

1. **Saleh Almarshad**; Kenneth Watterson; Simon Kennedy; 2025. Influence of Perivascular Adipose Tissue (PVAT) and Endothelium on the Response to Hypoxia in Rat Thoracic Aorta. The 38th Scientific Meeting of the Malaysian Society of Pharmacology and Physiology (MSPP), IMU University, August (2025), *Malaysia*.

2. **Saleh Almarshad**; Kenneth Watterson; Simon Kennedy; 2024. Effect of hypoxia on Perivascular adipose tissue (PVAT) function. British Pharmacological Society, Pharmacology 2024, December (2024), *Harrogate*.

3. **Saleh Almarshad**; Kenneth Watterson; Simon Kennedy; 2024. Effect of hypoxia on Perivascular adipose tissue (PVAT) function. Scottish Cardiovascular Forum, February (2024), *St Andrews*.

Chapter 1 Introduction

1.1 Cardiovascular system

The cardiovascular system (CVS), also known as the circulatory system, comprises the heart, blood, and an intricate network of blood vessels, including arteries, arterioles, capillaries, venules, and veins. Its primary function is to deliver oxygen, nutrients, hormones, electrolytes, and water to the cells and tissues throughout the body and to remove carbon dioxide and metabolic waste products, transporting them to excretory organs such as the lungs and kidneys (Aaronson et al., 2020, Matienzo and Bordoni, 2025). Furthermore, the cardiovascular system plays a critical role in regulating body temperature, maintaining water content in cells, and supporting immune system function (Aaronson et al., 2020).

The heart, a muscular pump located within the chest cavity, ensures continuous circulation of blood through two interconnected circuits: the systemic circulation and the pulmonary circulation. Oxygen-rich blood is pumped from the left ventricle through the aorta and systemic arteries, which progressively branch into smaller arteries, arterioles, and ultimately capillaries, the site of nutrient and gas exchange (Chaudhry et al., 2025, Aaronson et al., 2020). After exchange, capillaries merge to form venules, which in turn unite into progressively larger veins, returning deoxygenated blood to the heart via the superior and inferior vena cavae. Subsequently, the right ventricle pumps this blood into the lungs through the pulmonary arteries for oxygenation. Blood vessels themselves require nutrients and oxygen, which are delivered by a specialised network known as the vasa vasorum embedded within their walls (Aaronson et al., 2020, Matienzo and Bordoni, 2025).

1.2 Anatomy of the cardiovascular system

The walls of all blood vessels, except capillaries, consist of three distinct concentric layers: the tunica intima, tunica media, and tunica adventitia (externa) (Figure 1-1) (Aaronson et al., 2020, Touyz et al., 2018, Daly, 2019). The tunica intima is the innermost layer, composed of a single layer of flattened endothelial cells (ECs) supported by a basement membrane or basal lamina, providing a smooth lining essential for efficient blood flow and regulating substance exchange between blood and surrounding tissues. Beneath this lies the tunica media, predominantly comprising vascular smooth muscle cells (VSMCs) arranged in

circular or spiral layers, along with elastic fibres. This layer plays a critical role in controlling vascular tone, peripheral resistance, and the distribution of blood flow throughout the body (Touyz et al., 2018, Aaronson et al., 2020).

The outermost layer, the tunica adventitia, anchors the blood vessels to adjacent structures and comprises two key components: adventitia compacta, primarily containing fibroblasts and collagen fibres, and perivascular adipose tissue (PVAT), which surrounds most vessels and contributes to their physiological regulation (Touyz et al., 2018). Capillaries differ structurally from other blood vessels as they consist solely of a single endothelial cell layer resting on a basement membrane, facilitating efficient nutrient and waste product exchange between blood and tissues (Aaronson et al., 2020).

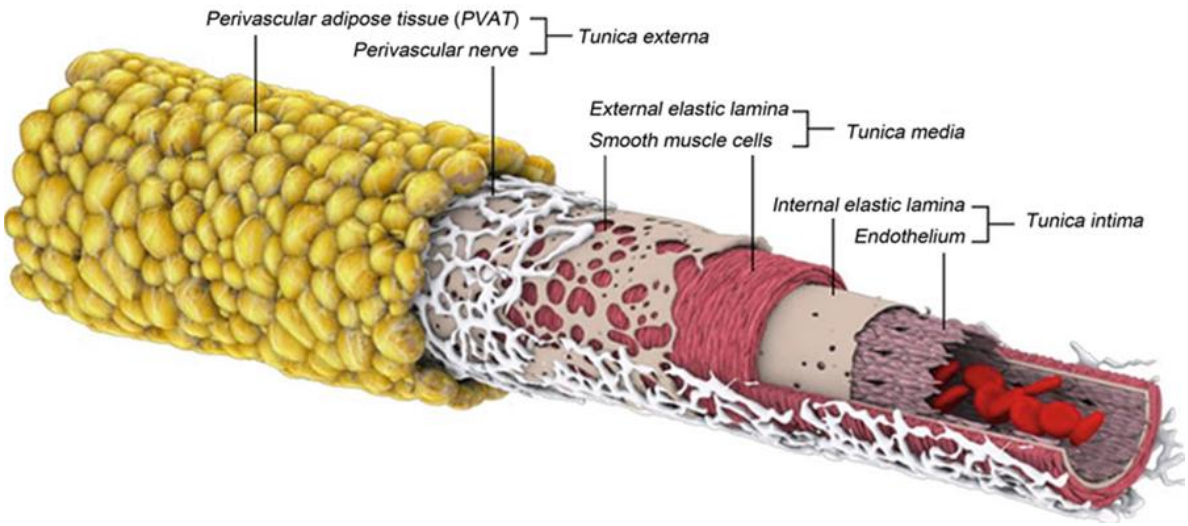

Figure 1-1 Vascular wall structure
Diagram illustrating the three distinct layers of the vascular wall: the inner layer (tunica intima) composed of endothelial cells; the middle layer (tunica media) containing vascular smooth muscle cells; and the outer layer (tunica externa) comprising nerve endings and perivascular adipose tissue (PVAT). Adapted from Daly (2019).

1.2.1 Endothelium (Tunica intima)

The vascular endothelium, also referred to as the tunica intima, consists of a single layer of flattened ECs lining the inner surface of all blood and lymphatic vessels. This endothelial layer creates a selective permeability barrier, mechanically and metabolically separating the vascular wall and peripheral tissues from circulating blood and lymph components (Luscher and Vanhoutte, 2020, Krüger-Genge et al., 2019). Once considered merely a passive barrier, the

endothelium is now recognised as an active participant in numerous physiological processes, including the regulation of vascular tone, immune responses, haemostasis, inflammation, and angiogenesis (Luscher and Vanhoutte, 2020, Deanfield et al., 2007). The vital role of endothelial cells in controlling vascular function was first identified by Furchgott and Zawadzki (1980), who demonstrated endothelium-dependent relaxation responses to acetylcholine in rabbit arteries.

ECs synthesise and secrete a diverse array of vasoactive substances crucial for maintaining vascular homeostasis. Among these are vasodilators, such as nitric oxide (NO), prostacyclin (PGI_2), and endothelium-derived hyperpolarising factor (EDHF), which collectively regulate blood flow, pressure, and vascular tone (Deanfield et al., 2007, Sandoo et al., 2010). Conversely, ECs also release vasoconstrictors, notably endothelin-1 (ET-1) and platelet-activating factor (PAF), which facilitate precise control over vascular responses (Sandoo et al., 2010, Galley and Webster, 2004). The delicate equilibrium between these relaxing and contracting mediators is essential for the normal physiological function of blood vessels and the systemic regulation of blood pressure (Galley and Webster, 2004). Disturbances in this equilibrium, characterised by enhanced vasoconstriction and decreased vasodilation, result in endothelial dysfunction, which is a feature seen in many chronic diseases including hypertension, diabetes, obesity, dyslipidaemia, and atherosclerosis (Wang et al., 2022a, Gallo et al., 2022).

Moreover, endothelial dysfunction is often driven by mechanisms involving oxidative stress, inflammation, and disrupted cellular signalling pathways (Wang et al., 2022a). Such dysfunction shifts endothelial phenotype towards a pro-inflammatory, pro-thrombotic, and proliferative state, increasing the risk of vascular pathology (Gallo et al., 2022). In hypertensive conditions for example, the imbalance between vasodilators like NO and vasoconstrictors like ET-1 exacerbates vascular constriction, elevating blood pressure (Nadar et al., 2004). Experimental models have shown that endothelium denudation enhances vascular contraction, as evidenced by increased responses to U46619, phenylephrine, and KCl in rat aortic rings, highlighting the protective and regulatory roles of an intact endothelium (Tang and Vanhoutte, 2008). Furthermore, endothelial cells communicate directly with VSMCs via myoendothelial gap junctions (MEGJs), facilitating the passage and influence of critical endothelium-derived mediators such as NO, PGI_2, ET-1, and EDHF. These interactions underscore the integral role

of the endothelium as both a structural and functional component, central to vascular integrity and cardiovascular health (Chaytor et al., 2005, Billaud et al., 2009, Sandow and Hill, 2000, Bryan Jr et al., 2005, Sandoo et al., 2010).

1.2.2 Vascular smooth muscle layer (Tunica media)

The tunica media, or vascular smooth muscle layer, predominantly comprises VSMCs interspersed with elastic fibres. These components are crucial for maintaining arterial wall integrity, regulating vascular tone, and facilitating vascular remodelling (Hu et al., 2019, Basatemur et al., 2019). VSMCs modulate vessel diameter and consequently blood pressure through coordinated contraction and relaxation processes. Contraction of these cells, induced by diverse stimuli such as hormonal (angiotensin II, ET-1), neural (noradrenaline), or mechanical factors, leads to narrowing of the vessel lumen and elevation of vascular resistance. Conversely, relaxation results in vessel dilation and decreased resistance, typically mediated by endothelium-derived NO diffusing into VSMCs and elevating cyclic guanosine monophosphate (cGMP) levels (Wilson, 2011, Walford and Loscalzo, 2003). VSMC contraction significantly modulates arterial diameter in muscular arteries and arterioles, whereas elastin produced by VSMCs is vital for elastic recoil in large arteries like the aorta. In smaller arteries and arterioles (resistance vessels), fewer elastic fibres are present, and VSMCs play a pivotal role in regulating peripheral vascular resistance and blood flow into capillary networks (Basatemur et al., 2019).

Intracellular calcium (Ca^{2+}) plays a central role in regulating VSMC contraction and relaxation. Increases in cytosolic Ca^{2+} concentration, either from extracellular influx through L-type voltage-gated calcium channels or via intracellular release from sarcoplasmic reticulum stores through inositol 1,4,5-trisphosphate (IP3) receptors, initiate contraction (Zhao et al., 2015b, Khalil, 2010). The Ca^{2+} binds to calmodulin, forming a complex that activates myosin light chain kinase (MLCK). MLCK phosphorylates myosin light chain (MLC), promoting actin-myosin cross bridge formation, thereby triggering cell shortening and smooth muscle contraction (Zhao et al., 2015b, Khalil, 2010). Conversely, VSMC relaxation is induced by mechanisms lowering intracellular Ca^{2+} levels. These mechanisms include closure of voltage-dependent calcium channels, calcium extrusion via sodium-calcium exchangers, and calcium sequestration within the sarcoplasmic

reticulum by the sarcoplasmic/endoplasmic reticulum Ca^{2+}-ATPase (SERCA) pump. This reduction in Ca^{2+} concentration activates MLC phosphatase and inhibits MLCK, resulting in muscle relaxation (Touyz et al., 2018, Brozovich et al., 2016).

Additionally, membrane potential significantly influences VSMC function through modulation of ion channel activity. Depolarisation of the cell membrane promotes calcium channel opening, increasing intracellular calcium concentration and thereby causing contraction. In contrast, hyperpolarisation, primarily mediated by potassium (K^+) channel activation, facilitates muscle relaxation. K^+ channels identified in VSMCs include ATP-sensitive (K^+_{ATP}), voltage-dependent (K_v), inward rectifying (Kir), and calcium-activated (K_{Ca}) channels (Touyz et al., 2018). Beyond regulating tone, VSMCs exhibit remarkable phenotypic plasticity in response to pathological stimuli. Under such conditions, they transition from a contractile phenotype to a proliferative, migratory, or even myofibroblast-like phenotype, contributing to vascular repair following injury or inflammation. However, these same phenotypic shifts also play a central role in the development of vascular pathologies, including atherosclerosis (Chen et al., 2023a, Cao et al., 2022, Owens et al., 2004).

Adrenergic receptors (ARs) are also highly expressed on VSMCs and play a central role in regulating vascular tone. Both α- and ß-AR subtypes are present, each activating distinct signalling pathways. Classically, α_1-ARs and α_2-ARs mediate vasoconstriction through Gq- and Gi-dependent mechanisms that elevate intracellular Ca^{2+} or suppress adenylyl cyclase and activate hyperpolarising K^+ currents (Gambardella et al., 2023). Among α_1-subtypes, α_1A- and α_1D-ARs are the principal mediators of agonist-induced VSMC contraction, while α_1B-AR contributes selectively to aortic and carotid vasoconstriction; α_2-ARs also mediate strong constrictor responses to endogenous neurotransmitters and exogenous agonists (Docherty and McGrath, 1980, Daly et al., 2002, Hussain and Marshall, 1997, Villalobos-Molina and Ibarra, 1996, Piascik et al., 1995, Muramatsu et al., 1990). In contrast, $ß_1$-, $ß_2$-, and $ß_3$-ARs expressed on VSMCs promote vasodilation via adenylyl cyclase–cAMP signalling (Gambardella et al., 2023). The dominant subtype varies by vascular bed: $ß_1$-AR-dependent relaxation is prominent in mesenteric arteries, while aortic dilation is mediated mainly by $ß_2$-AR and endothelial $ß_2$/$ß_3$-ARs (Flacco et al., 2013).

1.2.3 Adventitia and perivascular adipose tissue (Tunica externa)

The adventitia (tunica externa) is the outermost layer of blood vessel walls, composed primarily of connective tissue, fibroblasts, collagen fibres, and elastic fibres. It provides structural support and anchors vessels to surrounding tissues. Enveloping most systemic vessels, except capillaries and cerebral and pulmonary vessels, is perivascular adipose tissue (PVAT), a specialised adipose depot that modulates local vascular function (Hillock-Watling and Gotlieb, 2022, Queiroz and Sena, 2024). The detailed structure, function, and vascular roles of PVAT are discussed in Section 1.4.2.

1.3 Cardiovascular disease and obesity

Cardiovascular disease (CVD) remains one of the leading causes of morbidity and mortality worldwide and poses a major global health challenge. According to the World Health Organization (WHO, 2021), CVD is responsible for approximately 17.9 million deaths annually. Obesity is a major contributor to CVD through mechanisms such as metabolic dysfunction, inflammation, and vascular impairment. Cardiovascular risk factors including type 2 diabetes mellitus (T2DM), dyslipidaemia, and hypertension are frequently observed in individuals with obesity (Powell-Wiley et al., 2021). The WHO defines overweight as a body mass index (BMI) between 25 and 29.9 kg/m^2, and obesity as a BMI of 30 kg/m^2 or greater (WHO, 2000). The Global Burden of Disease Obesity Collaborators (2017) reported that 603.7 million adults were obese, with obesity rates doubling in 73 countries between 1980 and 2015 and continuing to rise globally. Recent data indicate that adult obesity more than doubled globally from 1990 to 2022 (WHO, 2025; Phelps et al. (2024)). An estimated 33% to 42% of the global population are currently overweight or obese (Islam et al., 2024). This widespread prevalence highlights the urgent need to better understand the mechanisms linking obesity to cardiovascular disease and to develop targeted therapeutic strategies.

Although obesity is driven by an energy imbalance between caloric intake and expenditure, it is fundamentally a disorder of adipose tissue, involving excessive lipid storage, altered fat distribution, and metabolic dysfunction (Jeremic et al., 2017, Reilly and Saltiel, 2017). Importantly, the phenotype and cardiometabolic consequences of obesity are significantly influenced by the regional distribution

of adipose tissue. Visceral and intra-abdominal fat depots are strongly associated with elevated cardiometabolic risk (Mathieu et al., 2009, Gesta et al., 2007) and PVAT is also implicated in obesity-related metabolic dysfunction (Nosalski and Guzik, 2017). In obesity, PVAT becomes dysfunctional, characterised by hypoxia, inflammation, and elevated oxidative stress, along with adipocyte abnormalities such as altered lipid metabolism, increased lipolysis, and reduced secretion of adipokines, including adiponectin. These changes contribute to a proinflammatory microenvironment and impaired regulatory function in vascular homeostasis (Stanek et al., 2021, Queiroz and Sena, 2024). In addition to PVAT dysfunction, obesity is associated with elevated circulating levels of sphingolipids in both humans and rodents. Among these, sphingosine-1-phosphate (S1P) and ceramides are involved in signalling pathways that contribute to metabolic syndrome and obesity-related complications (Lambert et al., 2018). The sphingolipid system, including the role of S1P, will be discussed in more detail in Section 1.6.

1.4 Adipose tissue biology

Adipose tissue (AT) is a dynamic and metabolically active organ composed of mature adipocytes and a stromal vascular fraction (SVF) that includes preadipocytes, vascular endothelial cells, fibroblasts, immune cells and stem cells (dos Santos Goldenberg and de Carvalho, 2023, Richard et al., 2020, Coelho et al., 2013). While traditionally considered a passive reservoir for energy storage, AT is now recognised as an endocrine organ that secretes numerous biologically active molecules known as adipokines, such as leptin and adiponectin. These adipokines exert autocrine, paracrine, and endocrine effects, influencing physiological processes such as energy metabolism, insulin sensitivity, inflammation, vascular function, and immune responses (Fernández-Alfonso et al., 2013, Petersen and Shulman, 2018, Koenen et al., 2021). AT depots are typically classified based on both anatomical location, for example subcutaneous and visceral fat, and functional phenotype, including white, brown, and beige AT.

1.4.1 White, brown, and beige adipose tissue

AT is broadly categorised into three major types: white adipose tissue (WAT), brown adipose tissue (BAT), and beige adipose tissue. These types differ in their cellular structure, mitochondrial content, thermogenic capacity, and

physiological roles (Stanek et al., 2021, Li et al., 2020). The distribution and activity of WAT and BAT vary significantly depending on factors such as age, sex, genetic background, and environmental stimuli including temperature, diet, and physical activity (Cinti, 2011, Berryman and List, 2017).

WAT is composed of unilocular adipocytes containing a single large lipid droplet occupying over 90% of cell volume and relatively few mitochondria. It is the predominant form of AT in adults and functions primarily in energy storage and endocrine signalling. WAT stores excess nutrients in the form of triglycerides and releases free fatty acids during periods of energy demand. It is also an active site of adipokine secretion, including leptin and adiponectin, which are central to metabolic regulation and systemic energy balance (Jeremic et al., 2017, Cinti, 2011, Funcke and Scherer, 2019). In humans, WAT is predominantly located in subcutaneous depots, such as the thighs, waist, and abdomen, and in visceral depots, including omental, mesenteric, retroperitoneal, gonadal, pericardial, and perivascular regions (Chusyd et al., 2016, Zwick et al., 2018). In obesity, WAT undergoes significant remodelling, characterised by adipocyte hypertrophy and hyperplasia, along with increased infiltration of immune cells, particularly macrophages. This remodelling leads to enhanced secretion of pro-inflammatory mediators, including interleukin-1ß (IL-1ß), interleukin-6 (IL-6), tumour necrosis factor-α (TNF-α), leptin, and monocyte chemoattractant protein-1 (MCP-1). These changes contribute to a sustained inflammatory environment that disrupts adipokine balance by suppressing adiponectin production and promoting metabolic disturbances such as insulin resistance, cardiovascular disease, and the metabolic syndrome (Koenen et al., 2021, Kwaifa et al., 2020).

BAT is composed of multilocular adipocytes rich in mitochondria and is primarily involved in non-shivering thermogenesis through the action of uncoupling protein 1 (UCP-1). This protein facilitates heat generation by uncoupling the mitochondrial proton gradient from ATP synthesis (Machado et al., 2022, Cannon and Nedergaard, 2004). BAT depots are most abundant in neonates but have been identified in adults, particularly in supraclavicular, suprarenal, perirenal, periovarian, cervical, and mediastinal regions, as well as around large vessels such as the thoracic aorta (Jeremic et al., 2017, Gil-Ortega et al., 2015, Hildebrand et al., 2018). In rodents, interscapular BAT is a well-characterised depot and commonly used in experimental models (Lidell et al., 2013). BAT also plays a role

in metabolic homeostasis by promoting lipid clearance, releasing BATokines, reducing insulin resistance, and improving glucose metabolism (van Marken Lichtenbelt et al., 2009, Gil-Ortega et al., 2015, Hildebrand et al., 2018). However, BAT activity is markedly reduced in overweight and obese individuals, often accompanied by diminished thermogenic capacity. Resting metabolic rate has been shown to positively correlate with BAT mass, underscoring its role in energy expenditure (van Marken Lichtenbelt et al., 2009). Accordingly, BAT activation has garnered attention as a potential therapeutic target for obesity and its related metabolic disorders, including T2DM. Enhancing the amount or activity of brown adipocytes has been associated with improved metabolic outcomes and greater resistance to obesity in animal studies (Cederberg et al., 2001, Kim et al., 2005).

Beige adipocytes, also known as brite (brown-in-white) cells, are inducible thermogenic adipocytes located within WAT depots (Chait and Den Hartigh, 2020, Li et al., 2022). They exhibit a phenotype that shares features of both white and brown adipocytes, including multilocular lipid droplets, increased mitochondrial content, and expression of UCP-1 in response to stimuli such as prolonged cold exposure or ß-adrenergic activation (Harms and Seale, 2013, Rosenwald et al., 2013, Bargut et al., 2017, Cuevas-Ramos et al., 2019). Unlike classical brown adipocytes, which originate from Myf5+ myogenic precursors, beige adipocytes are thought to derive either from smooth muscle-like pericytes or through transdifferentiation of mature white adipocytes in a process known as browning (Park et al., 2014a, Harms and Seale, 2013, Long et al., 2014). These cells are more prevalent in subcutaneous WAT and contribute to energy expenditure, thermogenesis, and improved metabolic regulation (Chait and Den Hartigh, 2020). Browning capacity varies by fat depot, with subcutaneous WAT showing greater propensity for beige adipocyte recruitment than visceral WAT, likely due to higher expression of PRDM16, a transcriptional co-regulator that promotes brown and beige adipocyte differentiation, and other thermogenic regulators in subcutaneous fat (Bargut et al., 2017, Li et al., 2021, Hondares et al., 2011). Although beige adipocytes have demonstrated metabolic benefits in animal models, their functional significance in human physiology remains an active area of research.

1.4.2 Perivascular adipose tissue (PVAT)

Perivascular adipose tissue (PVAT) is a specialised adipose depot that surrounds most systemic blood vessels, including the aorta and arteries such as the carotid, coronary, and mesenteric arteries, but is absent around capillaries, cerebral and pulmonary vessels (Hillock-Watling and Gotlieb, 2022, Queiroz and Sena, 2024). PVAT is anatomically positioned adjacent to the adventitia; although no physical barrier demarcates these layers, structural differences between them have been identified (Szasz et al., 2013). Initially regarded as a passive mechanical support tissue, PVAT was historically removed during vascular studies under the assumption that it merely interfered with the diffusion of pharmacological agents (Oriowo, 2015). This view began to change in 1991 when Soltis and Cassis demonstrated that PVAT attenuated noradrenaline-induced contraction in rat aortic rings, suggesting a functional role in modulating vascular tone (Soltis and Cassis, 1991).

Today, PVAT is recognised as an active endocrine, paracrine, and autocrine organ capable of releasing numerous bioactive substances that influence vascular homeostasis (Szasz and Webb, 2012). Its integral modulatory role in cardiovascular function has been increasingly recognised (Cheng et al., 2018). PVAT is primarily composed of adipocytes, but also contains immune cells, fibroblasts, endothelial cells, and components of the stromal vascular fraction (Nosalski and Guzik, 2017, Chang et al., 2020b). These diverse cellular elements endow PVAT with the capacity to secrete a range of adipokines and inflammatory mediators that contribute to vascular regulation.

PVAT exhibits significant heterogeneity in cellular composition and function depending on anatomical location and species (Kim et al., 2020). It may consist of WAT, BAT, or a mixture of both. For instance, rodent mesenteric PVAT is composed predominantly of WAT, while thoracic aortic PVAT more closely resembles BAT (Gálvez-Prieto et al., 2008, Barp et al., 2020, Gil-Ortega et al., 2015). In mixed aortic PVAT, characteristic features of BAT are observed, including multilocular adipocytes and the expression of UCP-1 (Fitzgibbons et al., 2011). Conversely, mesenteric PVAT lacks UCP-1 expression and exhibits lower vascularisation (Cinti, 2011). Heterogeneity can even exist within the same blood vessel: thoracic PVAT is enriched in brown adipocytes, while abdominal PVAT

contains primarily white adipocytes with fewer brown cells (Victorio et al., 2016, Brown et al., 2014, Padilla et al., 2013).

These regional and structural differences correlate with functional distinctions. Thoracic PVAT has been associated with BAT-like properties such as thermogenesis and higher resistance to inflammation, whereas abdominal PVAT demonstrates a greater pro-inflammatory profile and responsiveness to high-fat diets, indicating a more atherogenic phenotype (Padilla et al., 2013, Reynés et al., 2019, Fitzgibbons et al., 2011). Gene expression studies have confirmed that PVAT expresses lower levels of lipid metabolism and adipocyte differentiation markers, such as PPARγ, C/EBPα, and FABP4, compared with subcutaneous and visceral fat (Chatterjee et al., 2009, Adachi et al., 2022, Hu et al., 2021), further emphasising its distinct identity. Critically, PVAT is believed to originate from unique progenitor cells distinct from those of other adipose tissues, reinforcing its close developmental and functional association with the vascular system (Qi et al., 2018). Taken together, the structural, molecular, and functional features of PVAT underscore its significance as an active and highly specialised component of the cardiovascular system.

1.4.2.1 PVAT-derived mediators

PVAT significantly influences vascular function by releasing a diverse range of biologically active mediators, including adipokines, cytokines, reactive oxygen species (ROS), and gaseous molecules (Chang et al., 2020b, Almabrouk et al., 2014). These mediators include adiponectin, hydrogen sulphide (H_2S), NO, and superoxide (O_2^-) (Simonsen and Boedtkjer, 2016, Chang et al., 2020b, Szasz et al., 2013). The secretory profile of PVAT varies significantly depending on its anatomical location. For example, thoracic aortic PVAT releases higher levels of NO than abdominal aortic PVAT (Hwej et al., 2024, Victorio et al., 2016). Similarly, in mice, aortic PVAT secretes lower amounts of adiponectin, leptin, and resistin compared to subcutaneous and visceral AT (Chatterjee et al., 2009). PVAT also expresses components of the renin–angiotensin system (RAS) in a depot-specific manner. In Wistar Kyoto (WKY) rats, mesenteric PVAT demonstrates higher levels of angiotensin AT1a and AT2 receptors, angiotensin II, and chymase, but lower prorenin receptor expression compared to aortic PVAT, further modulating regional vascular responses (Gálvez-Prieto et al., 2008).

Beyond its secretory diversity and regional specialisation, PVAT also contributes to immune regulation and vascular remodelling through the release of both inflammatory mediators and growth factors. It secretes anti-inflammatory mediators such as adiponectin and adrenomedullin (Fésüs et al., 2007, Rajsheker et al., 2010), alongside pro-inflammatory adipokines including leptin, IL-6, IL-8, MCP-1, and TNF-α (Szasz and Webb, 2012, Şahin and Bariskaner, 2007). In addition to modulating inflammation, PVAT influences vascular structure through the secretion of growth factors that regulate VSMC proliferation and migration. These include thrombospondin-1, serpin-E1, transforming growth factor-beta (TGF-ß), vascular endothelial growth factor (VEGF), platelet-derived growth factor-BB (PDGF-BB), and placental growth factor (PLGF), which have been implicated in the development of vascular pathologies such as hypertension, atherosclerosis, and aneurysm formation (Chang et al., 2020b, Siegel-Axel et al., 2014, Rittig et al., 2012).

In summary, the PVAT secretome consists of a diverse range of bioactive substances that can be classified into six main functional groups. First, adipokines and adipocyte-derived proteins such as adiponectin, leptin, nesfatin and omentin are crucial for maintaining metabolic balance and vascular function. Second, inflammatory mediators, including cytokines and chemokines like TNF-α, IL-6, IL-8, and MCP-1, are central to immune signalling and vascular inflammation. Third, gaseous signalling molecules and oxidative species, including NO, H_2S, and hydrogen peroxide (H_2O_2), play roles in redox balance and endothelial function. Fourth, vasoactive peptides such as angiotensin II and angiotensin 1–7 contribute to the regulation of vascular tone and remodelling. Fifth, lipid-derived molecules, particularly free fatty acids released via lipolysis, exert paracrine and autocrine effects on vascular cells and lastly, PVAT generates steroid hormones like cortisol and oestradiol, which modulate vascular responses and systemic metabolic processes (Szasz and Webb, 2012, Akoumianakis et al., 2017). The functional balance among these mediators is essential for vascular homeostasis, and disturbances in this profile are closely associated with cardiovascular complications in obesity, hypertension, and diabetes (Nosalski and Guzik, 2017, Mitidieri et al., 2022).

1.4.2.2 Adrenergic innervation and adrenoceptor expression in PVAT

Sympathetic noradrenergic signalling is a key regulator of adipose tissue function. All major adrenoceptor subclasses (α_1, α_2, β_1, β_2 and β_3) are expressed on adipocytes, where they differentially control lipolysis, glucose metabolism and thermogenesis (Lafontan and Berlan, 1993). In brown adipocytes, α_1-adrenoceptors couple to Gq and activate PKC which contributes to thermogenic responses, whereas in white adipocytes α_1-adrenoceptor stimulation promotes glycogenolysis (Lafontan and Berlan, 1993). By contrast, α_2-adrenoceptors which are particularly abundant in WAT, are Gi-coupled inhibitory receptors that suppress adenylate cyclase activity, reduce cAMP and thereby limit lipolysis (Lafontan and Berlan, 1993). All three β-adrenoceptor subtypes are highly expressed in both WAT and BAT, where Gs–cAMP signalling drives lipolysis and, in brown and beige adipocytes, activates UCP-1-dependent thermogenesis (Lafontan and Berlan, 1993, Deng et al., 1996, Matthias et al., 2000). Within PVAT, adipocytes, sympathetic nerves and stromal vascular cells together form a local adrenergic system capable of synthesising, releasing, taking up and metabolising noradrenaline (Ayala-Lopez et al., 2014, Ayala-Lopez and Watts, 2017). Fluorescent ligand binding studies in mouse mesenteric PVAT have demonstrated the presence of both α- and β-adrenoceptors on PVAT cells (Bulloch and Daly, 2014). In addition to adipocytes, adrenoceptors are also expressed on PVAT-resident immune cells, including macrophages, lymphocytes and mast cells, providing further pathways through which sympathetic signalling can modulate inflammatory tone and influence vascular function (Abrass et al., 1985, Chi et al., 2003, Vida et al., 2011, Ayala-Lopez and Watts, 2017). Collectively, these findings indicate that PVAT is not only a passive target of sympathetic activity but also an active adrenergic organ that integrates neural inputs with local adipokine and cytokine release to regulate vascular tone.

1.4.2.3 PVAT regulation of vascular tone: anticontractile and contractile actions

PVAT is an active paracrine modulator of vascular tone due to its proximity to the vascular adventitia. Through secretion of vasoactive molecules, PVAT interacts with VSMCs and ECs, contributing to vascular homeostasis (Kim et al., 2020, Chang et al., 2020b). PVAT exhibits regional and depot-specific effects on vascular tone, demonstrated in mice, where thoracic aortic PVAT significantly attenuated

phenylephrine-induced vasoconstriction, an effect not seen with abdominal aortic PVAT. This effect correlated with higher expression of endothelial nitric oxide synthase (eNOS) and increased NO bioavailability in the thoracic region (Hwej et al., 2024, Victorio et al., 2016), reinforcing the concept of PVAT phenotypic heterogeneity (Gil-Ortega et al., 2015). The anticontractile nature of PVAT was first described by Soltis and Cassis (1991) in male Sprague-Dawley (SD) rat aortic rings, where intact PVAT attenuated norepinephrine-induced contraction and was initially attributed to enhanced sympathetic reuptake of norepinephrine. Subsequent work by Löhn et al. (2002) showed that in male SD rats, thoracic aortic rings with intact PVAT exhibited reduced contractile responses to phenylephrine, serotonin, and angiotensin II. This effect suggested the presence of a transferable adventitia-derived relaxing factor (ADRF), which was later reclassified as PVAT-derived relaxing factors (PVRFs) as they originated from PVAT itself (Szasz and Webb, 2012). The transferable nature of PVRFs has been validated in various studies using PVAT-conditioned solutions that induce relaxation in precontracted, PVAT-free vascular segments (Verlohren et al., 2004, Fésüs et al., 2007, Gao et al., 2007, Lu et al., 2011, Greenstein et al., 2009, Almabrouk et al., 2017). Identified PVRFs include adiponectin, leptin, H_2O_2, H_2S, omentin, methyl palmitate, prostacyclin, angiotensin 1–7 and NO (Tong et al., 2023, Victorio et al., 2016, Lee et al., 2011).

PVAT mediates vasorelaxation through both endothelium-dependent and independent mechanisms. Endothelium-dependent relaxation involves PVRFs stimulating eNOS in ECs, enhancing NO production which then activates soluble guanylate cyclase (sGC) in VSMCs, raising cGMP levels (Kim et al., 2020). Adiponectin, secreted by PVAT, plays a central role through the PI3K–Akt and AMP-activated protein kinase (AMPK) pathways that enhance eNOS phosphorylation (Almabrouk et al., 2017, Antoniades et al., 2009, Chen et al., 2003). Moreover, adiponectin contributes to vasorelaxation in murine mesenteric arteries by stimulating AdipoR1 receptors on ECs (Lynch et al., 2013). Additionally, apelin, another PVAT-derived adipokine, has been shown to enhance NO-dependent vasorelaxation both in vitro and in vivo, particularly in splanchnic and peripheral human arteries (Salcedo et al., 2007). In contrast, endothelium-independent effects are mediated by direct action of PVRFs on VSMC ion channels. In male SD rats, PVAT-induced relaxation in thoracic aorta involves K^+_{ATP} channels and

tyrosine kinase activation, functioning in a Ca^{2+}-dependent manner (Löhn et al., 2002). In Wistar rats, thoracic aortic relaxation is attributed to K_{Ca} channel activation and H_2O_2-stimulation of sGC (Gao et al., 2007). K_v channel-mediated relaxation has been observed in mesenteric arteries of SD rats and thoracic aorta of Wistar Kyoto rats (Verlohren et al., 2004, Lee et al., 2011). In human internal thoracic arteries, K_{Ca} channels also contribute to the anticontractile response (Gao et al., 2005). Additionally, adiponectin induces vasorelaxation in aortic and mesenteric vessel rings via opening K_v and large-conductance Ca^{2+}-activated K^+ (BK_{Ca}) channels (Fésüs et al., 2007, Weston et al., 2013, Lynch et al., 2013). Moreover, electrical field stimulation (EFS) of mesenteric arteries evokes an endothelium-independent anticontractile effect that depends partly on adiponectin derived from PVAT (Saxton et al., 2018). In addition, PVAT releases methyl palmitate, which modulates neurogenic (sympathetic–sensory interaction–mediated) vasorelaxation (Chang et al., 2020a). This diversity reflects the complexity of PVAT's regulatory role on vascular tone.

Concomitantly, PVAT also releases a range of contractile mediators, collectively referred to as PVAT-derived contracting factors (PVCFs). These include pro-inflammatory cytokines and vasoactive substances such as resistin, IL-6, TNF-α, leptin, angiotensin II, O_2^-, calpastatin, chemerin, catecholamines, prostaglandins and COX-derived vasoconstrictor prostanoids (Gao et al., 2007, Ramirez et al., 2017, Meyer et al., 2013, Kumar et al., 2019, Ferland et al., 2017, Owen et al., 2013, Ayala-Lopez et al., 2014, Valentini et al., 2023, Cheng et al., 2018). Notably, mediators such as H_2O_2, H_2S, prostanoids and leptin can exert dual actions, producing vasodilation or vasoconstriction depending on concentration, contractile state of the vessel, the vascular bed involved and pathological conditions (Santiago et al., 2016, Tong et al., 2023, Ahmed et al., 2023, Mendizábal et al., 2013, Quehenberger et al., 2002, Cacanyiova et al., 2019).

It is now well established that potassium channels are expressed in adipose tissue and adipocytes and contribute importantly to the anticontractile actions of PVAT. Human and rodent white adipocytes display prominent voltage-dependent K^+ currents, consistent with functional Kv channel expression on the adipocyte membrane (Ramırez-Ponce et al., 1996, Ramirez-Ponce et al., 2003). In vascular studies, PVRFs open smooth-muscle K^+ channels, including K_{ATP}, Ca^{2+}-activated K^+

(K_{Ca}) and delayed-rectifier Kv channels, to hyperpolarise VSMCs and limit Ca^{2+} entry (Oriowo, 2015, Lynch et al., 2013). Furthermore, pharmacological and genetic studies in small arteries identify XE991-sensitive KCNQ (Kv7.3–7.5) channels and BK_{Ca} channels as critical downstream targets of PVAT; blockade or deletion of these channels abolishes the anticontractile effect of PVAT, whereas KCNQ channel openers can restore PVAT-mediated relaxation in hypertensive and obese models (Lynch et al., 2013, Tano et al., 2014, Wang et al., 2021). Together, PVAT-derived mediators modulate vascular tone primarily through activation of defined K^+-channel subtypes in both adipocytes and adjacent VSMCs.

In conclusion, PVAT plays a pivotal and dynamic role in the regulation of vascular tone. Its anticontractile effects, primarily mediated by adiponectin, NO, and other PVRFs, promote vasodilation. Simultaneously, PVAT also produces PVCFs, which contribute to maintaining vascular homeostasis. The overall impact of PVAT on vascular tone depends on the balance between its vasodilatory and vasoconstrictive influences. Despite significant advancements, the precise mechanisms by which PVAT modulates vascular relaxation and contraction remain incompletely understood. Additionally, the full spectrum of vasoactive compounds produced by PVAT has yet to be fully elucidated, highlighting the need for further research in this area.

1.4.2.4 Adiponectin

Adiponectin is a 30 kDa protein hormone produced exclusively by adipose tissue and was first discovered in 1995 through subtractive hybridization studies that aimed to identify genes involved in adipocyte differentiation (Scherer et al., 1995). Initially detected in human plasma and differentiated 3T3-L1 adipocytes (Scherer et al., 1995, Nakano et al., 1996), adiponectin has since become a key focus in metabolic research due to its broad effects on insulin sensitivity, inflammation, and cardiovascular health (Sowka and Dobrzyn, 2021). Before the 1996 discovery that adiponectin mRNA expression is reduced in obesity, it was not widely recognised that adipose tissue could produce a hormone with insulin-sensitising properties (Combs and Marliss, 2014, Hu et al., 1996). Adiponectin exists predominantly in two isoforms: a full-length form and a globular fragment, with different biological activities that are still to be fully investigated (Kadowaki and Yamauchi, 2005, Kadowaki et al., 2006). Despite being rapidly cleared by the

liver, adiponectin is highly stable, maintaining relatively steady plasma levels with a short half-life of 45–75 minutes (Halberg et al., 2009b).

The effects of adiponectin are primarily mediated through two classical receptors, AdipoR1 and AdipoR2. Although they contain seven transmembrane domains similar to G-protein-coupled receptors (GPCRs), they are structurally distinct because their N-terminus is located intracellularly and their C-terminus extracellularly, which is the reverse orientation of typical GPCRs (Yamauchi et al., 2003). AdipoR1 is predominantly expressed in skeletal muscle, while AdipoR2 is enriched in the liver (Kadowaki et al., 2006). These receptors are also expressed in human and rodent adipose tissues and in 3T3-L1 adipocytes as well as in various metabolically active cells like immune cells, hepatocytes and neurons (Kadowaki et al., 2006, Wang et al., 2020b, Fry et al., 2006, Żelechowska et al., 2019, Pang and Narendran, 2008). A third adiponectin-binding protein, T-cadherin, is expressed predominantly in cardiovascular tissues and binds high-molecular-weight and hexameric adiponectin isoforms. However, due to its lack of an intracellular signalling domain, it is not considered a classical receptor (Hug et al., 2004, Denzel et al., 2010). Adiponectin binding to AdipoRs activates key downstream signalling pathways, particularly AMPK and PPAR alpha (PPARα), to exert anti-diabetic effects. This signalling is enhanced by APPL1, an adaptor protein, which promotes glucose uptake and insulin sensitivity via insulin receptor substrate 1 (IRS-1)(Luo and Liu, 2022). Osmotin, an adiponectin homolog, also activates AdipoRs to reduce abdominal fat accumulation in high-fat diet-fed mice (Jo et al., 2019).

Adiponectin shows a wide range of protective properties, including anti-inflammatory (Huang et al., 2008), anti-fibrotic (Shafiei et al., 2011), anti-apoptotic (Ye et al., 2014), and anti-lipotoxic effects (Xu et al., 2003), in addition to reducing ceramide accumulation and enhancing insulin sensitivity (Holland et al., 2010). In obese diabetic KKAy mice fed a high-fat diet, both adiponectin and its receptor mRNA expression in adipose tissues were significantly downregulated, which correlated with reduced insulin sensitivity (Yamauchi et al., 2001, Tsuchida et al., 2005). Furthermore, adiponectin knockout mice exhibit increased susceptibility to diet-induced insulin resistance, likely through increased TNF-α levels that impair insulin signalling through reduced fatty acid transport protein 1 (FATP-1) mRNA and IRS-1 expression (Maeda et al., 2002). Clinically, circulating

adiponectin levels are modulated by sex, pregnancy, and pathological conditions. Women and pregnant individuals generally exhibit higher levels (Combs et al., 2003), while reductions are observed in hypertension, coronary artery disease, metabolic syndrome, and diabetes (Yamauchi et al., 2001, Kumada et al., 2003, Chow et al., 2007, Salmenniemi et al., 2004).

Beyond metabolic regulation, adiponectin plays a critical role in vascular biology. It inhibits the proliferation and migration of vascular smooth muscle cells by binding directly to PDGF-BB and blocking ERK signalling, a pathway involved in atherosclerosis development (Arita et al., 2002). Moreover, as discussed in Section 1.4.2.2, adiponectin promotes vasodilation through both endothelium-dependent mechanisms, primarily via increased NO production, and endothelium-independent pathways, such as the activation of vascular smooth muscle potassium channels. Furthermore, the essential role of adiponectin in vascular homeostasis and blood pressure regulation is underscored by studies in adiponectin-deficient mice, which display elevated blood pressure (Ouchi et al., 2003, Ouchi et al., 2006). Overall, adiponectin functions as a crucial endocrine mediator linking adipose tissue with systemic metabolic, vascular, and inflammatory pathways.

1.5 Hypoxia and inflammation in adipose tissue: PVAT's role in metabolic and vascular dysfunction

1.5.1 PVAT in metabolic and cardiovascular disease

Dysfunctional PVAT has been implicated in a range of vascular diseases, including obesity, T2DM, atherosclerosis, and hypertension (Nosalski and Guzik, 2017). In many pathological states PVAT undergoes significant structural and functional changes. These include adipocyte hypertrophy, hypoxia, increased fibrosis, and dysregulated adipokine secretion, which collectively result in its dysfunction (Saxton et al., 2019a, Greenstein et al., 2009, Kim et al., 2019, Saxton et al., 2021). In obesity, PVAT secretes higher levels of inflammatory mediators such as TNF-α and IL-6, while the production of protective adipokines like adiponectin is significantly reduced (Saxton et al., 2021, Weisberg et al., 2003, Cai et al., 2023). This imbalance between pro- and anti-inflammatory factors contributes to endothelial dysfunction, reduced NO bioavailability, and impaired vasodilation,

thereby promoting hypertension and atherosclerosis (Chang et al., 2020b, Gálvez-Prieto et al., 2008, Quesada et al., 2018).

Furthermore, PVAT plays a critical role in vascular angiogenesis by releasing numerous angiogenic factors; thus, defects in PVAT signalling may be closely linked to the development of CVDs such as atherosclerosis and obesity-related vascular dysfunction (Mitidieri et al., 2022). In apolipoprotein E-deficient ($ApoE^{-/-}$) mice, inflammation within PVAT has been shown to precede both endothelial dysfunction and the development of atherosclerotic plaques (Skiba et al., 2017). High-fat diet (HFD) models in mice show a 70% reduction in adiponectin levels in PVAT and a complete loss of its anticontractile effect, a finding also confirmed in human subcutaneous arteries from obese patients (Aghamohammadzadeh et al., 2013, Almabrouk et al., 2018). Notably, this effect was reversed six months after bariatric surgery or treatment with antioxidant enzymes such as superoxide dismutase and catalase (Aghamohammadzadeh et al., 2013). These effects are partially attributed to increased oxidative stress, driven by elevated ROS production and impaired antioxidant defences (Qi et al., 2018, Queiroz and Sena, 2024).

PVAT dysfunction also plays a pivotal role in insulin resistance and metabolic disease. The inflammatory adipokines secreted by dysfunctional PVAT impair insulin signalling pathways, contributing to systemic insulin resistance, a core feature of T2DM (Gálvez-Prieto et al., 2012, Antonopoulos et al., 2015). The shift towards a proinflammatory immune profile within PVAT, including increased M1 macrophage infiltration, further exacerbates vascular inflammation and contributes to VSMC proliferation, migration and extracellular matrix remodelling (Chang et al., 2020b, Azul et al., 2020, Cai et al., 2023). In diabetes, thoracic PVAT contributes to inflammation through elevated expression of inflammatory markers such as CD36 and CCL2 (Azul et al., 2020). In diabetic db/db mice, whitening of PVAT and loss of UCP1 expression correlate with elevated cardiovascular risk (Wang et al., 2020a).

Importantly, therapeutic strategies targeting PVAT have demonstrated the potential to reverse its dysfunction. Bariatric surgery in obese patients not only restores the anticontractile function of PVAT but also increases adiponectin levels, improves NO bioavailability, and reduces inflammatory cell infiltration

(Aghamohammadzadeh et al., 2013). Similar benefits have been observed with dietary interventions that result in weight loss, with decreases in PVAT inflammation and enhanced endothelial NO synthase activity (Bussey et al., 2016, Emanuel et al., 2020). Furthermore, regular exercise restores PVAT anti-contractile function, reduces PVAT inflammation, increases β_3-adrenoceptor and organic cation transporter 3 (OCT3) expression, and improves systemic metabolic indices (blood glucose, plasma insulin); it also rescues adiponectin-mediated vasodilation (Saxton et al., 2021). These findings underline the importance of PVAT as a modifiable component in cardiometabolic disease and suggest that restoring its physiological function may provide a novel way for improving vascular health and reducing cardiovascular risk.

1.5.2 Inflammatory processes in PVAT

Inflammation within PVAT is a central mechanism linking metabolic disorders to cardiovascular dysfunction. In health, PVAT maintains an anti-inflammatory immune environment dominated by M2 macrophages and regulatory cells. However, obesity and insulin resistance drive a phenotypic shift towards proinflammatory M1 macrophages, leading to immune cell accumulation and local cytokine production. Macrophages in obese PVAT can constitute up to 50% of the immune cell population, compared to only 5–10% in lean tissue (Weisberg et al., 2003, Zeyda and Stulnig, 2007). This infiltration is mediated through several signalling pathways, including Toll-like receptor 4 (TLR4) activation, enhancing macrophage recruitment in obese patients and obese mouse AT (Saberi et al., 2009, Catalan et al., 2012). M1 macrophages then secrete TNF-α, IL-6, IL-1β, and iNOS, which promote systemic inflammation, impair insulin signalling, and compromise endothelial function (Zeyda and Stulnig, 2007, Weisberg et al., 2003, Schaffler et al., 2006). Moreover, inducible nitric oxide synthase (iNOS) expression is upregulated in the AT of obese humans and mice as well as diabetic mice, and its activity has been linked to mitochondrial dysfunction, reduced adiponectin synthesis, and impaired glucose uptake in 3T3-L1 adipocytes (Fite et al., 2015, Jeon et al., 2012, Jayarathne et al., 2018, Fujimoto et al., 2005, Engeli et al., 2004). Knockout or pharmacological inhibition of iNOS in high-fat diet (HFD) models improves insulin sensitivity and reduces inflammation, underlining its pathogenic role (Vilela et al., 2022, Dallaire et al., 2008, Tsuchiya et al., 2007).

Depot-specific immune responses have also been observed in PVAT. For example, in hypertensive models such as Dahl salt-sensitive rats, thoracic and mesenteric PVAT exhibit divergent inflammatory profiles, including hyperactivation of regulatory T cells (Tregs) and M2 macrophages (Kumar et al., 2021). In addition to macrophages, other immune cell subsets, including T cells, mast cells, monocytes and dendritic cells, also infiltrate PVAT under pathological conditions like obesity (Cai et al., 2023, Queiroz and Sena, 2024). These cells contribute to the proinflammatory microenvironment through the release of cytokines, chemokines such as CCL2, and adipokines like visfatin, leptin, and resistin, thereby amplifying inflammatory signalling and promoting vascular dysfunction (Queiroz and Sena, 2024). In summary, chronic low-grade inflammation within PVAT, especially in obesity and metabolic disease, is a critical contributor to vascular pathology.

1.5.3 Hypoxia in expanding adipose tissue

The onset of hypoxia within AT, particularly in PVAT, marks a pivotal transition from metabolically stressed adipose expansion to the development of vascular pathology. A central component of this transition is AT remodelling, a dynamic process supported by the tissue's inherent plasticity. Adipokines, secreted by adipocytes, mediate complex autocrine, paracrine, and endocrine signalling networks that regulate metabolic homeostasis and affect distant organs including the brain, liver, and muscle (Lee et al., 2019). In response to nutritional fluctuations and physiological demands, AT undergoes extensive remodelling involving coordinated changes in all resident cell types and tissue architecture to maintain health and accommodate growth (Huynh et al., 2025). AT expansion occurs via two primary mechanisms: hypertrophy, defined by the enlargement of existing adipocytes due to triacylglycerol (TAG) accumulation, and hyperplasia, marked by an increase in adipocyte number through de novo adipogenesis from precursor cells (Choe et al., 2016). While both modes contribute to overall adipose mass, hypertrophic growth is particularly implicated in the onset of local tissue hypoxia, which may impair vascular function and further exacerbate metabolic dysfunction. The interplay between hypertrophy and hyperplasia is governed by environmental and genetic factors, though the specific molecular regulators of this balance remain under active investigation (Huynh et al., 2025).

1.5.3.1 Mechanisms linking adipose expansion to hypoxia development

The shift from a well-oxygenated adipose environment to a hypoxic state during obesity-associated tissue expansion is driven by a combination of physical, vascular, and metabolic constraints. One of the primary mechanisms is the limitation of oxygen diffusion in enlarged adipocytes. Physiologically, the oxygen diffusion limit in tissues is approximately 100–200 μm (Brahimi-Horn and Pouysségur, 2007, Place et al., 2017), yet in both human and murine WAT, adipocyte diameters often exceed this threshold, reaching 150–200 μm in humans and surpassing 200 μm in obese mice (Skurk et al., 2007). It has been demonstrated that the partial pressure of oxygen (PO_2) may drop close to zero at distances just 100 μm from the vasculature (Folkman et al., 2000, Brahimi-Horn and Pouysségur, 2007). Despite the massive increase in adipose mass in obesity, the relative blood flow and proportion of cardiac output allocated to the tissue do not increase (Trayhurn, 2013). Moreover, postprandial increases in AT perfusion observed in lean individuals are notably absent in those with obesity (Goossens et al., 2011).

Vascular insufficiency further compounds this issue. Rapid adipose expansion, particularly via hypertrophy, is not matched by proportional increases in angiogenesis or capillary density. Studies in obese humans have shown 30–40% reductions in AT blood flow compared to lean individuals, alongside significantly decreased capillary density (Bolinder et al., 2000, Halberg et al., 2009a, Sun et al., 2012). This imbalance leads to reduced oxygen availability and lower PO_2 levels in the tissue. Measurements in both diet-induced and genetically obese (ob/ob) mice demonstrate that AT PO_2 can drop to 8–20 mmHg, compared to 27–40 mmHg in lean controls (Rausch et al., 2008, Sun et al., 2013, Ye et al., 2007). Human studies have similarly shown a decline, with obese subjects averaging PO_2 levels of 47 mmHg versus 55 mmHg in lean individuals (Pasarica et al., 2009).

In addition to structural constraints, metabolic dysfunction within adipocytes exacerbates local hypoxia. Obese adipocytes frequently exhibit heightened oxygen consumption due to mitochondrial alterations. Elevated levels of free fatty acids can activate adenine nucleotide translocase 2 (ANT2), a protein typically involved in BAT thermogenesis, resulting in uncoupled mitochondrial respiration and excessive oxygen use (Lefere et al., 2016, Lee et al., 2014). Hypoxia in AT has been confirmed by various methods, including pimonidazole staining, direct

oxygen tension measurement, and lactate/HIF-1α quantification in tissue biopsies (Lolmede et al., 2003, Huynh et al., 2025, Aguilera and Brekken, 2014, Ow et al., 2019). Notably, BAT is also susceptible to hypoxia in obesity. Shimizu et al. (2014) reported severe reductions in PO_2 (<15 mmHg) in BAT of diet-induced obese mice compared to levels around 50 mmHg in lean controls, likely due to BAT's inherently higher oxygen demands. This suggests that, despite differences in function and structure, both WAT and BAT are vulnerable to hypoxia under conditions of excessive nutrient surplus and impaired vascularisation.

1.5.3.2 Clinical and pathophysiological significance of PVAT hypoxia

As PVAT expands in obesity, it undergoes a pathological transformation from a vasoprotective to a dysfunctional and pro-inflammatory depot. This shift disrupts its paracrine signalling and promotes vascular pathology through "outside-in" mechanisms, whereby adipose-derived signals directly affect the underlying vascular wall (Kim et al., 2020). Hypoxia, commonly observed in expanding adipose depots, has been identified as a key driver of this inflammatory response. According to Rueda-Clausen et al. (2011), adult offspring exposed to gestational hypoxia did not show metabolic abnormalities when maintained on a low-fat diet, but when challenged with a high-fat diet they exhibited pronounced insulin resistance and glucose intolerance. This was accompanied by reduced IRS-1 expression and impaired Akt activation in liver and skeletal muscle, demonstrating that gestational hypoxia increased susceptibility to high-fat diet–induced insulin signalling defects, rather than these defects being caused by the diet alone. In both murine models and humans, hypoxia has been shown to alter the expression and secretion of inflammation-related adipokines, contributing to the pro-inflammatory environment characteristic of obese AT (Lolmede et al., 2003, Wang et al., 2007, Maenhaut et al., 2010). Hypoxic PVAT not only contributes locally to vascular inflammation and remodelling but also has systemic implications. Increased thoracic PVAT mass has been independently associated with major cardiovascular risk factors, including aortic stiffness, diabetes, coronary artery calcification, and hypertension (Villacorta and Chang, 2015, Chen et al., 2021, Lehman et al., 2010). Moreover, cardiac adiposity increases with obesity, and atherosclerotic plaques tend to localise in coronary arteries surrounded by PVAT. In these regions, coronary PVAT volume has been positively correlated with plaque burden, suggesting a direct pathogenic role (Owen et al., 2014). PVAT in obesity

also plays an active role in modulating vascular disease by responding to atherogenic stimuli and interacting with immune cells, sympathetic nerves, and vascular tissues (Kim et al., 2020). Together, these findings position PVAT hypoxia as a pivotal player in both localised vascular dysfunction and broader cardiometabolic risk.

1.5.4 Molecular and cellular responses to hypoxia in PVAT

Hypoxia in expanding PVAT triggers a range of molecular and cellular changes as the tissue adapts to low oxygen levels. While some responses are initially protective, they can become harmful over time, leading to PVAT dysfunction and contributing to vascular disease. A key player in this process is the hypoxia-inducible factor (HIF) pathway, which alters gene expression, affecting adipokine release, metabolism, and immune cell activity. Hypoxia may also interact with other important pathways, such as sphingolipid signalling, adding further complexity to the response. These complex and interrelated mechanisms are summarized in Figure 1-2, which illustrates how hypoxia in PVAT activates HIF-dependent pathways, reprograms adipocyte function, and promotes vascular inflammation and dysfunction.

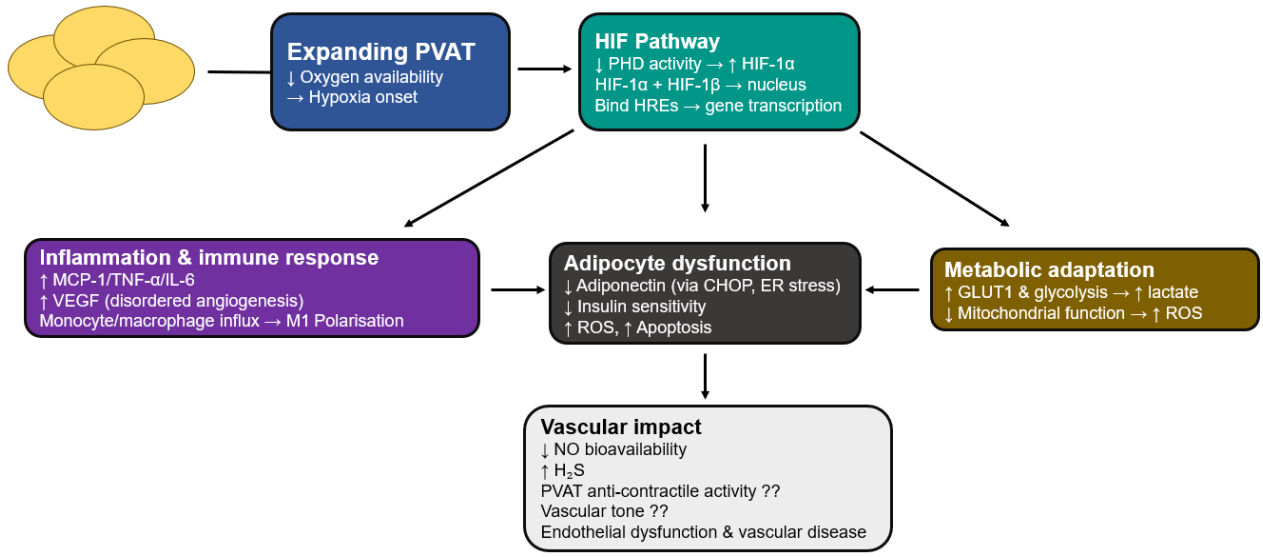

Figure 1-2 Summary of molecular and cellular effects of hypoxia in PVAT.
Hypoxia stabilizes HIF-α, which activates transcription of genes that reprogram metabolism, suppress protective adipokines like adiponectin, and promote inflammation and vascular dysfunction.

1.5.4.1 The HIF pathway: central regulator of the hypoxic response

Hypoxia-inducible factors (HIFs) are the primary transcriptional regulators that coordinate cellular adaptation to low oxygen conditions (Wang and Semenza, 1993, Lefere et al., 2016). The HIF complex is composed of an oxygen-sensitive α-subunit (mainly HIF-1α or HIF-2α) and a constitutively expressed ß-subunit (HIF-1ß, also known as ARNT) (Keith et al., 2012). Under normoxic conditions, proline residues on HIF-α are hydroxylated by prolyl hydroxylase domain (PHD) enzymes, allowing recognition by the von Hippel–Lindau (VHL) protein, which targets HIF-α for ubiquitination and proteasomal degradation (Keith et al., 2012, Lefere et al., 2016, Kaelin Jr, 2002). In hypoxia, PHD activity is suppressed due to their dependence on oxygen, allowing HIF-α to accumulate, translocate to the nucleus, and dimerise with HIF-1ß (Lin et al., 2013, Lefere et al., 2016). The active HIF complex then binds to hypoxia response elements (HREs) in the promoter regions of target genes, initiating transcriptional responses (Orlando et al., 2019, Weidemann and Johnson, 2008).

HIFs actively reprogram cellular functions to adapt to hypoxia but can also drive pathological processes in hypoxic AT. Key target genes include angiogenic factors such as VEGF, which promotes new vessel formation, although this process is often insufficiently regulated in obese AT (He et al., 2011, Engin, 2024). HIFs also enhance metabolic adaptation by inducing glucose transporters like GLUT1 and glycolytic enzymes to support anaerobic ATP production (Hu et al., 2007, Kierans and Taylor, 2021). In addition, HIF-1α promotes the expression of pro-inflammatory and fibrotic genes, thereby contributing to chronic inflammation and fibrosis within AT (Kang et al., 2023, Cifarelli et al., 2020). Although HIF-1α and HIF-2α share structural similarities and can regulate overlapping genes, they also exhibit distinct and sometimes opposing roles depending on cellular context and the duration of hypoxia (Bakleh and Al Haj Zen, 2025). This complex and context-dependent regulatory network is central to the emergence of a dysfunctional PVAT phenotype in obesity.

1.5.4.2 Altered adipokine secretion profile: the impact of hypoxia on PVAT's endocrine function

Hypoxia significantly alters the secretory profile of adipocytes and other resident cells within PVAT, shifting it from a predominantly anti-inflammatory,

vasoprotective state to one that is largely pro-inflammatory and which leads to vascular dysfunction. A key alteration is the suppression of adiponectin, an adipokine with potent anti-inflammatory, insulin-sensitising, and vasoprotective properties (Huynh et al., 2025, Chen et al., 2006). Hypoxic conditions have been shown to reduce adiponectin expression and secretion through multiple mechanisms, including endoplasmic reticulum (ER) stress. Specifically, the ER stress marker CHOP can inhibit adiponectin promoter activity, while hypoxia also destabilises adiponectin mRNA, further reducing its levels (Engin, 2024, Hosogai et al., 2007). This active suppression highlights a direct mechanistic link between PVAT hypoxia and the loss of a critical vascular protector. In contrast, hypoxia promotes the upregulation and release of several pro-inflammatory adipokines and cytokines, such as leptin, IL-6, TNF-α, MCP-1 (CCL2), angiopoietin-like 4 (Angptl4), and VEGF, which together contribute to a pro-inflammatory PVAT microenvironment (Trayhurn, 2013). This dysregulated secretome not only exacerbates local vascular inflammation but also plays a role in systemic low-grade inflammation associated with obesity and metabolic disease.

1.5.4.3 Cellular metabolic reprogramming: adapting to an oxygen-deficient environment

In response to hypoxia, cells within PVAT, including adipocytes, undergo metabolic reprogramming to sustain energy production under oxygen-limited conditions. A central adaptation is the shift from aerobic mitochondrial oxidative phosphorylation to anaerobic glycolysis, primarily mediated by HIF-1, which upregulates glucose transporters such as GLUT1 and key glycolytic enzymes to enhance glucose uptake and glycolytic flux (Kierans and Taylor, 2021). This metabolic shift results in elevated lactate production, a hallmark of anaerobic metabolism (Kierans and Taylor, 2021). However, prolonged hypoxia can impair mitochondrial function, disrupt energy balance, and elevate ROS, contributing to oxidative stress (Adzigbli et al., 2022, Kowalczyk et al., 2021). Concurrently, hypoxia and nutrient imbalance can induce ER stress and activate the unfolded protein response (UPR). Prolonged ER stress contributes to cellular dysfunction, inflammation, and apoptosis (Díaz-Bulnes et al., 2020, Chen et al., 2023b). These metabolic and stress-related adaptations are tightly interconnected, establishing a vicious cycle of dysfunction within hypoxic PVAT that exacerbates its pathogenic role in vascular disease.

1.5.4.4 Impact on immune cell recruitment and activation

The hypoxic microenvironment within AT, particularly in PVAT, contributes to the recruitment and activation of immune cells, increasing the inflammatory state described in Section 1.5.2. Activation of the HIF pathway promotes the expression of chemokines such as MCP-1 which attract monocytes, macrophages, and T lymphocytes into the tissue (Lin et al., 2013, Huynh et al., 2025). Hypoxia also influences immune cell function by promoting pro-inflammatory phenotypes, including macrophage polarisation (Engin, 2024). These recruited immune cells enhance local production of cytokines such as TNF-α and IL-6, along with ROS, which collectively enhance inflammation and oxidative stress within PVAT (Nosalski and Guzik, 2017, Wang et al., 2022b). This ongoing cycle of hypoxia, immune activation, and inflammation not only drives further adipose dysfunction but also disrupts the paracrine environment that regulates vascular tone and homeostasis, ultimately contributing to endothelial dysfunction and vascular disease.

1.5.5 Effect of hypoxia on vascular reactivity in PVAT

Hypoxia, which develops in the heart as a result of ischaemia, is a harmful insult that impairs cardiac function. In the coronary circulation, vasodilatation is a crucial physiological response to hypoxia that improves blood flow and, consequently, oxygenation of the hypoxic or ischaemic myocardium (Hedegaard et al., 2014). In relation to the role of PVAT in vascular function, it is important to highlight that there are conflicting reports on PVAT's response to hypoxia. On one hand, hypoxia is thought to exert a vasodilatory effect in a PVAT-dependent manner. For instance, Donovan et al. (2018) argue that PVAT enhances hypoxia-induced relaxation in porcine coronary arteries via a mechanism involving H_2S. Similarly, Maenhaut et al. (2010) reported that hypoxia, induced by bubbling with 95% N_2 and 5% CO_2 for 30 minutes, enhanced the vasorelaxant response of norepinephrine-precontracted thoracic aorta segments from male Swiss mice with intact PVAT, while this response was markedly reduced in PVAT-denuded vessels.

In contrast, other studies indicate that hypoxia may impair PVAT function. Badran et al. (2019) observed that gestational intermittent hypoxia caused a loss of anti-contractile activity of PVAT in abdominal aortic arteries from male offspring. This

dysfunction was rescued by exogenous application of adiponectin that was likely due to reduced adiponectin secretion under hypoxia (Chen et al., 2006). Moreover, PVAT in rat mesenteric arteries exposed to a hypoxic environment ex vivo (2.5 hours, 95% N_2/5% CO_2) demonstrated a loss of anti-contractile activity, which was prevented by the angiotensin-converting enzyme (ACE) inhibitor captopril and the angiotensin receptor blocker (AT1R antagonist; telmisartan) (Rosei et al., 2015), and was restored by incubation with anti-IL-6 or anti-TNF-α antibodies (Greenstein et al., 2009). In wild-type mice, this dysfunction was also rescued by activation of cGMP-dependent protein kinase via atrial natriuretic peptide (ANP) (Withers et al., 2014).

Obesity induces chronic PVAT hypoxia through adipocyte hypertrophy, impaired perfusion and limited angiogenesis, and this obesity-driven hypoxic environment contributes to PVAT dysfunction. Sousa et al. (2019) reported that in the thoracic aorta of obese sedentary male C57BL/6J mice, acetylcholine-induced vasorelaxation was significantly impaired in PVAT-intact compared to PVAT-denuded vessels. This dysfunction was associated with elevated inflammation and oxidative stress, which was attenuated by aerobic exercise training. Furthermore, Zaborska et al. (2016) found that maternal obesity led to the loss of PVAT's anti-contractile function in mesenteric arteries of offspring SD rats, due to reduced NO bioavailability and release of PVCFs. Interestingly, the inhibition of NO synthase using L-NMMA attenuated the anti-contractile effect, while activation of AMPK partially restored PVAT function, even in a NO-independent manner. Similarly, Saxton et al. (2022) showed that in obese mice, PVAT from mesenteric and gracilis arteries loses its anticontractile function; this function is mediated by both endothelial and neuronal NOS, and non-specific NOS activation with histamine restores function in mesenteric but not gracilis PVAT. These studies collectively highlight nitric oxide signalling as a critical mediator of PVAT integrity under hypoxic and metabolic stress.

Additional evidence on the regulatory mechanisms influencing PVAT function under hypoxic conditions is provided by Cui et al. (2023), who showed that chronic intermittent hypobaric hypoxia (CIHH) exerted a protective effect in male SD rats with metabolic syndrome by upregulating adiponectin and reducing inflammatory cytokines in PVAT, thereby improving mesenteric vascular reactivity. Moreover, Pelham et al. (2016) identified vitamin D as a key regulator of PVAT’s response to

hypoxia. In BALB/c mice, vitamin D deficiency activated hypoxia signalling and impaired PVAT's anti-contractile function in mesenteric arteries. Hypoxia further enhanced vasoconstrictor responses to serotonin and angiotensin II. Notably, this dysfunction was prevented by vitamin D supplementation and was less obvious in the thoracic aorta, suggesting vascular bed-specific effects. Altogether, these conflicting findings underscore the complexity of PVAT's role in vascular function under hypoxic conditions and indicate that the effects may vary depending on the specific vascular bed and experimental conditions.

In light of the effects of hypoxia and inflammation on adipose tissue and vascular function, attention has turned to the molecular pathways involved in these changes. One important pathway is the sphingolipid signalling system, especially S1P and the enzymes that produce it, the sphingosine kinases. Hypoxia can influence sphingolipid metabolism and affect S1P signalling, which in turn plays a role in regulating vascular tone and inflammation. The following section will introduce the sphingolipid system and explain how S1P is linked to hypoxia and vascular dysfunction in metabolic conditions.

1.6 Sphingolipid system

Sphingolipids are a structurally diverse class of lipids that function as essential components of eukaryotic plasma membranes and as bioactive molecules involved in critical cellular processes such as cell division, differentiation, signal transduction, and apoptosis (Kraft, 2017, Pralhada Rao et al., 2013). Sphingolipids are characterised by a sphingoid base backbone, predominantly sphingosine in mammals, which forms ceramide upon N-acylation with a fatty acid (Pralhada Rao et al., 2013, Pyne and Pyne, 2000). Ceramide plays a central role in sphingolipid metabolism, acting as both a precursor for complex sphingolipids like sphingomyelin and glycosphingolipids, and as a signalling molecule in various stress-related pathways (Pralhada Rao et al., 2013). The sphingolipid system functions through a range of bioactive metabolites, including ceramide, sphingosine, sphingomyelin, and sphingosine-1-phosphate (S1P). S1P is a particularly important phospholipid-derived metabolite that functions as both an extracellular mediator and an intracellular messenger (Xiao et al., 2023). The structural diversity of sphingolipids, driven by variations in the sphingoid base, acyl chain length, and head group, contributes to their broad functional range

(Issleny et al., 2023). In the context of obesity, adipose tissue expansion can induce hypoxia, which has been associated with increased levels of S1P in the tissue, highlighting the involvement of the sphingolipid system in metabolic dysfunction and inflammation (Samad et al., 2006, Ito et al., 2013).

1.6.1 Sphingosine-1-phosphate (S1P) overview

Sphingosine-1-phosphate is a lysophospholipid metabolite generated through the breakdown of sphingolipids in cell membranes (Cartier and Hla, 2019). It is produced by various cell types, including erythrocytes, endothelial cells, platelets, hepatocytes, neurons and adipocytes (Ito et al., 2013, Venkataraman et al., 2008, Hashimoto et al., 2009, Vu et al., 2017, Phan et al., 2024). S1P acts as a key signalling molecule involved in a range of physiological and pathological processes, including cell proliferation, survival, migration, invasion, angiogenesis, inflammation, immune cell movement, maintenance of vascular barrier function, and regulation of vascular tone (Cartier and Hla, 2019, Brinkmann and Baumruker, 2006, Takuwa et al., 2010, Wang et al., 2023). It also plays established roles in various pathophysiological conditions, including obesity, cancer, osteoporosis, diabetes, and atherosclerosis (Maceyka et al., 2012, Kajita et al., 2024). Because of its important roles in the cardiovascular and immune systems, S1P is being widely studied as both a factor in disease development and a possible target for therapy.

1.6.1.1 Sphingosine-1-phosphate synthesis and degradation

The cellular levels of S1P are meticulously controlled through a dynamic balance between its synthesis and degradation. Sphingosine, the backbone of sphingolipids, is formed by the cleaving of fatty acids from ceramide by the enzyme ceramidase (Spiegel and Milstien, 2011, Maceyka and Spiegel, 2014, Pyne and Pyne, 2011). Subsequently, S1P is synthesised intracellularly by the phosphorylation of sphingosine, by two closely related sphingosine kinases (SKs), illustrated in Figure 1-3 (Pyne and Pyne, 2000, Hannun and Obeid, 2008, Spiegel and Milstien, 2003). The levels of S1P are closely regulated by SphKs and by the enzymes responsible for its degradation in response to environmental alterations and stimulation (Maceyka et al., 2012, Pyne et al., 2016).

The catabolism of S1P is equally important for regulating its bioavailability and signalling activity. Degradation of S1P can be classified as reversible or irreversible. Reversible degradation occurs by dephosphorylation of S1P via S1P phosphatases (S1PP) / lipid phosphate phosphatases (LPPs) that convert it to sphingosine. Thereafter, sphingosine is acylated by ceramide synthase to generate ceramide. Irreversible degradation by S1P lyase enzyme (SPL) generates hexadecenal and phosphoethanolamine (Pyne and Pyne, 2000, Pyne et al., 2009). Ceramide can be produced through several pathways: de novo synthesis via dihydroceramides, the breakdown of glycosphingolipids such as glucosylceramide, hydrolysis of sphingomyelin, and the salvage of sphingosine through reacylation by ceramide synthases (CerS) (Pyne et al., 2016, Strub et al., 2010, Kitatani et al., 2008). De novo synthesis occurs in the endoplasmic reticulum and begins with the condensation of serine and palmitoyl-CoA by serine palmitoyltransferase (SPT), forming 3-ketodihydrosphingosine. This intermediate is reduced to dihydrosphingosine by 3-ketodihydrosphingosine reductase, followed by N-acylation by ceramide synthases (CerS) to generate dihydroceramide. Finally, dihydroceramide is desaturated by dihydroceramide desaturase (DES) to produce ceramide (Pyne and Pyne, 2000). Generally, ceramide and S1P have opposing effects: ceramide promotes antiproliferative processes such as apoptosis, cell cycle arrest, and senescence, while S1P enhances cell survival, motility, and proliferation (Hannun and Obeid, 2008, Pyne et al., 2016). Earlier research introduced the ceramide-sphingosine-S1P rheostat model, which proposes that the balance between these lipids determines cell fate. In this model, ceramide and sphingosine are associated with apoptosis, whereas S1P supports cell survival (Cuvillier et al., 1996, Pyne and Pyne, 2010).

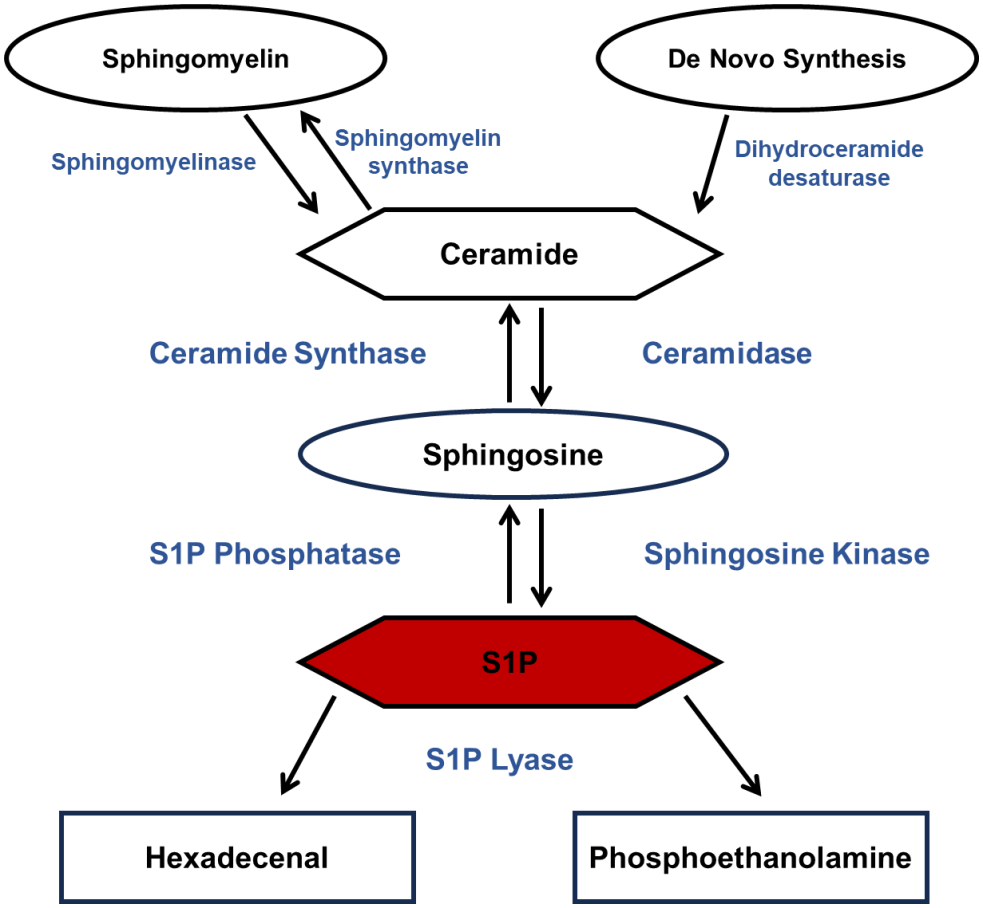

Figure 1-3 The steps of sphingosine-1-phosphate synthesis and degradation.
S1P production begins with the generation of ceramide. Ceramide can be synthesised from sphingomyelin by the sphingomyelinase enzyme or from de novo synthesis. Then, ceramide and sphingosine are interconverted by ceramidase and ceramide synthase. Thereafter, sphingosine and S1P are interconverted by S1P phosphatase and sphingosine kinase. S1P is irreversibly cleaved by the S1P lyase enzyme to produce hexadecenal and phosphoethanolamine.

1.6.1.2 S1P in circulation

S1P is present at high concentrations in the blood and lymph, typically ranging from 0.1 to 0.6 μM in plasma but remains low in interstitial tissues (0.5–75 pmol/mg), forming a concentration gradient critical for lymphocyte trafficking and vascular barrier integrity (Xiong and Hla, 2014, Proia and Hla, 2015, Książek et al., 2015). This gradient is actively maintained through S1P synthesis by producing cells and its degradation by tissue-resident enzymes. Erythrocytes and vascular endothelial cells are the primary sources of circulating S1P under basal conditions, while platelets contribute upon activation due to their high sphingosine kinase 1 (SphK1) activity and absence of S1P-degrading enzymes (Książek et al., 2015, Sah et al., 2020). Additionally, SphK1 contributes significantly to the S1P level in the plasma (Venkataraman et al., 2006). Although erythrocytes have lower SphK1 activity per cell, their abundance and inability to degrade S1P allow for sustained production (Xiong and Hla, 2014). Adipose tissue

is also a contributor to circulating S1P. Plasma S1P levels are elevated in both diet-induced and genetic obesity models in mice, and in obese humans compared to lean controls. In humans, elevated circulating S1P levels correlate with increased body fat percentage, waist circumference, BMI, HbA1c, fasting insulin, insulin resistance (HOMA-IR) and higher total and low-density lipoprotein (LDL) cholesterol levels, indicating its association with adiposity and metabolic dysfunction (Kowalski et al., 2013). In circulation, S1P is stabilised by carrier proteins, mainly high-density lipoprotein (HDL) via apolipoprotein M (ApoM), and to a lesser extent by albumin (Cartier and Hla, 2019). These carriers protect S1P from degradation and facilitate its interaction with receptors, linking S1P dynamics to lipid metabolism, vascular signalling, and immune regulation.

1.6.1.3 S1P transporter

Due to the hydrophilic nature of its phosphate group, S1P cannot passively diffuse across the hydrophobic lipid bilayer of cell membranes (Reitsema et al., 2014). Therefore, the export of intracellularly synthesised S1P into the extracellular space, an essential step for activating S1P receptors in a process termed "inside-out" signalling, requires specific transporter proteins (Spiegel et al., 2019). These transporters serve as key regulators of S1P export, controlling its release and thereby influencing its availability for autocrine and paracrine signalling. Several dedicated S1P transporters have been identified that contribute to the establishment of S1P gradients. Among them, Spinster homolog 2 (SPNS2), a member of the major facilitator superfamily (MFS), is a key exporter in vascular and lymphatic endothelial cells (Spiegel et al., 2019). SPNS2 is essential for maintaining blood and lymph S1P levels and plays critical roles in immune cell trafficking and hearing, as SPNS2 deficiency is associated with lymphopenia and auditory dysfunction (Spiegel et al., 2019, Li et al., 2025b). Moreover, SPNS2 mediates the export of S1P-mimicking FTY720-phosphate (fingolimod-P), underlining its pharmacological relevance (Li et al., 2025b).

Another MFS transporter, MFSD2B, has been identified as the primary S1P exporter in erythrocytes and platelets, the main cellular sources of circulating S1P (Polzin et al., 2023, Vu et al., 2017). In addition to MFS transporters, members of the ATP-binding cassette (ABC) transporter family, such as ABCA1, ABCC1, and ABCG2, also contribute to S1P efflux, particularly in specific cell types or under

pathological conditions (Kotlyarov and Kotlyarova, 2021, Nagahashi et al., 2014). Hypoxia has been shown to induce S1P release from adipocytes through ABCA1 and ABCC1 transporters, and inhibition of ABCA1 with glibenclamide significantly decreases this release, highlighting a functional role for these transporters in modulating extracellular S1P levels under hypoxic conditions (Ito et al., 2013). The expression of these transporters is cell-type specific, with SPNS2 predominantly found in endothelial cells and MFSD2B in red blood cells and platelets. This differential expression allows for spatially regulated S1P export and contributes to the formation of precise extracellular gradients. Such cell-specific control not only supports local and systemic S1P signalling but also highlights these transporters as potential therapeutic targets distinct from S1P receptors or synthetic enzymes.

1.6.1.4 S1P receptors and biological role for S1P

The majority of extracellular actions of S1P are mediated by five high-affinity G protein-coupled receptors (GPCRs), designated $S1P_1$ through $S1P_5$. These receptors, previously referred to as endothelial differentiation gene (EDG) receptors, initiate diverse intracellular signalling cascades upon S1P binding (Yuan et al., 2021, Blaho and Hla, 2014). Each receptor subtype exhibits distinct tissue and cellular expression profiles and couples selectively to heterotrimeric G proteins, enabling S1P signalling to exert context- and cell-specific effects. Among these, $S1P_1$, $S1P_2$, and $S1P_3$ are broadly distributed in cardiovascular, immune, nervous and adipose tissues (Obinata and Hla, 2019, Choi and Chun, 2013, Jun et al., 2006), while $S1P_4$ is predominantly found in lymphoid and hematopoietic cells as well as in airway smooth muscle cells, and $S1P_5$ is expressed in central nervous system oligodendrocytes and natural killer cells (Obinata and Hla, 2012). These receptors couple to different G proteins: $S1P_1$ couples to G_i to activate PI3K/Akt pathway, MAPK/ERK, and Rac, along with PLC activation and Ca^{2+} mobilisation, and inhibition of adenylyl cyclase (Mahajan-Thakur et al., 2017, Gonda et al., 1999, Okamoto et al., 1998), while $S1P_2$ and $S1P_3$ couple to G_i, Gq, and $G_{12/13}$, enabling broader signalling that includes PLC/IP_3/ Ca^{2+} signalling, mitogen-activated protein kinase (MAPK) family pathways (ERK1/2, JNK, and p38), Rho/Rho kinase, and Rac, as well as suppression of cAMP via adenylyl cyclase inhibition (Figure 1-4) (Gonda et al., 1999, Means and Brown, 2009, Skoura and Hla, 2009, Kluk and Hla, 2002).

In addition to endogenous ligands like S1P and dihydro-S1P (Contos et al., 2000), selective pharmacological modulators have been developed to target individual S1P receptor subtypes. SEW2871 selectively activates $S1P_1$ (Pan et al., 2006), CYM5478 is a potent agonist of $S1P_2$ (Herr et al., 2016), and CYM5541 targets $S1P_3$ (Jo et al., 2012). Receptor-specific antagonists include W146 for $S1P_1$ (Sanna et al., 2006), JTE-013 for $S1P_2$ (Parrill et al., 2004), and BML-241 (CAY10444) for $S1P_3$ (Salomone and Waeber, 2011). These modulators have helped to clarify receptor-specific roles and support the development of targeted S1P-based therapies.

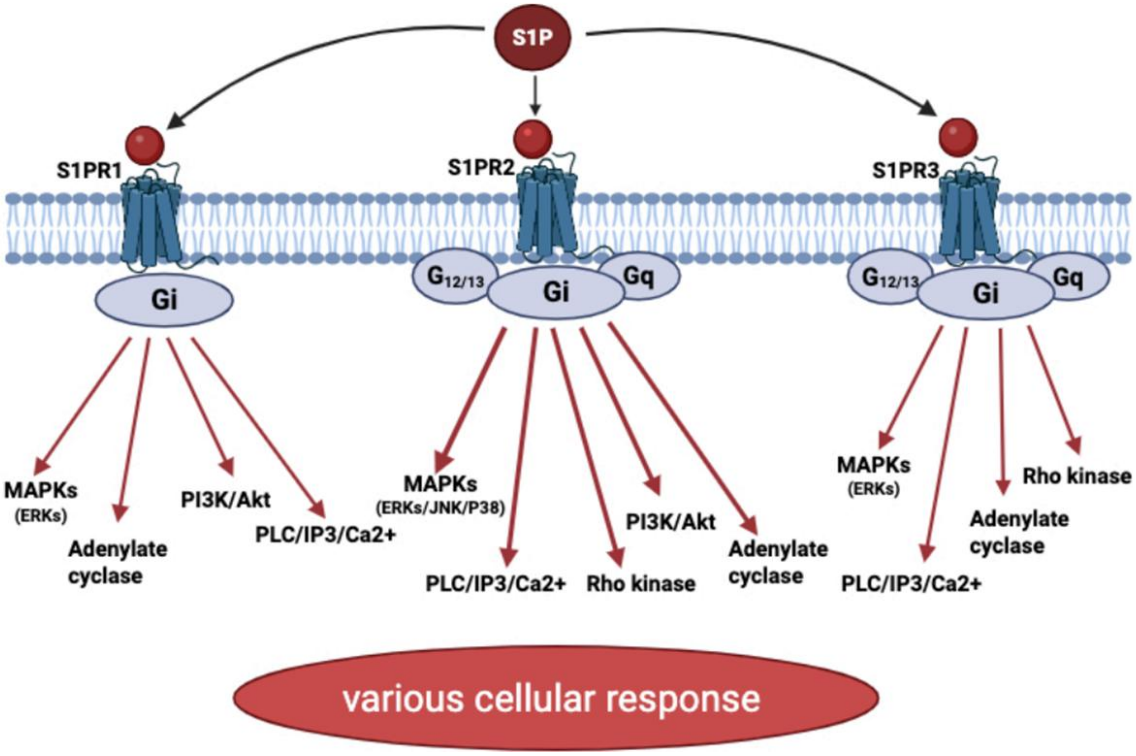

Figure 1-4 S1P–S1PR-mediated signalling pathways.
This figure illustrates the intracellular signalling cascades triggered by sphingosine-1-phosphate (S1P) binding to its receptors $S1P_1$, $S1P_2$, and $S1P_3$. These G protein-coupled receptors activate distinct G proteins (Gi, Gq, and $G_{12}/_{13}$) each of which drives specific downstream pathways. Gi inhibits adenylate cyclase, reducing cAMP levels, and activates PI3K/Akt, ERK/MAPK, PLC/IP_3/Ca^{2+}, and Rac signalling, depending on receptor subtype. Gq stimulates phospholipase C (PLC), leading to IP_3 production and Ca^{2+} mobilisation, and also contributes to MAPK activation. $G_{12}/_{13}$ activates Rho and Rho kinase pathways, regulating cytoskeletal dynamics and contractility. Together, these pathways contribute to diverse cellular responses depending on the receptor subtype and cellular context. Created with BioRender.com.

1.6.1.5 Intracellular signalling role of S1P and regulation of cell biology in health and disease

For two decades, very few studies addressed the receptor-independent, intracellular role for S1P. However, evidence has emerged that S1P plays an important role in regulating several intracellular proteins. For example, S1P

regulates the release of calcium from thapsigargin-sensitive intracellular stores (zu Heringdorf et al., 2003). Additionally, S1P stimulates E3 ligase activity in TNF receptor-associated factor 2 (TRAF2), and it regulates anti-apoptotic, inflammatory and immune processes (Alvarez et al., 2010). Moreover, S1P interacts with Prohibitin 2 (PHB2) to regulate respiration of the mitochondria and cytochrome-c oxidase assembly (Strub et al., 2011). Recent studies have demonstrated that S1P binds to peroxisome proliferator-activated receptor gamma (PPARγ), a transcription factor that regulates neoangiogenesis and this results in upregulation of PPARγ target genes in human endothelial cells (ECs) (Parham et al., 2015). In that study, Parham et al reported that SphK1(-/-) SphK2(+/-) mice showed decreased vascular development, which means that S1P-activation of PPARγ may play a pivotal role in manipulating neovascularisation. Overexpression of PPARγ has also been observed in human cancers, such as prostate, colon and breast cancers (Parham et al., 2015). Moreover, both S1P and PPARγ play a role in regulating the transport of nutrition to cancer cells and mediating the formation of blood vessels in normal and pathological states (Parham et al., 2015).

1.6.2 Sphingosine kinases

S1P is synthesised intracellularly by two isoforms of sphingosine kinase: SphK1 and SphK2. These enzymes play pivotal roles in cellular signalling by regulating the "sphingolipid rheostat" which is the balance between pro-apoptotic lipids, such as ceramide and sphingosine, and the pro-survival lipid S1P (Schulz et al., 2019, Spiegel and Milstien, 2003). This balance is essential for determining cell fate in response to various physiological and pathological stimuli (Pyne et al., 2009). SphK1 and SphK2 are encoded by separate genes, SphK1 on chromosome 17 and SphK2 on chromosome 19 (Cannavo et al., 2017, Liu et al., 2000). Although the isoforms share approximately 80% sequence similarity, they differ significantly in structure, size, and localisation. SphK1a is composed of 384 amino acids, whereas SphK2a consists of 618 amino acids due to the presence of two additional segments at its N-terminal and central regions, resulting in a length difference of about 250 residues (Liu et al., 2000). Both isoforms contain conserved functional domains, designated C1 through C5, which include an ATP-binding site and a sphingosine recognition domain. The catalytic activity resides within domains C1 to C3 (Pitson et al., 2002, Pyne et al., 2009). SphK1 exists in three isoform variants: SphK1a

with a molecular mass of 38 kDa, SphK1b at 39 kDa, and SphK1c at 47 kDa, while SphK2 has two known variants: SphK2a and SphK2b (64 and 80 kDa) (Venkataraman et al., 2006). Both SphK isoforms are ubiquitously expressed in human tissues, with SphK1 showing higher levels in the heart, lung, spleen, and leukocytes, and SphK2 more abundant in the liver and kidney (Liu et al., 2000, Melendez et al., 2000, Hatoum et al., 2017). The subcellular localisation of SphK1 is primarily cytosolic, with the ability to translocate to the plasma membrane in response to stimulation (Hengst et al., 2009). SphK2, in contrast, localises to the nucleus, mitochondria, cytoplasm, and endoplasmic reticulum, with distribution varying by cell line (Cannavo et al., 2017). For example, in HeLa cells, SphK2 is predominantly nuclear, while in HEK293 cells it is mainly cytoplasmic (Hait et al., 2005, Igarashi et al., 2003). Within the nucleus, SphK2-derived S1P regulates gene transcription by inhibiting histone deacetylases (Hait et al., 2009). Functionally, SphK1 is commonly associated with enhanced cell proliferation, survival, and neoplastic transformation (Xia et al., 2000), while SphK2 has been shown to suppress cell growth and promote cell cycle arrest (Okada et al., 2005, Igarashi et al., 2003). However, other studies have indicated that SphK2 may also contribute to cell survival, as siRNA-mediated knockdown of SphK2 has resulted in increased apoptosis and decreased chemoresistance in several cancer cell lines (Sankala et al., 2007).

1.6.2.1 Role and regulation of SphK1

SphK1 is the most extensively studied of the two isoforms of sphingosine kinase due to its central role in promoting cell survival, proliferation, migration, inflammation, and angiogenesis (Bryan et al., 2008). Under basal conditions, SphK1 resides in the cytoplasm. However, upon stimulation by a variety of extracellular signals such as growth factors including PDGF, cytokines including TNF-α and IL-1β, hormones such as oestrogen, GPCR agonists, and hypoxic stress, SphK1 undergoes translocation to the plasma membrane (Bryan et al., 2008, ter Braak et al., 2009, Pitson et al., 2005, Alganga et al., 2019, Gomez-Brouchet et al., 2022, Anelli et al., 2008, Billich et al., 2005). This translocation is often mediated by phosphorylation of serine residue 225 (Ser225) by extracellular signal-regulated kinases 1 and 2 (ERK1/2), which significantly enhances its catalytic activity and facilitates localised production of S1P at the cell periphery (Pitson et al., 2003). At the plasma membrane, SphK1 interacts with regulatory

proteins such as calcium- and integrin-binding protein 1 (CIB1), which promotes its membrane localisation in a calcium-dependent manner (Jarman et al., 2010). Phosphorylation-independent mechanisms, including activation via Gq protein signalling in response to muscarinic receptor or K-Ras stimulation, have also been described (ter Braak et al., 2009, Gault et al., 2012).

Beyond translocation, SphK1 is regulated at the transcriptional and post-transcriptional levels. Several transcription factors, including specificity protein 1 (Sp1), activator protein 1 (AP-1), activator protein 2 (AP-2), HIF2α, the E2F family members E2F1 and E2F7, and LIM domain only protein 2 (LMO2), have been shown to modulate SphK1 gene expression particularly in cancer and in endothelial cells under pathological conditions (Hazar-Rethinam et al., 2015, Bonica et al., 2020, Wang et al., 2020d). Additionally, post-transcriptional regulation is mediated by microRNAs (miRNAs), which are short non-coding RNAs that suppress gene expression by binding to the messenger RNA (mRNA) of target genes. Several miRNAs, including miR-124 in ovarian cancer, miR-506 in hepatocellular carcinoma, miR-3677 in osteosarcoma, and miR-6862 in neural cells, have been identified to negatively regulate SphK1 expression by promoting mRNA degradation or inhibiting translation (Zhang et al., 2013b, Lu et al., 2015, Yao et al., 2020, Xue et al., 2020).

Protein–protein interactions further modulate both the activity and subcellular localisation of SphK1. Several activating interactions have been identified with proteins such as the Src family tyrosine kinases Lyn and Fyn, delta-catenin, eukaryotic elongation factor 1A (eEF1A), TRAF2, and filamin A. These proteins enhance SphK1 activity and facilitate downstream signalling processes (Urtz et al., 2004, Fujita et al., 2004, Leclercq et al., 2008, Xia et al., 2002, Maceyka et al., 2008). In contrast, other proteins including SphK1-interacting protein (SKIP), platelet endothelial cell adhesion molecule-1 (PECAM-1), four-and-a-half LIM domain protein 2 (FHL2), and aminoacylase 1 have been shown to inhibit SphK1 catalytic activity under specific cellular conditions (Lacaná et al., 2002, Fukuda et al., 2004, Sun et al., 2006, Maceyka et al., 2004). The subcellular localisation of SphK1 is also influenced by its interaction with membrane phospholipids. Binding to plasma membrane phospholipids such as phosphatidic acid (PA) and phosphatidylserine (PS) helps anchor SphK1 at the plasma membrane and enhances its activity. This membrane interaction is particularly pronounced

following Ser225 phosphorylation, which induces conformational changes that expose key lipid-binding residues on the enzyme surface (Delon et al., 2004, Stahelin et al., 2005). These complex regulatory mechanisms underscore the importance of SphK1 as a tightly controlled signalling molecule, essential in maintaining cellular homeostasis and frequently utilised in disease states such as cancer.

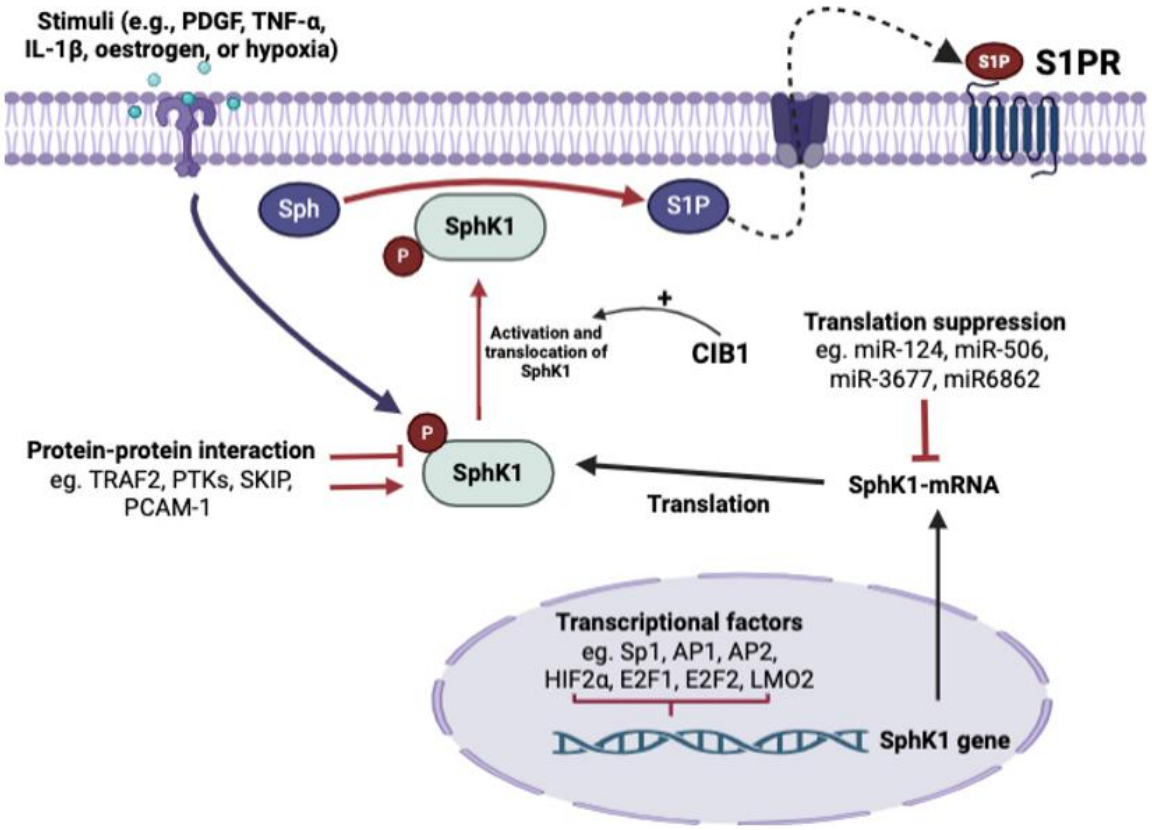

Figure 1-5 Regulatory mechanisms controlling SphK1 expression, stability, and activity. This figure summarises the transcriptional, post-transcriptional, and post-translational mechanisms regulating sphingosine kinase 1 (SphK1). Transcription factors such as Sp1, AP-1, AP-2, HIF-1α, E2F1, E2F2, and LMO2 influence SphK1 gene expression. MicroRNAs including miR-124, miR-506, miR-3677, and miR-6862 suppress translation at the post-transcriptional level. Post-translational control involves phosphorylation and translocation in response to various stimuli, such as platelet-derived growth factor (PDGF), tumour necrosis factor-alpha (TNF-α), interleukin-1β (IL-1β), oestrogen, and hypoxia. CIB1 promotes membrane localisation of SphK1, enabling interaction with regulatory proteins (e.g., TRAF2, PTKs, SKIP, PCAM-1) and access to its substrate sphingosine (Sph), which it converts to sphingosine-1-phosphate (S1P) for receptor-mediated signalling via S1PRs. Created with BioRender.com.

1.6.2.2 SphK2 regulation

SphK2 is regulated in response to a range of extracellular stimuli, including TNF-α, IL-1β, lipopolysaccharide (LPS), epidermal growth factor (EGF), and hypoxia (Mastrandrea et al., 2005, Hait et al., 2005, Weigert et al., 2019, Wacker et al., 2009). Among these, hypoxic conditions have been shown to upregulate SphK2

expression in cerebral microvascular endothelial cells (Wacker et al., 2009). Moreover, in cardiomyocytes, hypoxic preconditioning protects against hypoxia-reoxygenation injury by upregulating SphK2 and activating the focal adhesion kinase (FAK)/Akt signalling pathway (Zhang et al., 2016). At the molecular level, SphK2 is phosphorylated at Ser351 and Thr578 by ERK1/2, which enhances its catalytic activity and supports processes such as EGF-induced cell migration (Hait et al., 2007).

1.6.2.3 Degradation and inhibitors of SphKs

SphKs, particularly SphK1, are regulated not only through transcriptional and post-translational mechanisms but also via targeted degradation, which provides an additional level of control over S1P signalling. DNA-damaging agents such as etoposide, doxorubicin, actinomycin D, and UV irradiation reduce SphK1 protein levels without affecting mRNA expression, suggesting post-translational regulation via degradation pathways, with UV-induced effects shown to involve a p53-dependent mechanism (Taha et al., 2004, Heffernan-Stroud et al., 2012). SphK1 is subject to proteasomal degradation, especially in response to various inhibitors including SKi, N,N-dimethylsphingosine (DMS), FTY720, and PF-543 (McNaughton et al., 2016, Loveridge et al., 2010, Bu et al., 2021). Proteasomal involvement is confirmed by the rescue of SphK1 stability in numerous cells upon treatment with MG-132, a proteasome inhibitor (McNaughton et al., 2016, Loveridge et al., 2010, Tonelli et al., 2010, Alganga et al., 2019). Interestingly, PF-543, a selective and potent SphK1 inhibitor, reduces SphK1 expression and S1P levels through proteasomal degradation and is widely used to study SphK1 function (Alganga et al., 2019, Byun et al., 2013, Yi et al., 2023, Schnute et al., 2012). It has also been shown to reduce SphK1 expression in pulmonary artery smooth muscle cells (PASMC), with MG-132 reversing this effect, further confirming proteasome involvement (Byun et al., 2013). However, PF-543 and VPC9609, another nanomolar-range SphK1 inhibitor, did not significantly inhibit DNA synthesis in PASMC (Byun et al., 2013). In a chronic hypoxia model, PF-543 reduced right ventricular hypertrophy without altering vascular remodelling, and this was linked to decreased cardiomyocyte apoptosis (MacRitchie et al., 2016). SphK1 degradation also occurs via the lysosomal pathway, as evidenced by findings that SKi-induced loss of SphK1 is blocked by chloroquine and CA-074ME, a cathepsin B inhibitor, and by the colocalisation of SphK1 with lysosomes and cathepsin B in

MCF-7 cells (Taha et al., 2006a, Taha et al., 2005, Ren et al., 2010). SphK1b appears more resistant to SKi-induced degradation in some prostate cancer cell lines, possibly due to isoform-specific regulation or compensatory expression (Loveridge et al., 2010). Furthermore, acetylation of Lys27 and Lys29 has been shown to stabilise SphK1 by preventing its ubiquitination, suggesting competitive regulation between acetylation and ubiquitin-mediated degradation (Yu et al., 2012). For SphK2, Selective SphK2 inhibitors such as ABC294640 and (R)-FTY720-Ome (ROME) have been shown to decrease SphK2 expression and S1P production in cancer models (Lim et al., 2011, Watson et al., 2013). Interestingly, ABC294640 also induces proteasomal degradation of SphK1 in prostate cancer cells (McNaughton et al., 2016). While the mechanisms underlying SphK2 degradation are not fully understood, SphK2 can be cleaved by caspase-1 (Weigert et al., 2010) or degraded via non-proteasomal, non-lysosomal mechanisms, particularly in response to ROME (Lim et al., 2011). Overall, SphK inhibitors not only modulate kinase activity but also induce isoform-specific degradation through proteasomal and lysosomal pathways, with important implications for therapeutic strategies, especially in hypoxia-related conditions.

1.6.3 The role of SphKs /S1P in vascular tone

S1P, produced by SphKs, plays a critical role in the regulation of vascular tone. Early studies using isolated mesenteric and intrarenal arteries from male Wistar rats demonstrated that S1P induces vasoconstriction through GPCR activation and elevated intracellular calcium levels (Bischoff et al., 2000). The vascular response to S1P depends on several factors, including receptor distribution, vascular bed, vessel type, species differences and S1P concentration (Michel et al., 2007, Hedemann et al., 2004). Subsequent investigations highlighted that the vascular effects of S1P are mediated via both endothelium-dependent and endothelium-independent mechanisms. In ECs, S1P primarily acts via $S1P_1$ and $S1P_3$ to promote vasodilation (Igarashi and Michel, 2009). This effect happens through activation of the calcium-sensitive and PI3K/Akt pathways leading to eNOS activation and NO production, as demonstrated in rat mesenteric arteries, the human corpus cavernosum (HCC) and the penile artery (di Villa Bianca et al., 2006, Dantas et al., 2003). In rat aortic rings and coronary arteries, S1P also promoted endothelium-dependent vasodilation via $S1P_3$ and eNOS activation (Mair et al., 2010, Alganga et al., 2019, Roviezzo et al., 2006). Moreover, S1P analogue

(FTY720) induced vasodilation in mouse aorta via $S1P_3$ and Akt-dependent eNOS activation (Tölle et al., 2005). Additionally, S1P enhances endothelial barrier function by strengthening intercellular junctions, a process mediated through $S1P_1$, particularly in human pulmonary artery ECs (Singleton et al., 2005, Weigel et al., 2023). This barrier protection is supported by the interaction of S1P with heat shock protein 90 (Hsp90), which facilitates eNOS activation and NO production (Roviezzo et al., 2006, Brouet et al., 2001).

Conversely, S1P can also exert vasoconstrictive effects via its action on VSMCs, which predominantly express $S1P_2$, with lower expression of $S1P_1$ and $S1P_3$ (Alewijnse et al., 2004). S1P-induced VSMC contraction involves multiple mechanisms, including calcium influx through L-type channels, activation of RhoA/Rho-kinase via $G_{12/13}$ signalling, and increased intracellular calcium from sarcoplasmic stores (Bischoff et al., 2000, Hemmings et al., 2006, Coussin et al., 2002). Additional pathways involved in S1P-induced vasoconstriction include the phosphorylation of p38 MAPK and ERK1/2 (Hemmings et al., 2006), as well as store-operated calcium entry (SOCE), which promotes intracellular calcium accumulation (El-Shewy et al., 2018). In SD rat cerebral arteries, S1P-induced vasoconstriction was mediated by both $S1P_2$ and $S1P_3$ through calcium mobilisation and Rho-kinase signalling, while the response in the aorta was less significant due to lower receptor expression (Coussin et al., 2002). S1P-triggered vasoconstriction has also been observed in other species and vascular beds, including porcine pulmonary arteries (Hsiao et al., 2005), hamster gracilis muscle resistance arteries, possibly mediated by increased reactive oxygen species production (Keller et al., 2006) and human placental vessels, where it may occur via Rho-kinase activation (Hemmings et al., 2006). Notably, S1P can have dual effects based on concentration. For example, vasoconstriction in rat mesenteric arteries occurred only at high doses ($>3\times10^{-5}$ M) (Hedemann et al., 2004), while vasodilation is observed at lower, more physiological concentrations (1×10^{-10} to 1×10^{-7} M) (Dantas et al., 2003). Thus, S1P plays a dual role in regulating vascular tone, acting as a vasodilator or vasoconstrictor depending on receptor distribution, cell type, and concentration.

1.6.4 The role of SphKs /S1P in adipose tissue function

A few studies are now being conducted to learn more about SphKs/S1P expression in AT and how it affects cell function. Recent research has revealed that sphingolipids have a detrimental effect on adipocyte metabolism. Solid evidence exists that SphK1 is essential for lipolysis-driven inflammation (Wang et al., 2014). Additionally, SphK1 mRNA expression was induced by isoproterenol, an adrenergic receptor agonist used for studying lipolysis, in both 3T3-L1 adipocytes and mouse gonadal adipose tissue. Moreover, IL-6 production from lipolysis was attenuated by SphK1 depletion (Lambert et al., 2018, Wang et al., 2014). It also has been found that ob/ob mouse subcutaneous adipose tissue expresses more SphK1, but not SphK2, compared to wild type mice (Hashimoto et al., 2009). Furthermore, mice given a high-fat diet exhibited higher levels of SphK1 expression in isolated mature adipocytes and in epididymal adipose tissue than did those fed a low-fat diet (Wang et al., 2014). In subcutaneous adipose tissue in humans, similar results were observed in inflamed compared to less inflamed tissue (Fayyaz et al., 2014). It has also been reported that S1P concentrations are considerably higher in subcutaneous adipose tissue from obese patients compared to lean individuals (Blachnio-Zabielska et al., 2012). Paradoxically however, a study has reported that SphK1 may act as a barrier against increased LPS inflammation in rat WAT. This research has demonstrated that LPS may boost the expression of SphK1 in adipocyte tissue (Tous et al., 2014). In summary, more research is needed to establish the role of the sphingolipid system within not just PVAT but other AT and what its role is in health and disease.

1.6.5 Crosstalk between SphKs /S1P signalling and hypoxia

Hypoxia occurs within fat depots as adipose tissue expands. This adipose tissue hypoxia is not merely a passive consequence of tissue expansion but an active pathophysiological state that can trigger a cascade of cellular and molecular responses, including significant alterations in sphingolipid metabolism. It has been observed that pulmonary vessels constrict in response to hypoxia. Interestingly, it has been reported that in hypoxia-induced pulmonary hypertension SphK2 expression is increased in human arterial pulmonary smooth muscle cells. Additionally, patients with pulmonary arterial hypertension had higher levels of SphK1 expression, while SphK1$^{-/-}$ mice are protected from hypoxia-mediated

pulmonary hypertension (Pyne et al., 2016). Moreover, there has been evidence of hypoxia-induced SphK1 transcriptional upregulation in a variety of cell types, including endothelial cells, renal carcinoma, and brain cancer (Pulkoski-Gross and Obeid, 2018). In response to oxygen levels, there is a proposed feedback circuit between hypoxia-inducible factors and SphK1/S1P (Salama et al., 2015, Bouquerel et al., 2016). Hypoxia (provoked by cobalt chloride or oxygen deprivation) elevated the expression of SphK1, HIF1α, and HIF2α in glioma cells and SphK1 expression was lowered when HIF2α was knocked down (Anelli et al., 2008). In addition, it was shown that treatment with SphK inhibitors or S1P receptor antagonists inhibited increases in the concentration of the HIF1α induced by hypoxia (Sanagawa et al., 2016). S1P produced in response to hypoxia promotes the expression of plasminogen activator inhibitor-1(PAI-1) in mouse 3T3-L1 adipocytes (Ito et al., 2013) and in HepG2 cells through HIF1α (Sanagawa et al., 2016). PAI-1, the physiological inhibitor of fibrinolysis in circulation, is markedly enhanced in adipose tissues of obese mice and people. It has been demonstrated that S1P binding to S1P2 receptors in an autocrine or paracrine manner can be enhanced by hypoxia in obese adipose tissue (Ito et al., 2013).

In ischaemia and hypoxia, promoting the SphK/S1P pathway also lengthens the survival of cardiomyocytes. For instance, administration of exogenous S1P during hypoxia increases the lifespan of neonatal rat cardiomyocytes (Karliner et al., 2001, Karliner, 2013). It has also been discovered that compared to wild type controls during hypoxia, ventricular cardiomyocytes with the SphK1 gene deleted had an increase in cytochrome c release and cell death (Tao et al., 2007). S1P also was found to have an important role in vascular function during hypoxia. An example of this is the study carried out by Alganga et al. (2019) in which they reported a vasodilation response of rat aortic rings after a brief period of hypoxia. This effect was due to a rise in SphK1 expression in endothelium, which also enhances the vasorelaxation impact of S1P via activation of $S1P_3$ receptors. In conclusion, the induction of vasodilation by hypoxia, whether directly on the vascular beds or indirectly via the paracrine action of PVAT, is still contentious and requires further research.

1.6.6 Interplay between the sphingolipid signalling system and adiponectin

The interaction between adiponectin signalling and the sphingolipid system forms a crucial axis in regulating cellular metabolism, membrane composition, and survival. Adiponectin, through its receptors AdipoR1 and AdipoR2, exhibits intrinsic ceramidase activity that degrades ceramide into sphingosine, which is subsequently phosphorylated by SphKs to produce S1P (Holland et al., 2010, Sharma and Holland, 2017). Activation of AdipoR1 and AdipoR2 also stimulates the production of sphingosine and S1P, leading to improved metabolic outcomes, including enhanced insulin sensitivity, reduced inflammation, and activation of AMPK (Bikman and Summers, 2011). Overexpression of either receptor isoform reduces hepatic ceramide levels and enhances ceramidase activity (Tao et al., 2014). Furthermore, S1P produced through AdipoR1/2 signalling activates downstream transcriptional regulators, including sterol regulatory element-binding protein 1 (SREBP1) and PPARγ, particularly via S1P3 activation, leading to increased expression of stearoyl-CoA desaturase (SCD). This promotes the synthesis of monounsaturated fatty acids, which are essential for maintaining membrane lipid fluidity and homeostasis (Ruiz et al., 2022). In differentiated C2C12 myotubes, globular adiponectin treatment enhances both the expression and phosphorylation of SphK1 and SphK2 and increases $S1P_4$ mRNA expression (Bernacchioni et al., 2022). Inhibition of SphK1 and SphK2 using PF543 and ABC294640, respectively, significantly impairs adiponectin-induced improvements in mitochondrial oxidative metabolism and electrophysiological responses in skeletal muscle (Bernacchioni et al., 2022). Additionally, adiponectin promotes the extracellular release of S1P, which binds to surface S1P receptors and protects cells from palmitate-induced oxidative stress and apoptosis (Botta et al., 2020). Notably, S1P signalling also regulates adiponectin expression. Treatment of 3T3-L1 preadipocytes with S1P inhibits adipocyte differentiation and lipid accumulation, accompanied by downregulation of key transcriptional factors including PPARγ and C/EBPα, as well as reduced adiponectin expression (Moon et al., 2014). Conversely, pharmacological or genetic inhibition of $S1P_2$ promotes adipogenesis, lipid accumulation, and upregulation of these transcriptional factors, along with increased adiponectin expression (Moon et al., 2015, Jeong et al., 2015). Supporting this, deletion of SphK1 in obese mice reduces pro-inflammatory cytokines and increases anti-inflammatory mediators, including the

cytokine IL-10 and the adipokine adiponectin, in epicardial adipose tissue (Wang et al., 2014). Importantly, in the absence of both AdipoR1 and AdipoR2, ceramidase activity is severely reduced, resulting in ceramide accumulation and increased susceptibility to lipotoxic cell death (Holland et al., 2010). Although this axis has been studied in skeletal muscle, liver, and adipocytes, the interplay between adiponectin and sphingolipid signalling in the context of blood vessels and PVAT remains to be fully elucidated.

1.7 Hypothesis and Aim

Hypoxia is a hallmark of expanding adipose depots and acutely modulates PVAT signalling. I hypothesise that acute hypoxia reprograms PVAT and adipocyte secretory and signalling pathways, particularly adiponectin and the SphK1/S1P axis. In systemic vessels, PVAT will augment hypoxia-induced vasorelaxation, while specific receptor pathways, $ß_3$-adrenoceptor and AdipoR1, and S1P and $S1P_2$, will differentially modulate this response depending on PVAT presence and endothelial integrity.

Thus, the principal research aim of this thesis was to define how acute hypoxia remodels adipocyte and PVAT signalling and how this controls vascular reactivity in rat thoracic aorta and mesenteric arteries. This was achieved through the following experimental aims:

1. To determine the effects of hypoxia on phenylephrine-induced contraction and cromakalim-induced relaxation in rat thoracic aorta and mesenteric arteries with and without PVAT and endothelium, and to compare pre-exposure to hypoxia with acute hypoxia applied to constricted arteries.

2. To test whether adiponectin signalling contributes to hypoxic vasorelaxation by defining acute hypoxia effects on adiponectin protein, mRNA and release in 3T3-L1 adipocytes and in thoracic versus mesenteric PVAT, and by pharmacologically modulating $ß_3$-adrenoceptors and AdipoR1 during hypoxia in thoracic aorta.

3. To investigate whether hypoxia regulates the SphK/S1P pathway in adipocytes and PVAT by measuring SphK1 and SphK2 mRNA, SphK1 phosphorylation and abundance, and S1P levels and release, and to assess how exogenous S1P or selective $S1P_2$ activation influence hypoxia-induced relaxation.

Chapter 2 - Materials and Methods

Materials

2.1 Animals

All animal experiments were conducted in accordance with United Kingdom Home Office Legislation under the Animals (Scientific Procedures) Act 1986 and under project licence PP1756142, held by Professor Simon Kennedy. All procedures on the licence have been reviewed and approved by the local Animal Welfare and Ethical Review Body (AWERB). Male Sprague-Dawley (SD) rats, weighing between 180–210g, were acquired from ENVIGO (UK) and housed in the Central Research Facility (CRF) at the University of Glasgow. The animals were maintained under controlled conditions, including a 12-hour light-dark cycle and a stable room temperature of 21°C, with free access to food and water. Animals were fed a standard maintenance chow diet (RM1, Rat and Mouse No.1 Maintenance, Special Diets Services), composed of wheat, barley, wheatfeed, de-hulled extracted toasted soya, soya protein concentrate, macro minerals, soya oil, whey powder, amino acids, vitamins, and micro minerals. The calculated approximate analysis of RM1 is : moisture 10.0%, crude protein 14.38%, crude oil 2.71%, crude fibre 4.65%, ash 6.0%, and nitrogen-free extract 61.73%, with metabolisable energy of 10.74 MJ/kg. All animals were humanely euthanised using an approved Schedule 1 method before any experimental procedures were conducted.

2.2 Materials and chemicals

A list of the materials and chemicals used, along with their suppliers, is provided in Table 2-1.

Table 2-1 Materials and chemicals by supplier

Supplier	Materials & chemicals (catalogue number)
Tocris Bioscience, Bristol, UK	▪ Sphingosine 1 Phosphate (1370) ▪ Troglitazone (3114) ▪ CL 316243 disodium salt (1499)
Cayman Chemical, USA	▪ CYM 5478 (29024)
Sigma-Aldrich (Merck Life Science UK Ltd, Gillingham, Dorset, UK)	▪ Cobalt (II) chloride hexahydrate (C8661) ▪ PF543 (PZ0234) ▪ Bovine Serum Albumin Fraction V, heat shock 250g (3116956001) ▪ Bovine Serum Albumin (BSA) (PB1600-100)

	▪ Phenylephrine (P6126) ▪ Lactate Dehydrogenase Activity Assay Kit (MAK066) ▪ 3-Isobutyl-1-methylxanthine (IBMX) (I5879) ▪ Dexamethasone (D4902) ▪ Acetylcholine (A6625) ▪ Tween-20 (P2287-MKBQ9465V) ▪ Porcine Insulin (I5523) ▪ Cromakalim (C1055-10MG) ▪ Cycloheximide (239763) ▪ CA-074 Me (205531) ▪ Protran® Premium Western blotting membranes, nitrocellulose, pore size 0.2 µM, roll W × L 300 mm × 4 m (GE10600004) ▪ Corning tissue culture T75/T150 flasks ▪ 10 cm diameter dishes
Pall Corporation, Portsmouth, UK	▪ Transfer Membrane, BioTrace™ NT, Nitrocellulose, Pore Size: 0.2 µm, Rolls, 300×3000 (66485)
Thermo Fisher Scientific, UK	▪ Pierce™ BCA Protein Assay Kits (23227) ▪ RIPA Lysis and Extraction Buffer (89900) ▪ Halt™ Protease and Phosphatase Inhibitor Cocktail (100X) (78440) ▪ Ammonium persulfate, 99+%, for molecular biology, DNAse, RNAse, and Protease free (327085000) ▪ Taqman® Fast Advance Master Mix (4444557) ▪ High-Capacity cDNA Reverse Transcription Kit (4368814) ▪ Taqman® Universal Master Mix II (4440040)
Bio-Techne Ltd./R&D Systems, Abingdon, Oxfordshire, UK	▪ Rat Total Adiponectin/Acrp30 Quantikine ELISA Kit (RRP300) ▪ Proteome Profiler Rat Adipokine Array Kit (ARY016)
Stratech, Ely, Cambridgeshire, UK	▪ Adiponectin blocking peptide (GTX31718-PEP-GTX 50 ul), Manufacturer: GeneTex ▪ MG-132 (A2585-APE), Manufacturer: Apexbio
Invitrogen (GIBCO Life Technologies Ltd), Paisley, UK	▪ NuPAGE™ LDS Sample Buffer (4X) (NP0007) ▪ Trypsin (T4049-844169) ▪ Foetal calf serum (FCS) (EU origin) ▪ Foetal calf serum (FCS) (USA origin) ▪ Phosphate Buffered Saline (PBS) (14190144)

	▪ Dulbecco's Modified Eagles Media (DMEM), high glucose (11965092) ▪ Penicillin/Streptomycin (15140-122) ▪ Newborn calf serum (NCS)
Clinisciences, France/UK	▪ Rat Sphingosine 1 Phosphate (S1P) ELISA Kit (MBS1600586-96), Manufacturer: MyBioSource
Enzo Life Sciences, Exeter, UK	▪ Blocking peptide for Adiponectin receptor 1 pAb (ALX-210-645 ALX-151-045 100UL) ▪ Lactacystin (BML-PI104-0200)
LI-COR, Biosciences, Lincoln, NE, USA	▪ REVERT Total Protein Stain (926-11010)
New England Biolabs Inc, Hitchin, UK	▪ Blue Prestained Protein Standard, Broad Range (11-250 kDa) (P7719S)
Qiagen Ltd, Manchester, UK	▪ RNeasy Lipid Tissue Mini Kit (74804) ▪ RNeasy Mini Kit (74104)
Severn Biotech Ltd, Kidderminster, Hereford, UK	▪ Acrylamide:Bisacrylamide (37.5:1; 30% (w/v) Acrylamide) (20-2100-10)
VWR International Ltd, Leicestershire, UK	▪ Falcon tissue culture 6/12 well plates ▪ Falcon tissue culture 10 cm diameter dishes

2.3 List of specialist equipment and suppliers

A list of the equipment used, along with the respective suppliers, is provided in Table 2-2.

Table 2-2 Equipment and supplier

Supplier	Equipment
LI-COR Biotechnology, USA	▪ Odyssey Sa Infrared Imaging System and Software
Thermo Scientific, Thermo Fisher Scientific, Waltham, MA, USA	▪ Multiskan™ FC Microplate Photometer ▪ Nanodrop spectrophotometer
Bio-Rad Laboratories Ltd, UK	▪ Mini Trans-Blot Electrophoretic Transfer Cell + Power pack
BMG Labtech, Ortenberg, Germany	▪ FLUORstar OPTIMA Microplate Reader
Danish Myo Technology, Aarhus, Denmark	▪ Nanodrop spectrophotometer

ADInstruments, Oxford, UK	▪ LabChart™ 8 Pro software
Applied Biosystems, Thermo Fisher Scientific, Waltham, MA, USA	▪ QuantStudio™ 12K Flex Real-Time PCR System
Billups-Rothenberg, Inc., San Diego, CA, USA	▪ Modular Incubator Chamber

2.4 Standard solutions

A list of the buffers and solutions used is provided in Table 2-3. Unless otherwise specified, all solutions and reagents were prepared using distilled water.

Table 2-3 Buffers and solutions

Name	Composition
RIPA lysis buffer (1X)	50 mM Tris-HCl pH 7.4, 50 mM NaF, 1 mM Na pyrophosphate, 1 mM EGTA, 1 mM EDTA, 150 mM NaCl, 1.0% (v/v) Nonidet P-40 (NP-40), 1% (w/v) sodium deoxycholate, 0.1% (w/v) SDS, 250 mM mannitol, 1 mM DTT, 1 mM benzamidine, 0.1 mM PMSF, 1 mM Na vanadate, 5 µg/mL soybean trypsin inhibitor.
Sodium Dodecyl Sulfate-Polyacrylamide Gel Electrophoresis (SDS-PAGE) Resolving Gel Solution (8–15% Acrylamide)	8–15% (v/v) acrylamide, 0.163–0.408% (v/v) bisacrylamide, 125 mM Tris-HCl (pH 8.8), 0.1% (w/v) SDS, 0.1% (w/v) ammonium persulfate, and 0.05% (v/v) TEMED.
SDS-PAGE Stacking Gel Solution	250 mM Tris-HCl (pH 6.8), 5% (v/v) acrylamide, 0.1% (w/v) SDS, 0.1% (w/v) ammonium persulfate, and 0.05% (v/v) TEMED.
SDS-PAGE Running Buffer	25 mM Tris base, 190 mM glycine, and 0.1% (w/v) SDS.
Transfer Buffer	25 mM Tris base, 192 mM glycine, and 20% (v/v) ethanol.
Tris-Buffered Saline (TBS)	20 mM Tris-HCl (pH 7.5) and 137 mM NaCl.
Tris-Buffered Saline with Tween 20 (TBST)	20 mM Tris-HCl (pH 7.5), 137 mM NaCl, and 0.1% (v/v) Tween 20.

5% Blocking Buffer	Prepared by dissolving 1 g of milk powder in 20 mL of TBST.
Physiological Salt Solution (PSS)	4.7 mM KCl, 1.2 mM $MgSO_4$, 24.9 mM $NaHCO_3$, 1.2 mM KH_2PO_4, 2.5 mM $CaCl_2$, 11.1 mM glucose, and 119.0 mM NaCl; pH 7.4.
High Potassium Physiological Salt Solution (KPSS)	62.5 mM KCl, 1.2 mM $MgSO_4$, 24.9 mM $NaHCO_3$, 1.2 mM KH_2PO_4, 2.5 mM $CaCl_2$, and 11.1 mM glucose; pH 7.4.

2.5 Antibodies

Details of the primary and secondary antibodies used in these experiments for Western blotting are presented in Table 2-4 and Table 2-5. All primary antibodies were diluted in TBST with 5% (w/v) bovine serum albumin (BSA) and incubated overnight at 4°C, according to the manufacturer's instructions. Similarly, all secondary antibodies were prepared in TBST with 5% (w/v) BSA and incubated at room temperature for 1 hour with shaking, following the manufacturer's instructions.

Table 2-4 Primary antibodies for immunoblotting

Antibody	Clonality	Host species	Dilution	Manufacturer (product number)
SphK1	Polyclonal	Mouse	1:500	Santa Cruz (sc-365401)
Phospho-SphK1 (Ser225)	Polyclonal	Rabbit	1:1000	ECM Biosciences (SP1641)
Phospho-SphK1 (Ser225)	Polyclonal	Rabbit	1:1000	Proteintech Group, Inc (19561-1-AP)
GAPDH	Polyclonal	Rabbit	1:1000	Invitrogen (PAI-988)
Adiponectin	Monoclonal	Rabbit	1:1000	Cell Signalling Technology (2789)

Table 2-5 Secondary antibodies for immunoblotting

Conjugate	Epitope	Host species	Dilution	Manufacturer (product number)
IRDye® 680CW	Mouse	Donkey	1:10000	LI-COR Biosciences, USA (925-68072)

IRDye® 800CW	Mouse	Donkey	1:10000	LI-COR Biosciences, USA (926-32212)
IRDye® 680CW	Rabbit	Donkey	1:10000	LI-COR Biosciences, USA (926-68073)
IRDye® 800CW	Rabbit	Donkey	1:10000	LI-COR Biosciences, USA (926-32213)

2.6 List of TaqMan probes

The TaqMan probes used for quantitative real-time PCR (qPCR) analysis to assess gene expression levels were obtained from Thermo Fisher Scientific and are presented in Table 2-6.

Table 2-6 TaqMan probes for quantitative real-time PCR (qPCR)

TaqMan probe name(mRNA)	Species	Assay ID	Fluorophore (reporter dye)
Sphingosine kinase 2 (SphK2)	Mouse	Mm00445021_m1	Fluorescein Amidite (FAM)
Sphingosine kinase 1 (SphK1)	Mouse	Mm00448841_g1	FAM
Sphingosine kinase 1 (SphK1)	Rat	Rn00682794_g1	FAM
Adiponectin (Adipoq)	Mouse	Mm04933656_m1	FAM
Adiponectin (Adipoq)	Rat	Rn00595250_m1	FAM
TATA box binding protein (Tbp)	Mouse	Mm01277042_m1	FAM
TATA box binding protein (Tbp)	Rat	Rn01455646_m1	FAM

Methods

2.7 Functional study (Wire Myography)

2.7.1 Vessel preparation and mounting for functional studies

For the preparation of arteries for functional studies, SD rats weighing 180–300 g were humanely euthanised either by intraperitoneal administration of pentobarbital (200 mg/mL) or by gradually increasing CO_2 concentration in an enclosed chamber. For logistical reasons, pentobarbital was used only for the initial thoracic aorta experiments described in Section 3.3.2, which included a small number of vessels (n = 1–2 per condition). All subsequent vascular experiments were conducted in rats euthanised by CO_2 overdose. Following euthanasia, either the thoracic aorta or first- or second-order branches of mesenteric arteries (from the ileum) were carefully dissected and immediately placed into cold PSS.

Thoracic aortae were cut into 2–3 mm rings, while mesenteric arteries were cut into 1–2 mm segments, both under a binocular microscope and PVAT was either removed or preserved depending on the experimental design. Thoracic aortic rings were mounted on pins in a four-channel myograph (Figure 2-1), whereas mesenteric rings were mounted in a four-channel wire myograph (Figure 2-2) using two 40 µm diameter, 2 cm long stainless steel wires passed through the vessel lumen and secured between stainless steel jaws. One jaw was connected to a force transducer to measure isometric tension, and the other to an adjustable micrometer for precise control of resting force. Mounted vessels were incubated at 37°C in PSS, continuously gassed with 95% O_2 and 5% CO_2, and allowed to equilibrate at a resting tension of 0 mN for 30 minutes. Arterial rings were then stretched incrementally (~2 mN steps), with each stretch held for approximately 5 minutes until reaching an optimal tension of 9.81 mN, as previously established for rat aorta using similar myographic protocols (Alganga et al., 2019). Mesenteric arteries were normalised using the DMT Normalisation Module in LabChart, following the manufacturer's procedure. Vessels were gradually stretched in small increments (~50 µm) using the micrometer, and passive tension was recorded at each step. The software automatically generated the tension–internal circumference curve and calculated the internal circumference corresponding to

a transmural pressure of 100 mmHg (IC_{100}). Each vessel was then set to 90% of this value (IC_1/IC_{100} = 0.9), which is the recommended setting for rat mesenteric arteries. This ensured that each segment was standardised to its optimal resting tension before experiments. The internal diameter of the mesenteric arteries was calculated from the IC_{100} values. Across all experiments, the mean internal diameter was 304.3 ± 83.5 µm.

To assess vessel viability post-mounting, all arterial segments were stimulated twice with 5 mL pre-warmed (37°C) high potassium physiological salt solution (KPSS, 62.5 mM). Between stimulations, vessels were washed three times with pre-warmed PSS to ensure adequate recovery. This procedure confirmed tissue responsiveness and sensitised the vessels before exposure to pharmacological agents. Thoracic aortic rings were considered viable only if they produced a KPSS-induced contraction of at least 4.90 mN (0.5 g). For mesenteric arteries, only PVAT-intact segments generated contractions greater than 2 mN and were therefore deemed viable. LabChart™ 8 Pro software was used to record and analyse vessel responses to various reagents. All force measurements were initially recorded in milliNewtons (mN). For analysis of concentration–response curves, contractile responses were normalised to the maximal contraction induced by KPSS and expressed as a percentage of KPSS (%KPSS). No length-normalisation (mN/mm) was applied.

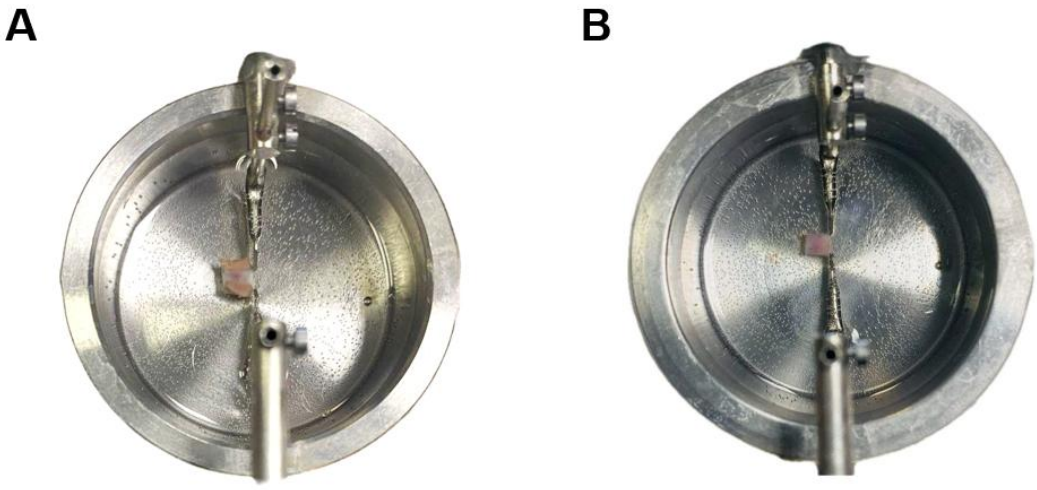

Figure 2-1 Representative images of rat thoracic aortic rings mounted on pins in a myograph. Thoracic aortic segments (2–3 mm) with PVAT (A) and without PVAT (B) were mounted on two pins. One pin was connected to a force transducer linked to a computer for recording changes in vessel tone, while the other was attached to an adjustable micrometer to precisely regulate tension on the arterial ring.

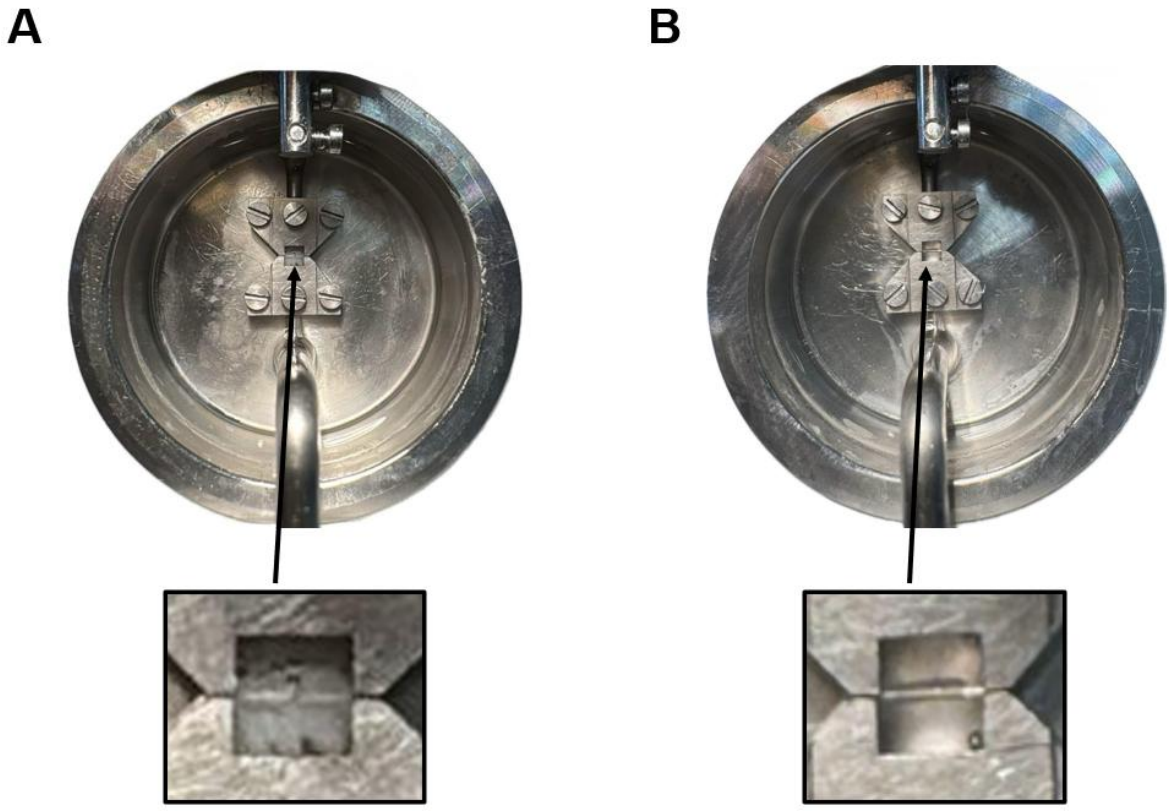

Figure 2-2 Representative images of rat mesenteric arterial rings mounted on a wire myograph. Mesenteric artery segments (1–2 mm) with PVAT (A) and without PVAT (B) were secured on two 40 μm diameter wires. One wire was connected to a force transducer linked to a computer for recording changes in vessel tone, while the other was attached to an adjustable micrometer to precisely regulate tension on the arterial ring.

2.7.2 Testing the viability of the endothelium for vessel functional studies

To test the viability of the endothelium, mesenteric and thoracic arterial rings were precontracted with phenylephrine (PE) at 10 μM for mesenteric arteries and 1 μM for thoracic arteries, until a stable contraction plateau was reached. Endothelial function was then assessed by adding acetylcholine (ACh) at 10 μM for mesenteric arteries and 1 μM for thoracic arteries. A relaxation of ≥ 50% in response to ACh confirmed an intact endothelium, whereas a relaxation of ≤ 20% indicated successful endothelial denudation (Figure 2-3). In some experiments, the endothelium was mechanically removed by gently rubbing the intimal surface with forceps, which was applied to thoracic aorta only. Rings with denuded endothelium were then used to compare vascular responses with those of endothelium-intact segments. For mesenteric arteries, no mechanical removal was required; PVAT-intact rings showed functional endothelial relaxation, whereas PVAT-denuded mesenteric segments did not relax to ACh and were therefore classified as endothelium-denuded.

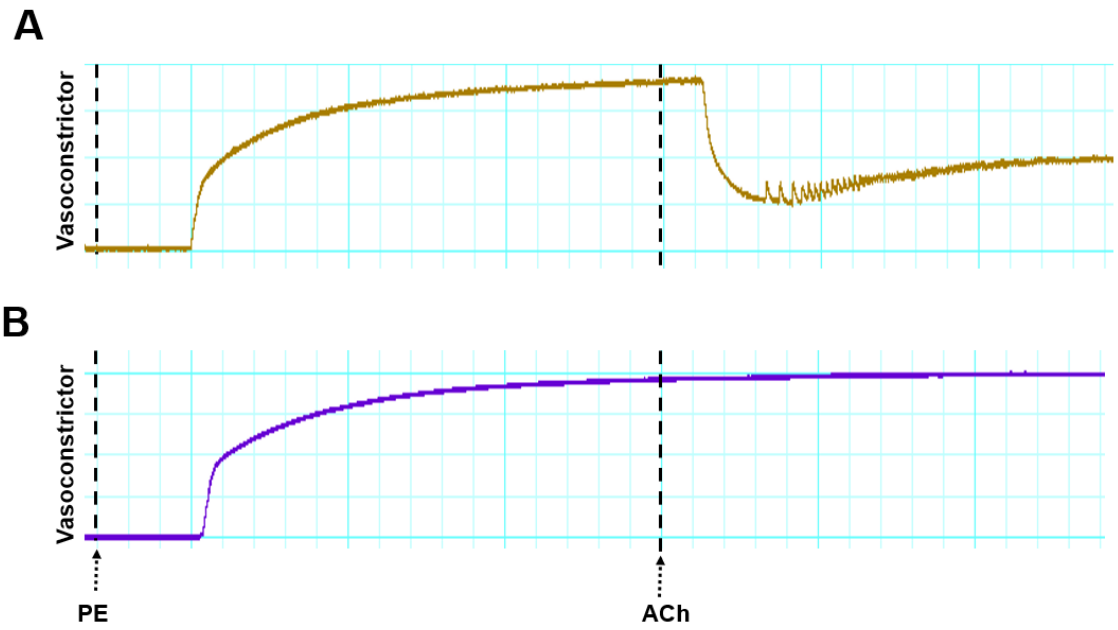

Figure 2-3 Assessing endothelial viability
Vessels were mounted in myograph baths and precontracted with phenylephrine (PE). Once a stable tension was achieved, the endothelium-dependent vasodilator acetylcholine (ACh) was administered. **(A)** Vessels exhibiting ≥50% relaxation in response to ACh were classified as endothelium-intact rings, while **(B)** vessels showing ≤20% relaxation were considered endothelium-denuded rings.

2.7.3 Hypoxia induction protocol

Hypoxia was induced by altering the gas composition used to bubble the myograph chamber, replacing 95% O_2 and 5% CO_2 with 95% N_2 and 5% CO_2 for 30 minutes. In some experiments, the gas mixture was returned to control conditions before conducting dose-response curves for PE and the vasodilator cromakalim (CK).

2.7.3.1 Hypoxia exposure followed by dose-response curves to phenylephrine

To investigate the impact of hypoxia on the contraction response to PE, thoracic aortic and mesenteric rings were subjected to a 30-minute hypoxic period followed by re-oxygenation and maintenance under normoxic conditions. Subsequently, concentration-response curves were constructed by incrementally adding phenylephrine (ranging from 1×10^{-9} M to 3×10^{-5} M), with a 10-minute interval between each addition.

2.7.3.2 Hypoxia exposure followed by dose-response curves to cromakalim

Thoracic aortic rings were pre-contracted using PE (1×10^{-6} M). Once a stable contraction level was achieved, concentration-response curves to the potassium-channel opener cromakalim were generated by gradually adding increasing concentrations (ranging from $1x10^{-9}$ M to $1x10^{-6}$ M) at intervals of 10 minutes. The responses were calculated as the percentage decrease in PE-induced tone.

2.7.3.3 Effect of hypoxia on precontracted vessels

Hypoxia was induced in the organ baths for 30 minutes following pre-contraction with PE. Measurements were recorded during hypoxic conditions, 30 minutes after induction, without re-oxygenation.

2.7.4 Effect of S1P and $S1P_2$ agonist (CYM 5478) on vascular reactivity

To investigate whether S1P is involved in modulating vascular reactivity under hypoxic conditions, vehicle, S1P (10 μM) or the $S1P_2$ agonist CYM 5478 (10 μM) was added to the organ bath containing the vessel precontracted with PE, followed by hypoxia induction for 30 minutes. Measurements were then recorded at the end of the hypoxic period. These concentrations (10 μM) match those previously used

to activate S1P signalling (Moon et al., 2014, Mensah et al., 2017, Wang et al., 2020c).

2.7.5 Effects of β_3-Adrenoceptor agonists and adipoR1B on vascular reactivity

To examine the role of adiponectin in PVAT-induced relaxation under hypoxic conditions, endothelium-intact or denuded thoracic aortic rings, with or without PVAT were precontracted with PE. Adiponectin blocking peptide against adiponectin receptor 1 (AdipoR1B) (5 µg/mL) or β_3-AR agonist (CL-316,243; 10 µM) was then added before inducing hypoxia for 30 minutes. Measurements were recorded at the end of the hypoxic period. The concentrations used for AdipoR1B (5 µg/mL) and CL-316,243 (10 µM) were selected based on previous studies (Almabrouk et al., 2017, Saxton et al., 2018, Weston et al., 2013).

2.8 Cell culture procedures

2.8.1 Recovery of cryopreserved cell stocks from liquid nitrogen

3T3-L1 preadipocytes, a mouse fibroblast cell line originally obtained from the American Type Culture Collection (ATCC, Manassas, VA, USA), were kindly provided by Dr. Ian Salt (School of Molecular Bioscience, University of Glasgow). The cells were stored frozen in cryogenic vials in liquid nitrogen until use. When required, the vials were rapidly thawed by immersion in a 37°C water bath. The thawed cells were then transferred under sterile conditions to a Corning T75 culture flask containing 10 mL of pre-warmed Dulbecco's Modified Eagle's Medium (DMEM) supplemented with 10% (v/v) newborn calf serum (NCS) and 1% (v/v) penicillin/streptomycin. The culture medium had been pre-equilibrated to 37°C in a humidified incubator maintained at 10% (v/v) CO_2. The cells were incubated overnight at 37°C in a humidified atmosphere with 10% (v/v) CO_2. The following day, the medium was aspirated to remove cryoprotective agents and cellular debris, and fresh DMEM was added to provide optimal conditions for cell viability and growth.

2.8.2 Cell culture growth media and passaging 3T3-L1 cells

The preadipocytes were cultured at 37°C in a humidified atmosphere containing 10% (v/v) CO_2 in T75 flasks using DMEM supplemented with 10% (v/v) newborn calf serum (NCS). The culture medium was replenished every two days. When the cells reached approximately 80% confluency, they were routinely passaged. To do so, the cell growth medium was aspirated, and the cells were rinsed with 5 mL of pre-warmed sterile phosphate-buffered saline (PBS). Subsequently, the cells were detached from the flasks by adding 3 mL of sterile trypsin-EDTA solution (0.05% v/v) to each T75 flask and incubating at 37°C for one minute. The trypsin activity was then halted by adding an appropriate volume of DMEM/NCS, and the cell suspension was divided as needed. For experimental purposes, 3T3-L1 preadipocytes were cultured in Falcon 10 cm diameter dishes or Falcon 6 or 12-well plates. For all 3T3-L1 culture experiments, each 'n' value represents an independent vial of cells subjected to the full experimental protocol.

2.8.3 Preparation of 3T3-L1 cells for freezing

The culture medium was aspirated from the T75 flasks, and the cells were detached by adding 3 mL of sterile 0.05% (v/v) trypsin-EDTA per flask. The flasks were then incubated at 37°C for one minute to facilitate cell detachment. To neutralize the trypsin, 7 mL of DMEM was added to each flask before transferring the cell suspension into 15 mL universal tubes. The cells were then pelleted by centrifugation at 350 × g for 5 minutes. After removing the supernatant, the pellets were resuspended in freezing medium, consisting of foetal calf serum (FCS) supplemented with 10% (v/v) dimethyl sulfoxide (DMSO). The cell suspension was then aliquoted into polypropylene cryogenic vials, which were placed in a polycarbonate freezing container and stored at -80°C for 24 hours before being transferred to liquid nitrogen for long-term preservation.

2.8.4 Preparation of 3T3-L1 preadipocyte differentiation medium

To induce the maturation of 3T3-L1 preadipocytes into adipocytes, an adipogenic mixture was prepared. The differentiation medium contained DMEM supplemented with 10% (v/v) fetal calf serum (FCS), 0.5 mM 3-isobutyl-1-methylxanthine (IBMX), 0.25 mM dexamethasone, 1 µg/mL insulin, and 5 µM troglitazone, which

underwent 0.22 µm filter (Millipore® Stericup® Quick Release Vacuum Filtration System) sterilization before use.

2.8.5 3T3-L1 preadipocyte differentiation protocol

3T3-L1 cells were cultured in DMEM supplemented with 10% NCS and antibiotics (100 µg/ml (w/v) penicillin-streptomycin). Upon reaching confluence, typically within two days, the cells were incubated with the differentiation medium. By day 3, the medium was replaced with DMEM containing 10% FCS, 5 µM troglitazone, and 1 µg/ml insulin, which underwent 0.22 µm filter sterilization before use. By day 6, the medium was changed again to DMEM with just 10% FCS and antibiotics, and cells were typically utilised between day 8 and day 12 of the culture period. In this study, the successful differentiation of 3T3-L1 preadipocytes into mature adipocytes was confirmed by observing morphological changes under the microscope. Mature adipocytes typically exhibit a rounded, lipid-laden appearance, in contrast to the spindle-shaped, fibroblast-like form of preadipocytes (Figure 2-4).

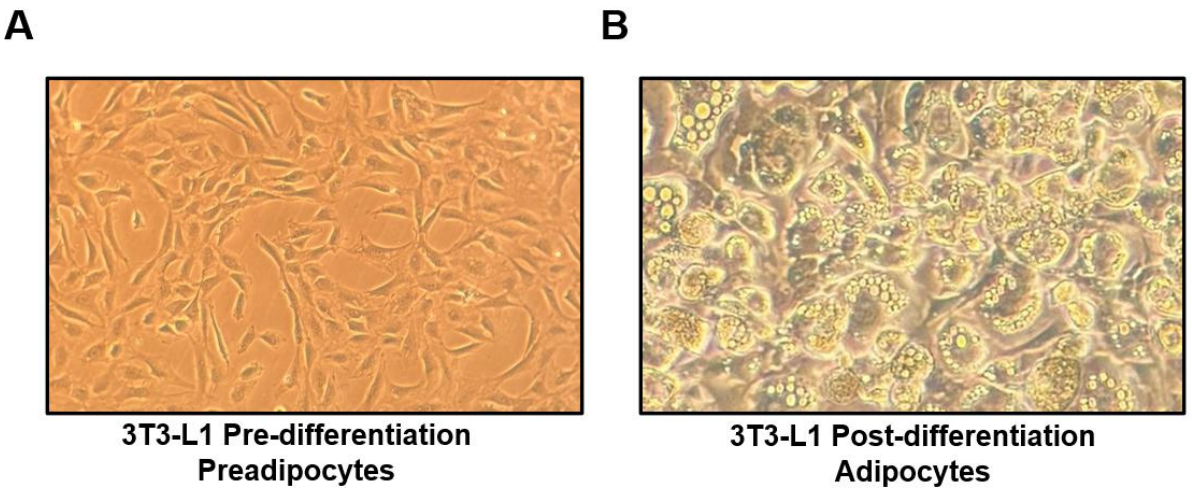

Figure 2-4 Morphological changes in 3T3-L1 cells during adipocyte differentiation
3T3-L1 fibroblasts were differentiated into mature adipocytes as described in the methods. **(A)** Representative image of 3T3-L1 preadipocytes at Day 0, displaying their morphology before differentiation. **(B)** Representative image of fully differentiated 3T3-L1 adipocytes at Day 8, illustrating the morphological changes associated with adipogenesis.

2.8.6 Hypoxia induction protocol for 3T3-L1 adipocytes

Hypoxia was induced in 3T3-L1 adipocytes between day 8 and day 12 post-differentiation using either chemical or physical methods. For chemical hypoxia, cells were serum-starved in serum-free DMEM for 2 hours at 37°C in 10% (v/v) CO_2 before being treated with 200 µM cobalt chloride ($CoCl_2$). $CoCl_2$ acts as a chemical

hypoxia mimetic by stabilising HIF-1α through inhibition of prolyl hydroxylase (PHD) enzymes, thereby preventing HIF-1α degradation and activating hypoxia-responsive cellular pathways even under normoxic oxygen conditions. The $CoCl_2$ concentration (200 μM) was selected based on a previous study showing reliable HIF-1α stabilisation and chemical hypoxia induction in adipocytes (Wang et al., 2007).

For physical hypoxia, a Modular Incubator Chamber (Figure 2-5) was used to create a controlled low-oxygen environment. Cells were serum-starved for 2 hours at 37°C in 10% (v/v) CO_2, then placed inside the chamber. The inlet and outlet ports were connected to a pre-mixed hypoxic gas cylinder (1% O_2, 5% CO_2, balance N_2) via tubing, and a flow meter was used to flush the chamber with the hypoxic gas mixture for 2–5 minutes to ensure complete displacement of ambient air. The chamber was then sealed and incubated at 37°C for different time points, up to a maximum of 6 hours, as for time points beyond this the hypoxic gas mixture would require to be refilled.

Figure 2-5 Modular incubator chamber for hypoxia induction.
The Modular Incubator Chamber was used for physical hypoxia induction in 3T3-L1 adipocytes by creating a controlled low-oxygen environment. The chamber is equipped with a ring clamp to secure the lid tightly, preventing gas leakage and maintaining hypoxic conditions. The gas inlet port is connected to a pre-mixed hypoxia gas cylinder (1% O_2, 5% CO_2, balance N_2), while the gas outlet port ensures controlled gas flow within the chamber. The chamber lid securely encloses the culture plates, allowing stable hypoxic conditions to be maintained.

2.8.7 Preparation of 3T3-L1 cell lysates

Cells were cultured in 6-well plates, differentiated, and between day 8 and day 12, preincubated for 30 minutes at 37°C with either vehicle, S1P (10 μM), MG132 (10 μM), lactacystin (10 μM), CA-074ME (10 μM), a combination of MG132 and CA-074ME, or left untreated as a control. Preincubation was performed in serum-free DMEM. Following this, the medium was removed, and cells were re-incubated with the same treatments in fresh media, either under normoxic or hypoxic conditions, as described in the previously outlined protocol.

After treatment, the culture medium was aspirated, and the cells were rinsed with ice-cold PBS. Subsequently, 150 μL of ice-cold RIPA (Radio-Immunoprecipitation Assay) lysis buffer was added to each well. The cells were then gently scraped on ice and transferred to pre-chilled microcentrifuge tubes. To ensure efficient lysis, the samples were briefly sonicated for 5 seconds, followed by centrifugation at 17,000 × g for 10 minutes at 4°C. Finally, the supernatants were collected and stored at -20°C for future analysis.

2.9 PVAT tissue procedures

2.9.1 PVAT treatment and hypoxia exposure protocol

Mesenteric and thoracic PVAT samples were carefully dissected from male SD rats and weighed. A portion of these samples, weighing approximately 20–30 mg, was preincubated at 37°C for 30 minutes in 500 μL of preoxygenated PSS, composed of: 118 mM NaCl, 4.7 mM KCl, 1.2 mM $MgSO_4$, 25 mM KH_2PO_4, 11 mM glucose, and 2.5 mM $CaCl_2$. The samples were either left untreated (control) or treated with cycloheximide (10 μM), MG132 (10 μM), lactacystin (10 μM), CA-074ME (10 μM), or a combination of MG132 and CA-074ME. The concentrations of cycloheximide, MG132, lactacystin and CA-074ME (all 10 μM) were based on the study by Alganga et al. (2019), who used these doses to investigate protein synthesis and degradation pathways in rat aorta. These pharmacological inhibitors were used to assess whether proteasomal or lysosomal turnover contributes to changes in SphK1 stability under hypoxic conditions. Cycloheximide inhibits new protein synthesis, MG132 and lactacystin inhibit proteasomal degradation, and CA-074ME blocks cathepsin-dependent lysosomal degradation. Combined MG132 and CA-074ME treatment allows simultaneous inhibition of both pathways. This approach was

used to test whether protein synthesis or degradation mechanisms regulate SphK1 stability in PVAT. Following preincubation, the tissues were subjected to either normoxic or hypoxic conditions for 30 minutes. Normoxic conditions were maintained with a 95% O_2 and 5% CO_2 gas mixture, while hypoxic conditions were induced by switching to 95% N_2 and 5% CO_2 for the same duration. After treatment, the tissues were immediately snap-frozen in liquid nitrogen and stored at -80°C for further analysis. Additionally, the conditioned media was collected, rapidly frozen in liquid nitrogen, and stored at -80°C for subsequent experiments.

2.9.2 Preparation of PVAT tissue lysates

Mesenteric and thoracic PVAT samples were retrieved from -80°C storage and transferred to pre-chilled microcentrifuge tubes. The tissues were homogenized in 250 µL of ice-cold RIPA lysis buffer using a battery-operated pestle motor mixer (Sigma-Aldrich, UK). To ensure efficient disruption, the samples underwent sonication for 20 seconds, followed by vortexing and incubation on ice for 15 minutes. The lysates were then centrifuged at 17,000 × g for 10 minutes at 4°C, and the resulting supernatants were collected and stored at -20°C for future use.

2.10 RNA extraction and reverse transcription polymerase chain reaction (RT-PCR)

2.10.1 3T3-L1 cell RNA extraction and purification

Adipocytes cultured in 6-well plates were incubated in serum-free DMEM at 37°C with 10% (v/v) CO_2 for 2 hours before hypoxia induction, which was achieved using either chemical or physical methods. For chemical hypoxia, cells were treated with 200 µM $CoCl_2$ in serum-free DMEM and maintained at 37°C with 10% CO_2 for different time points as specified in the experimental protocol. For physical hypoxia, after 2 hours of serum starvation, cells were placed inside a Modular Incubator Chamber. The chamber was connected to a pre-mixed hypoxic gas cylinder containing 1% O_2, 5% CO_2, and 94% N_2. Once sealed, the chamber was incubated at 37°C for different time points, up to a maximum of 6 hours. Following treatment, the medium was aspirated, and cells were washed twice with ice-cold PBS.

Total RNA extraction was performed using the RNeasy Mini Kit according to the manufacturer's protocol. All steps were carried out at room temperature. Each well was lysed with 350 µL of RNeasy lysis buffer (RLT), and the lysate was collected using a cell scraper. The collected lysate was transferred to a RNeasy Mini spin column and homogenized by centrifugation at maximum speed (17,000 × g) for 2 minutes. An equal volume of 70% (v/v) ethanol was gently mixed into each lysate by pipetting, followed by transfer to separate RNeasy Mini spin columns and centrifugation at maximum speed for 1 minute. After discarding the flow-through, the columns were washed with 700 µL of wash buffer 1 (RW1) and centrifuged at maximum speed for 30 seconds. The flow-through was discarded, and 500 µL of wash buffer (RPE) was added to each column, followed by centrifugation for 30 seconds. This washing step was repeated with an additional 500 µL of buffer RPE, followed by centrifugation for 2 minutes. The columns were then transferred to fresh 2 mL collection tubes and centrifuged for an additional 3 minutes at maximum speed to remove any residual buffer. Finally, the columns were placed into new 1.5 mL collection tubes, and RNA was eluted using 30 µL of RNase-free water by centrifugation at maximum speed for 1 minute. The quality and concentration of the extracted RNA were assessed using a NanoDrop™ 1000 spectrophotometer, measuring absorbance at 260 nm and 280 nm. RNA purity was determined based on the A260/A280 ratio, with all samples falling within the acceptable range of 1.8–2.1. Samples were subsequently stored at −80 °C for future use.

2.10.2 PVAT RNA extraction and purification

Mesenteric and thoracic PVAT samples from male SD rats were carefully dissected and weighed before being immersed in physiological salt solution (PSS) and incubated at 37°C for 30 minutes. Following preincubation, tissues were exposed to either normoxic or hypoxic conditions for 30 minutes. Normoxic conditions were maintained using a gas mixture of 95% O_2 and 5% CO_2, while hypoxic conditions were induced by replacing oxygen with 95% N_2 and 5% CO_2 in a myograph chamber at 37°C. Total RNA was extracted following the Qiagen RNeasy Lipid Tissue Mini Kit protocol. Briefly, PVAT samples were transferred into 2 mL collection tubes containing two stainless steel beads (5 mm in diameter). QIAzol lysis reagent (1 mL) was added, and the tissues were homogenized using a TissueLyser LT (Qiagen) for 5 minutes. The homogenates were then incubated at room temperature (15–

25°C) for 5 minutes before the addition of 200 µL chloroform, followed by vigorous shaking for 15 seconds. After incubation for 2–3 minutes, the tubes were centrifuged at 12,000 × g for 15 minutes at 4°C, leading to the separation into three distinct phases: a clear aqueous phase containing RNA, a white interphase, and a red organic phase. The upper aqueous phase was carefully transferred to a fresh tube and mixed thoroughly with an equal volume of 70% ethanol.

The RNA-containing solution was then loaded onto a RNeasy Mini spin column fitted into a 2 mL collection tube and centrifuged at 8,000 × g for 15 seconds at room temperature. The column membrane was washed by adding 350 µL of Buffer RW1, followed by centrifugation at 8,000 × g for 15 seconds. To remove genomic DNA contamination, 80 µL of DNase I solution was applied directly onto the spin column membrane and left at room temperature for 15 minutes. Another 350 µL of Buffer RW1 was then added and centrifuged under the same conditions. The flow-through was discarded, and the column was washed twice with 500 µL of Buffer RPE, followed by centrifugation at 8,000 × g for 15 seconds, then an additional 2 minutes to ensure complete removal of residual contaminants. To eliminate any residual buffer and ensure column dryness, the RNeasy Mini spin column was transferred to a fresh 2 mL collection tube and centrifuged again. Finally, the column was placed into a new 1.5 mL collection tube, and 30 µL of RNase-free water was applied directly to the membrane to elute the RNA. The elution step was completed by centrifugation at 8,000 × g for 1 minute, producing a highly concentrated RNA sample. The RNA concentration and purity were assessed using a NanoDrop™ 1000 spectrophotometer, and the extracted RNA was stored at −80°C for future analysis.

2.10.3 cDNA generation by polymerase chain reaction (PCR)

To synthesise cDNA, the High-Capacity cDNA Reverse Transcription Kit was used following the manufacturer's protocol. For each 20 µL reaction, 1 µg of DNase I-treated RNA was diluted to 10 µL with RNase-free H_2O in a 0.5 mL PCR reaction tube and kept on ice. The reverse transcription reaction was prepared by adding 2 µL of 10X Reverse Transcriptase buffer, 0.8 µL of 25X dNTP Mix (100 mM), 2 µL of 10X RT random primers, 1 µL of Multiscribe Reverse Transcriptase, and 4.2 µL of RNase-free water to each tube, bringing the final reaction volume to 20 µL. The reaction mixture was vortexed briefly and centrifuged for 15 seconds at 17,000 ×

g, then loaded into a thermal cycler (Eppendorf® Mastercycler®) for reverse transcription. The cycling conditions were set as follows: 25°C for 10 minutes, 37°C for 120 minutes, 85°C for 5 minutes, and 4°C until the tubes were removed from the thermal cycler for storage. The synthesised cDNA was stored at -80°C for long-term preservation.

2.10.4 Quantitative real time-PCR (qPCR)

The mRNA expression of selected genes in adipocytes and PVAT was analysed using TaqMan® probes and TaqMan® PCR Master Mix. In a 384-well PCR plate, each well contained 1 µL of TaqMan® gene-specific probe (Table 2-6), 2 µL of cDNA, 2 µL of Nuclease-free water, and 5 µL of TaqMan® master mix, bringing the total reaction volume to 10 µL per well. The plate was sealed with qPCR transparent plastic adhesive and centrifuged at 2000 × g for 5 minutes.

Real-time PCR was performed using the QuantStudio™ 12K Flex Real-Time PCR System equipped with a 384-Well Block Module (Applied Biosystems™, Thermo Fisher Scientific). The thermal cycling conditions followed a standard qPCR protocol, consisting of an initial denaturation step at 95°C for 10 minutes, followed by 40 cycles of 95°C for 15 seconds and 60°C for 1 minute, and a final step at 55°C for 80 cycles. The mRNA expression levels of SphK1, SphK2, adipoq, and the housekeeping gene TATA binding protein (TBP) were quantified using QuantStudio™ Real-Time PCR Software. To confirm the suitability of TBP as a reference gene, raw Ct values were compared across all experimental conditions (normoxia vs hypoxia). TBP expression was stable with no significant variation between groups, supporting its use as an appropriate housekeeping gene for qPCR normalisation (Figure 2-6). Gene expression was normalised to TBP mRNA levels, and relative quantification was calculated using the $^{\Delta\Delta}$Ct method (Rao et al., 2013).

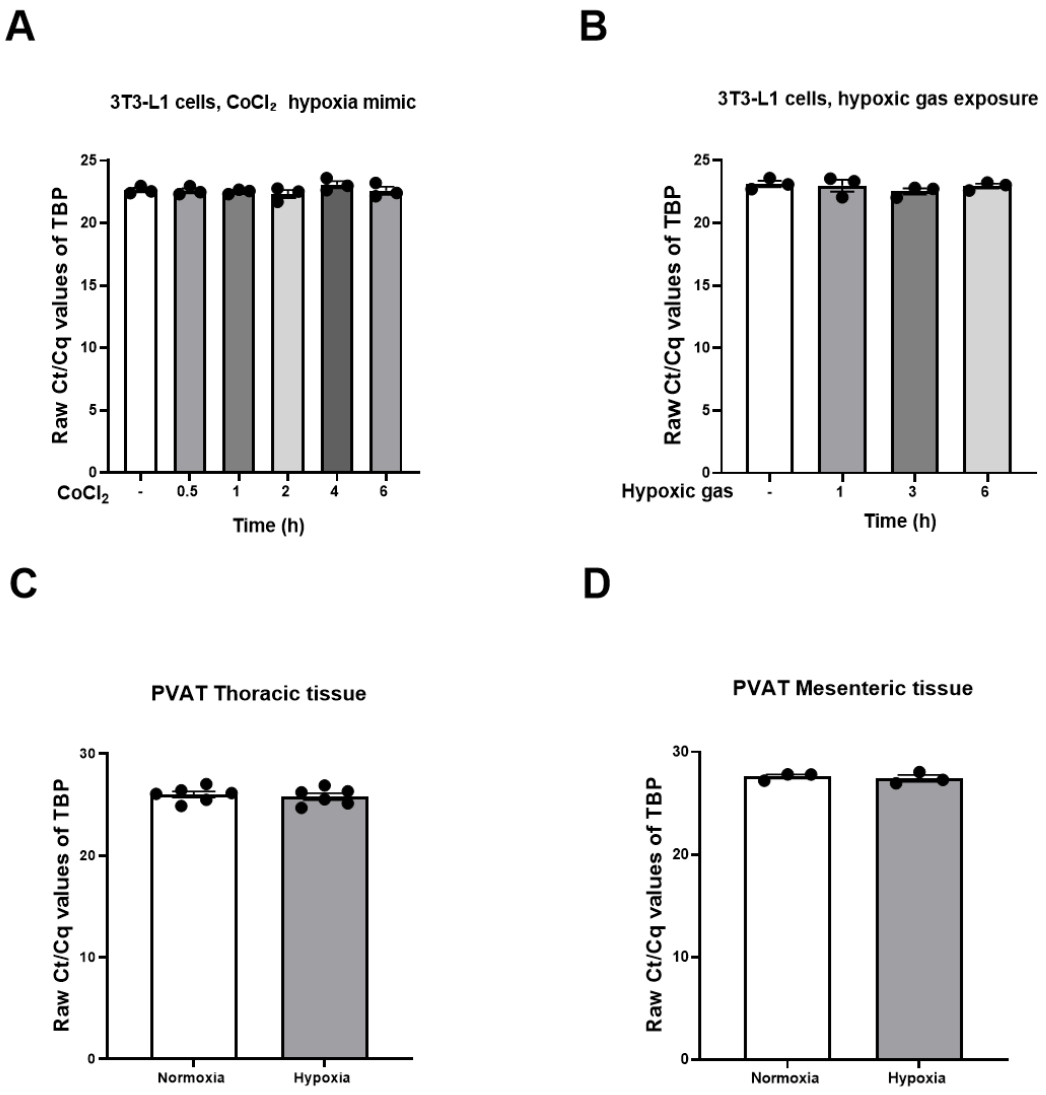

Figure 2-6 Raw Ct values for TBP across experimental groups.
Raw Ct/Cq values for TBP measured in 3T3-L1 adipocytes and PVAT samples under normoxia and hypoxia. **(A)** TBP expression in 3T3-L1 cells exposed to $CoCl_2$ for 0–6 h (n=3). **(B)** TBP expression in 3T3-L1 cells subjected to hypoxic gas exposure for 1, 3, and 6 h (n=3). **(C)** TBP expression in thoracic aorta PVAT tissue under normoxic and hypoxic conditions (n=6). **(D)** TBP expression in mesenteric PVAT tissue under normoxia and hypoxia (n=3). TBP expression remained stable across all conditions, supporting its use as the reference housekeeping gene for ΔΔCt normalisation. Data are presented as mean ± SEM with individual biological replicates shown. Statistical significance was assessed using a one-way ANOVA with Dunnett's post-hoc test for multiple comparisons, and unpaired Student's t-tests were used for pairwise group comparisons.

2.11 Protein analysis

2.11.1 Protein concentration estimation assays

2.11.1.1 Bicinchoninic acid method (BCA)

The bicinchoninic acid (BCA) protein assay was used to determine the protein concentration of 3T3-L1 adipocytes and PVAT lysates. A standard protein calibration curve was generated using BSA dilutions ranging from 0.2 mg/mL to 2

mg/mL, with distilled water as the blank. The assay was performed in a 96-well plate, where 2 µL of lysate (in duplicate) was added to each well and brought to a final volume of 10 µL with distilled water. A working reagent (WR) was freshly prepared using the Pierce™ BCA Protein Assay Kit, by mixing BCA Reagent A with BCA Reagent B in a 50:1 ratio. A volume of 200 µL of WR was added to each well containing either samples or BSA standards. The plate was then covered and incubated at 37°C for 10 minutes. Following incubation, the absorbance was measured at 595 nm using either a FLUOstar OPTIMA Microplate Reader or a Multiskan™ FC Microplate Photometer. The average absorbance of each sample was determined in duplicate, and the protein concentration was quantified by comparison with the BSA standard curve.

2.11.2 SDS–polyacrylamide gel electrophoresis

Protein samples containing 40 µg of total protein were prepared by mixing with 2 µL of 1 mM dithiothreitol (DTT) and 8 µL of NuPAGE® LDS sample buffer (4X), adjusting the final volume to 40 µL. The samples were then heated at 95°C for 5 minutes before being loaded onto the gel.

Proteins were separated by sodium dodecyl sulfate-polyacrylamide gel electrophoresis (SDS–PAGE) based on their molecular weight. The polyacrylamide gels were prepared at either 10% or 12% acrylamide concentration and polymerised before being assembled in a Mini-PROTEAN® Tetra Vertical Electrophoresis Cell. The system was filled with SDS–PAGE running buffer, composed of 190 mM glycine, 25 mM Tris base, and 0.1% (w/v) SDS. Equal amounts of protein lysates, as determined by BCA protein quantification, were loaded into individual wells, along with a pre-stained broad-range protein standard (11–250 kDa) in the first lane for molecular weight reference. Electrophoresis was conducted in two stages: initially at 80 V for 20 minutes to facilitate stacking, followed by an increased voltage of 130–140 V until the tracking dye migrated to the bottom of the gel, typically within 60–75 minutes.

2.11.3 Immunoblotting

Following SDS-PAGE separation, proteins were transferred onto nitrocellulose membranes using a wet transfer method. The gels were carefully removed and

placed on pre-wetted nitrocellulose membranes, ensuring direct contact. Both the gel and membrane were layered between two 3MM Whatman filter papers and transfer sponges, forming a sandwich-like structure (Figure 2-7). This assembly was then positioned within a Bio-Rad Mini-Transblot Cell transfer cassette and submerged in transfer buffer (192 mM glycine, 25 mM Tris base, and 20% (v/v) ethanol). Protein transfer was carried out at 60 V for 135 minutes. Upon completion, the nitrocellulose membranes were removed and placed in Tris-buffered saline (TBS) for further processing.

In some experiments, total protein staining was performed as an internal loading control. Membranes were stained with REVERT™ Total Protein Stain for 5 minutes, followed by three washes with TBS (5 minutes per wash) before imaging. Imaging was performed using a LI-COR instrument, detecting blue-stained proteins in the 700 nm red channel. Protein quantification was carried out using densitometry analysis in Image Studio™ Acquisition Software. Following imaging, membranes were stripped with 0.2 M NaOH for 5 minutes, then washed three times with TBS before proceeding to antibody incubation.

After transfer, membranes were incubated in 5% (w/v) milk powder prepared in TBS for 30–60 minutes at room temperature with continuous shaking to prevent non-specific antibody binding. The membranes were then washed three times with TBS (5 minutes per wash) and incubated overnight at 4°C with primary antibodies (Table 2-4) diluted 1:1000 in TBST (TBS + 0.1% (v/v) Tween-20) supplemented with 5% (w/v) bovine serum albumin (BSA). Two loading-normalisation approaches were used. GAPDH (~37 kDa) was used in one early adiponectin experiment and one early SphK1 experiment in 3T3-L1 adipocytes. However, SphK1 (~34 kDa) and adiponectin (~30 kDa) lie close to the molecular weight of GAPDH, increasing the risk of band overlap or loss of signal when membranes are stripped and re-probed. Consequently, GAPDH was not used for subsequent blots. All later 3T3-L1 Western blots and all PVAT blots were normalised using total-protein staining, which avoids co-migration issues. Following overnight incubation, membranes were washed three times with TBST (5 minutes per wash) and then incubated for 1 hour at room temperature in the dark with IRDye-labelled donkey anti-rabbit or anti-mouse IgG secondary antibodies (Table 2-5). Secondary antibodies were diluted 1:10,000 in TBST supplemented with 5% (w/v) BSA and gently shaken during incubation. After secondary antibody incubation, membranes were washed three times with TBST

(5 minutes per wash) to remove unbound antibodies. The signal was then visualised using the Odyssey Sa Infrared Imaging System, which was operated through Odyssey Sa Infrared Imaging System software. Full-length, uncropped Western blot images with visible molecular weight ladders for each protein analysed are provided in Appendix A.

2.11.4 Stripping of nitrocellulose membranes

Nitrocellulose membranes were incubated in 0.2 M NaOH stripping buffer at room temperature with continuous shaking for 5 minutes. Following incubation, the membranes were washed three times with TBS, each wash lasting 5 minutes.

2.11.5 Densitometric quantification of protein bands

Images acquired using the LI-COR Odyssey® Sa Imaging System were processed in Image Studio™ Acquisition Software (LI-COR Biotechnology, USA). Protein band intensity was analysed using the same software, and quantification was typically expressed as a ratio of phosphorylated to total protein immunoreactivity or normalized against an independent loading control.

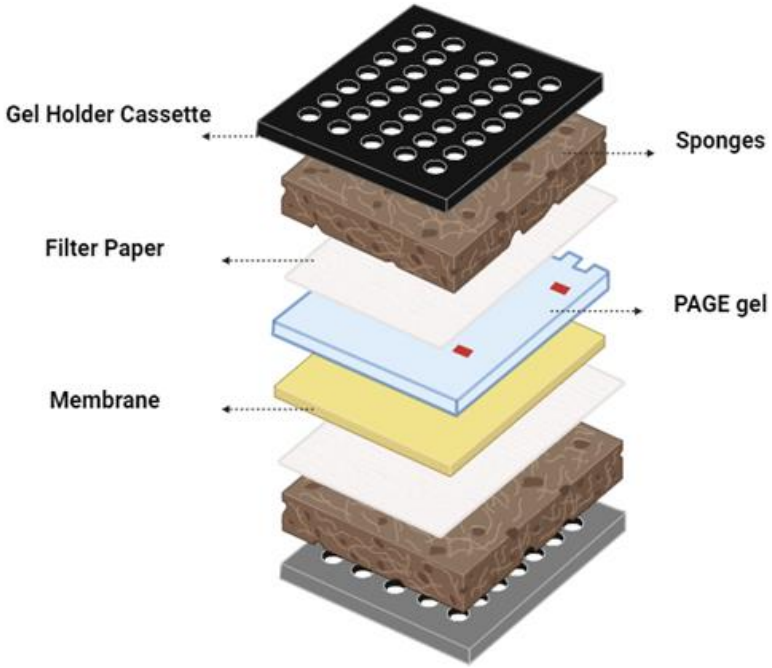

Figure 2-7 Protein transfer process following SDS-PAGE
After SDS-PAGE separation, gels were carefully removed from the plates and placed onto pre-wetted nitrocellulose membranes. Both components were then positioned between two layers of filter paper and transfer sponges, forming a sandwich-like assembly. This structure was inserted into the transfer cassette, ensuring that the gels faced the cathode while the membranes faced the anode to facilitate electrophoretic protein transfer. Illustration created using BioRender.com.

2.12 ELISA, LDH activity, and adipokine array assays

2.12.1 Preparation of PVAT and 3T3-L1 samples for ELISA and LDH assay

3T3-L1 cells were cultured in 6-well plates, differentiated, and at a time point between days 8 and 12, they were preincubated for 30 minutes at 37°C in 1 mL serum-free DMEM under normoxic or hypoxic conditions. Hypoxia was induced across different time points using 200 µM $CoCl_2$ or by exposure to a pre-mixed hypoxic gas mixture (1% O_2, 5% CO_2, balance N_2) in a hypoxia chamber. After treatment, conditioned media was collected, rapidly frozen in liquid nitrogen, and stored at -80°C.

Thoracic and mesenteric PVAT from male SD rats was dissected, weighed, and preincubated at 37°C for 30 minutes in 350 µL of PSS. For S1P ELISA, samples were either left untreated (control) or treated with the SphK1 inhibitor PF543 (100 nM) before exposure to normoxic or hypoxic conditions for 30 minutes. Following treatment, conditioned media was collected and stored at -80°C, while tissues were homogenized in 250 µL of ice-cold RIPA buffer, sonicated for 20 seconds, vortexed, and incubated on ice for 15 minutes. Lysates were then centrifuged at 17,000 × g for 10 minutes at 4°C, and supernatants were stored at -20°C for further analysis.

2.12.2 S1P ELISA protocol

Sphingosine 1-Phosphate (S1P) levels in thoracic and mesenteric PVAT lysates, PVAT conditioned media, and 3T3-L1 adipocyte conditioned media were measured using a sandwich enzyme-linked immunosorbent assay (ELISA) kit, following the manufacturer's protocol. Samples of PVAT and conditioned media were prepared using the method described above. Before analysis, conditioned media and lysate supernatants were centrifuged at 2000–3000 × g for 20 minutes to remove cellular debris, with the supernatants retained for testing.

For the assay, pre-coated ELISA plates containing a rat S1P-specific antibody were used. Serially diluted S1P standards ranging from 1.5 to 48 ng/mL were prepared alongside experimental samples. 50 µL of standard or 40 µL of sample plus 10 µL of anti-S1P antibody was added to each well, followed by 50 µL of Streptavidin-

HRP conjugate. The plate was incubated at 37°C for 60 minutes, then washed five times with wash buffer, allowing each well to soak for 30 seconds to 1 minute per wash. Subsequently, 50 µL of substrate solutions A and B were added, and the plate was incubated at 37°C for 10 minutes in the dark. The reaction was stopped with 50 µL of stop solution, causing an immediate colour change. Optical density (OD) was measured at 450 nm using a Multiskan™ FC Microplate Photometer within 10 minutes. The S1P concentration in each sample was determined by interpolation from a standard curve, with a sensitivity range down to 1.5 ng/mL.

2.12.3 Adiponectin ELISA protocol

Samples of thoracic and mesenteric PVAT and conditioned media were prepared using the method described above. Protein concentrations in these samples were estimated accordingly. Adiponectin concentrations were determined using a Rat Total Adiponectin/Acrp30 Quantikine ELISA Kit (R&D Systems), specifically designed for the quantitative measurement of rat adiponectin concentrations. Standards ranging from 0.156 ng/mL to 10 ng/mL were prepared according to the provided protocol. PVAT lysate samples were diluted 1000-fold with Calibrator Diluent RD5-26 (diluted 1:4) according to the manufacturer's instructions. Conditioned media samples underwent multiple dilution trials until a suitable dilution of 100-fold was identified. Dilutions less than 100-fold resulted in some sample absorbance values exceeding the standard curve limits, hence 100-fold was selected as the optimal dilution.

According to the manufacturer's instructions, 50 µL of Assay Diluent RD1W was added to each well of the pre-coated microplate, followed by 50 µL of standard, appropriately diluted PVAT lysate, or conditioned media samples. The microplate was sealed and incubated for 1 hour at room temperature on a horizontal orbital shaker set at 500 ± 50 rpm. Wells were then aspirated and washed five times with Wash Buffer (400 µL per well). Rat Adiponectin Conjugate (100 µL) was added to each well, and the plate was sealed again and incubated for another hour at room temperature on the shaker. After an additional five washes, 100 µL of Substrate Solution was added to each well, and the microplate was incubated for 30 minutes at room temperature, protected from direct light. The reaction was stopped by adding 100 µL of Stop Solution, and the absorbance was measured within 30 minutes using a Multiskan™ FC Microplate Photometer set at 450 nm with

wavelength correction at 540 nm or 570 nm (Figure 2-8). Mean absorbance values from duplicate wells were calculated, and adiponectin concentrations were determined by comparison to the standard curve generated using the standards provided in the kit.

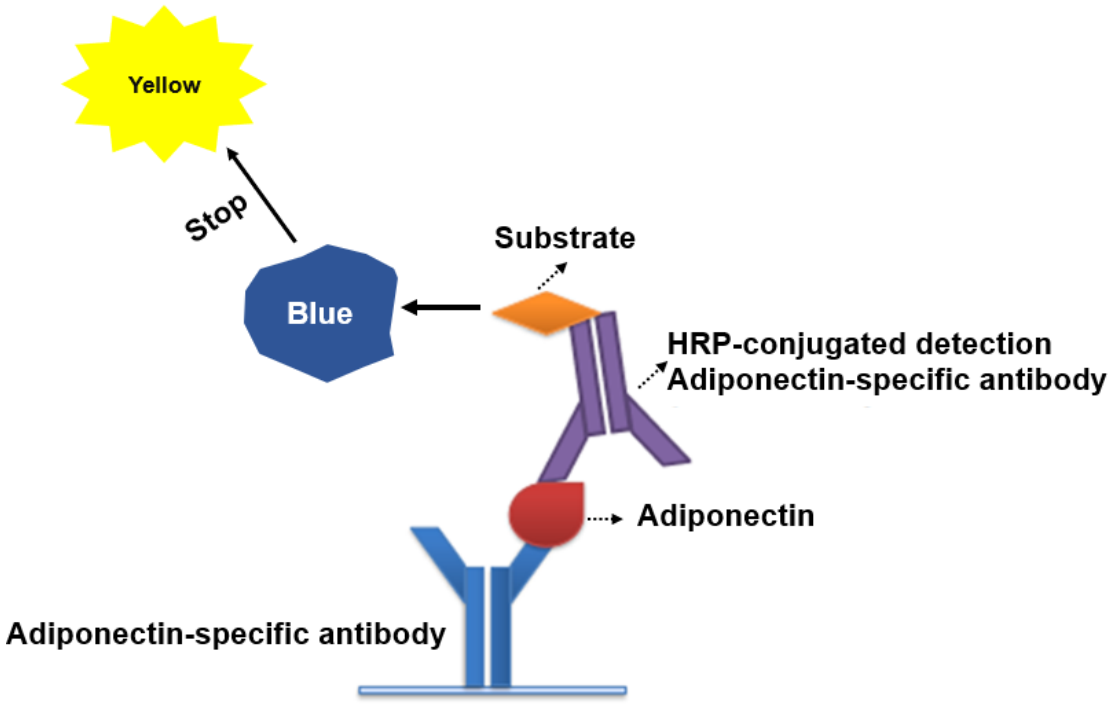

Figure 2-8 Principle of adiponectin ELISA for PVAT conditioned media
The Adiponectin ELISA is based on a sandwich enzyme-linked immunosorbent assay (ELISA) principle. A capture antibody specific to adiponectin is pre-coated onto the ELISA plate, allowing selective binding of adiponectin from thoracic and mesenteric PVAT-conditioned media. After washing, an HRP-conjugated detection antibody is added, which binds to the captured adiponectin. The reaction is then developed using a chromogenic substrate, producing a colour change proportional to the adiponectin concentration, which is quantified by measuring optical density at 450 nm.

2.12.4 Lactate dehydrogenase (LDH) activity assay protocol

LDH activity was determined in conditioned media collected from cultured 3T3-L1 adipocytes and thoracic and mesenteric PVAT using the Lactate Dehydrogenase Activity Assay Kit. Samples of PVAT and 3T3-L1 adipocytes were prepared using the methods described above. After preliminary optimization experiments, appropriate sample volumes and dilutions were identified to ensure absorbance readings fell within the linear detection range of the assay. Specifically, conditioned media from 3T3-L1 adipocytes were used at a final volume of 10 µL per well (5-fold dilution), while thoracic and mesenteric PVAT-conditioned media were used at 5 µL per well (equivalent to a 10-fold dilution).

LDH activity was quantified according to the manufacturer's instructions. Briefly, standards ranging from 0 to 12.5 nM/well NADH were prepared to generate a standard curve. Standards and samples were loaded into clear 96-well plates, and the total volume was adjusted to 50 µL per well using LDH Assay Buffer. Subsequently, a master reaction mix containing 48 µL of LDH Assay Buffer and 2 µL of LDH Substrate Mix per well was freshly prepared and 50 µL was added to each well. Plates were mixed thoroughly using a horizontal shaker. Absorbance was measured immediately (initial reading, $T_{initial}$) at 450 nm using a Multiskan™ FC Microplate Photometer, followed by additional measurements every 5 minutes. The final absorbance measurement (T_{final}) was selected as the last value within the linear range of the standard curve. LDH activity (nmol/min/mL) was calculated from the NADH standard curve provided with the kit. All measurements were performed in duplicate, and average values were reported.

2.12.5 Preparation of thoracic PVAT conditioned media for adipokine array

Thoracic PVAT samples from male SD rats were carefully dissected and weighed, then immersed in 1 mL of preoxygenated PSS within a myograph chamber at 37°C for 30 minutes. After preincubation, tissues were either continuously oxygenated (normoxia) or exposed to hypoxic conditions for 30 minutes. Following treatment, PVAT was collected, and the conditioned media was stored at -80°C.

2.12.6 Rat adipokine array (proteome profiler)

Adipokine profiling was performed using the Rat Adipokine Array Kit, designed to simultaneously detect 30 rat adipokines spotted in duplicate on nitrocellulose membranes. Samples of conditioned media from thoracic PVAT were prepared using the method described above. Briefly, membranes were incubated with the provided blocking buffer (Array Buffer 6) for 1 hour at room temperature on a rocking platform shaker. Then, 1 mL of thoracic PVAT-conditioned media was combined with 0.5 mL of Array Buffer 6 and 15 µL of reconstituted Rat Adipokine Detection Antibody Cocktail and incubated at room temperature for 1 hour. Following aspiration of blocking buffer, the sample/antibody mixture was added to each membrane and incubated overnight at 2–8°C on a rocking shaker.

After incubation, membranes were washed twice using the provided Wash Buffer and incubated with 2 mL of IRDye 800CW Streptavidin (1:2000 dilution in Array Buffer 6) at room temperature for 30 min on a rocking shaker. Membranes were then washed twice more with wash buffer. Fluorescent signals were detected by imaging the membranes using a LiCor Odyssey Imager. The resulting images were analysed using Image Studio software. Signal intensity for each adipokine was quantified and normalised against internal reference control spots included on each array. All measurements were performed in duplicate, and the final normalised values were calculated and analysed using GraphPad Prism 10.0 software (California, USA).

2.13 Statistical analysis

Statistical analyses were conducted using GraphPad Prism 10. Data are presented as mean ± standard error of the mean (SEM), with *n* representing either the number of experiments performed, or the number of rats used. Normality was assessed using the Shapiro–Wilk test. Comparisons between two groups were analysed using an unpaired Student's *t*-test for normally distributed data or the Mann–Whitney U test for non-normally distributed data. For multiple group comparisons, one-way or two-way ANOVA was used for normally distributed data, followed by appropriate post-hoc tests, whereas the Kruskal–Wallis test followed by Dunn's multiple comparisons test was applied for non-normally distributed data. For concentration–response curves, a two-way ANOVA with post-hoc testing was applied. In all cases, statistical significance was set at $p < 0.05$.

Chapter 3 Vascular Responses to Hypoxia: Influence of PVAT and Endothelium in the Rat Thoracic Aorta and Mesenteric Arteries

3.1 Introduction

A key modulator of vascular function within the systemic circulation is perivascular adipose tissue (PVAT), a metabolically active adipose layer that surrounds most systemic blood vessels, excluding capillaries, cerebral vessels, and those of the pulmonary circulation, and exerts significant paracrine and vasocrine influence on vascular tone (Hillock-Watling and Gotlieb, 2022, Queiroz and Sena, 2024). PVAT exhibits distinct depot-specific phenotypes determined by anatomical location. In rodents, thoracic PVAT resembles brown adipose tissue (BAT), characterised by thermogenic activity and relative resistance to inflammation, whereas mesenteric and abdominal PVAT more resemble white adipose tissue (WAT), displaying lower thermogenic capacity and greater susceptibility to inflammatory activation (Padilla et al., 2013, Gálvez-Prieto et al., 2008, Cinti, 2011). These phenotypic differences are associated with increased risk of vascular pathologies, as WAT-like abdominal PVAT depots are more strongly linked to the development of aortic aneurysms and atherosclerosis than thoracic vessels (Padilla et al., 2013, Yap et al., 2021).

PVAT contributes to vascular homeostasis by secreting various vasoactive molecules collectively referred to as PVAT-derived relaxing factors (PVRFs), such as adiponectin and nitric oxide (NO). These factors act on both vascular smooth muscle cells (VSMCs) and endothelial cells to promote vasodilation and suppress contraction (Soltis and Cassis, 1991, Löhn et al., 2002, Gil-Ortega et al., 2010, Victorio et al., 2016, Almabrouk et al., 2017, Fésüs et al., 2007). The critical interaction between PVAT and endothelium in maintaining vascular tone has been demonstrated in a study showing that PVAT-induced relaxation required endothelial integrity and was mediated through NO and Ca^{2+}-activated potassium channels (Gao et al., 2007). Supporting this, Tan et al. (2004) reported that circulating adiponectin correlated with endothelium-dependent vasodilation in humans and directly enhanced NO production in endothelial cells. Moreover, PVAT-mediated regulation of vascular tone varies not only across different vascular beds but also within distinct regions of the same vessel. For example, thoracic aortic PVAT in mice significantly attenuates phenylephrine-induced vasoconstriction compared to abdominal aortic PVAT. This difference is associated with higher eNOS expression and NO bioavailability in the thoracic region (Hwej et al., 2024, Victorio et al., 2016). In addition to its anticontractile actions, PVAT

can also release PVAT-derived contracting factors (PVCFs) including angiotensin II, superoxide (O_2^-), catecholamines and leptin. These factors contribute to vascular homeostasis and modulate the local PVAT microenvironment (Ramirez et al., 2017, Meyer et al., 2013). Therefore, the net impact of PVAT on vascular reactivity represents a dynamic equilibrium between relaxing and contracting mediators.

Obesity significantly dysregulates adipokine secretion and synthesis within adipose tissue (AT), leading to a chronic inflammatory state (Maenhaut et al., 2010). As obesity progresses, AT expands primarily through two mechanisms: hypertrophy (increased adipocyte size) and hyperplasia (increased adipocyte number) (Jo et al., 2009). Increased thoracic PVAT mass has been independently associated with major cardiovascular risk factors, including aortic stiffness, diabetes, coronary artery calcification, and hypertension (Villacorta and Chang, 2015, Chen et al., 2021, Lehman et al., 2010). Furthermore, PVAT in obesity plays an active role in modulating vascular disease by responding to atherogenic stimuli and interacting with immune cells, sympathetic nerves, and adjacent vascular tissues (Kim et al., 2020). These morphological changes are often accompanied by inadequate neovascularization and limited oxygen diffusion, particularly in hypertrophic adipocytes, resulting in local tissue hypoxia (Trayhurn, 2013, Bolinder et al., 2000, Sun et al., 2011, Trayhurn and Wood, 2004). Hypoxia activates hypoxia-inducible factors (HIFs), especially HIF-1α, which in turn promotes the expression of pro-inflammatory cytokines, angiogenic factors, and fibrotic genes within AT (Kang et al., 2023, Cifarelli et al., 2020, He et al., 2011).

Hypoxia exerts complex effects on vascular reactivity, and these effects are both vessel-specific and context-dependent. Systemic arteries generally dilate under hypoxia to enhance tissue perfusion via metabolites like adenosine, NO, and HIF activation (Böger and Hannemann, 2020, Hannemann and Böger, 2022). In contrast, pulmonary arteries constrict to redirect blood flow towards well-oxygenated lung areas, driven by mitochondrial oxygen sensing and redox signalling that inhibit potassium channels, causing depolarization and calcium influx (Waypa and Schumacker, 2010). Notably, pulmonary vessels lack PVAT, which plays an important modulatory role in systemic vessels. PVAT also plays a key role in modulating vascular responses to hypoxia. However, this interaction remains poorly explored, highlighting the novelty and significance of current

research in this area. Existing data suggest that PVAT may enhance hypoxia-induced vasorelaxation in aortic vessels via the release of ADRFs, including hydrogen sulphide (H_2S), or through mechanisms involving ATP-sensitive potassium channels, independent of NO and endothelium (Donovan et al., 2018, Maenhaut et al., 2010). Conversely, other evidence shows that hypoxia impairs PVAT's anti-contractile function, particularly in mesenteric arteries under conditions of obesity or metabolic stress, due to inflammation, oxidative stress, and reduced NO bioavailability (Greenstein et al., 2009, Zaborska et al., 2016). Similarly, Badran et al. (2019) observed that gestational intermittent hypoxia led to a loss of PVAT-mediated relaxation in abdominal aortic arteries of male offspring. Sousa et al. (2019) further demonstrated that in the thoracic aorta of obese sedentary mice, acetylcholine-induced vasorelaxation was more impaired in PVAT-intact than in PVAT-denuded vessels. These findings underscore the dual and context-specific role of PVAT in hypoxic vascular environments.

The thoracic aorta and mesenteric arteries exhibit distinct anatomical and functional properties that influence their vascular responses. The thoracic aorta, as a large elastic conduit, is rich in elastin and functions to buffer pulsatile pressure waves from the left ventricle, while mesenteric arteries are smaller muscular resistance vessels with a higher smooth muscle-to-elastin ratio, allowing them to tightly regulate regional perfusion and systemic vascular resistance (Leloup et al., 2015). These structural differences are accompanied by functional disparities in endothelial activity. For instance, the thoracic aorta exhibits higher basal NO release than mesenteric arteries, contributing to greater tonic suppression of smooth muscle contraction (Leloup et al., 2015). Notably, PVAT surrounding these vessels also differs in its regulatory influence on vascular tone, which is further modulated under hypoxic conditions. In BALB/c mice, hypoxia has been shown to augment vasoconstrictive responses in mesenteric arteries, while having minimal or no effect on contractility in the thoracic aorta (Pelham et al., 2016). The interaction between hypoxia, PVAT phenotype, and vascular reactivity remains complex and incompletely understood.

Although the impact of hypoxia on vascular function has been previously studied, the modulatory role of PVAT under hypoxic conditions remains poorly defined, particularly across different vascular beds and in relation to endothelial status. Importantly, the timing and context of hypoxia exposure, whether through pre-

exposure before pharmacological induction of contraction, or acute application during an established vasoconstriction, may distinctly influence vascular responses. However, this aspect has received limited investigation.

3.2 Aims

- To investigate the effects of hypoxia on the contractile response of rat thoracic aorta and mesenteric arteries to phenylephrine (PE), in rings with and without PVAT and endothelium.
- To assess the relaxation response of thoracic aorta to cromakalim (CK) following precontraction with PE, under normoxic and hypoxic conditions.
- To determine how acute hypoxia, applied during PE-induced contraction, alters vascular tone in the presence or absence of PVAT and endothelium.

3.3 Results

To explore how hypoxia and PVAT interact to modulate arterial tone, a series of functional experiments was conducted using wire myography on thoracic aorta and mesenteric artery segments isolated from male Sprague-Dawley (SD) rats. The contractile responses of endothelium-intact (E+) and endothelium-denuded (E–) arterial rings, both with and without PVAT, were assessed following stimulation with phenylephrine (PE) under normoxic and hypoxic conditions. Hypoxia was induced by bubbling the chambers with 95% N_2/5% CO_2 for 30 min (see Section 2.7.3). PE dose–response curves were run after re-oxygenation with 95% O_2/5% CO_2 (see 2.7.3.1). After re-oxygenation, rings were precontracted with PE, and CK dose–response curves were also obtained (see 2.7.3.2). In a separate protocol, acute hypoxia was applied for 30 min after PE precontraction and responses were recorded during hypoxia, without re-oxygenation (see 2.7.3.3). Endothelial integrity/removal was verified by the presence or absence of ACh–induced relaxation after PE precontraction, as discussed in Section 2.7.2 (Figure 2-3). Throughout the Results chapters, ‘control’ refers to the relevant reference group for each experiment, as stated in the corresponding text or figure legend. In some experiments this refers to untreated normoxic samples, whereas in others it refers to the baseline treatment condition (e.g., hypoxia only). No separate vehicle-only control group was included.

3.3.1 KPSS responses in vessels used in this study

Before examining the effects of hypoxia and pharmacological interventions, KPSS-induced contractions were used to confirm the viability of all vessels. Within each vessel type, KPSS-induced contractions were similar across PVAT(+) and PVAT(–) and across endothelium-intact and -denuded rings (Figure 3-1).

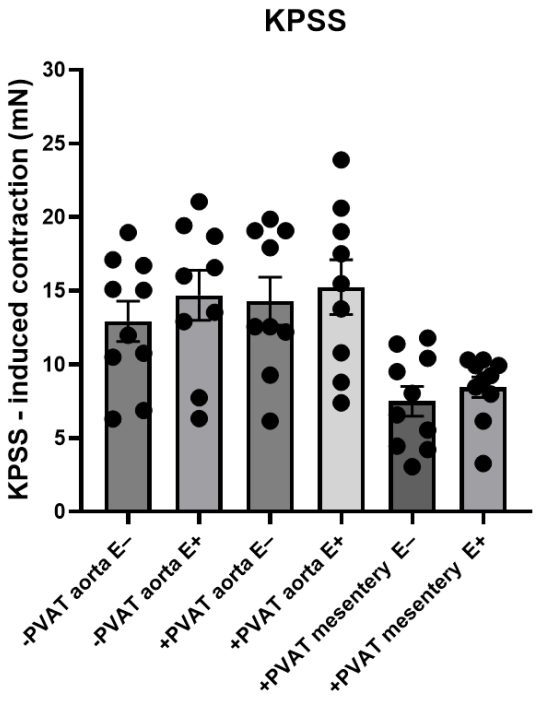

Figure 3-1 KPSS-induced contractions in aortic and mesenteric arteries under different PVAT and endothelial conditions.
Bar chart showing contractile responses to KPSS (62.5 mM) in thoracic aorta (±PVAT, ±endothelium) and mesenteric arteries (±PVAT). Within each vessel type, KPSS responses were consistent irrespective of PVAT or endothelial status. Thoracic and mesenteric KPSS values have not been compared directly. Data are presented as mean ± SEM (n=9–10). Statistical analysis was performed using a one-way ANOVA followed by Tukey's post-hoc test.

3.3.2 Concentration-dependent contractile response of thoracic aorta to PE under normoxia and hypoxia

3.3.2.1 Normoxic conditions

To determine the effects of PE on vascular reactivity under normoxic conditions, concentration–response curves to PE (1×10^{-9} to 3×10^{-5} M) were generated in thoracic aortic rings with intact endothelium (E+) or denuded endothelium (E–), and with or without intact PVAT. The symbols used to represent different experimental groups in the dose–response curves are described in Table 3-1.

Under normoxic conditions, a significant reduction in the magnitude of contraction was observed in E+ rings with intact PVAT (n = 6) compared to E+ rings without PVAT (n = 5; $p < 0.0001$) (Figure 3-2A). In contrast, this anticontractile effect of PVAT was lost in E– rings, with no significant difference detected between rings with or without PVAT ($p = 0.1329$) (Figure 3-2B). Comparison between E+ and E– rings with intact PVAT showed a trend towards a reduced contractile response in E+ rings compared to E– rings; however, this difference did not reach statistical

significance (p = 0.0575; Figure 3-2C). Additionally, in the absence of PVAT, E+ rings exhibited significantly greater contractions to PE compared to E- rings (n = 5; $p < 0.0001$) (Figure 3-2D).

In summary, under normoxic conditions, PVAT significantly reduced PE-induced contractions in the presence of an intact endothelium, while this anticontractile effect was abolished when the endothelium was removed.

Table 3-1 Graphical symbol key used in vascular function dose-response curves

Symbol	PVAT Status	Endothelium	Condition	Line Style
●	PVAT(-)	E+	Normoxia	Solid red line
○	PVAT(-)	E-	Normoxia	Solid red line
■	PVAT(+)	E+	Normoxia	Solid blue line
□	PVAT(+)	E-	Normoxia	Solid blue line
●	PVAT(-)	E+	Hypoxia	Dashed red line
○	PVAT(-)	E-	Hypoxia	Dashed red line
■	PVAT(+)	E+	Hypoxia	Dashed blue line
□	PVAT(+)	E-	Hypoxia	Dashed blue line

Graphical key indicating symbol, colour, and line style representations for PVAT status, endothelium integrity, and oxygen conditions in dose–response figures.

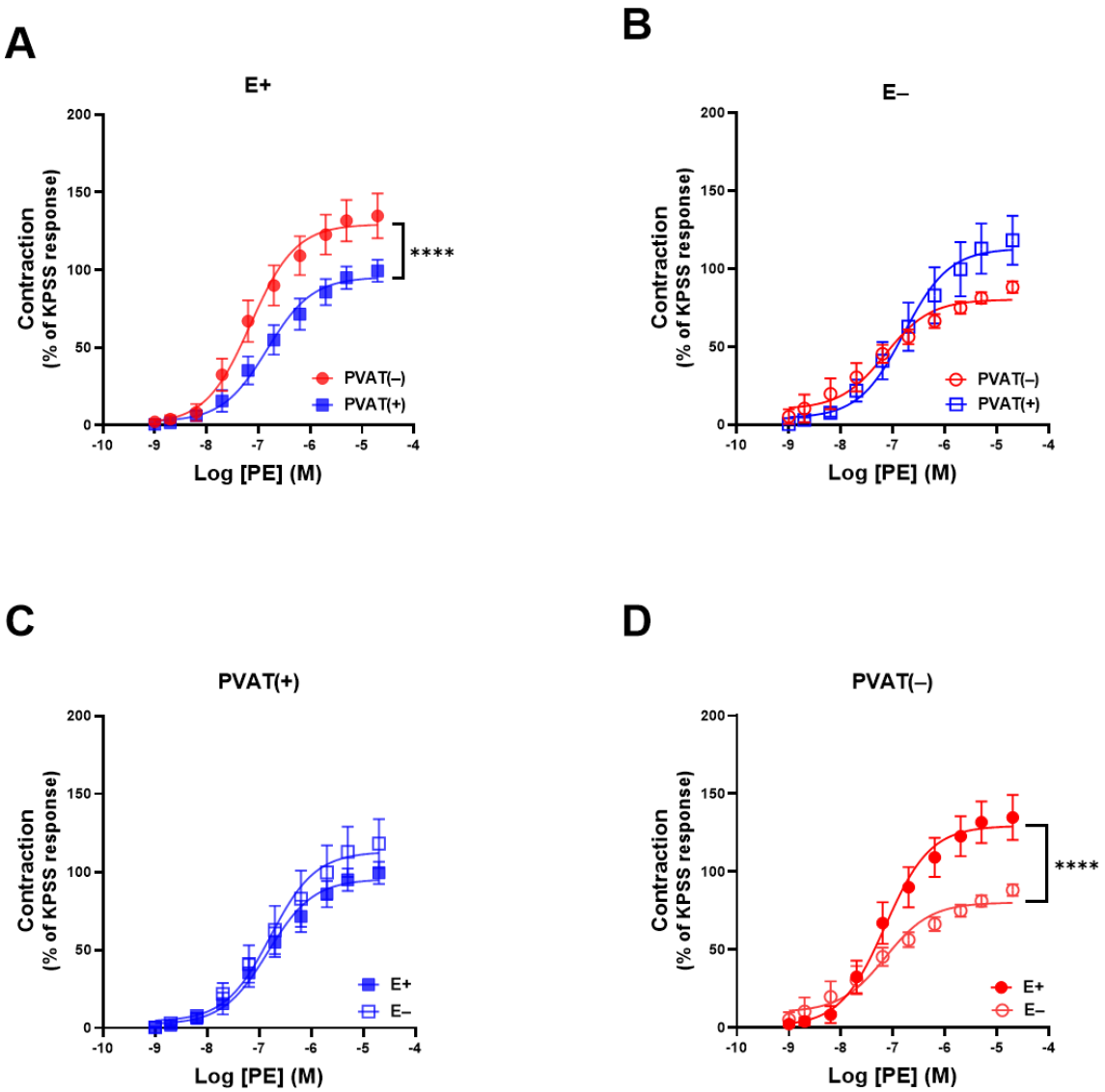

Figure 3-2 Contractile response to PE in rat thoracic aorta under normoxic conditions. Concentration–response curves for the contractile effect of PE (1×10^{-9} to 3×10^{-5} M) were generated in thoracic aortic rings under normoxic conditions. **(A)** Endothelium-intact (E+) aortic rings with PVAT (PVAT+) and without PVAT (PVAT–). **(B)** Endothelium-denuded (E–) aortic rings with PVAT(+) and without PVAT(–). **(C)** Comparison between PVAT(+) rings with E+ and E–. **(D)** Comparison between PVAT(–) rings with E+ and E–. The data are normalised to the maximum contraction induced by KPSS and expressed as mean ± SEM from arteries obtained from different animals. Data are presented as mean ± SEM from six independent experiments for PVAT(+) /E+ and PVAT(+) /E–, and five independent experiments for PVAT(–)/E+ and PVAT(–)/E–. Statistical analysis was performed using two-way ANOVA followed by Bonferroni's multiple comparisons test. Asterisks indicate statistical significance (****$p < 0.0001$).

3.3.2.2 Hypoxic conditions

Thoracic aortic rings were exposed to hypoxia (95% N_2 and 5% CO_2) for 30 minutes, then re-oxygenated (95% O_2/5% CO_2) and maintained under normoxia while concentration–response curves to PE (1×10^{-9} to 3×10^{-5} M) were generated in E+ and E– rings, with and without PVAT. No significant difference was found between E+ rings with PVAT present and absent ($p = 0.0748$) (Figure 3-3A). In E– rings, the presence of PVAT significantly increased contractions to PE compared to rings without PVAT ($p < 0.0001$) (Figure 3-3B). Comparison between PVAT(+) rings with E+ and E– showed a significant increase in contraction in the E– group ($p < 0.001$) (Figure 3-3C). Furthermore, in PVAT(–) rings, no significant difference in contraction was observed between E+ and E– rings ($p = 0.1119$) (Figure 3-3D). In summary, hypoxia abolished the anticontractile effect of PVAT in E+ rings, while promoting increased contractions in E– rings.

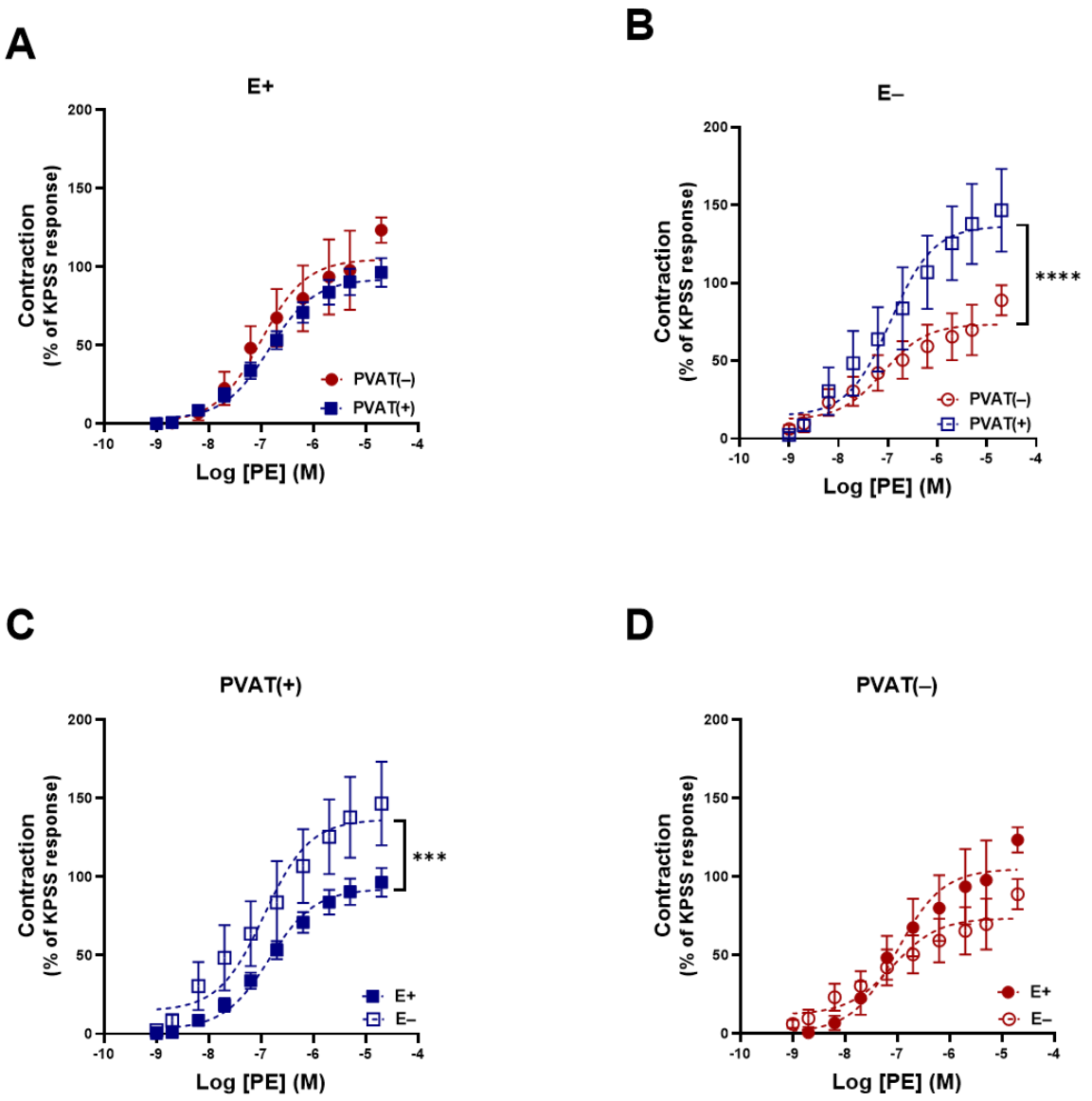

Figure 3-3 Contractile response to PE in rat thoracic aorta under hypoxic conditions. Concentration–response curves for the contractile effect of PE (1×10^{-9} to 3×10^{-5} M) were generated in thoracic aortic rings following 30 minutes of hypoxic exposure. **(A)** Endothelium-intact (E+) aortic rings with PVAT (PVAT+) and without PVAT (PVAT–). **(B)** Endothelium-denuded (E–) aortic rings with PVAT(+) and PVAT(–). **(C)** Comparison between PVAT(+) rings with E+ and E–. **(D)** Comparison between PVAT(–) rings with E+ and E–. The data are normalised to the maximum contraction induced by KPSS and expressed as mean ± SEM from arteries obtained from different animals. Data are presented as mean ± SEM from seven independent experiments for PVAT(+) /E+, five for PVAT(+) /E–, five for PVAT(–)/E+, and six for PVAT(–)/E–. Statistical analysis was performed using two-way ANOVA followed by Bonferroni's multiple comparisons test. Asterisks indicate statistical significance (***$p < 0.001$, ****$p < 0.0001$).

3.3.2.3 Comparison between normoxia and hypoxia

To directly assess the effect of hypoxia on vascular reactivity, contractile responses to PE were compared between aortic rings exposed to normoxic conditions and those subjected to 30 minutes of hypoxia. No significant differences were observed in PVAT-intact rings with E+ between normoxic and hypoxic conditions ($p = 0.7589$) (Figure 3-4A). In contrast, in PVAT(+) with E– rings, a significantly greater contraction was observed following exposure to hypoxia compared to normoxia ($p < 0.01$) (Figure 3-4B). Additionally, in PVAT(–) rings with E+, a significant anticontractile effect was noted under hypoxic conditions compared to normoxia ($p < 0.01$) (Figure 3-4C). However, in PVAT(–) rings with E-, no significant differences were observed between normoxic and hypoxic conditions ($p = 0.4477$) (Figure 3-4D). In summary, hypoxia increased PE-induced contractions in PVAT-denuded aortic rings, while no significant changes were observed in PVAT-intact rings.

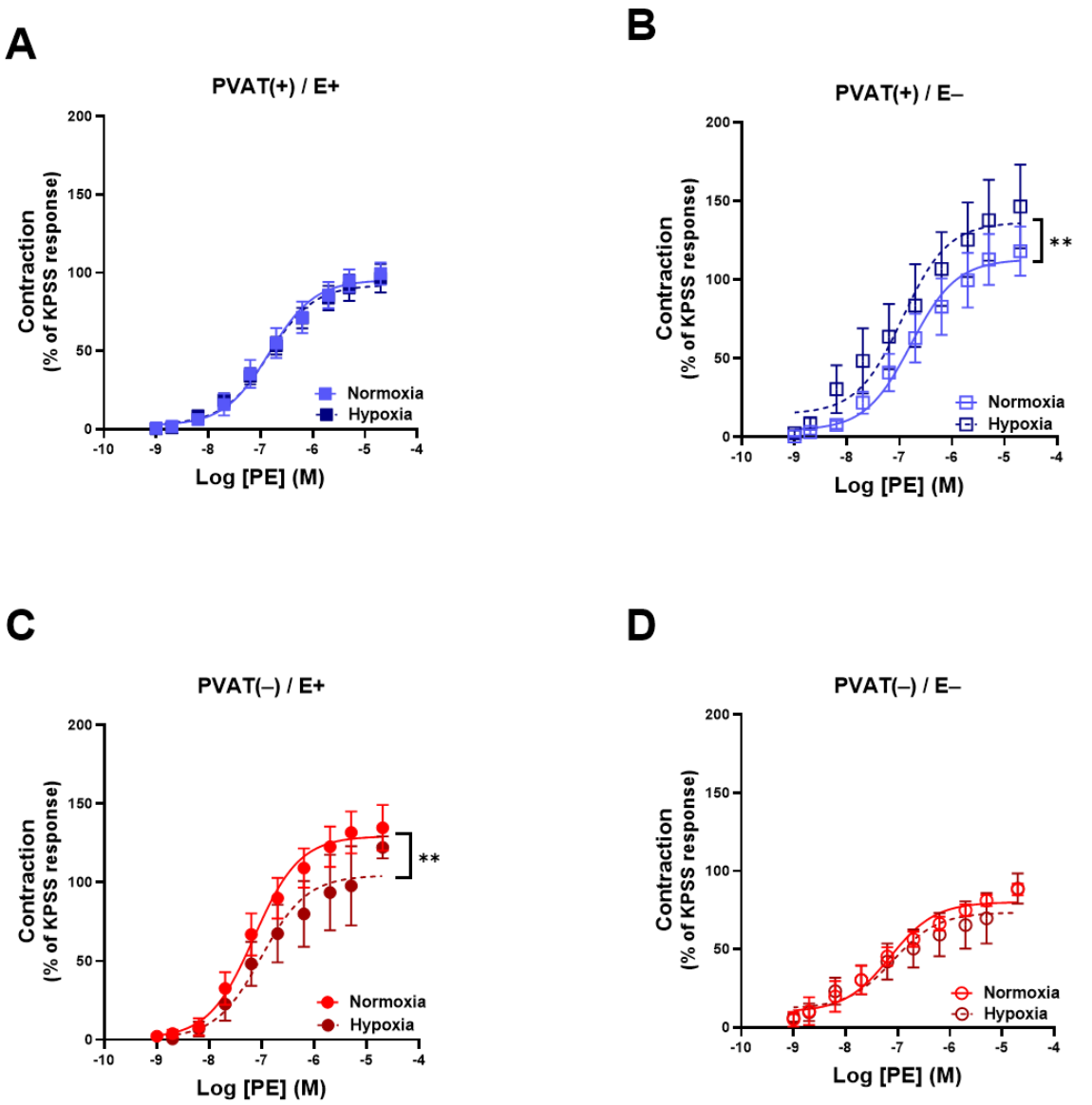

Figure 3-4 Contractile response to PE in rat thoracic aorta under normoxic and hypoxic conditions.
Thoracic aortic rings were exposed to either normoxic (95% O_2 and 5% CO_2) or hypoxic (95% N_2 and 5% CO_2) conditions for 30 minutes before concentration–response curves to PE were generated. **(A)** PVAT(+) /E+ rings. **(B)** PVAT(+) /E– rings. **(C)** PVAT(–)/E+ rings. **(D)** PVAT(–)/E–rings. The data are normalised to the maximum contraction induced by KPSS and expressed as mean ± SEM from arteries obtained from different animals. Data are presented as mean ± SEM from independent experiments with group sizes ranging from five to seven (n=5–7). Statistical analysis was performed using two-way ANOVA followed by Bonferroni's multiple comparisons test. Asterisks indicate statistical significance (**p < 0.01).

3.3.3 Contractile response of mesenteric arteries with PVAT to PE under normoxic and hypoxic conditions

Following the evaluation of thoracic aortic contractile responses, the contractility of mesenteric arteries was next assessed. The influence of PVAT and hypoxia on PE-induced contractions was examined in E+ and E- mesenteric artery rings. As with the thoracic aorta, concentration-response curves to PE (1×10^{-9}-3×10^{-5} M)

were generated in separate rings under normoxia or after a 30-min hypoxic exposure (95% N_2/5% CO_2) followed by re-oxygenation.

Under normoxic conditions, no significant differences in PE-induced contraction were observed between E+ and E- rings ($p = 0.7948$) (Figure 3-5A). Similarly, under hypoxic conditions, no significant difference in contraction was detected between E+ and E- rings, although E+ rings exhibited a trend toward greater contraction compared to E- rings ($p = 0.0522$) (Figure 3-5B).

When comparing normoxia and hypoxia, E+ mesenteric rings with PVAT demonstrated a significantly greater contraction in response to PE following exposure to hypoxia ($p < 0.05$) (Figure 3-6A). However, no significant difference was observed between normoxic and hypoxic conditions in E- mesenteric rings ($p = 0.8239$) (Figure 3-6B).

Interestingly, mesenteric arteries without PVAT did not exhibit any measurable contractile response to PE under either normoxic or hypoxic conditions.

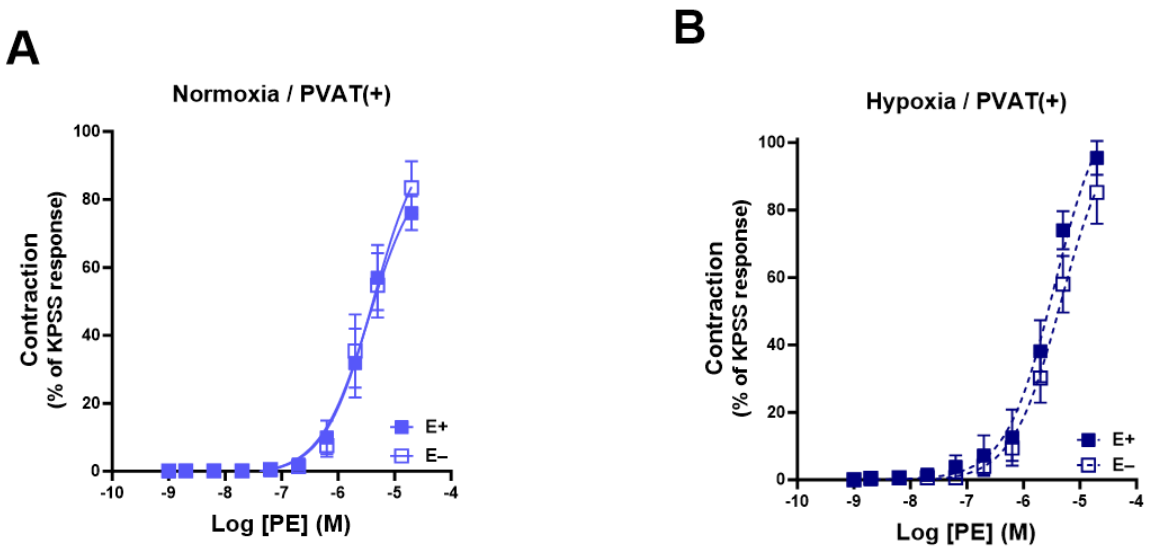

Figure 3-5 Effect of endothelium (E+/E–) on PE-induced contraction of mesenteric arteries with PVAT under normoxic and hypoxic conditions.
Concentration–response curves to PE (1×10^{-9} to 3×10^{-5} M) were generated in mesenteric arteries with intact PVAT under normoxic and hypoxic conditions. **(A)** Contractile responses in E+ and E– rings under normoxia. **(B)** Contractile responses in E+ and E– rings under hypoxia. The data are normalised to the maximum contraction induced by KPSS and expressed as mean ± SEM from arteries obtained from different animals. Data are presented as mean ± SEM from six independent experiments for normoxic E+, seven for normoxic E–, six for hypoxic E+, and five for hypoxic E–. Statistical analysis was performed using two-way ANOVA followed by Bonferroni's multiple comparisons test.

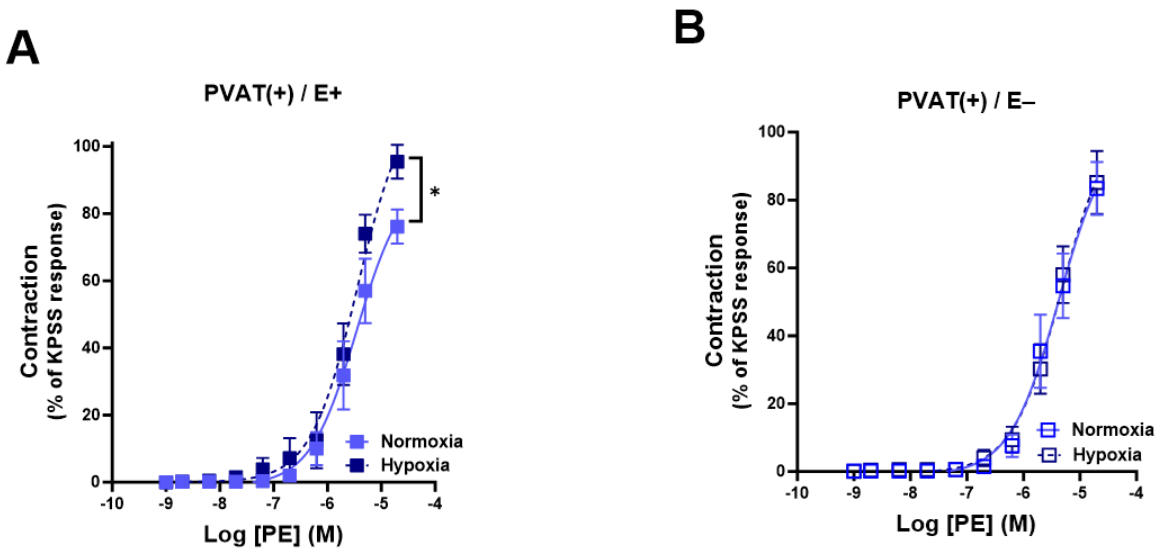

Figure 3-6 Effect of oxygenation (normoxia vs. hypoxia) on PE-induced contraction of PVAT(+) mesenteric arteries with E+ and E– endothelium
Mesenteric artery rings with intact PVAT were exposed to either normoxic (95% O_2 and 5% CO_2) or hypoxic (95% N_2 and 5% CO_2) conditions for 30 minutes before concentration–response curves to PE (1×10^{-9} to 3×10^{-5} M) were generated. **(A)** Comparison of contractile responses in PVAT(+) /E+ rings between normoxia and hypoxia. **(B)** Comparison of contractile responses in PVAT(+) /E– rings between normoxia and hypoxia. The data are normalised to the maximum contraction induced by KPSS and expressed as mean ± SEM from arteries obtained from different animals. Data are presented as mean ± SEM from six independent experiments for normoxic E+, seven for normoxic E–, six for hypoxic E+, and five for hypoxic E–. Statistical analysis was performed using two-way ANOVA followed by Bonferroni's multiple comparisons test (*p< 0.05).

3.3.4 Relaxation response of thoracic aorta to cromakalim (CK) under normoxic and hypoxic conditions

3.3.4.1 Normoxic conditions

Next, the effect of thoracic PVAT on endothelium-independent relaxation responses under normoxic conditions was evaluated using cromakalim (CK). Concentration–response curves to CK (1 nM to 10 μM) were generated in E+ and E- thoracic aortic rings, with either intact PVAT (PVAT+) or removed PVAT (PVAT-), following precontraction with PE (1 μM). In E+ vessels, no significant differences were observed in relaxation responses between PVAT(+) and PVAT(-) rings (Figure 3-7A). In contrast, in E- vessels, a significant increase in relaxation was observed in PVAT(-) rings compared to PVAT(+) rings ($p<0.001$) (Figure 3-7B). Comparison of PVAT(+) rings between E+ and E- groups revealed a significant enhancement of relaxation in E+ rings ($p<0.001$) (Figure 3-7C). However, in PVAT(-) rings, E+ rings exhibited a significantly lower relaxation response to CK compared to E- rings ($p<0.01$) (Figure 3-7D). In summary, under normoxia PVAT did not change CK relaxation in endothelium-intact rings; in PVAT-absent rings, removing the

endothelium increased relaxation, whereas in endothelium-denuded rings, the presence of PVAT reduced relaxation.

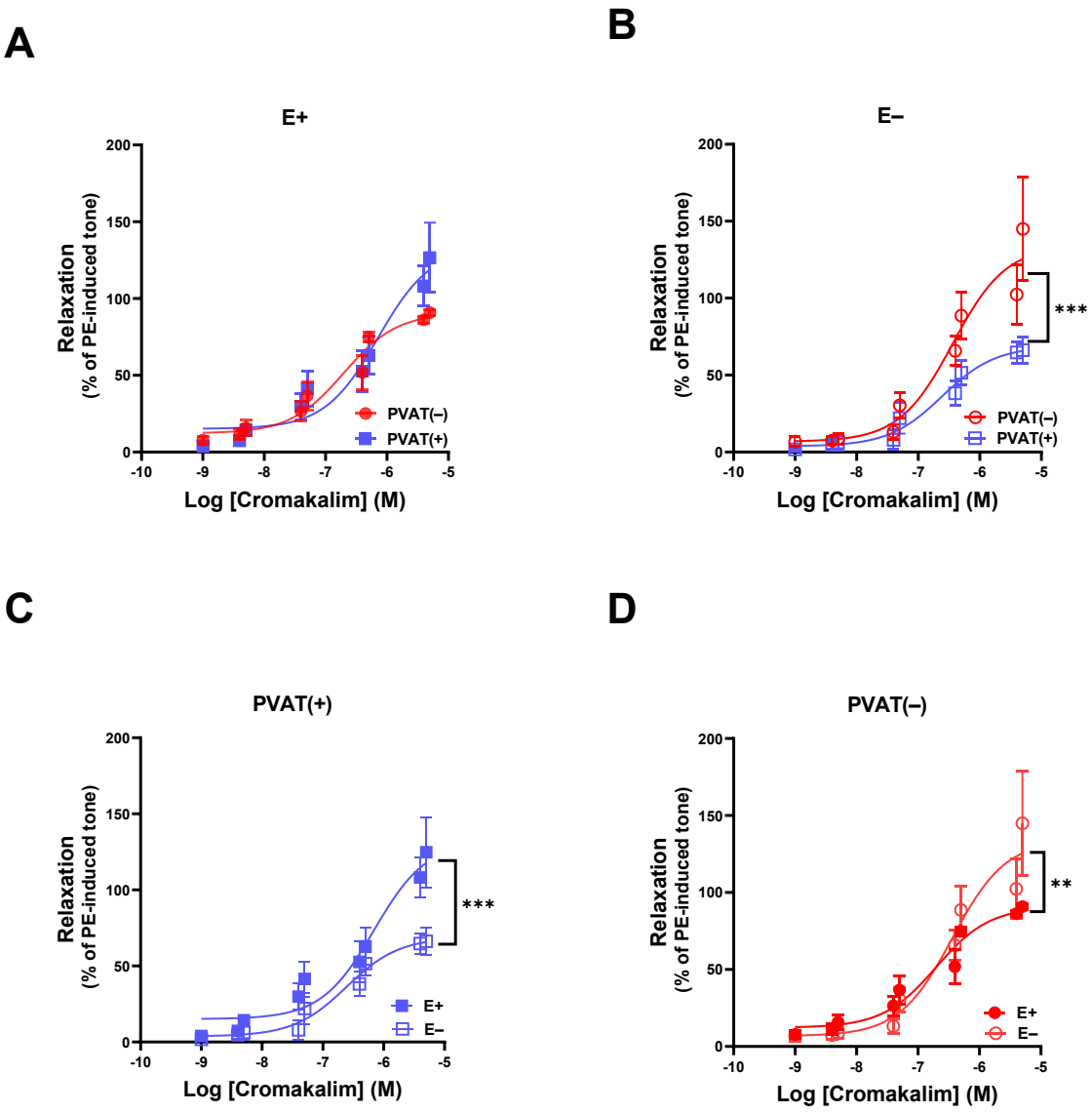

Figure 3-7 Effect of PVAT and endothelium on cromakalim-induced relaxation of thoracic aorta under normoxic conditions.
Thoracic aortic rings were precontracted with PE (1 μM) and then exposed to cumulative additions of cromakalim (CK) ranging from 1 nM to 10 μM. **(A)** Relaxation responses in E+ rings with PVAT(+) and PVAT(–). **(B)** Relaxation responses in E– rings with PVAT(+) and PVAT(–). **(C)** Comparison of relaxation responses between E+ and E– rings in PVAT(+) arteries. **(D)** Comparison of relaxation responses between E+ and E– rings in PVAT(–) arteries. Relaxation is expressed as a percentage of the precontracted tone induced by PE and presented as mean ± SEM from arteries obtained from different animals. Data are presented as mean ± SEM from seven independent experiments for PVAT(+) /E+, five for PVAT(–)/E+, four for PVAT(+) /E– and five for PVAT(–)/E–. Statistical analysis was performed using two-way ANOVA followed by Bonferroni's multiple comparisons test. Asterisks indicate statistical significance (**p < 0.01, ***p < 0.001).

3.3.4.2 Hypoxic conditions

To determine whether the anti-contractile properties of thoracic PVAT were influenced by hypoxia, relaxation responses to CK were assessed following

exposure to hypoxia (95% N_2 and 5% CO_2 for 30 minutes). Concentration–response curves to CK (1 nM to 10 μM) were generated in PE-precontracted aortic rings with or without PVAT, and with either E+ or E– rings.

In E+ rings, no significant differences were observed in CK-induced relaxation between PVAT(+) and PVAT(–) vessels (Figure 3-8A). In E– rings, a similar non-significant difference was seen between PVAT(+) and PVAT(–) groups (Figure 3-8B). When comparing PVAT(+) rings between E+ and E– groups, there was no significant difference in relaxation responses (Figure 3-8C). Likewise, in PVAT(–) rings, no significant difference was found between E+ and E– rings (Figure 3-8D). In summary, under hypoxia, CK-induced relaxation was similar across all groups, eliminating the between-group differences observed at normoxia; direct comparisons with normoxia are presented in Section 3.3.4.3.

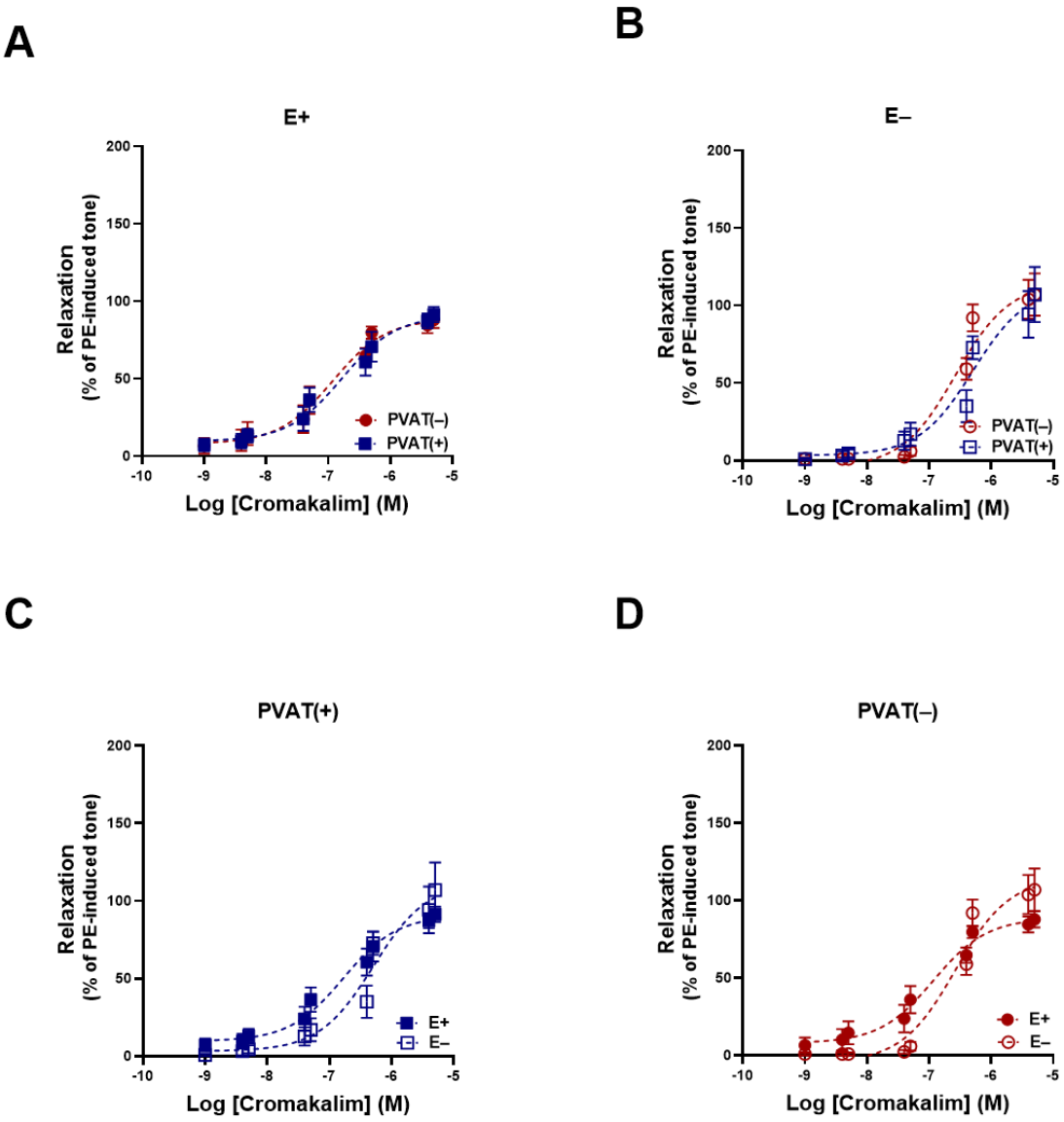

Figure 3-8 Effect of PVAT and endothelium on cromakalim-induced relaxation of thoracic aorta under hypoxic conditions.
Thoracic aortic rings were exposed to hypoxia (95% N_2 and 5% CO_2) for 30 minutes, then precontracted with PE (1 μM) before cumulative addition of CK ranging from 1 nM to 10 μM . **(A)** Relaxation responses in E+ rings with PVAT(+) and PVAT(–). **(B)** Relaxation responses in E– rings with PVAT(+) and PVAT(–). **(C)** Comparison of relaxation responses between E+ and E– rings in PVAT(+) arteries. **(D)** Comparison of relaxation responses between E+ and E– rings in PVAT(–) arteries. Relaxation is expressed as a percentage of the precontracted tone induced by PE and presented as mean ± SEM from arteries obtained from different animals. Data are presented as mean ± SEM from seven independent experiments for PVAT(+)/E+, eight for PVAT(–)/E+, four for PVAT(+)/E–, and three for PVAT(–)/E–. Statistical analysis was performed using two-way ANOVA followed by Bonferroni's multiple comparisons test.

3.3.4.3 Comparison between normoxia and hypoxia

To determine whether hypoxia influenced relaxation responses to CK, thoracic aortic rings were compared after exposure to normoxic or hypoxic conditions. No significant differences in CK-induced relaxation were observed between PVAT(+)/E+ rings under normoxia and hypoxia (Figure 3-9A). In PVAT(+)/E– rings, a significantly greater relaxation response was observed following hypoxic exposure compared to normoxia ($p < 0.05$) (Figure 3-9B). In PVAT(–)/E+ rings, hypoxia resulted in a non-significant increase in relaxation compared to normoxic rings (Figure 3-9C). Similarly, in PVAT(–)/E– rings, no significant differences were detected between normoxic and hypoxic conditions (Figure 3-9D). In summary, hypoxia enhanced CK-induced relaxation only in PVAT(+) rings with denuded endothelium, while no significant differences were observed in other groups.

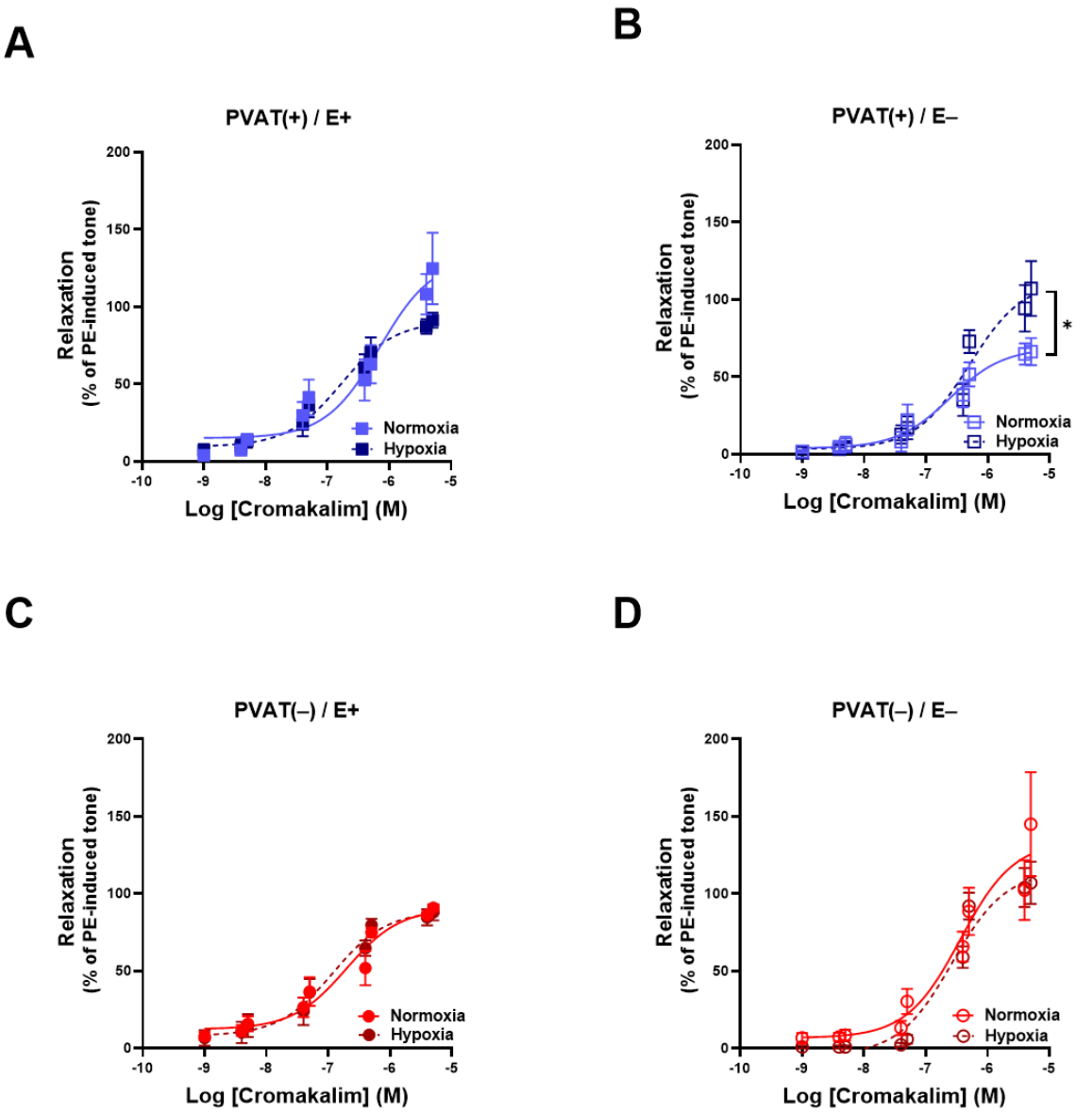

Figure 3-9 Comparison of cromakalim-induced relaxation in thoracic aorta under normoxic and hypoxic conditions.
Thoracic aortic rings were exposed to either normoxic (95% O_2 and 5% CO_2) or hypoxic (95% N_2 and 5% CO_2) conditions for 30 minutes before concentration–response curves to CK were generated. **(A)** PVAT(+)/E+ rings. **(B)** PVAT(+)/E– rings. **(C)** PVAT(–)/E+ rings. **(D)** PVAT(–)/E– rings. Relaxation is expressed as a percentage of the precontracted tone induced by PE and presented as mean ± SEM from arteries obtained from different animals. Group sizes are the same as described for Figure 3-7 and Figure 3-8. Statistical analysis was performed using two-way ANOVA followed by Bonferroni's multiple comparisons test. Asterisks indicate statistical significance (*$p < 0.05$).

3.3.5 Effect of hypoxia on PE-precontracted thoracic aorta with and without PVAT

The previous vascular function experiments investigated contractile and relaxation responses through concentration–response curves to PE and CK, following 30 minutes of pre-exposure to normoxic or hypoxic conditions. In contrast, the subsequent experiments were designed to assess the direct effects

of acute hypoxia on vascular tone. In these studies, thoracic aortic rings were first precontracted with a single concentration of PE (1 μM) under normoxic conditions. Once a stable contraction was achieved, myograph chambers were bubbled with hypoxic gas (95% N_2 and 5% CO_2) for 30 minutes, and the real-time effect of hypoxia on vascular tone was measured.

Following the onset of hypoxia, thoracic aortic rings with intact endothelium exhibited significant relaxation in both PVAT(+) and PVAT(–) groups compared to their baseline contraction under normoxic conditions ($p < 0.0001$) (Figure 3-10A). Additionally, PVAT(+) rings showed a significantly greater relaxation response to hypoxia compared to PVAT(–) rings ($p < 0.01$). Relaxation began within minutes of switching to hypoxia, with a rapid initial drop followed by a slower decline to a new steady state at 30 min; values reported are at 30 min. A representative control recording from a PVAT(+) ring is provided in Figure 3-10B to illustrate hypoxia-induced relaxation.

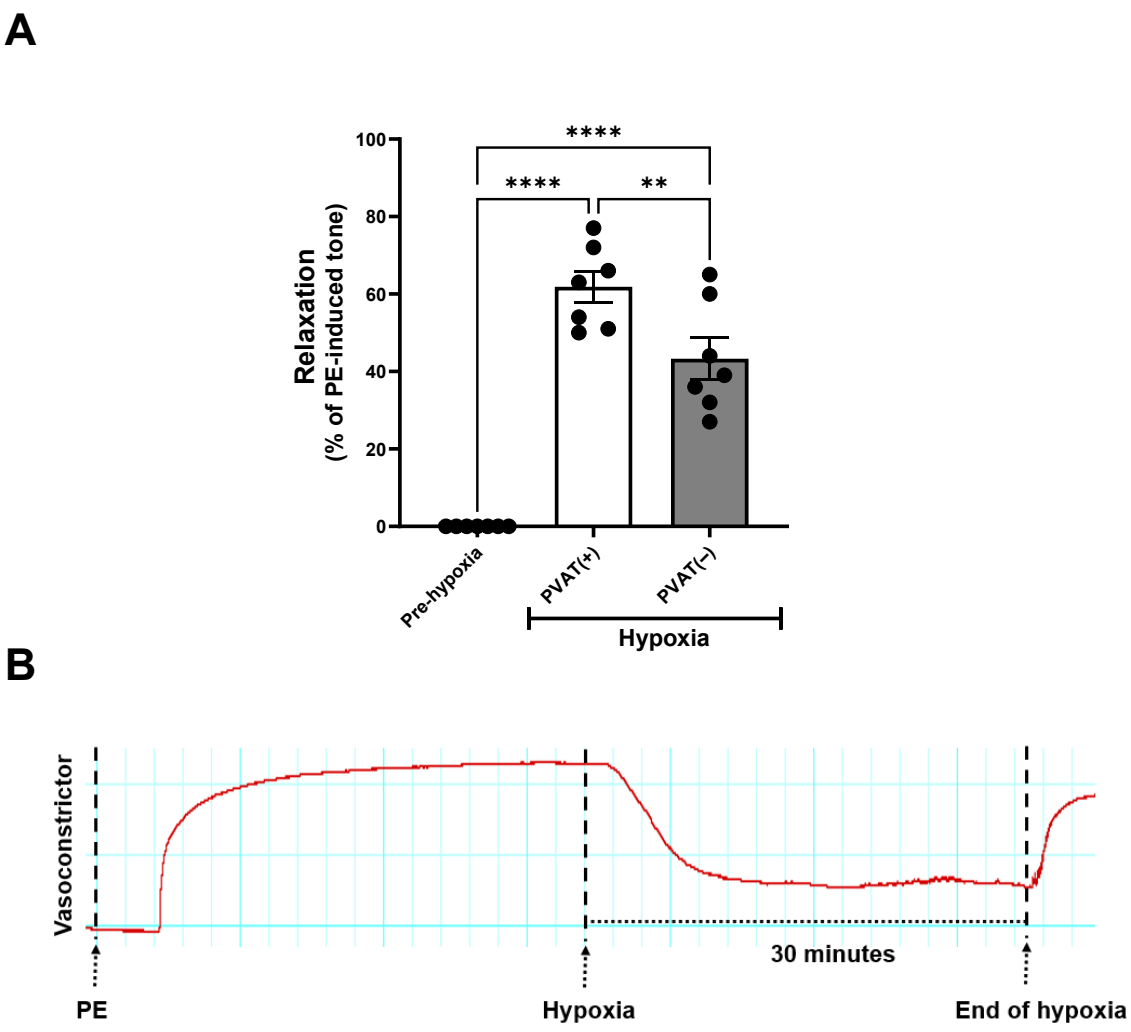

Figure 3-10 Hypoxia-induced relaxation in endothelium-intact (E+) thoracic aorta with and without PVAT.
Thoracic aortic rings with E+ were precontracted with PE (1 μM) under normoxic conditions. After achieving a stable contraction, rings were exposed to hypoxia (95% N_2 and 5% CO_2) for 30 minutes. **(A)** Relaxation is expressed as a percentage of the precontracted tone induced by PE and presented as mean ± SEM from seven independent experiments per group. **(B)** Representative myograph recording from a PVAT(+) ring showing PE pre-contraction, the onset of hypoxia and the subsequent relaxation. Statistical analysis was performed using one-way ANOVA followed by Tukey's post-hoc test. Asterisks indicate statistical significance (**p < 0.01, ****p < 0.0001).

3.3.6 Effect of PVAT and endothelium on hypoxia-induced relaxation

In vessels lacking endothelium, hypoxia induced significant relaxation in PVAT(+) rings compared with normoxic baseline ($p < 0.001$), while PVAT(-) rings showed no significant response. Consequently, relaxation was significantly greater in PVAT(+)/E- than in PVAT(-)/E- rings ($p < 0.01$) (Figure 3-11). In summary, hypoxia-induced relaxation was significant in PVAT(+)/E+, PVAT(+)/E-, and PVAT(-)/E+ groups, but not in PVAT(-)/E- rings.

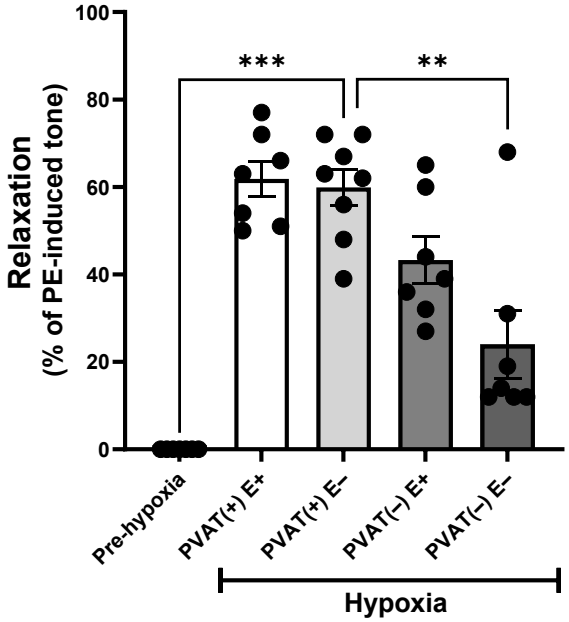

Figure 3-11 Effect of PVAT and endothelium on hypoxia-induced relaxation in PE-precontracted thoracic aorta.
Thoracic aortic rings were precontracted with PE (1 μM) under normoxic conditions. Once a stable contraction was achieved, rings were exposed to hypoxia (95% N_2 and 5% CO_2) for 30 minutes. Relaxation is expressed as a percentage of the precontracted tone induced by PE and presented as mean ± SEM from arteries obtained from different animals. Data are presented as mean ± SEM from seven independent experiments for PVAT(+) /E+ and PVAT(–)/E+, eight for PVAT(+) /E–, and six for PVAT(–)/E–. Statistical analysis was performed using the Kruskal–Wallis test followed by Dunn's multiple comparisons test. Comparisons between PVAT(+)/E– and PVAT(–)/E– groups were additionally analysed using the Mann–Whitney U test. Asterisks indicate statistical significance (*$p < 0.05$, ***$p < 0.001$, ****$p < 0.0001$).

3.4 Discussion

The present study investigates the effect that acute or reversible hypoxia has on PVAT and endothelial function and how that modulates vascular tone in rat thoracic aorta and mesenteric arteries. Two experimental approaches were employed using wire myography. The first involved generating concentration–response curves to PE and CK following 30 minutes of hypoxic pre-exposure. The second assessed real-time vascular responses to acute hypoxia applied for 30 minutes during sustained PE-induced contraction. My findings reveal that the timing and context of hypoxia exposure critically influence vascular reactivity. Specifically, pre-exposure to hypoxia enhanced PE-induced contractile responses in both thoracic and mesenteric arteries. Conversely, CK-induced relaxation showed modest enhancement under hypoxia in thoracic PVAT. In contrast to the variable effects observed following pre-exposure to hypoxia, acute hypoxia in a pre-contracted ring induced significant vasorelaxation in thoracic aorta. These effects were further modulated by the presence or absence of PVAT and functional endothelium (Figure 3-12). The dual experimental approach, involving both pre-exposure to hypoxia and acute hypoxic challenge, offers valuable insight into how the effect of hypoxia differs dependent on the contractile state of the vascular rings and also on whether endothelium and PVAT are present.

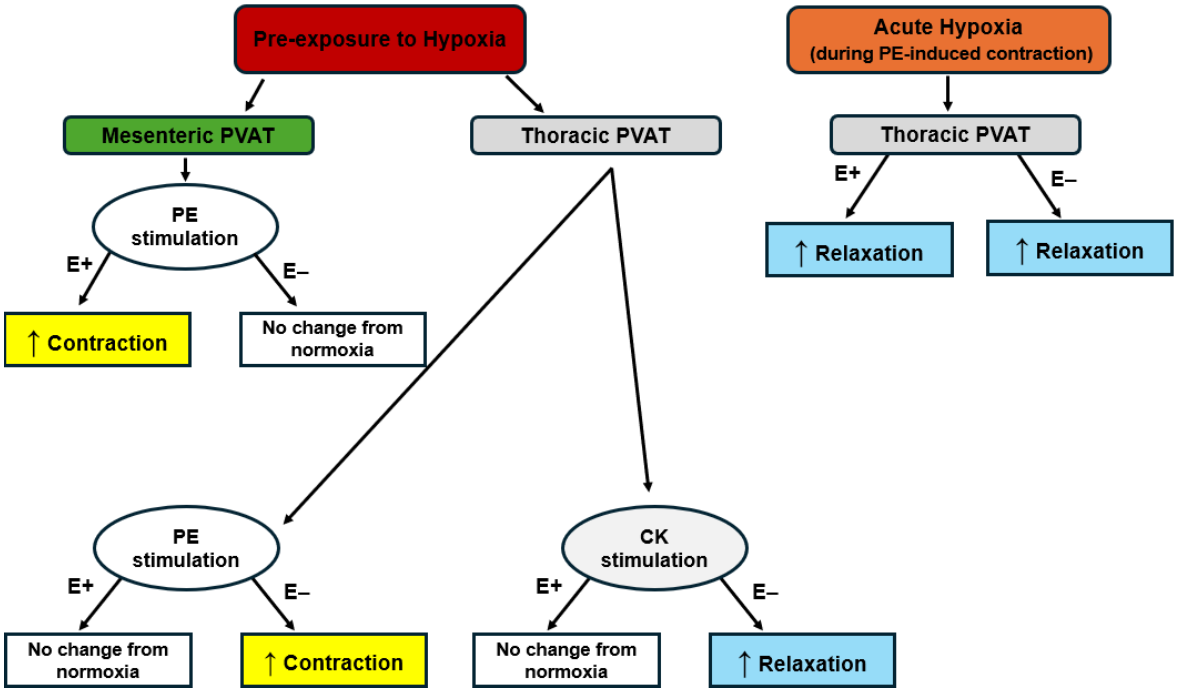

Figure 3-12 Schematic summary of PVAT and endothelium contributions to hypoxia-induced vascular responses in thoracic and mesenteric arteries.
A schematic flowchart illustrating the impact of pre-exposure to hypoxia (30 minutes of 95% N_2 and 5% CO_2) and acute hypoxia (applied during phenylephrine (PE)-induced contraction) on vascular responses in rat thoracic and mesenteric arteries with intact perivascular adipose tissue (PVAT). The diagram distinguishes outcomes based on vascular bed (thoracic versus mesenteric), type of stimulation (PE or cromakalim (CK)), and endothelial status (E+ or E–).

Initial experiments under normoxic conditions clarified the fundamental roles of PVAT and the endothelium in modulating PE-induced contractions in the rat thoracic aorta. In vessels with intact endothelium (E+), the presence of PVAT significantly attenuated contractile responses to PE compared to PVAT (-) rings (Figure 3-2A), consistent with earlier findings demonstrating that PVAT reduces vasoconstriction induced by agents such as norepinephrine, phenylephrine, serotonin, and angiotensin II (Soltis and Cassis, 1991, Löhn et al., 2002, Verlohren et al., 2004). This anticontractile effect has been demonstrated across a wide range of arterial beds, including the aorta (Soltis and Cassis, 1991, Wang et al., 2009, Fang et al., 2009), mesenteric arteries (Li et al., 2013), skeletal muscle arteries (Meijer et al., 2013), and subcutaneous arteries (Greenstein et al., 2009). It is primarily attributed to the release of various vasoactive substances known as PVRFs (Szasz and Webb, 2012). The transferable nature of PVRFs has been validated in various studies using PVAT-conditioned solutions that induce relaxation in precontracted, PVAT-free vascular segments (Verlohren et al., 2004, Fésüs et al., 2007, Gao et al., 2007, Lu et al., 2011, Greenstein et al., 2009, Almabrouk et al., 2017). These include, but are not limited to, nitric oxide (NO), hydrogen sulphide (H_2S), prostacyclin, hydrogen peroxide (H_2O_2), palmitic acid

methyl ester, angiotensin 1-7, adiponectin, leptin, and omentin (Tong et al., 2023, Victorio et al., 2016, Lee et al., 2011). Interestingly, this anticontractile effect of PVAT was abolished in endothelium-denuded (E-) rings, where no significant difference was observed between PVAT(+) and PVAT(–) groups (Figure 3-2B), highlighting the essential role of an intact endothelium in mediating PVRF actions. This interdependence is further supported by my observation that E+ rings with intact PVAT displayed a trend toward reduced contractile responses compared to their E− counterparts (Figure 3-2C), suggesting that PVAT and the endothelium may act synergistically through overlapping or complementary mechanisms. My findings accord with previous studies demonstrating the importance of both PVAT and endothelium in vascular regulation. For instance, Gao et al. (2007) demonstrated that PVAT potentiates endothelial NO release, while Löhn et al. (2002) reported that PVAT-derived factors can also induce endothelium-independent relaxation via activation of K^{+}_{ATP} channels and tyrosine kinases. Gao et al. (2007) further proposed a dual mechanism by which PVAT exerts its effects: one endothelium-dependent, involving NO and Ca^{2+}-activated potassium channels (K_{Ca}), and another endothelium-independent, mediated by H_2O_2 and subsequent soluble guanylyl cyclase (sGC) activation. Conversely, in the absence of PVAT, E+ rings showed significantly greater contractile responses to PE than E− rings (Figure 3-2D). Although this result contrasts with typical expectations, it may suggest that, in the absence of PVAT, the endothelium compensates by upregulating the release of EDCFs like endothelin or PGI_2 to maintain vascular tone (Rapoport and Williams, 1996, Yanagisawa et al., 1988, Koga et al., 1989). Collectively, these findings and my data support the concept that both PVAT and the endothelium contribute critically to the regulation of vascular tone under physiological conditions.

Pre-exposure to a hypoxic environment (30 minutes of 95% N_2 and 5% CO_2) significantly altered PE-induced vascular responses in the thoracic aorta, highlighting a complex interplay between hypoxia, PVAT, and endothelium. Under normoxic conditions, PVAT(+) E+ rings showed reduced contraction compared to PVAT(–) E+ rings, consistent with the modulatory influence of PVAT (Figure 3-2A). However, this difference was abolished under hypoxic conditions (Figure 3-3A), suggesting a context-dependent modulation.

Direct comparison between normoxia and hypoxia in PVAT-intact E+ rings showed no significant change in contraction (Figure 3-4A), indicating that the presence of PVAT prevents the hypoxia-induced relaxation typically mediated by the endothelium. This is further supported by the contrasting observation in PVAT(-) E+ rings, where hypoxia significantly reduced PE-induced contraction (Figure 3-4C), suggesting that in the absence of PVAT, the endothelium can exert a vasorelaxant effect under hypoxic conditions. In E- rings, PVAT presence significantly increased contraction compared to PVAT(-) rings (Figure 3-3B) and contraction was significantly greater in PVAT(+) E- rings under hypoxia compared to normoxia (Figure 3-4B), indicating that oxygen deprivation may impair relaxant signalling or amplify PVAT-derived vasoconstrictors. Finally, under hypoxia, PVAT(+) E- rings exhibited significantly higher contraction than PVAT(+) E+ rings (Figure 3-3C), reinforcing the notion that the endothelium plays a critical protective role in buffering PVAT-driven vasoconstriction during hypoxic stress.

The literature presents conflicting reports regarding PVAT's role under hypoxic conditions. Some studies report that hypoxia promotes vasorelaxation in a PVAT-dependent manner, such as in porcine coronary arteries and mouse thoracic aorta (Donovan et al., 2018, Maenhaut et al., 2010). However, these findings come from acute hypoxia protocols in which vessels were first precontracted and then switched to hypoxic gassing (95% N_2/5% CO_2) for 30 min while relaxation was recorded during the sustained tone; these will be discussed in the context of my acute-exposure experiments. Conversely, a growing body of evidence suggests that hypoxia may impair PVAT function, diminishing its vasomodulatory capacity or even shifting it toward a procontractile profile. Badran et al. (2019) demonstrated that gestational intermittent hypoxia reduced the anti-contractile activity of PVAT in abdominal aortic arteries from male offspring, an effect reversed by adiponectin. Similarly, Han et al. (2018) restored PVAT function using calycosin via the adiponectin/AMPK/eNOS pathway. In mesenteric arteries, hypoxia-induced PVAT dysfunction has been consistently reported (Greenstein et al., 2009, Rosei et al., 2015, Withers et al., 2014). My findings, where the presence of PVAT blocked hypoxia-induced relaxation and promoted vasoconstriction in E- rings, may be mediated by enhanced release of PVCFs, including angiotensin II, superoxide anion, chemerin, and prostaglandins (Ramirez et al., 2017).

Furthermore, obesity drives persistent PVAT hypoxia and oxidative stress, which together promote and sustain this dysfunction. Sousa et al. (2019) reported impaired vasorelaxation in PVAT-intact aortic rings from obese mice, attributed to increased inflammation. Similarly, Zaborska et al. (2016) found that maternal obesity reduced NO bioavailability and disrupted PVAT's regulatory function in mesenteric arteries. Although the present study used non-obese animals, obesity is associated with chronic PVAT hypoxia due to adipocyte hypertrophy, limited oxygen diffusion, and inadequate neovascularisation, which activates HIF-1α and pro-inflammatory/fibrotic signalling (Trayhurn, 2013, Sun et al., 2011, He et al., 2011, Cifarelli et al., 2020). In obese states, this adipose hypoxia and dysfunction are tightly linked to systemic endothelial dysfunction, characterised by reduced NO bioavailability, eNOS uncoupling, oxidative stress, and an imbalance between vasodilators and vasoconstrictors such as endothelin-1 and angiotensin II (Lobato et al., 2012, Kajikawa and Higashi, 2022). Visceral and perivascular fat depots from obese individuals show increased production of pro-inflammatory cytokines, reduced adiponectin, and a shift from anti-contractile to pro-contractile signalling; changes that promote insulin resistance, oxidative stress and impaired endothelium-dependent vasodilation (Arcaro et al., 1999, De Jongh et al., 2004, Romero-Corral et al., 2010, Mazurek et al., 2003, Mazzotta et al., 2021, Lau et al., 2017). Notably, in the absence of PVAT, several studies confirm that the endothelium contributes significantly to hypoxia-induced vasorelaxation, likely via nitric oxide (Hedegaard et al., 2011, Van Mil et al., 2002). Consistent with this, in my pre-exposure experiments (30 min at 95% N_2/5% CO_2 followed by re-oxygenation), PVAT(–) E+ rings showed attenuated PE contractions relative to normoxia (Figure 3-4C), supporting a prominent endothelial contribution and no change in PVAT(–) E– rings (Figure 3-4D). These findings are therefore compatible with the concept that, in healthy non-obese vessels, acute hypoxia/re-oxygenation can unmask a protective, NO-dependent endothelial response, whereas in obesity, chronic PVAT hypoxia, adipose inflammation and vascular oxidative stress would be expected to blunt this endothelial compensation and promote enhanced tone and hypertension (Lobato et al., 2012, Kajikawa and Higashi, 2022, Jonk et al., 2007). Conversely, studies by Donovan et al. (2017) and Hedegaard et al. (2014) also highlight H_2S as a key mediator in vascular smooth muscle under hypoxia in PVAT-denuded segments. Interestingly, Alganga et al. (2019) reported an opposing effect, where 30 minutes of hypoxia enhanced

contractility in rat thoracic aortic rings precontracted with U46619. Such discrepancies may reflect species-specific responses, the type and timing of hypoxic exposure, the contractile agent used or the interplay between endothelial and PVAT-derived signals. Altogether, the available evidence emphasises that PVAT's role under hypoxia is highly context dependent.

The mesenteric arteries, as resistance vessels, have distinct structural and functional characteristics compared to the thoracic aorta. Under normoxic conditions, no significant differences in PE-induced contraction were observed between E+ and E– mesenteric artery rings with intact PVAT (Figure 3-5A). In contrast, thoracic aortic rings showed a trend toward reduced contraction in E+ compared to E– rings (Figure 3-2C). These observations reflect the known regional and depot-specific effects of PVAT on vascular tone. For example, in mice, thoracic aortic PVAT, primarily composed of brown adipose tissue (BAT), markedly attenuates phenylephrine-induced vasoconstriction, whereas abdominal aortic PVAT (white adipose tissue, WAT) does not. This differential effect has been linked to higher eNOS expression and greater NO bioavailability in BAT-rich regions (Hwej et al., 2024, Victorio et al., 2016). Similarly, in Wistar Kyoto (WKY) rats, mesenteric PVAT (WAT) exhibits elevated levels of angiotensin II, angiotensin AT1a and AT2 receptors, and chymase, but lower expression of the prorenin receptor compared to periaortic PVAT (BAT), contributing to region-specific modulation of vascular responses (Gálvez-Prieto et al., 2008). These functional differences align with the distinct physiological and pathological roles of each vascular bed. Thoracic aorta is a large elastic conduit vessel often involved in atherosclerosis, whereas mesenteric vessels are smaller resistance arteries primarily regulating peripheral blood pressure (Lusis, 2000, Bridges et al., 2011, Peixoto-Neves et al., 2015, Simões et al., 2021).

Under hypoxic conditions, a trend toward increased PE-induced contraction was observed in E+ mesenteric artery rings compared to E– rings (Figure 3-5B), suggesting that the endothelium may contribute to hypoxia-induced vasoconstriction in this vascular bed. This contrasts with the thoracic aorta, where the endothelium appears to play a more protective role during hypoxia by limiting vasoconstriction. When comparing normoxia to hypoxia, only the E+ mesenteric rings demonstrated a significant increase in contractile response (Figure 3-6A), while E– rings remained unchanged (Figure 3-6B). These findings are consistent

with previous studies showing that mesenteric PVAT loses its regulatory function under hypoxic stress. For instance, it has been reported that a longer period of hypoxia (2.5 h, 95% N_2/5% CO_2) abolished the modulatory effect of mesenteric PVAT, an effect prevented by the ACE inhibitor captopril and the AT1R antagonist telmisartan (Rosei et al., 2015) and was reversed by aldosterone receptor antagonism (eplerenone) (Withers et al., 2011). Similarly, Greenstein et al. (2009) found that this dysfunction, likely driven by oxidative stress and inflammation, could be reversed by anti-IL-6 or anti-TNF-α treatment. Withers et al. (2014) further demonstrated that cGMP-dependent protein kinase activation via atrial natriuretic peptide (ANP) restored PVAT function in wild-type mice. Moreover, in C57BL/6J mice, a 32-week high-fat diet abolished the anticontractile effect of PVAT in mesenteric arteries, and PVAT significantly impaired endothelium-dependent relaxation in these vessels (Gil-Ortega et al., 2014).

Notably, in my experiments using young SD rats (180–300 g), mesenteric arteries showed no contractile response to phenylephrine, U46619, or high K^+ solution following PVAT removal, under both normoxic and hypoxic conditions. This lack of reactivity was consistent across all samples and was not due to technical error, as parallel tests using mesenteric arteries from hypertensive rats confirmed normal contractile responses. Other studies investigating PVAT effects in mesenteric arteries of SD rats have typically used older or heavier animals (e.g. ~300–500 g Cruz-López et al. (2024); or more than 420 g Liao et al. (2021)). It is possible that the lack of responsiveness observed here is related to the developmental stage or small diameter of the arteries or may reflect a strong PVAT-dependent modulation of vascular tone.

Building upon the investigation of vessel contraction, I then investigated relaxation responses using cromakalim (CK), a K_{ATP} channel opener, under both normoxic and hypoxic conditions in the thoracic aorta. Under normoxic conditions, in endothelium-intact (E+) vessels, no significant differences were observed in CK-induced relaxation between PVAT(+) and PVAT(–) rings (Figure 3-7A). This suggests that the influence of PVAT on K_{ATP} channel-mediated relaxation is not overtly significant when the endothelium is intact.

In contrast, endothelium-independent effects of PVAT are primarily mediated by the direct actions of PVRFs on VSMC ion channels. These effects vary across

vascular beds and experimental models. In male SD rats, PVAT-induced relaxation in the thoracic aorta involves activation of K_{ATP} channels and tyrosine kinase pathways, functioning in a calcium-dependent manner (Löhn et al., 2002). In Wistar rats, thoracic aortic relaxation is associated with K_{Ca} channel activation and hydrogen peroxide-stimulated soluble guanylate cyclase (sGC) activity (Gao et al., 2007). K_v channel-mediated relaxation has also been observed in the mesenteric arteries of SD rats and in the thoracic aorta of Wistar Kyoto rats (Verlohren et al., 2004, Lee et al., 2011). Additionally, adiponectin, a key PVRF, induces vasorelaxation in both aortic and mesenteric vessel rings through activation of voltage-gated potassium (K_v) and large-conductance calcium-activated potassium (BK_{Ca}) channels (Fésüs et al., 2007, Weston et al., 2013, Lynch et al., 2013). Consistent with an endothelium-independent PVAT pathway, Almabrouk et al. (2017) showed that PVAT augments CK-induced relaxation in endothelium-denuded mouse aorta via AMPKα1-dependent actions of adiponectin.

Consistent with the patterns observed in the PE dose-response curves, a significant enhancement of CK-induced relaxation was observed in PVAT(–)/E– rings compared to both PVAT(+)/E– and PVAT(–)/E+ rings (Figure 3-7B and 3.6D). One possible explanation is improved drug access to VSMCs once PVAT and the endothelial layer are removed, which shortens the adventitial diffusion path and reduces intramural barriers within the vessel wall (Lew et al., 1989, Tankó et al., 1999, Steinhorn et al., 1994), thereby increasing CK's apparent efficacy at K_{ATP} channels. However, PVAT(+)/E+ rings relaxed more than PVAT(+)/E– at the same CK concentrations (Figure 3-7C), which argues against access alone. This pattern suggests that an intact endothelium amplifies VSMC K_{ATP}-mediated relaxation, for example via basal NO/cGMP–mediated Ca^{2+} desensitisation (Francis et al., 2010, Lee et al., 1997) and EDHF-type myoendothelial coupling (Sandow and Hill, 2000, Sandow et al., 2002). Thus, CK acts directly on VSMC K_{ATP} channels, but endothelial status and PVAT presence set the magnitude of the relaxation.

Under hypoxic conditions, vascular responses to cromakalim (CK) differed markedly from those observed under normoxia. While no significant differences were found among groups under hypoxia alone (Figure 3-8A–D), a clearer interpretation emerged when comparing normoxic and hypoxic conditions directly. Notably, CK-induced relaxation was significantly enhanced in PVAT(+)/E–

rings under hypoxia compared to normoxia (Figure 3.8B), suggesting that PVAT compensates for the absence of endothelium by promoting K_{ATP} channel activity in hypoxic conditions. Additionally, hypoxia may increase PVAT release of vasodilators, especially H_2S, which promotes K^+-channel opening and augments relaxation (Donovan et al., 2018, Fang et al., 2009). This may represent an adaptive mechanism to maintain vasodilation when oxygen supply is low and endothelial function is compromised.

This interpretation is supported by findings from Maenhaut et al. (2010), who demonstrated that hypoxia enhanced vasorelaxation in norepinephrine-precontracted thoracic aorta segments from male Swiss mice through a mechanism involving K_{ATP} channel activation, independent of both the endothelium and soluble guanylyl cyclase. This indicates that hypoxia-induced relaxation can proceed via an endothelium-independent pathway. The response was significantly reduced by high extracellular K^+ (60–120 mM), and by tetraethylammonium (TEA), a non-selective K^+ channel blocker, as well as by glibenclamide, a selective K_{ATP} channel inhibitor. These results strongly implicate K^+ channels, particularly K_{ATP} channels, in mediating the hypoxic vasodilatory response. Moreover, K_{ATP} channels are known to be activated by endogenous vasodilators released during hypoxia (Daut et al., 1990) and are expressed not only in vascular smooth muscle but also in adipocytes.

K_{ATP} channels are composed of four Kir6.x pore-forming subunits and four regulatory sulfonylurea receptor (SUR) subunits, as characterised in various tissues (Clement et al., 1997). While this structure is well established in vascular smooth muscle, functional K_{ATP} channels have also been identified in adipocytes. For instance, glibenclamide has been shown to induce a dose-dependent increase in intracellular calcium ($[Ca^{2+}]_i$) in adipocytes (Shi et al., 1999), supporting the presence of functional K_{ATP} channels in these cells. This suggests that both vascular and PVAT-derived K_{ATP} channels may contribute to the enhanced CK-induced relaxation observed under hypoxia in endothelium-denuded vessels.

Beyond the pre-exposure experiments, my study employed another approach to directly assess the real-time effects of acute hypoxia on vascular tone. In these experiments, thoracic aortic rings were precontracted with PE under normoxic conditions and then exposed to acute hypoxia. This was important given the

conflicting reports on whether hypoxia causes contraction or relaxation, often without distinguishing the timing of exposure. Upon exposure to acute hypoxia, E+ thoracic aortic rings showed significant relaxation in both PVAT(+) and PVAT(–) groups compared to their baseline contraction under normoxic conditions (Figure 3-10). The presence of PVAT further amplified this relaxation relative to PVAT(–) rings. Notably, E– vessels demonstrated hypoxia-induced relaxation, which was evident in PVAT(+) rings (Figure 3-11). This suggests a direct effect of PVAT on vascular smooth muscle or the release of factors that act independently of the endothelium to promote vasodilation during acute hypoxic stress.

This finding aligns with a previous study by Maenhaut et al. (2010), which demonstrated that hypoxia (30 min of 95% N_2/5% CO_2) induced vasorelaxation in norepinephrine-precontracted thoracic aorta segments from male Swiss mice. This closely resembles the acute hypoxia approach used in my study, though performed in rats. In Maenhaut's study, hypoxia significantly relaxed precontracted aortic rings with intact adipose tissue, whereas only minimal relaxation was observed in arteries without adipose tissue; critically, removal of the endothelium did not alter the hypoxic relaxation, and inhibition of sGC had no effect, while high extracellular K^+, TEA and glibenclamide attenuated the response, consistent with K^+/K_{ATP} channel involvement via an endothelium-independent mechanism. Notably, this vasorelaxant effect of PVAT was preserved when vessels were precontracted with prostaglandin F2α or U46619, suggesting that hypoxia enhances PVAT-mediated relaxation across different constrictors. Similar findings were reported in porcine coronary arteries, where PVAT significantly enhanced hypoxia-induced relaxation following U46619-induced contraction (Donovan et al., 2018). In that study, exposure to hypoxic gas (95% N_2/5% CO_2 for 30 min) promoted vasorelaxation via a mechanism involving H_2S generated by cystathionine-ß-synthase (CBS), a transsulfuration enzyme that produces H_2S from L-cysteine and homocysteine (Zuhra et al., 2020). Additionally, Donovan et al. (2017) demonstrated that in vessels lacking PVAT, H_2S-mediated hypoxic relaxation was attributable to the vascular smooth muscle itself, further supporting H_2S as a key mediator of hypoxia-induced vasodilation independent of PVAT.

In my acute hypoxia protocol (hypoxia applied during PE tone), relaxation was robust and PVAT-dependent even in E– rings, consistent with K^+/KATP-dominated,

endothelium-independent mechanisms and PVAT-derived vasodilators (e.g. H_2S) augmenting the response (Maenhaut et al., 2010, Donovan et al., 2018). By contrast, in the pre-exposure + re-oxygenation protocol, subsequent PE and CK curves were recorded under normoxia. Re-oxygenation increases ROS from mitochondria, xanthine oxidase and NADPH oxidases, activates inflammatory signalling, and can impair endothelial NO bioavailability, classically blunting ACh- but not sodium nitroprusside (SNP)–mediated relaxation (Granger and Kvietys, 2015, Ku, 1982, VanBenthuysen et al., 1987, Tsao et al., 1990, Pearson et al., 1990, Kaeffer et al., 1996). In parallel, adipocytes up-regulate inflammatory adipokines (IL-1ß, IL-8, TNF-α) during hypoxia/re-oxygenation, with peaks often on re-oxygenation or during intermittent hypoxia–re-oxygenation (He et al., 2014, Hong et al., 2014). Together, these dynamics likely explain the pre-exposure findings: re-oxygenation may (i) modify the endothelial contribution, diminishing it when PVAT is present (ROS/inflammatory cross-talk) but preserving or enhancing it in PVAT(–)/E+ rings, and (ii) shift PVAT/VSMC signalling, thereby normalising CK responses across groups while augmenting PE contraction and CK relaxation in PVAT(+)/E– rings.

3.5 Conclusion

In conclusion, this study provides important insight into the complex and context-dependent roles of PVAT and the endothelium in regulating vascular tone under hypoxic conditions. The findings demonstrate that both the timing and nature of hypoxia exposure critically shape vascular responses. Pre-exposure to hypoxia elicited dual effects of PVAT in endothelium-denuded vessels, depending on the pharmacological stimulus. With PE, hypoxia enhanced contraction, while with CK, it promoted increased relaxation. The presence of an intact endothelium in the pre-exposure experiments played a compensatory protective role, preventing hypoxia-induced contraction with PE and relaxation with CK. In contrast, in the mesenteric arteries with PVAT, endothelial presence appeared to contribute to hypoxia-induced vasoconstriction. Notably, acute hypoxia applied during active contraction triggered a robust vasorelaxant response, which was significantly amplified by PVAT and occurred independently of the endothelium. These findings highlight the dynamic interplay between PVAT, the endothelium, and vascular smooth muscle, underscoring the vessel-specific heterogeneity in responses to oxygen deprivation.

Chapter 4 Depot-Specific Effects of Hypoxia on Adiponectin in 3T3-L1 Adipocytes and PVAT

4.1 Introduction

Adipose tissue (AT) is a dynamic endocrine organ that secretes various bioactive molecules known as adipokines; including leptin and adiponectin. These adipokines exert autocrine, paracrine, and endocrine effects, influencing physiological processes such as energy metabolism, insulin sensitivity, inflammation, immune responses and vascular function (Fernández-Alfonso et al., 2013, Petersen and Shulman, 2018, Koenen et al., 2021). Among adipose depots, PVAT is especially important as it envelops most blood vessels and influences vascular tone through paracrine and vasocrine mechanisms (Hillock-Watling and Gotlieb, 2022, Queiroz and Sena, 2024).

PVAT mediates anticontractile effects in multiple vascular beds, including the rat aorta (Löhn et al., 2002), coronary vessels (Aghamohammadzadeh et al., 2012) and mesenteric arteries (Verlohren et al., 2004, Lee et al., 2011). Consistent with this, in Chapter 3 I showed that under normoxic conditions, PVAT significantly attenuated PE-induced contractions in endothelium-intact rat thoracic aorta compared with PVAT(–) rings, highlighting the anticontractile influence of PVAT in the presence of the endothelium. Separately, Chapter 3 also demonstrated that in rat thoracic aorta, acute hypoxia applied during active contraction induces a robust vasorelaxation that is augmented by PVAT, although the mediators of this hypoxia-sensitive response remain to be defined. Under normoxic conditions, these effects are primarily mediated through the release of PVRFs, such as adiponectin (Chen et al., 2003), hydrogen peroxide (H_2O_2) (Gao et al., 2007), hydrogen sulphide (H_2S) (Fang et al., 2009) and nitric oxide (NO) (Gil-Ortega et al., 2014, Victorio et al., 2016). PVAT promotes vasodilation via both endothelium-dependent and endothelium-independent mechanisms (Gao et al., 2007). Importantly, the secretory profile of PVAT differs from other adipose depots, resulting in depot-specific differences in PVAT-mediated anticontractile effects. In mice, aortic PVAT secretes lower levels of adiponectin and leptin while releasing higher levels of IL-6, IL-8, and MCP-1, compared to subcutaneous and perirenal AT (Chatterjee et al., 2009). These differences reflect anatomical and phenotypic diversity. For instance, thoracic PVAT exhibits BAT-like features, whereas mesenteric and abdominal PVAT resembles WAT (Padilla et al., 2013, Gálvez-Prieto et al., 2008, Cinti, 2011). This phenotypic heterogeneity influences regional vascular responses. For example, thoracic PVAT shows greater

anticontractile activity, likely due to higher eNOS expression and NO availability, compared to abdominal PVAT (Hwej et al., 2024, Victorio et al., 2016). Norepinephrine (NE) levels in thoracic PVAT are approximately seven times higher than in mesenteric PVAT (Ahmad et al., 2019). Jeong et al. (2018) attributed this elevated NE to the BAT-like nature of thoracic PVAT, which is thermogenically active and also to rich sympathetic innervation. These depot-specific characteristics may contribute to regional disparities in vascular risk, as WAT-like PVAT depots are more associated with atherosclerosis and vascular dysfunction (Padilla et al., 2013, Yap et al., 2021). However, how hypoxia differentially regulates BAT-like thoracic versus WAT-like mesenteric PVAT remains poorly characterised.

Adiponectin was first identified in human plasma and differentiated 3T3-L1 adipocytes (Scherer et al., 1995, Nakano et al., 1996). Before its metabolic significance was fully understood, it was not widely recognised that adipose tissue could produce a hormone with insulin-sensitising properties (Combs and Marliss, 2014, Hu et al., 1996). Since then, adiponectin has emerged as a key regulator of metabolic homeostasis, demonstrating anti-inflammatory (Huang et al., 2008), anti-fibrotic (Shafiei et al., 2011), anti-apoptotic (Ye et al., 2014), and anti-lipotoxic effects (Xu et al., 2003). It also enhances insulin sensitivity and reduces ceramide accumulation (Holland et al., 2010). In the vascular system, adiponectin acts as a key PVRF with potent vasodilatory properties (Sena et al., 2017, Chen et al., 2003). These effects are mediated by the adiponectin receptors AdipoR1 and AdipoR2, which are expressed in adipose and vascular tissues and signal via AMPK to activate eNOS, thereby enhancing endothelial NO bioavailability (Chen et al., 2003, Antoniades et al., 2009, Kadowaki et al., 2006, Yamauchi and Kadowaki, 2008). In murine mesenteric arteries, adiponectin promotes vasorelaxation via AdipoR1 on endothelial cells (Lynch et al., 2013). In VSMCs, it induces vasorelaxation through the activation of Kv and BK_{Ca} channels in both aortic and mesenteric vessel rings (Fésüs et al., 2007, Lynch et al., 2013). In mesenteric arteries, $ß_3$-adrenergic receptor stimulation by the sympathetic neurotransmitter, norepinephrine (NE), triggers PVAT to release adiponectin, which then activates BK_{Ca} channels and induces NO release, leading to vasodilation (Weston et al., 2013). However, the hypoxic environment present in obese individuals markedly suppresses adiponectin expression. This reduction in adiponectin levels is, at least

in part, due to endoplasmic reticulum (ER) stress, with the ER stress marker CHOP known to suppress adiponectin promoter activity. Hypoxia-induced mRNA destabilisation further lowers adiponectin production (Engin, 2024, Hosogai et al., 2007).

Adipose tissue hypoxia is increasingly recognised as a central mechanism linking obesity to vascular dysfunction and chronic inflammation. As adipose depots expand, particularly via hypertrophy, limited oxygen diffusion and insufficient angiogenesis result in localised hypoxia that drives metabolic stress, inflammation, and altered adipokine secretion (Trayhurn, 2013, Sun et al., 2011, Brahimi-Horn and Pouysségur, 2007, Huynh et al., 2025). In both murine (3T3-F442A and 3T3-L1) and in primary human adipocytes differentiated from subcutaneous preadipocytes, hypoxia triggers a shift in adipokine expression toward a pro-inflammatory profile, including the upregulation of leptin, VEGF, IL-6, PAI-1, and matrix metalloproteinases (MMPs), while concurrently downregulating adiponectin and haptoglobin (Wang et al., 2007, Chen et al., 2006, Lolmede et al., 2003). This imbalance between pro- and anti-inflammatory factors contributes to endothelial dysfunction, reduced NO bioavailability, and impaired vasodilation, thereby promoting hypertension and atherosclerosis. (Chang et al., 2020b, Gálvez-Prieto et al., 2008, Quesada et al., 2018). Hypoadiponectinemia resulting from adipose tissue hypoxia under conditions of obesity has subsequently been linked with insulin resistance, type 2 diabetes, cardiovascular disease, and other metabolic complications (Kadowaki et al., 2006). Supporting this, Badran et al. (2019) demonstrated that hypoxia abolishes the anticontractile function of PVAT in the abdominal aorta, an effect reversed by exogenous adiponectin. In obese diabetic KKAy mice fed a HFD, both adiponectin and its receptor mRNA were significantly downregulated, which correlated with reduced insulin sensitivity (Yamauchi et al., 2001, Tsuchida et al., 2005). Furthermore, adiponectin knockout mice exhibit increased susceptibility to diet-induced insulin resistance, linked to increased TNF-α levels and decreased FATP-1 and IRS-1 expression (Maeda et al., 2002). HFD-fed mice exhibit a ~70% reduction in PVAT adiponectin and a complete loss of its anticontractile effect, findings that were also observed in obese patients (Aghamohammadzadeh et al., 2013, Almabrouk et al., 2018). Notably, this effect was reversed after bariatric surgery or treatment with antioxidant enzymes (Aghamohammadzadeh et al., 2013).

Given the importance of adiponectin in vascular regulation and the evidence that hypoxia suppresses its expression, several questions remain regarding how acute hypoxia alters Adipoq transcription, adiponectin protein and secretion in a depot-dependent manner, and whether any such changes contribute to PVAT-dependent vasorelaxation. Thus, this study examines the impact of acute hypoxia on adiponectin levels and Adipoq mRNA in 3T3-L1 adipocytes and in thoracic versus mesenteric PVAT, and, building on Chapter 3 where PVAT amplified hypoxia-induced relaxation in rat thoracic aorta, tests whether adiponectin signalling contributes to that response.

4.2 Aims

1. To analyse changes in adiponectin expression and Adipoq mRNA under hypoxia in 3T3-L1 adipocytes.
2. To investigate the impact of hypoxia on adiponectin (Adipoq) gene expression, protein levels, and secretion in thoracic and mesenteric PVAT.
3. To explore the role of pharmacological modulators, including $ß_3$-AR agonists and the adiponectin receptor-1 blocker (AdipoR1B), in modulating hypoxia-induced vascular relaxation.
4. To analyse the broader adipokine profile in thoracic PVAT and its modulation by hypoxia.

4.3 Results

4.3.1 LDH release as a marker of hypoxia-induced cytotoxicity in 3T3-L1 adipocytes

To determine whether hypoxic exposure induces cytotoxic effects in 3T3-L1 adipocytes, lactate dehydrogenase (LDH) activity in the culture medium was measured as an indicator of LDH released from damaged cells and thus plasma membrane injury. The LDH assay has previously been used to assess cytotoxic responses in 3T3-L1 adipocytes and other adipose tissue models (Chung and Hyun, 2021, Aboy-Pardal et al., 2024). LDH activity was measured under both $CoCl_2$- and gas-induced hypoxic conditions. Cells treated with 200 µM $CoCl_2$ for 1 or 4 hours showed no significant changes in extracellular LDH activity compared with normoxic controls. Under gas-induced hypoxia, no significant changes were detected at 1 or 3 hours, whereas a significant increase in extracellular LDH activity was observed at 6 hours ($p<0.05$) (Figure 4-1).

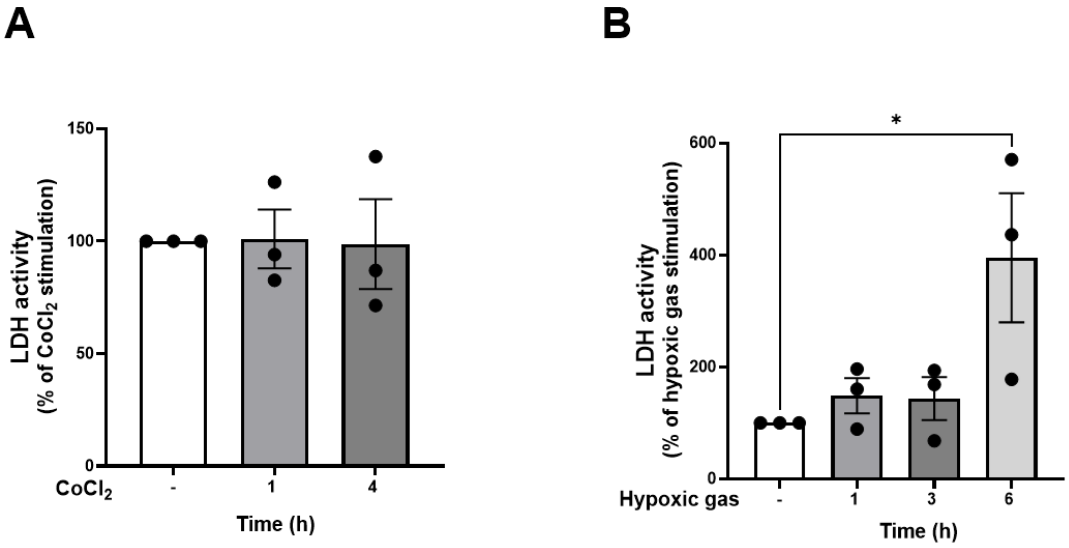

Figure 4-1 Effect of hypoxia on LDH activity in 3T3-L1 adipocyte cells.
Lactate dehydrogenase (LDH) activity was measured in the culture medium of 3T3-L1 adipocytes under normoxic and hypoxic conditions. **(A)** Cells were treated with 200 µM $CoCl_2$ for 1 and 4 hours. **(B)** Cells were exposed to a hypoxic gas mixture (94% N_2, 5% CO_2, 1% O_2 (sealed chamber)) for 1, 3, or 6 hours. In both experiments, untreated cells maintained under normoxia served as the control group. LDH levels are presented as percent fold-change relative to untreated control cells and expressed as mean ± SEM from three independent experiments (n=3). Statistical analysis was performed using one-way ANOVA followed by Dunnett's post-hoc test to compare each treatment group with untreated cells. Asterisks indicate statistical significance (*$p < 0.05$).

4.3.2 Cytotoxicity assessment (LDH activity) in thoracic and mesenteric PVAT under normoxia and hypoxia

To assess whether hypoxia induced cytotoxic effects in PVAT, lactate dehydrogenase (LDH) activity was measured in the conditioned media from thoracic and mesenteric PVAT samples. PVAT samples were initially incubated under normoxic conditions for 30 minutes, followed by continued normoxia or exposure to hypoxia for an additional 30 minutes. In thoracic PVAT, no significant differences in LDH activity were observed between normoxia and hypoxia (Figure 4-2A). Similarly, no significant changes in LDH activity were detected in mesenteric PVAT under either condition (Figure 4-2B).

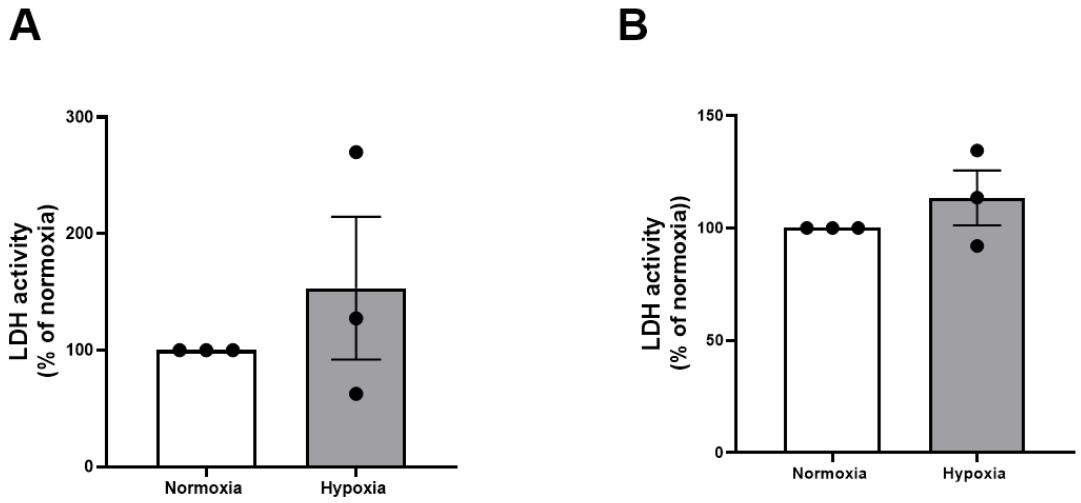

Figure 4-2 Effect of hypoxia on LDH activity in thoracic and mesenteric PVAT of rats under normoxic and hypoxic conditions.
Thoracic and mesenteric PVAT samples were initially incubated under normoxic conditions (95% O_2 and 5% CO_2) for 30 minutes, followed by either continued normoxia or exposure to hypoxia (95% N_2 and 5% CO_2 (open bath)) for an additional 30 minutes. LDH activity in the conditioned media was measured as an indicator of cytotoxicity. **(A)** LDH activity in thoracic PVAT-conditioned media. **(B)** LDH activity in mesenteric PVAT-conditioned media. Data are presented as mean ± SEM from three independent experiments (n=3) and as percent fold-change relative to normoxia. Statistical analysis was performed using an unpaired Student's t-test.

4.3.3 Hypoxia suppresses adiponectin expression in 3T3-L1 adipocytes

Adiponectin, secreted by adipose tissue, exerts anti-inflammatory and vasodilatory effects and promotes NO signalling via AMPK–eNOS (Ebrahimi-Mamaeghani et al., 2015, Yamauchi and Kadowaki, 2008, Withers et al., 2014). Since obesity is associated with PVAT hypoxia and inflammation, and Saxton et al. (2021) showed PVAT dysfunction in a relatively acute diet-induced obesity model, including reduced adiponectin secretion and loss of adiponectin vasodilator action, I hypothesised that hypoxia would suppress adiponectin expression in 3T3-L1 adipocytes. Protein expression of adiponectin was measured first to establish the primary phenotypic effect of hypoxia. The accompanying transcriptional response under gas hypoxia was then reported (Section 4.3.4). To test this, cells were treated with 200 μM $CoCl_2$ for 4 hours. Western blot analysis revealed a significant reduction in adiponectin protein levels compared with untreated cells ($p < 0.0001$; Figure 4-3). To confirm these findings under more physiologically relevant conditions, I exposed cells to a hypoxic gas mixture in a sealed chamber filled with (94% N_2, 5% CO_2, 1% O_2) for 1, 3, and 6 hours. As shown in Figure 4-4, gas-induced hypoxia significantly downregulated adiponectin expression at all time points examined ($p < 0.01$). Notably, although 6 hours of gas hypoxia produced a significant rise in extracellular LDH (Section 4.3.1), downregulation of adiponectin was already obvious at 1–3 hours when LDH was unchanged, indicating a hypoxia-driven regulatory effect rather than secondary toxicity; the 6-hour time point is included as an upper-limit time point to illustrate the trend under more severe stress.

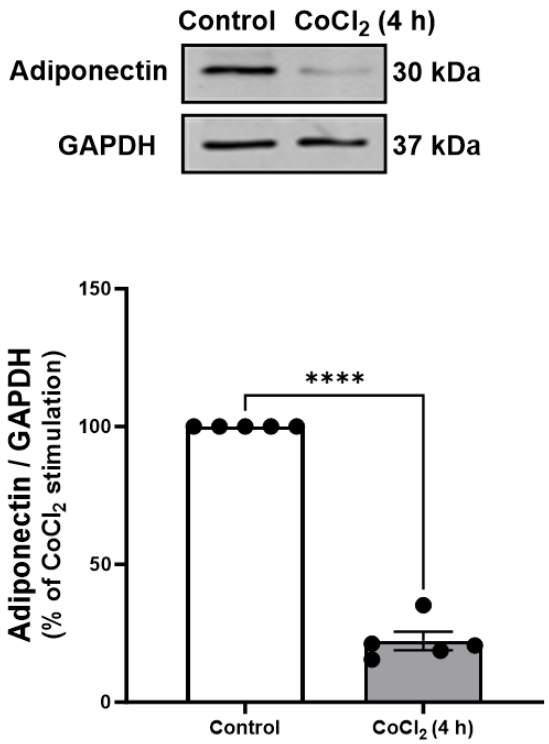

Figure 4-3 The effect of cobalt chloride-induced hypoxia on adiponectin expression in 3T3-L1 adipocytes.
Representative immunoblot and quantitative analysis showing the effect of $CoCl_2$-induced hypoxic conditions (200 µM, 4-hour exposure) on adiponectin expression in 3T3-L1 adipocytes compared with untreated cells. Adiponectin levels were normalised to GAPDH, and data are expressed as percent fold-change relative to untreated control cells. The adiponectin band quantified corresponded to ~30 kDa, and GAPDH corresponded to ~37 kDa. Results are presented as mean ± SEM from five independent experiments (n = 5). Statistical analysis was performed using an unpaired Student's t-test. Asterisks indicate statistical significance (****$p < 0.0001$).

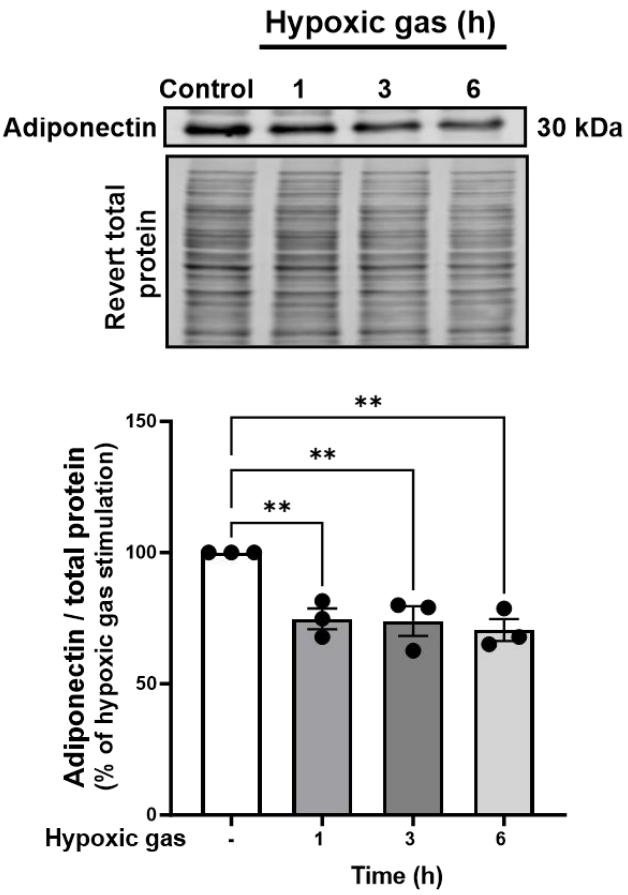

Figure 4-4 The effect of gas-induced hypoxia on adiponectin expression in 3T3-L1 adipocytes.
Representative Western blot images and quantitative analysis of adiponectin expression in 3T3-L1 adipocytes exposed to a hypoxic gas mixture (94% N_2, 5% CO_2, 1% O_2) for 1, 3, and 6 hours. Adiponectin levels were normalised to total protein stain, and data are expressed as percent fold-change relative to untreated control cells. The adiponectin band quantified corresponded to ~30 kDa. Results are presented as mean ± SEM from three independent experiments (n=3). Statistical analysis was performed using one-way ANOVA followed by Dunnett's post-hoc test. Asterisks indicate statistical significance (**$p < 0.01$).

4.3.4 Adipoq gene expression during gas-induced hypoxia in 3T3-L1 adipocytes

Given the observed reduction in adiponectin protein levels under gas-induced hypoxia, I next investigated whether this effect was reflected at the transcriptional level by examining Adipoq gene expression. Because both $CoCl_2$ and gas hypoxia reduced adiponectin protein to a similar extent (Figure 4-3; Figure 4-4), gene expression was assessed under gas hypoxia only, as this more closely models physiological oxygen deprivation and avoids potential side effects associated with chemical mimetics. 3T3-L1 adipocytes were exposed to a hypoxic gas mixture (94% N_2, 5% CO_2, 1% O_2) for 1, 3, and 6 hours. Quantitative RT-PCR analysis revealed a time-dependent suppression of Adipoq mRNA expression, with a significant downregulation observed at 3 hours ($p<0.01$) and 6 hours ($p < 0.05$)

compared to normoxic controls. A slight, non-significant upward trend was noted at 1 hour (p = 0.0642), before declining significantly at later time points (Figure 4-5).

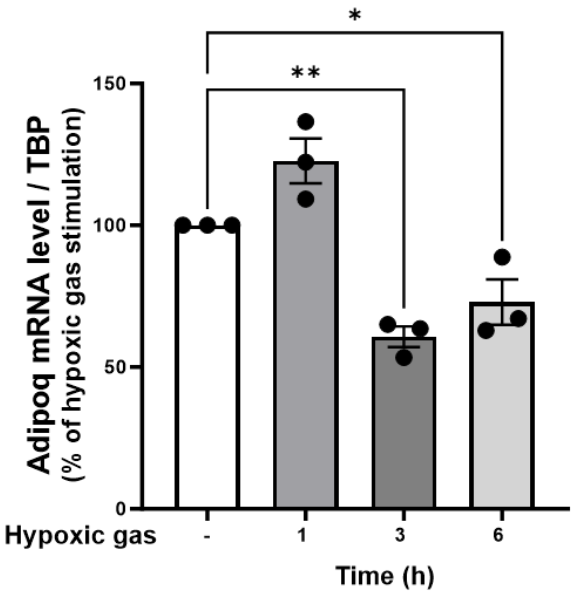

Figure 4-5 Effects of gas-induced hypoxia on Adipoq mRNA level in 3T3-L1 adipocytes. 3T3-L1 adipocytes were exposed to a hypoxic gas mixture (94% N_2, 5% CO_2, 1% O_2) for 1, 3, or 6 hours. Total RNA was extracted, and Adipoq mRNA levels were quantified by quantitative RT-PCR. Expression levels were normalised to TATA-binding protein (TBP) mRNA and are presented as percent fold-change relative to untreated control cells. Data represent the mean ± SEM from three independent experiments (n=3). Statistical analysis was performed using one-way ANOVA followed by Dunnett's post-hoc test. Asterisks indicate statistical significance (*p < 0.05, **p < 0.01).

4.3.5 Effect of hypoxia on Adipoq gene expression in thoracic and mesenteric PVAT

Following the assessment of Adipoq gene expression in 3T3-L1 adipocytes, I next investigated the effect of hypoxia on adiponectin (Adipoq) gene expression in thoracic and mesenteric PVAT. Adipoq mRNA levels were measured by quantitative RT-PCR in PVAT samples that were initially maintained under normoxic conditions and then either continued under normoxia or changed to hypoxic conditions. In thoracic PVAT, hypoxia induced a significant decrease in Adipoq mRNA expression compared to normoxia ($p < 0.001$) (Figure 4-6A). In contrast, no significant differences in Adipoq mRNA expression were observed between normoxic and hypoxic conditions in mesenteric PVAT (Figure 4-6B).

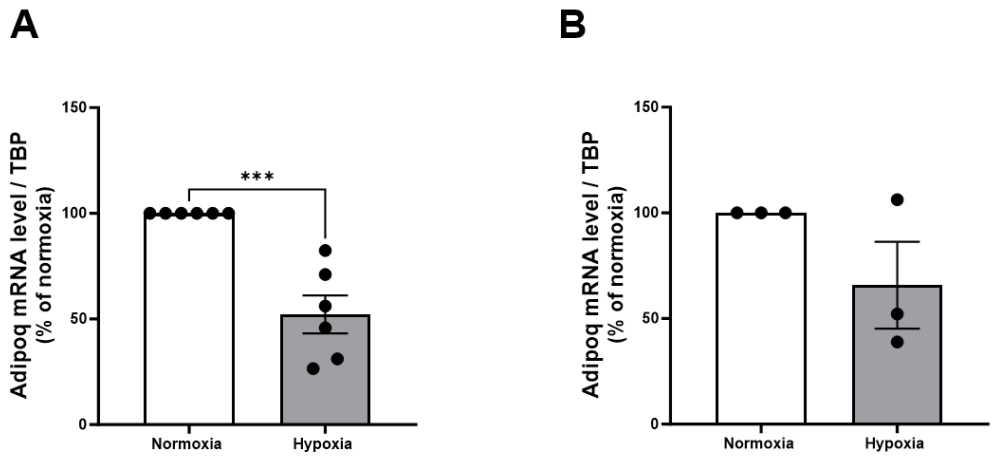

Figure 4-6 Effect of hypoxia on Adipoq mRNA expression in thoracic and mesenteric PVAT. Thoracic and mesenteric PVAT samples were initially incubated under normoxic conditions (95% O_2 and 5% CO_2) for 30 minutes, followed by continued normoxia or exposure to hypoxia (95% N_2 and 5% CO_2) for an additional 30 minutes. Total RNA was extracted, and Adipoq mRNA levels were quantified by quantitative RT-PCR. Expression levels were normalised to TATA-binding protein (TBP) mRNA and are presented as percentage relative to normoxic controls. Data are presented as mean ± SEM from six independent experiments for thoracic PVAT **(A)** and three independent experiments for mesenteric PVAT **(B)**. Statistical analysis was performed using unpaired Student's t-test. Asterisks indicate statistical significance (***p < 0.001).

4.3.6 Effect of hypoxia on adiponectin protein expression in thoracic and mesenteric PVAT lysates

The effect of hypoxia on adiponectin protein levels was investigated in thoracic and mesenteric PVAT tissue lysates. PVAT samples were initially incubated under normoxic conditions for 30 minutes, followed by either continued normoxia or exposure to hypoxic gas for an additional 30 minutes. Western blot analysis revealed a significant decrease in adiponectin protein levels in thoracic PVAT under hypoxia compared to normoxia ($p < 0.0001$) (Figure 4-7A). In contrast, no significant differences in adiponectin expression were observed in mesenteric PVAT between normoxic and hypoxic conditions (Figure 4-7B). To assess adiponectin secretion, conditioned media collected from thoracic PVAT were analysed by Western blotting. No significant differences in adiponectin levels in the media were detected between normoxic and hypoxic conditions (Figure 4-8).

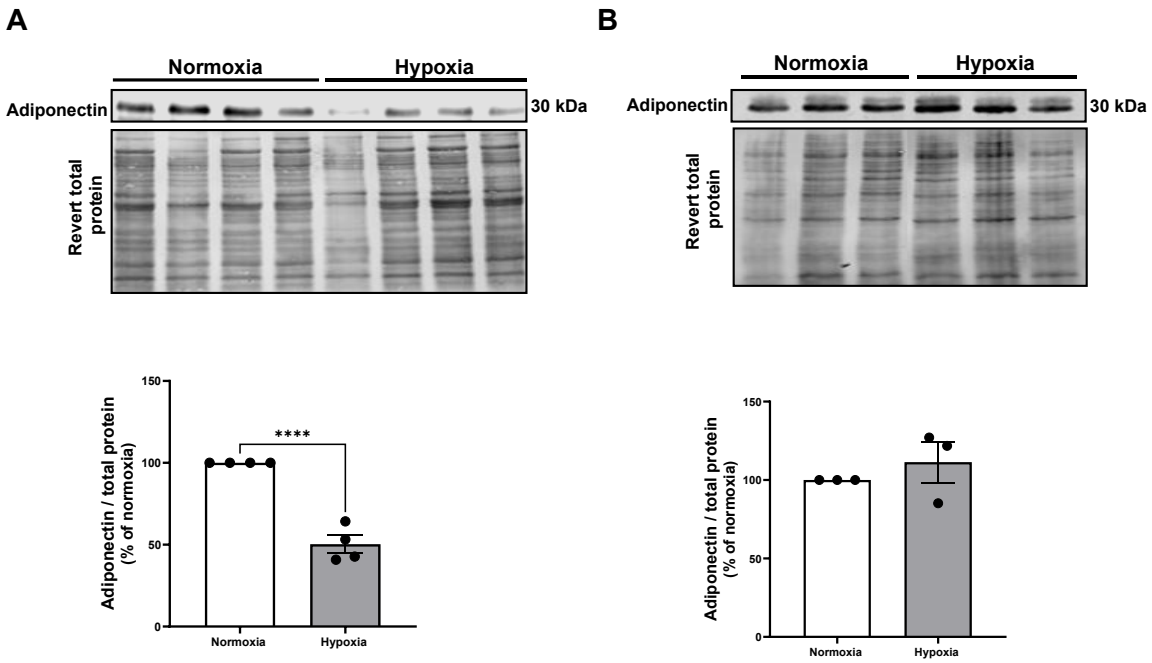

Figure 4-7 Adiponectin expression in thoracic and mesenteric PVAT under normoxic and hypoxic conditions.

Immunoblot and quantification showing adiponectin expression in rat PVAT samples. **(A)** Thoracic PVAT under normoxic and hypoxic conditions. **(B)** Mesenteric PVAT under normoxic and hypoxic conditions. Adiponectin levels were quantified relative to total protein stain. The adiponectin band quantified corresponded to ~30 kDa. Data are presented as mean ± SEM from four independent experiments for thoracic PVAT (n=4) and three independent experiments for mesenteric PVAT (n=3) and are presented as percentage relative to normoxic controls. Statistical analysis was performed using an unpaired Student's t-test. Asterisks indicate statistical significance (****$p < 0.0001$).

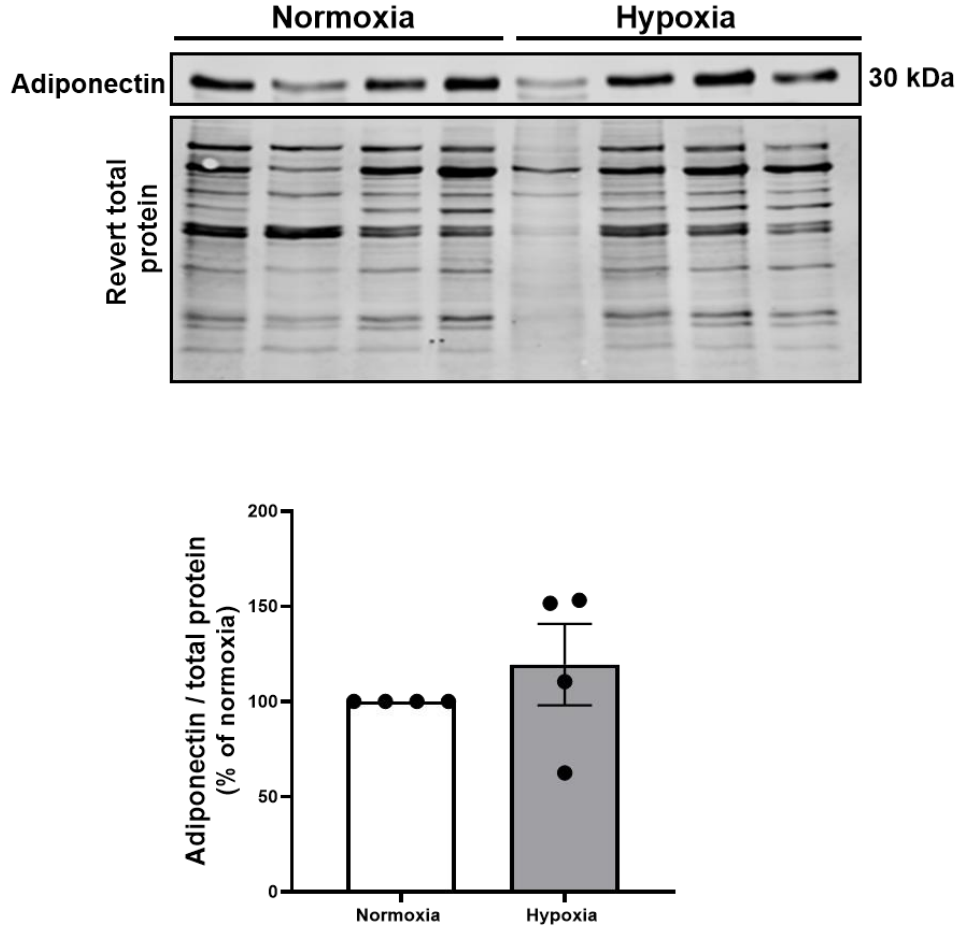

Figure 4-8 Expression of adiponectin in the conditioned media of thoracic PVAT under normoxic and hypoxic conditions.
Western blot analysis of adiponectin in conditioned media collected from thoracic PVAT. PVAT samples were initially incubated under normoxic conditions (95% O_2 and 5% CO_2) for 30 minutes, followed by continued normoxia or exposure to hypoxia (95% N_2 and 5% CO_2) for an additional 30 minutes. Adiponectin levels in the conditioned media were normalised to total protein stain. The adiponectin band quantified corresponded to ~30 kDa. Data are presented as mean ± SEM from four independent experiments (n=4) and are presented as percentage relative to normoxic controls. Statistical analysis was performed using an unpaired Student's t-test.

4.3.7 Adiponectin levels in PVAT lysates under normoxia and hypoxia

Given the observed effects of hypoxia on adiponectin protein expression in thoracic PVAT, adiponectin content within PVAT lysates was assessed to determine whether hypoxia altered baseline intracellular levels. Thoracic and mesenteric PVAT samples were initially maintained under normoxic conditions for 30 minutes, followed by either continued normoxia or exposure to hypoxia for an additional 30 minutes. Adiponectin protein levels were quantified by ELISA. No significant differences in adiponectin content were observed between normoxic and hypoxic conditions in either thoracic or mesenteric PVAT. However, independent of

oxygenation, thoracic PVAT had significantly higher baseline adiponectin levels than mesenteric PVAT (Figure 4-9; $p < 0.05$).

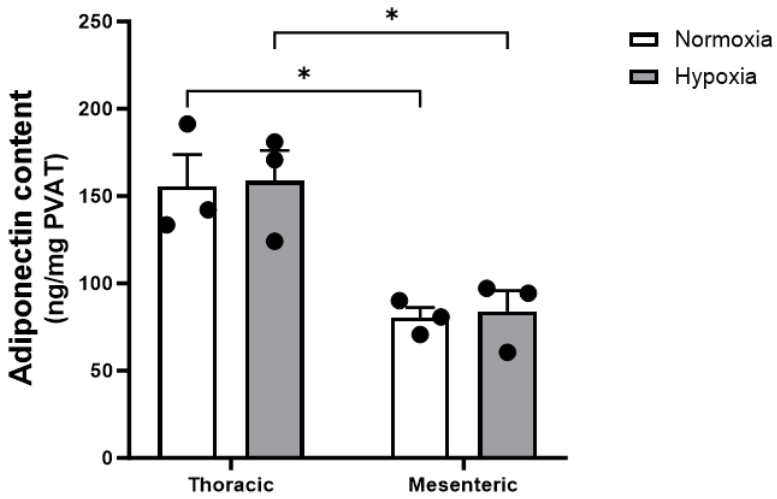

Figure 4-9 Adiponectin levels in thoracic and mesenteric PVAT lysates under normoxic and hypoxic conditions.
Adiponectin levels were quantified by ELISA in lysates of thoracic and mesenteric PVAT from rats exposed to normoxic or hypoxic conditions. PVAT samples were maintained under normoxic conditions or exposed to hypoxia for 30 minutes. Adiponectin concentrations are expressed as ng adiponectin per mg tissue. Data are presented as mean ± SEM from three independent experiments (n = 3). Statistical analysis was performed using two-way ANOVA followed by Tukey's post-hoc test. Asterisks indicate statistical significance (*$p < 0.05$, **$p < 0.01$).

4.3.8 Effect of normoxic and hypoxic conditions on adiponectin release in the conditioned media of thoracic and mesenteric PVAT

Although PVAT across different anatomical locations may exhibit features of either brown or white adipose tissue, its secretory profile shows distinct differences compared to other fat depots. For example, compared to subcutaneous and perirenal adipose tissue, mouse aortic PVAT has been shown to secrete substantially less adiponectin and leptin, while producing higher levels of pro-inflammatory cytokines including IL-6, IL-8, and MCP-1 (Chatterjee et al., 2009). To investigate whether hypoxia influenced adiponectin secretion from PVAT, conditioned media collected from thoracic and mesenteric PVAT samples under normoxia or hypoxia were analysed. Adiponectin concentrations in conditioned media were quantified by ELISA. A trend toward increased adiponectin release was observed in conditioned media from hypoxic thoracic PVAT compared to normoxic controls ($p = 0.0506$), while no significant difference was detected in mesenteric PVAT. Thoracic PVAT released significantly higher levels of

adiponectin compared to mesenteric PVAT under both normoxic ($p < 0.01$) and hypoxic conditions ($p < 0.0001$) (Figure 4-10).

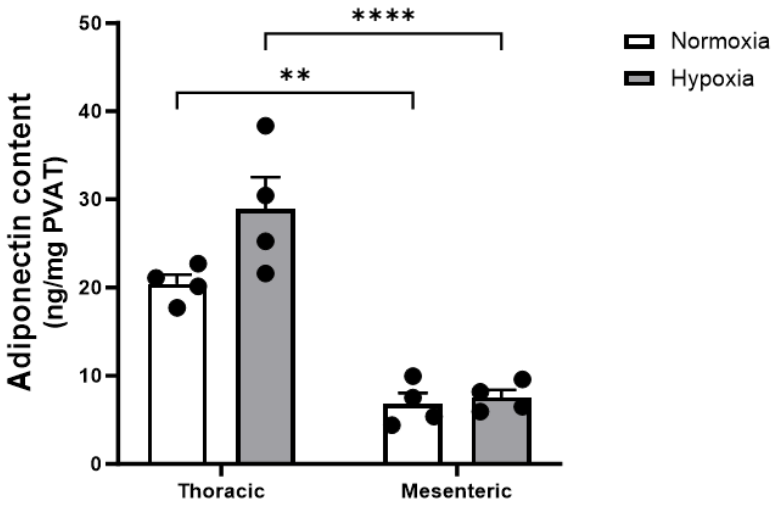

Figure 4-10 Adiponectin levels in conditioned media from thoracic and mesenteric PVAT under normoxic and hypoxic conditions.
Adiponectin concentrations were measured by ELISA in conditioned media collected from thoracic and mesenteric PVAT samples exposed to normoxic or hypoxic conditions. Adiponectin concentrations are expressed as ng adiponectin per mg tissue. Data are presented as mean ± SEM from four independent experiments (n=4). Statistical analysis was performed using two-way ANOVA followed by Tukey's post-hoc test. Asterisks indicate statistical significance (**$p < 0.01$, ****$p < 0.0001$).

4.3.9 Effect of β_3-AR agonist and AdipoR1B on hypoxia-induced relaxation of thoracic aorta

Since previous studies have shown that β_3-adrenoceptor stimulation in PVAT produces adiponectin-dependent anticontractile/vasodilatory effects (Saxton et al., 2018, Weston et al., 2013), this experiment investigated whether modulating β_3-AR signalling or blocking adiponectin receptors would alter hypoxia-induced relaxation in thoracic aortic rings. To test this, rings precontracted with a single concentration of PE (1 μM) were pretreated with the β_3-AR agonist CL-316,243 (10 μM) or a selective adiponectin receptor 1 blocker (AdipoR1B; 5 μg/mL) prior to 30 minutes hypoxic exposure.

In PVAT(+) /E+ and PVAT(+) /E- rings, CL-316,243 and AdipoR1B did not significantly change hypoxia-induced relaxation compared with hypoxia-only rings (controls) (Figure 4-11A, B). However, in PVAT(-)/E+ rings, treatment with CL-316,243 significantly reduced relaxation responses ($p < 0.05$) (Figure 4-11C). In PVAT(-)/E- rings, no significant differences were observed among the group

treated with CL-316,243 compared to hypoxia-only rings (controls) (Figure 4-11D). Taken together, these data indicate that acute hypoxic relaxation in rat thoracic aorta is largely independent of AdipoR1 signalling and β_3-AR drive when PVAT is present, while β_3-AR activation can oppose hypoxic relaxation via an endothelium-dependent pathway that is revealed when PVAT is removed.

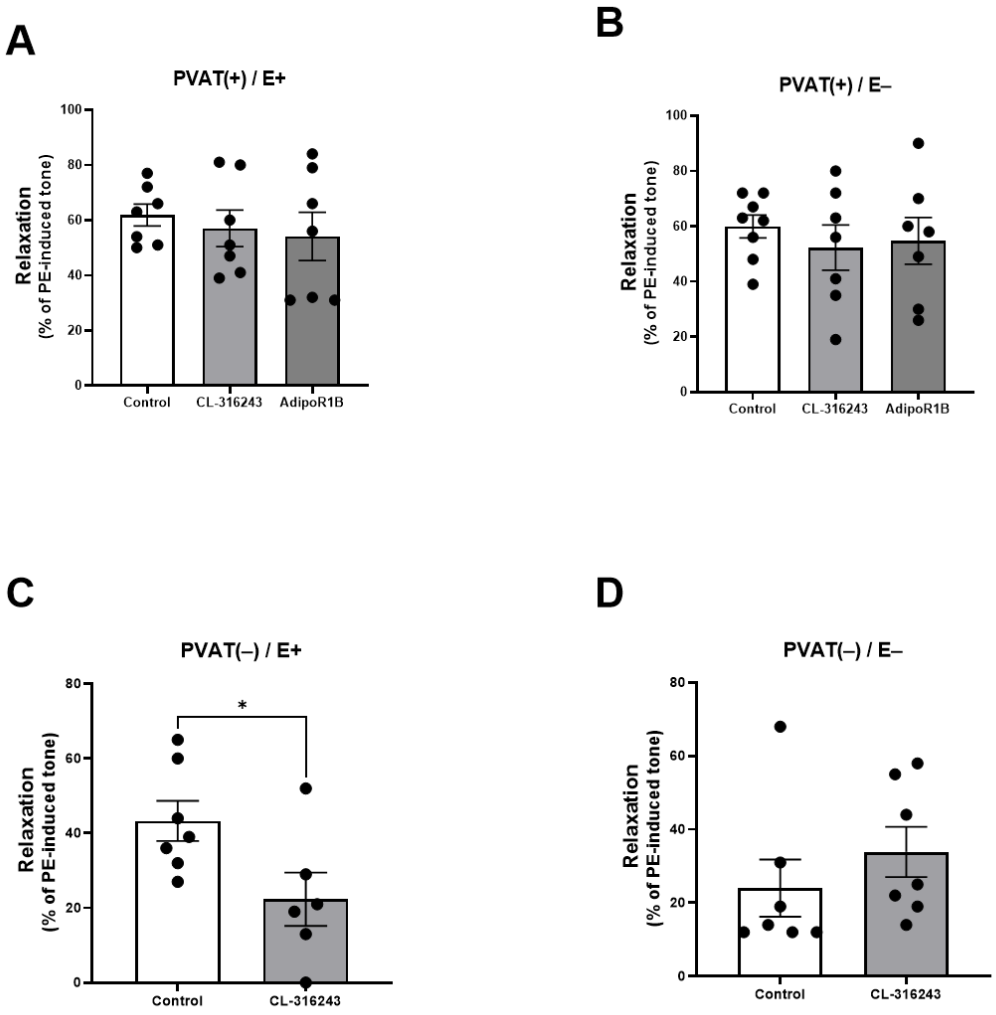

Figure 4-11 Effect of β_3-AR agonist and AdipoR1B on hypoxia-induced relaxation in thoracic aorta.
Thoracic aortic rings were precontracted with PE (1 µM) and treated with either the β_3-adrenoceptor agonist CL-316,243 (10 µM), the adiponectin receptor-1 blocker AdipoR1B (5 µg/mL), or left untreated as hypoxia-only control rings prior to hypoxic exposure (95% N_2 and 5% CO_2 for 30 minutes). Relaxation is expressed as a percentage of the precontracted tone induced by PE and presented as mean ± SEM from arteries obtained from different animals. **(A)** PVAT(+) /E+ rings (n = 7 for all groups). **(B)** PVAT(+) /E– rings (n = 8 control, 7 for all treatment groups). **(C)** PVAT(–)/E+ rings (n = 7 control, 6 for treatment groups). **(D)** PVAT(–)/E– rings (n = 7 for all groups). Statistical analysis was performed using one-way ANOVA followed by Dunnett's multiple comparisons test for panels A and B. As data in panel D were not normally distributed, panel C and D was analysed using the Mann–Whitney U test. Asterisks indicate statistical significance (*$p < 0.05$).

4.3.10 Exploratory adipokine profiling of thoracic PVAT under acute hypoxia

To broaden the analysis beyond single mediators, adipokines in thoracic PVAT-conditioned media under normoxia and acute hypoxia were profiled, complementing the adiponectin work in this chapter. Conditioned media were collected after an initial 30-minute normoxic incubation and after a further 30 minutes in either normoxia or hypoxia (95% N_2, 5% CO_2), then analysed using the Proteome Profiler Rat Adipokine Array (30 analytes). Hypoxia qualitatively reduced several adipokines, including leukaemia inhibitory factor (LIF), insulin-like growth factor-binding protein-1 (IGFBP-1), interleukin-10 (IL-10) and resistin (Figure 4-12). Given the exploratory sample size (n = 2), no statistical testing was performed; these data provide a broader view of PVAT adipokines and highlight candidates for future investigation.

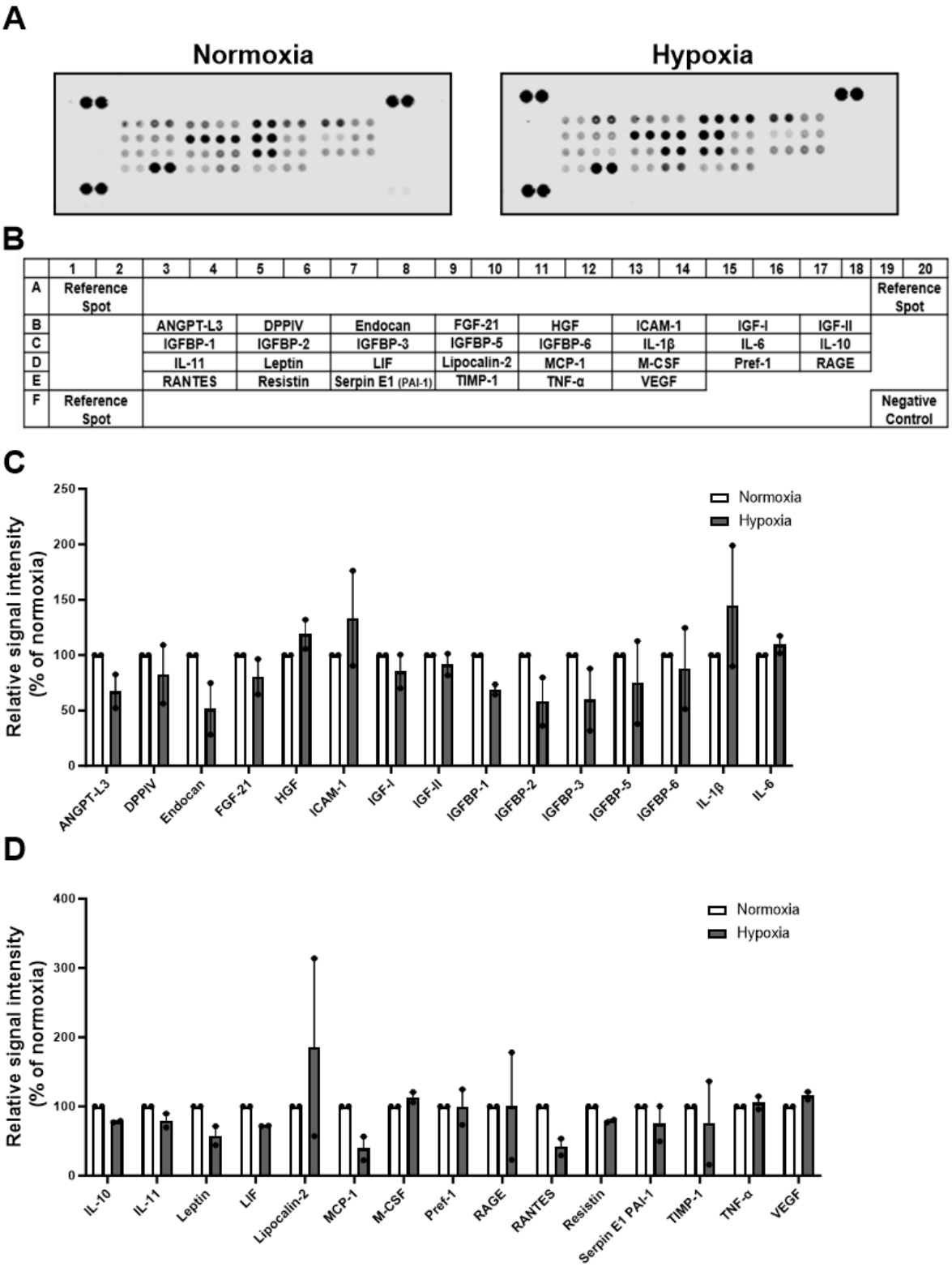

Figure 4-12 Adipokine expression levels in thoracic PVAT-conditioned medium under normoxic and hypoxic conditions.

Conditioned media were collected from thoracic PVAT samples maintained under normoxic conditions or exposed to hypoxic conditions, and adipokine levels were assessed using a Proteome Profiler Rat Adipokine Array kit containing 30 adipokine and adipokine-related antibodies spotted in duplicate. **(A)** Representative array images showing fluorescent detection of adipokines under normoxic and hypoxic conditions. **(B)** Array layout map indicating the position and identity of each adipokine on the membrane. **(C–D)** Quantification of 30 adipokines in thoracic PVAT-conditioned media. Signal intensities are presented as percentage relative to normoxia. Data are expressed as mean ± SD from two independent experiments (n=2) and expressed in arbitrary units. No statistical analysis was performed.

4.4 Discussion

The present study investigated whether acute hypoxia alters adiponectin in 3T3-L1 adipocytes (Adipoq mRNA and protein) and in thoracic versus mesenteric PVAT (Adipoq mRNA, protein and secretion), and whether adiponectin/β_3-adrenoceptor signalling contributes to the hypoxic relaxation of the rat thoracic aorta observed previously (Chapter 3). The data show that acute hypoxia selectively suppresses adiponectin expression in 3T3-L1 adipocytes and thoracic PVAT, but not mesenteric PVAT, with no evidence of acute cytotoxicity. This reduction in adiponectin under hypoxia is consistent with prior reports in adipocytes and adipose tissue exposed to low oxygen or obesity-associated hypoxia (Tsuchida et al., 2004, Hosogai et al., 2007, Ye et al., 2007, Wang et al., 2007, Chen et al., 2006, Magalang et al., 2009), supporting the effectiveness of the hypoxic challenge used here. Furthermore, thoracic PVAT exhibited higher basal adiponectin content than mesenteric PVAT irrespective of oxygenation. Functionally, hypoxic relaxation of thoracic aortic rings was preserved when PVAT was present, regardless of β_3-adrenoceptor or AdipoR1 manipulation. However, in PVAT-removed, endothelium-intact rings, β_3-adrenoceptor activation significantly reduced hypoxic relaxation, an effect absent when the endothelium was removed. These results indicate that acute hypoxic vasorelaxation is largely independent of PVAT-derived adiponectin and reveal an inhibitory, endothelium-dependent β_3-adrenoceptor pathway that is masked by PVAT (Table 4-1). Collectively, these findings highlight depot-specific and pathway-specific responses of PVAT to acute hypoxic stress.

Table 4-1 Summary of hypoxia-driven changes in Adiponectin and vascular function

<table>
<tr><th>3T3-L1 adipocytes (1–6 h hypoxia)</th><th>PVAT molecular changes (30 min hypoxia)</th></tr>
<tr><td>• Protein: ↓ adiponectin ($CoCl_2$ 4 h; 1–6 h gas hypoxia)
• mRNA (Adipoq): ↓ at 3–6 h (ns at 1 h)
• Cytotoxicity (LDH): ↔ (↑ only at 6 h)</td><td>• Thoracic PVAT: Adipoq mRNA ↓; Protein ↓; Secretion ↔ (trend ↑)
• Mesenteric PVAT: Adipoq mRNA ↔; Protein ↔; Secretion ↔
• Note: No acute cytotoxicity in either depot (LDH: ↔)</td></tr>
<tr><th colspan="2">Functional responses: hypoxic relaxation of thoracic aortic rings</th></tr>
<tr><td>• PVAT(+)/E+
• CL-316,243 (β_3-AR agonist): ↔
• AdipoR1 blocker: ↔
• → Hypoxic relaxation maintained (PVAT-supported)</td><td>• PVAT(+)/E-
• CL-316,243: ↔
• AdipoR1B: ↔
• → Hypoxic relaxation maintained (PVAT-supported)</td></tr>
<tr><td>• PVAT(-)/E+
• CL-316,243: ↓ relaxation*
•AdipoR1B: ↔
• → Endothelium-dependent β_3-AR effect opposes hypoxic relaxation
*Only significant effect observed across all modulators.</td><td>• PVAT(-)/E-
• CL-316,243: ↔
• AdipoR1B: ↔
• → Hypoxic relaxation unchanged</td></tr>
</table>

Before examining the specific effects on adiponectin, it was crucial to establish that the observed changes were not due to hypoxia-induced cytotoxicity. An LDH release assay confirmed that the hypoxic conditions used were not significantly cytotoxic to either cultured adipocytes or PVAT samples, except for a moderate increase after 6 h of gas-induced hypoxia in 3T3-L1 cells. These results are consistent with previous reports indicating that 3T3-L1 adipocytes exhibit elevated LDH levels only under high-stress conditions such as treatment with high dose of pinostilbene hydrate (200 μM) (Chung and Hyun, 2021, Aboy-Pardal et al., 2024). These findings indicate that the observed changes in adiponectin result directly from hypoxia, reflecting regulated transcriptional and post-transcriptional processes rather than non-specific cell death.

Both chemical ($CoCl_2$) and gas-induced hypoxia significantly reduced adiponectin protein levels in 3T3-L1 adipocytes. Gas hypoxia also induced a time-dependent suppression of Adipoq mRNA, with significant downregulation at 3 h and 6 h but not at 1 h, where a non-significant transient increase was observed. Adipoq mRNA was not measured under $CoCl_2$. This temporal pattern aligns with earlier findings by Ye et al. (2007) and Chen et al. (2006), who reported delayed transcriptional

downregulation of Adipoq under hypoxia in 3T3-L1 adipocytes, potentially reflecting early compensatory mechanisms followed by HIF-1α–mediated PPARγ suppression (Yun et al., 2002) and/or activation of ER-stress pathways (Hosogai et al., 2007). Mechanistically, CHOP suppresses adiponectin transcription in 3T3-L1 cells, with CHOP-10 disrupting the C/EBP binding site (−117/−73) (Chevillotte et al., 2007). Consistent with an ER-stress mechanism, Guo et al. (2017) showed that 5% O_2 reduced adiponectin mRNA and protein via PERK and IRE1 activation, and that inhibiting either branch restored expression. Notably, hypoxia can also reduce Adipoq expression via a HIF-1α–driven decrease in C/EBPα (with no change in PPARγ), as reported by Chen et al. (2006), indicating that distinct upstream signals ultimately act through C/EBP-dependent downregulation of the adiponectin promoter. Finally, the degree of protein suppression in my study appeared greater than mRNA suppression at early time points, consistent with a lag between transcript and protein changes (Wang et al., 2007) and compatible with additional post-transcriptional/post-translational regulation, such as impaired multimerisation or altered redox-dependent stability, given that hypoxia disrupts cellular redox balance (Magalang et al., 2009, Li and Shah, 2004).

In PVAT, acute hypoxia reduced Adipoq mRNA and adiponectin protein in thoracic PVAT (Figure 4-6, 4-7A) but not in mesenteric PVAT (Figure 4-6B, 4-7B). Independent of oxygenation, thoracic PVAT contained significantly more adiponectin than mesenteric PVAT in my study (Figure 4-9), and it released more adiponectin into conditioned media under both conditions (Figure 4-10). This depot specificity aligns with the known phenotypic heterogeneity of PVAT. Thoracic PVAT exhibits BAT-like characteristics with higher eNOS expression and NO production (Hwej et al., 2024, Victorio et al., 2016), whereas mesenteric PVAT is more WAT-like and pro-inflammatory (Cinti, 2011, Chatterjee et al., 2009). Higher adiponectin (and BAT characteristics) in thoracic PVAT may be particularly important for protecting the aorta (an artery prone to atherosclerosis), while lower adiponectin in mesenteric PVAT relates to its role in small artery function and blood pressure control. These differences align with reports that PVAT is richly innervated by the sympathetic nervous system, with ~97–98% of adipose nerves being sympathetic, and that $ß_3$-AR signalling is prominent in perivascular depots (Giordano et al., 2006, Saxton et al., 2019b). In mesenteric arteries, $ß_3$-AR stimulation of PVAT induces adiponectin release, activating BK_{Ca} channels and

enhancing NO-dependent dilation (Weston et al., 2013, Hanscom et al., 2024), and PVAT buffers norepinephrine by taking it up within the fat layer, so less reaches vascular smooth muscle to cause contraction (Saxton et al., 2018). Prior work also reports ~7-fold higher NE content in thoracic vs mesenteric PVAT, consistent with the BAT-like, highly innervated thoracic phenotype (Ahmad et al., 2019, Jeong et al., 2018, Hanscom et al., 2024, Sheng et al., 2016). While I did not quantify β_3-AR expression, NE content, or innervation here, these adrenergic features provide a plausible explanation for my observations: the higher basal adiponectin in thoracic PVAT may make hypoxic downregulation more readily detectable over the short exposure period, whereas the low-adiponectin mesenteric depot has limited scope for further reduction. Consistent with this, hypoxic relaxation in PVAT(+) rings was unchanged by β_3-AR or AdipoR1 manipulation, suggesting PVAT-derived dilator pathways were already involved, while in PVAT(–)/E+ rings β_3-AR agonism reduced relaxation, revealing an endothelium-dependent inhibitory β_3-AR influence that is normally masked by PVAT support.

Despite the intracellular suppression of adiponectin in thoracic PVAT under hypoxia, extracellular levels in conditioned media over 30 min did not change significantly, although there was a trend toward increased release, indicating a temporal dissociation between tissue content and measurable release within this short exposure period. This is consistent with hypoxia-related redox effects on protein processing (Li and Shah, 2004), and similar dissociations have been reported in adipocytes under hypoxia (Wang et al., 2007, Magalang et al., 2009).

Given evidence that β_3-adrenoceptor activation in PVAT produces adiponectin-dependent anticontractile/vasodilatory effects, including β_3-dependent adiponectin secretion during EFS (Saxton et al., 2018) and β_3-induced, adiponectin-mediated hyperpolarization (Weston et al., 2013), I hypothesised that pharmacological modulation of these pathways would alter hypoxic vasorelaxation. Contrary to this expectation, in PVAT(+) rings β_3-AR agonism or AdipoR1 blockade produced no significant change in hypoxia-induced relaxation, implying that PVAT-mediated hypoxic vasodilation was already at or near a functional ceiling and not further enhanced by additional β_3 drive. By contrast, in PVAT(–), endothelium-intact rings the β_3-AR agonist attenuated hypoxic relaxation, an effect absent after endothelial denudation, localising an inhibitory,

PVAT-independent action to the endothelium. Moreover, AdipoR1 blockade was ineffective across preparations, indicating that, in this acute condition, hypoxic vasorelaxation of the thoracic aorta occurs largely independent of adiponectin signalling. While β_3-AR–induced adiponectin release from PVAT is established in other conditions, my findings suggest it is not the dominant contributor to acute hypoxic relaxation in the thoracic aorta. Instead, an endothelial β_3-AR–dependent inhibitory pathway is unmasked when PVAT support is removed.

My results extend reports that chronic hypoxia or obesity-associated conditions reduce adiponectin by showing that acute hypoxia already induces depot-selective suppression in thoracic but not mesenteric PVAT, while extracellular adiponectin over 30 minutes and PVAT-dependent hypoxic relaxation are preserved. In abdominal aorta from male offspring exposed to gestational intermittent hypoxia, Badran et al. (2019) showed loss of the PVAT anticontractile effect together with lower circulating adiponectin and reduced PVAT adiponectin at protein and mRNA levels, and exogenous adiponectin restored function. In mouse aorta, HFD lowers PVAT adiponectin by ~70% and abolishes the anticontractile effect via an AMPK-related mechanism (Almabrouk et al., 2018). Systemically, obesity is associated with adipose hypoxia and reduced adiponectin expression (mRNA/protein) in epididymal WAT of ob/ob and diet-induced obese mice (Ye et al., 2007), and with downregulation of adiponectin and its receptors in adipose tissues that correlates with insulin resistance (Yamauchi et al., 2001, Tsuchida et al., 2005), including AdipoR1/R2 decreases in WAT, BAT and skeletal muscle of ob/ob mice (Tsuchida et al., 2004). In metabolic-syndrome rats, Cui et al. (2023) reported adipocyte hypertrophy, hypoadiponectinaemia, heightened contractile responses with impaired relaxation, a pro-inflammatory PVAT profile with reduced adiponectin, and reduced AdipoR1, AdipoR2, APPL and phosphorylated eNOS in the mesenteric artery, and further showed that chronic intermittent hypobaric hypoxia increased PVAT adiponectin, attenuated inflammatory cytokines and improved mesenteric vasorelaxation. Differences across studies likely reflect hypoxia protocol and exposure, including intermittent versus continuous stimuli, hypobaric versus normobaric gas, and exposure duration or severity. Taken together, my thoracic aorta data suggest that over a short exposure PVAT can maintain extracellular adiponectin and preserve hypoxic relaxation, possibly through mobilisation of existing stores or via compensatory dilators such as NO, H_2O_2 and H_2S (Gil-Ortega

et al., 2014, Gao et al., 2007, Fang et al., 2009), and that $ß_3$-adrenoceptor activation can exert an endothelium-dependent inhibitory influence when PVAT is absent, helping explain why $ß_3$-AR agonism enhanced PVAT anti-contractility in the work of Saxton et al. (2018) whereas it attenuated hypoxic relaxation in my PVAT(–)/E+ rings.

Although limited (n=2), the adipokine array was designed to provide a wider view of the thoracic PVAT secretome under acute hypoxia, and it suggests that 30 min hypoxia suppresses several adipokines, including LIF, IGFBP-1, IL-10, and resistin, supporting my adiponectin findings and indicating rapid reprogramming. Because n=2, statistical analysis was not possible. In line with this study, IL-10 falls at 2% O_2 in placenta (Royle et al., 2009) and is generally anti-inflammatory and reduced in obesity/metabolic syndrome (Esposito et al., 2003). In contrast, obese stromal vascular fraction shows higher basal TNF-α and IL-10 (O'rourke et al., 2011) and obese PVAT displays increased resistin and visfatin (Park et al., 2014b), underscoring that depot composition and chronic inflammatory status shape the baseline secretome and may mask or dilute the early hypoxia-induced pattern. IGFBP biology is context dependent. Hypoxia upregulates IGFBP-1 mRNA in HepG2 cells (Tazuke et al., 1998), whereas my PVAT data indicate an early decrease in secreted IGFBP-1, consistent with translational or release control. LIF also shows marked temporal dynamics in hypoxic–ischaemic models, with elevations decreasing by 48–72 h (Lin et al., 2020), reinforcing time sensitivity. Future work should determine whether these acute adipokine shifts contribute to PVAT-dependent hypoxic relaxation by add-back or neutralisation during PVAT(+/–) wire-myography under hypoxia.

4.5 Conclusion

This chapter demonstrates that acute hypoxia selectively suppressed adiponectin expression in 3T3-L1 adipocytes and in thoracic PVAT without evidence of cytotoxicity, whereas mesenteric PVAT was unchanged over the same short exposure. In the thoracic aorta, hypoxic vasorelaxation was largely adiponectin independent. When PVAT was present, neither $ß_3$-AR agonist nor AdipoR1 blockade altered the response. In PVAT-depleted rings with an intact endothelium, the $ß_3$-AR agonist attenuated relaxation. Regarding adiponectin measurements, thoracic PVAT showed higher basal adiponectin content and greater release into conditioned media than mesenteric PVAT under both normoxia and hypoxia. Collectively, these findings highlight depot-specific regulation of adiponectin under acute hypoxia and indicate that the impact of $ß_3$-AR signalling on vascular tone depends on PVAT presence and endothelial integrity. Although hypoxia reduced adiponectin, these molecular changes did not translate into a measurable acute effect on hypoxic vascular relaxation. Thus, the role of adiponectin in the acute hypoxic contractile response remains inconclusive. Future work should test causality by manipulating adiponectin signalling during acute hypoxia (e.g., adiponectin replacement or neutralisation, selective AdipoR agonists/antagonists, or PVAT from Adipoq-deficient animals). In parallel, inhibiting alternative PVAT-derived dilators (NO, H_2O_2, H_2S) would assess compensatory pathways.

Chapter 5 Effects of Hypoxia on SphK1/S1P Signalling and Secretory Profiles in 3T3-L1 Adipocytes and PVAT

5.1 Introduction

Sphingolipids are fundamental structural components of mammalian cell membranes that also function as bioactive signalling molecules (Pyne and Pyne, 2000). Among them, sphingosine-1-phosphate (S1P) is a central regulator of numerous physiological processes, including cell survival, proliferation, migration, and angiogenesis (Spiegel and Milstien, 2011, Maceyka and Spiegel, 2014, Pyne and Pyne, 2011). S1P is generated intracellularly through the phosphorylation of sphingosine by two closely related kinases, sphingosine kinase 1 (SphK1) and sphingosine kinase 2 (SphK2) (Pyne and Pyne, 2000, Hannun and Obeid, 2008). The balance between S1P synthesis and degradation tightly regulates cellular S1P levels, allowing cells to adapt to environmental and metabolic stress (Maceyka et al., 2012, Pyne et al., 2016).

Although both SphK isoforms are widely expressed, their cellular distribution and functions differ. SphK1 is primarily cytosolic and has been associated with enhanced cell proliferation and survival, while SphK2 is localised to the nucleus and other organelles (Kohama et al., 1998, Igarashi et al., 2003). However, within a cell, both SphKs can move to other compartments (Pyne and Pyne, 2010). There are three isoforms for SphK1 (SphK1a/b/c) and there are two isoforms for SphK2 (SphK2a/b) (Liu et al., 2000, Okada et al., 2005). Importantly, SphK1 overexpression has been linked to inflammation, cancer, and metabolic dysfunction (Xia et al., 2000, Wang et al., 2014, Pyne and Pyne, 2010), whereas SphK2 displays more complex and context-dependent roles in cellular homeostasis, with evidence for both pro-apoptotic and pro-survival effects depending on cell type and conditions (Okada et al., 2005, Hait et al., 2009, Sankala et al., 2007).

The extracellular actions of S1P are mediated through its binding to a family of five G protein–coupled receptors ($S1P_1$–$S1P_5$), with $S1P_{1-3}$ being particularly relevant to the CVS (Strub et al., 2010). Through these receptors, S1P can produce divergent vascular responses. In ECs, activation of $S1P_1$ and $S1P_3$ promotes endothelium-dependent vasodilation through PI3K/Akt-mediated eNOS activation and nitric oxide (NO) release (Igarashi and Michel, 2009, Dantas et al., 2003, Mair et al., 2010, Tölle et al., 2005, di Villa Bianca et al., 2006). In contrast, VSMCs express higher levels of $S1P_2$, with lower expression of $S1P_1$ and $S1P_3$, resulting in

predominantly $S1P_2$ -mediated vasoconstriction through RhoA/Rho-kinase activation and calcium mobilisation, and cytoskeletal remodelling (Alewijnse et al., 2004, Hemmings et al., 2006, Bischoff et al., 2000, Medlin et al., 2010). Moreover, pathological conditions such as hypoxia, inflammation, and obesity can shift receptor expression, potentially altering the balance between vasodilatory and vasoconstrictive effects (Anelli et al., 2008, Salama et al., 2015, Fayyaz et al., 2014, Zhang et al., 2013a).

Adipose tissue (AT) is a metabolically active endocrine organ that releases adipokines, cytokines, and bioactive lipids such as sphingosine-1-phosphate (S1P). Both SphK1 and SphK2 are expressed in cultured adipocytes and in several adipose depots including subcutaneous, epididymal white- and brown AT, while $S1P_{1-3}$ are also widely detected in AT and cultured adipocytes (Hashimoto et al., 2009, Kitada et al., 2016, Mastrandrea, 2013, Chakrabarty et al., 2022, Morishige et al., 2023, Lee et al., 2017). Functionally, SphK1 has been implicated in adipocyte metabolism and inflammation, where its expression is upregulated by lipolytic stimuli and high-fat feeding, and is elevated in inflamed AT in both humans and mice (Wang et al., 2014, Fayyaz et al., 2014, Blachnio-Zabielska et al., 2012). These findings suggest that the SphK1/S1P axis contributes to obesity-related adipose dysfunction, although paradoxical anti-inflammatory effects have also been reported (Tous et al., 2014). Present around the blood vessels, PVAT exerts a paracrine influence on vascular tone by releasing adipokines, NO and ROS, with profiles that vary by depot (Barp et al., 2020). Thoracic PVAT resembles BAT, while mesenteric PVAT is more similar to WAT, and each depot exhibits distinct metabolic and secretory features (Gálvez-Prieto et al., 2008). Recent work further suggests that PVAT contains a functional SphK1–S1P–$S1P_3$ signalling axis, which can modulate vascular relaxation through HDL-S1P interactions, thereby providing the first molecular evidence of S1P signalling within PVAT (Li et al., 2025a). In line with this, observations reported in Aljaezi's thesis indicate that IL-1β upregulates SphK1 mRNA expression in PVAT and that the SphK1/S1P pathway contributes to IL-1β-induced hyporeactivity in rat aortic rings with intact PVAT, but not in rings without PVAT (Aljaezi, 2024).

Interestingly, SphK1 is tightly controlled at the post-translational level. SphK1 activity and stability can be reduced through dephosphorylation at Ser225 by protein phosphatase 2A (Barr et al., 2008), and the enzyme is also degraded

through both the ubiquitin–proteasome system and cathepsin B–mediated lysosomal pathways (Taha et al., 2006b, Loveridge et al., 2010). Pharmacological agents such as the SphK1 inhibitor PF543 utilise this mechanism by promoting proteasome-dependent SphK1 degradation (Byun et al., 2013). Evidence further suggests that hypoxia itself may enhance both SphK1 expression and degradation simultaneously in vascular endothelial cells (Alganga et al., 2019). Thus, proteasomal and lysosomal pathways represent key mechanisms in regulating the abundance and function of SphK1.

Hypoxia is a hallmark of expanding adipose depots and is a key driver of adipose tissue dysfunction. In adipocytes and other cell types, hypoxia stabilises hypoxia-inducible factors (HIFs) and increases SphK1 transcription and S1P production (Ito et al., 2013, Pulkoski-Gross and Obeid, 2018). Mechanistic studies show that HIF-2α directly upregulates SphK1 under hypoxic stress, leading to increased S1P release and angiogenic signalling (Anelli et al., 2008). Similarly, in clear cell renal cell carcinoma with constitutive HIF stabilisation, SphK1 is overexpressed and elevated S1P drives invasion and angiogenesis, correlating with poor survival (Salama et al., 2015). In adipocytes, hypoxia-induced S1P promotes the expression of PAI-1, pro-inflammatory mediators via $S1P_2$ (Ito et al., 2013), while in HepG2 cells, this response occurs through HIF-1α signalling (Sanagawa et al., 2016). In the vasculature, hypoxia-driven SphK1/S1P signalling has been associated with both vasodilatory and vasoconstrictive outcomes depending on tissue type and receptor distribution (Alganga et al., 2019, Ahmad et al., 2006, Chen et al., 2014). Collectively, these findings suggest that hypoxia-induced activation of the SphK/S1P pathway has context-dependent metabolic and vascular effects, but its specific contribution within PVAT remains poorly understood.

Therefore, this chapter investigates the effects of hypoxia on SphK1/S1P signalling and adipokine secretion in both cultured 3T3-L1 adipocytes and ex vivo PVAT depots. By integrating molecular, biochemical, and vascular function experiments, this work aims to clarify the mechanisms through which hypoxia modulates adipocyte and PVAT function, and how this may contribute to altered vascular responses. In Chapter 3 I demonstrated that acute hypoxia induces significant PVAT-dependent relaxation of the thoracic aorta and, to build on that finding, the current chapter examines whether the SphK1/S1P axis is involved in

this hypoxia-induced relaxation and contributes to the vascular effects associated with PVAT.

5.2 Aims

1. To determine how hypoxia regulates the SphK/S1P axis in 3T3-L1 adipocytes, by assessing SphK1 and SphK2 mRNA expression, SphK1 phosphorylation and total protein, and the contribution of proteasomal/lysosomal pathways to SphK1 stability.
2. To determine how hypoxia regulates the SphK/S1P axis in thoracic and mesenteric PVAT, by assessing SphK1 mRNA, SphK1 phosphorylation and total protein, and the contribution of proteasomal/lysosomal pathways to SphK1 abundance.
3. To determine the impact of hypoxia on S1P metabolism, by measuring extracellular S1P release in 3T3-L1 adipocytes, and both intracellular and extracellular S1P levels in thoracic and mesenteric PVAT.
4. To explore the role of pharmacological modulators, including exogenous S1P and CYM 5478 (a selective $S1P_2$ agonist), in modulating hypoxia-induced vascular relaxation.

5.3 Results

5.3.1 Hypoxia upregulates SphK1 but not SphK2 mRNA expression in 3T3-L1 adipocytes

5.3.1.1 $CoCl_2$-induced hypoxia:

Previous studies have demonstrated that hypoxia can upregulate SphK1 expression and its enzymatic product, sphingosine-1-phosphate (S1P), in various cell lines and tissues (Pulkoski-Gross and Obeid, 2018, Pyne et al., 2016). To assess whether a similar regulatory mechanism occurs in adipocytes, the mRNA expression levels of SphK1 and SphK2 were analysed in differentiated 3T3-L1 adipocytes treated with cobalt chloride ($CoCl_2$), a chemical inducer of hypoxia. Cells were incubated with $CoCl_2$ at a concentration of 200 µM for 0.5, 1, 2, 4, and 6 hours. Quantitative RT-PCR analysis revealed a transient increase in SphK1 mRNA expression at the 4-hour time point ($p<0.05$; Figure 5-1A), returning to basal levels by 6 hours. In contrast, no significant alterations were detected in SphK2 mRNA expression at any time point (Figure 5-1B).

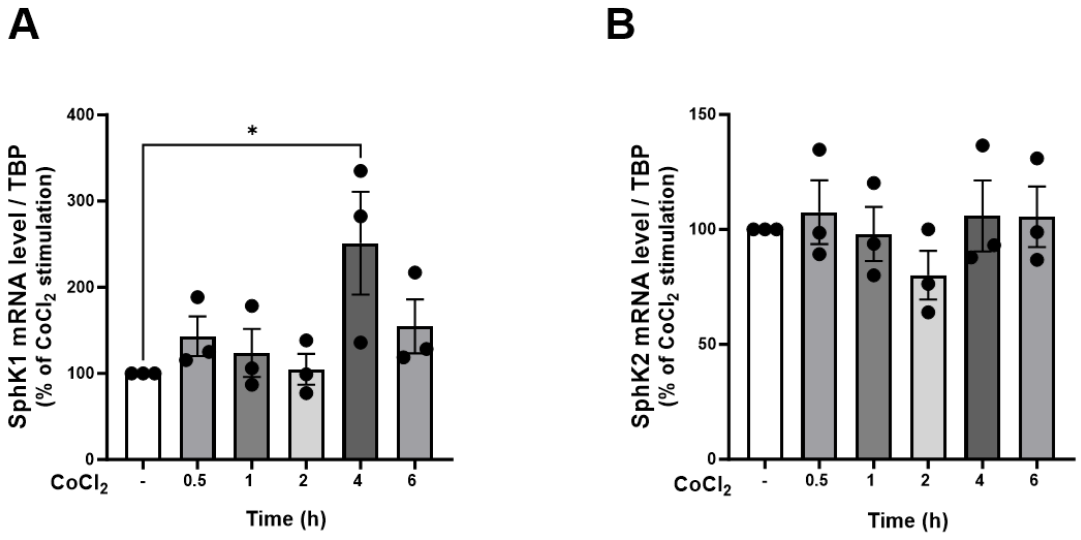

Figure 5-1 Effects of cobalt chloride-induced hypoxia on SphK1 and SphK2 mRNA expression in 3T3-L1 adipocytes.
3T3-L1 adipocytes were treated with 200 µM $CoCl_2$ for 0.5, 1, 2, 4, and 6 hours. RNA was isolated and analysed by RT-PCR to measure the expression of **(A)** SphK1 and **(B)** SphK2 mRNA. Expression levels were normalized to TATA-binding protein (TBP) mRNA as an internal control. Data represent mean ± SEM from three independent experiments (n=3) and are expressed as fold change relative to untreated cells. Statistical analysis was performed using one-way ANOVA followed by Dunnett's post-hoc test. Asterisks indicate statistical significance (*$p < 0.05$).

5.3.1.2 Gas-induced hypoxia:

To further investigate the effects of hypoxia on the expression of SphK isoforms, 3T3-L1 adipocytes were exposed to a controlled hypoxic gas mixture (1% O_2, 5% CO_2, and 94% N_2) for durations of 1, 3, and 6 hours. Because the hypoxia chamber is a sealed environment, sampling additional time points would have required breaking the atmosphere and re-gassing and so to minimise disturbance and maintain a constant 1% O_2, three a priori time points were selected. In contrast, $CoCl_2$ experiments permitted more frequent sampling (0.5–6 h) because the stimulus is applied directly to the culture medium without altering atmospheric conditions. Quantitative RT-PCR analysis demonstrated a significant elevation ($p < 0.05$) in SphK1 mRNA expression at the 3-hour time point relative to untreated normoxic control cells (Figure 5-2A). Conversely, no significant alteration in SphK2 mRNA expression was observed at any time point studied (Figure 5-2B).

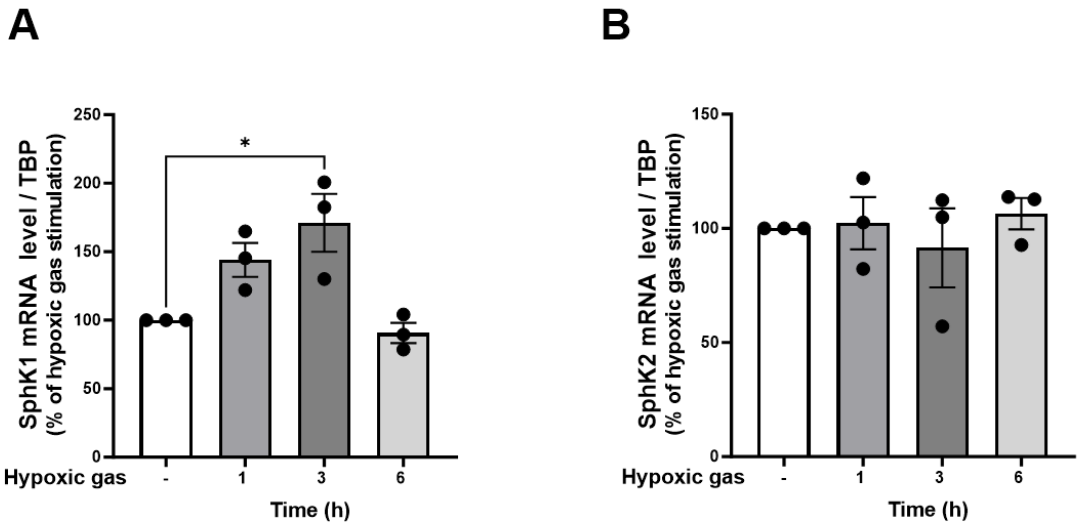

Figure 5-2 Effects of gas-induced hypoxia on SphK1 and SphK2 mRNA expression in 3T3-L1 adipocytes.
3T3-L1 adipocytes were exposed to a hypoxic gas mixture (94% N_2, 5% CO_2, 1% O_2) for 1, 3, or 6 hours. Total RNA was extracted, and mRNA levels of **(A)** SphK1 and **(B)** SphK2 were quantified by RT-PCR. Expression levels are presented as fold-change relative to untreated control cells, normalised to TATA-binding protein (TBP) mRNA as an internal control. Data are presented as mean ± SEM from three independent experiments (n=3). Statistical significance was assessed using one-way ANOVA followed by Dunnett's post-hoc test. Asterisks indicate statistical significance (*$p < 0.05$).

5.3.2 SphK1 phosphorylation induced by hypoxia in 3T3-L1 adipocytes

The previous results demonstrated that hypoxia selectively upregulated SphK1 mRNA expression without affecting SphK2. To investigate whether hypoxia also modulates the activation of SphK1 through phosphorylation, differentiated 3T3-L1 adipocytes were exposed to hypoxic conditions using either $CoCl_2$ (200 μM) or a hypoxic gas mixture (94% N_2, 5% CO_2, and 1% O_2) at various time points.

Western blot analysis revealed no significant change in SphK1 phosphorylation levels at any time point tested (5, 15, 30, 60, and 120 minutes) following $CoCl_2$ treatment (Figure 5-3A). However, exposure to the hypoxic gas mixture significantly enhanced SphK1 phosphorylation at the 1-hour time point ($p < 0.01$; Figure 5-3B). Notably, both increases in phosphorylation and mRNA expression appeared transient. Earlier gas-hypoxia time points (<1 h) were not sampled because hypoxia was applied using a sealed modular chamber: plates were removed from the incubator, the chamber was fully flushed/re-gassed to 1% O_2, sealed, and then returned to the incubator. To avoid short-term temperature fluctuations during chamber handling outside the incubator and re-equilibration, and because the gas acted on the chamber atmosphere rather than being bubbled directly through the medium (unlike the wire-myograph system), I selected 1, 3, and 6 h time points; sub-one hour sampling was not practicable in this setup.

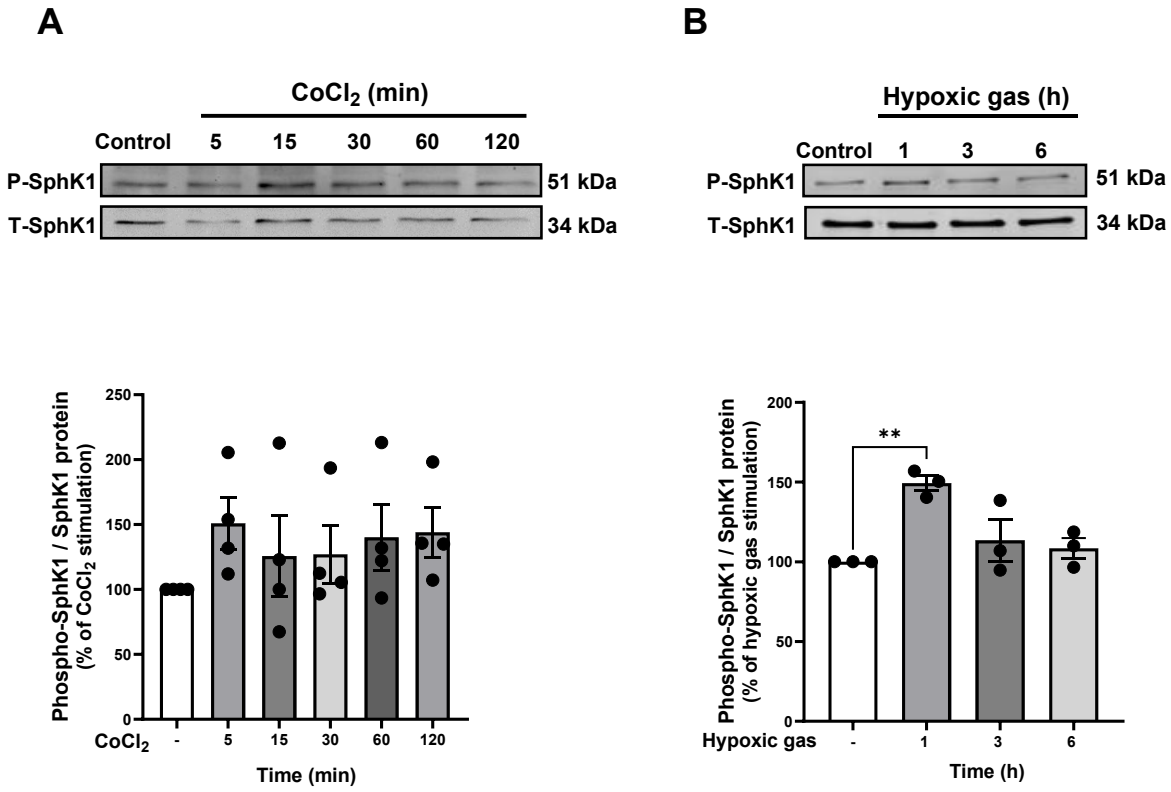

Figure 5-3 The effect of hypoxia on SphK1 phosphorylation in 3T3-L1 adipocytes. Representative western blot images and quantitative analysis of phosphorylated SphK1 (P-SphK1) normalized to total SphK1 (T-SphK1) in adipocytes exposed to **(A)** cobalt chloride ($CoCl_2$; 200 μM) for 5, 15, 30, 60, and 120 minutes, and **(B)** a hypoxic gas mixture (94% N_2, 5% CO_2, and 1% O_2) for 1, 3, and 6 hours. The quantified P-SphK1 band was located at ~51 kDa, while the quantified T-SphK1 band was located at ~34–36 kDa. Data are presented as mean ± SEM of percent fold-change relative to untreated control cells, from 3–4 independent experiments (n = 4 for $CoCl_2$, n = 3 for gas). Statistical significance was assessed using one-way ANOVA followed by Dunnett's post-hoc test; asterisks indicate statistical significance (**p < 0.01).

5.3.3 The effect of hypoxia on SphK1 expression levels in 3T3-L1 adipocytes

Having demonstrated that gas-induced hypoxia upregulates SphK1 mRNA expression and enhances its phosphorylation, I next investigated whether hypoxia also affects total SphK1 protein levels in 3T3-L1 adipocytes. Cells were exposed to hypoxia using either $CoCl_2$ (200 μM) or a hypoxic gas mixture (94% N_2, 5% CO_2, and 1% O_2) for the indicated durations. Western blot analysis showed no significant change in total SphK1 protein expression following $CoCl_2$ treatment at any of the assessed time points (1, 2 and 4 hours; Figure 5-4A). Similarly, gas-induced hypoxia did not produce any statistically significant alterations in SphK1 levels across the tested time points (1, 3, and 6 hours; Figure 5-4B).

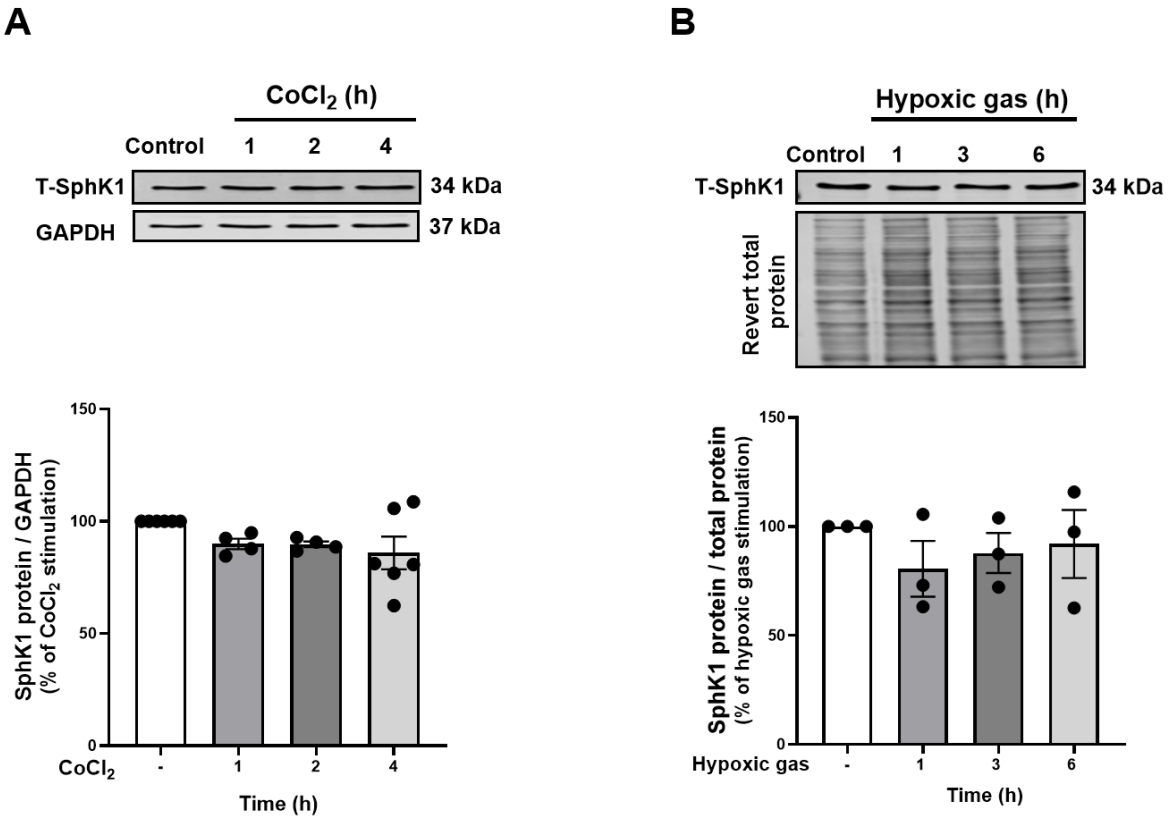

Figure 5-4 The effect of hypoxia on total SphK1 expression levels in 3T3-L1 adipocytes. Representative western blot images and quantification of total SphK1 (T-SphK1) levels in adipocytes treated with **(A)** $CoCl_2$ for 1, 2 and 4 hours, or **(B)** a hypoxic gas mixture (94% N_2, 5% CO_2, and 1% O_2) for 1, 3, and 6 hours. The quantified SphK1 band was located at ~34–36 kDa, and GAPDH at ~37 kDa. SphK1 expression was normalized to GAPDH for $CoCl_2$-treated samples and to total protein stain for gas-treated samples. Data are expressed as percent fold-change relative to untreated control cells and presented as mean ± SEM from independent experiments (n=4, except for the 4-hour time point where n=6). Statistical analysis was performed using one-way ANOVA followed by Dunnett's post-hoc test.

5.3.4 Role of protein degradation on SphK1 expression in 3T3-L1 adipocytes

5.3.4.1 $CoCl_2$ hypoxia in the presence of proteasome/lysosome inhibitors

As previously shown, treatment with 200 μM $CoCl_2$ for 4 hours significantly increased SphK1 mRNA levels but did not alter SphK1 phosphorylation or total protein levels. To determine whether this lack of change at the protein level was due to post-translational degradation, protein degradation pathways were pharmacologically inhibited.

Previous studies have demonstrated that SphK1 is subject to degradation via the ubiquitin–proteasome system and/or cathepsin B-mediated lysosomal degradation (Taha et al., 2006b, Loveridge et al., 2010). Furthermore, evidence suggests that hypoxia can increase SphK1 expression while simultaneously promoting its degradation via both pathways in endothelial cells (Alganga et al., 2019). To assess whether similar mechanisms are active in 3T3-L1 adipocytes exposed to hypoxia, cells were pretreated with the proteasome inhibitors lactacystin (10 μM) or MG132 (10 μM), the cathepsin B inhibitor CA-074ME (10 μM), or a combination of MG132 and CA-074ME. Cells were then exposed to $CoCl_2$ for 4 hours, corresponding to the time point where the increase in SphK1 mRNA was previously observed. Western blot analysis showed that none of these inhibitor treatments resulted in a significant increase in total SphK1 protein levels compared to untreated controls (Figure 5-5).

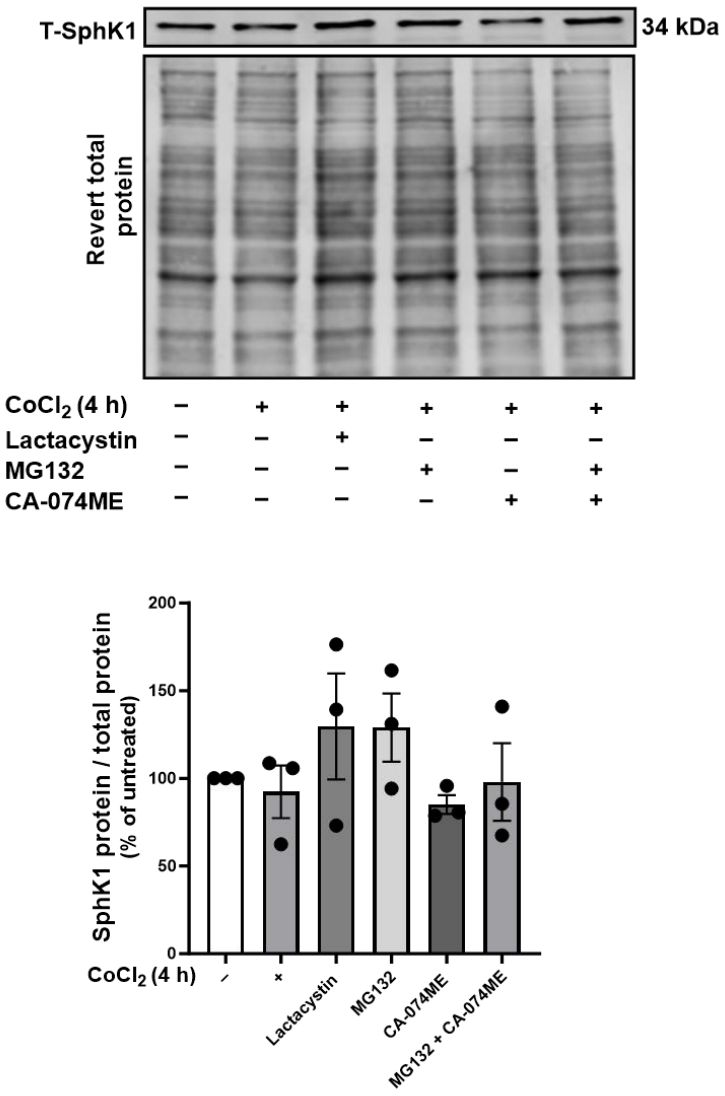

Figure 5-5 The effect of cobalt chloride on SphK1 expression in the presence of protein degradation inhibitors in 3T3-L1 adipocyte cells.
Representative immunoblot and quantification showing the effect of pre-treatment with lactacystin (10 µM, 30 min), MG132 (10 µM, 30 min), CA-074ME (10 µM, 30 min), or a combination of MG132 and CA-074ME on SphK1 protein expression in 3T3-L1 adipocytes exposed to $CoCl_2$-induced hypoxia for 4 hours. The quantified SphK1 band was located at ~34–36 kDa. Total SphK1 (T-SphK1) levels were normalized to total protein stain. Data are expressed as percent fold-change relative to untreated control cells and presented as mean ± SEM from three independent experiments (n=3). Statistical analysis was performed using one-way ANOVA followed by Dunnett's post-hoc test.

5.3.5 Differential S1P release in gas- and $CoCl_2$-induced hypoxia

In a previous study using 3T3-L1 adipocytes and $CoCl_2$-induced hypoxia, Ito et al. (2013) demonstrated that $CoCl_2$ stimulation promotes S1P production and its extracellular release. However, they did not investigate hypoxia induced by gas exposure, which may more accurately reflect in vivo conditions. To address this, I assessed S1P release in response to both $CoCl_2$ and gas-induced hypoxia as part of our optimisation of hypoxia induction in this model. S1P concentrations in conditioned media from 3T3-L1 adipocytes were quantified using an ELISA-based

assay following exposure to either $CoCl_2$ or gas-induced hypoxia. Cells treated with 200 µM $CoCl_2$ for 4 hours exhibited a significant increase in S1P release compared with normoxic untreated controls ($p < 0.05$; Figure 5-6A). In contrast, exposure to a hypoxic gas mixture (94% N_2, 5% CO_2, 1% O_2) for 1 or 6 hours resulted in a significant reduction in S1P release at 1 hour ($p < 0.01$), with no significant difference observed at 6 hours, when compared with normoxic untreated controls (Figure 5-6B).

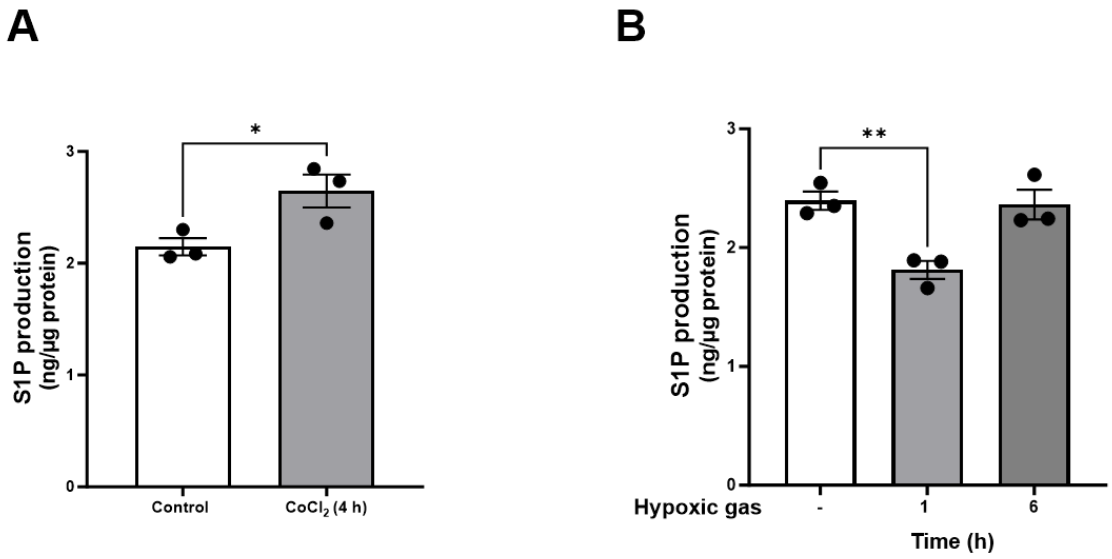

Figure 5-6 Effect of hypoxia on S1P release into conditioned media from 3T3-L1 adipocyte cells.
S1P levels were measured by ELISA in conditioned media from 3T3-L1 adipocytes subjected to hypoxia. **(A)** Cells were treated with 200 µM $CoCl_2$ for 4 hours and compared with untreated normoxic controls. **(B)** Cells were exposed to a hypoxic gas mixture (94% N_2, 5% CO_2, 1% O_2) for 1 and 6 hours and compared with untreated normoxic controls. S1P concentrations were normalised to total protein content and expressed as ng/µg protein. Data represent the mean ± SEM from three independent experiments (n=3). Statistical analysis was performed using an unpaired Student's t-test for $CoCl_2$ treatment and one-way ANOVA followed by Dunnett's post-hoc test for gas treatment. Asterisks indicate statistical significance (*$p < 0.05$, **$p < 0.01$).

5.3.6 SphK1 gene expression in thoracic and mesenteric PVAT under normoxia and hypoxia

Building on the adipocyte findings, I extended the analysis to rat PVAT, a more physiological context than 3T3-L1 cells, comparing thoracic (BAT-like) and mesenteric (WAT-like) depots to test whether brief gas hypoxia alters SphK1 mRNA. PVAT isolated from the thoracic aorta and mesenteric artery of rats was initially incubated under normoxia (95% O_2 and 5% CO_2) for 30 minutes, then maintained in normoxia or exposed to hypoxia (95% N_2, 5% CO_2) for a further 30 minutes. Quantitative RT-PCR analysis revealed no significant change in SphK1

mRNA expression in thoracic PVAT under hypoxia (Figure 5-7A). In mesenteric PVAT, no significant difference in SphK1 expression was detected between normoxic and hypoxic conditions, with considerable inter-replicate variability observed (Figure 5-7B).

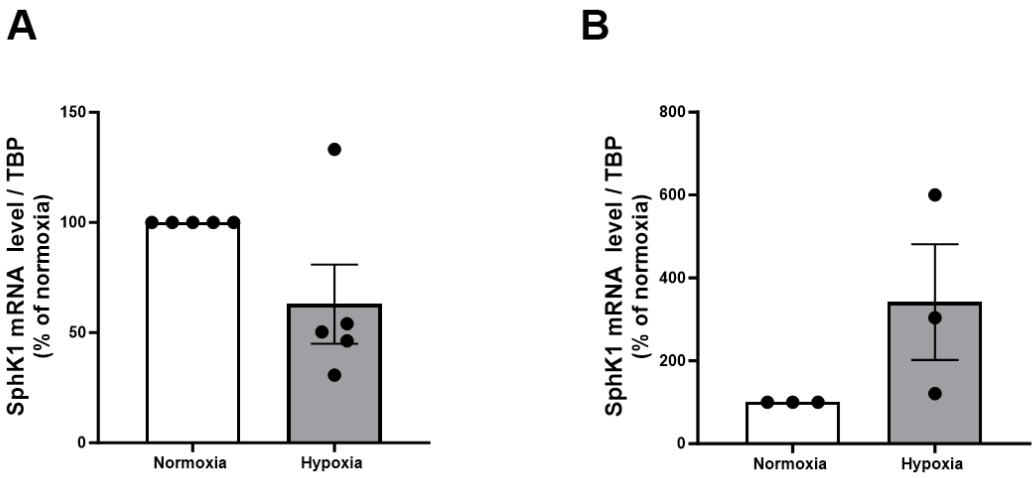

Figure 5-7 Effect of hypoxia on SphK1 mRNA expression in thoracic and mesenteric PVAT. Thoracic and mesenteric PVAT samples were initially incubated under normoxic conditions (95% O_2 and 5% CO_2) for 30 minutes, followed by continued normoxia or exposure to hypoxia (95% N_2 and 5% CO_2) for an additional 30 minutes. Total RNA was extracted and SphK1 mRNA levels were quantified by quantitative RT-PCR. Expression levels were normalised to TATA-binding protein (TBP) mRNA and are presented as percentage relative to normoxic controls. Data are presented as mean ± SEM from five independent experiments for thoracic PVAT **(A)** and three independent experiments for mesenteric PVAT **(B)**. Statistical analysis was performed using the Mann–Whitney U test.

5.3.7 Expression of SphK1 phosphorylation and SphK1 in thoracic and mesenteric PVAT under normoxia and hypoxia

As SphK1 mRNA expression showed no significant reduction in thoracic PVAT under short-term hypoxia, I next assessed whether changes occurred at the protein level. Specifically, I investigated whether hypoxia influences SphK1 activation through phosphorylation (P-SphK1) or alters total SphK1 (T-SphK1) protein in thoracic and mesenteric PVAT. PVAT samples were incubated under normoxia for 30 minutes, followed by continued normoxia or exposure to hypoxic gas (95% N_2, 5% CO_2) for an additional 30 minutes. Western blot analysis revealed no significant differences in P-SphK1 (Figure 5-8A) or T-SphK1 (Figure 5-8B) in thoracic PVAT. Similarly, no significant changes in P-SphK1 (Figure 5-9A) or T-SphK1 (Figure 5-9B) were observed in mesenteric PVAT.

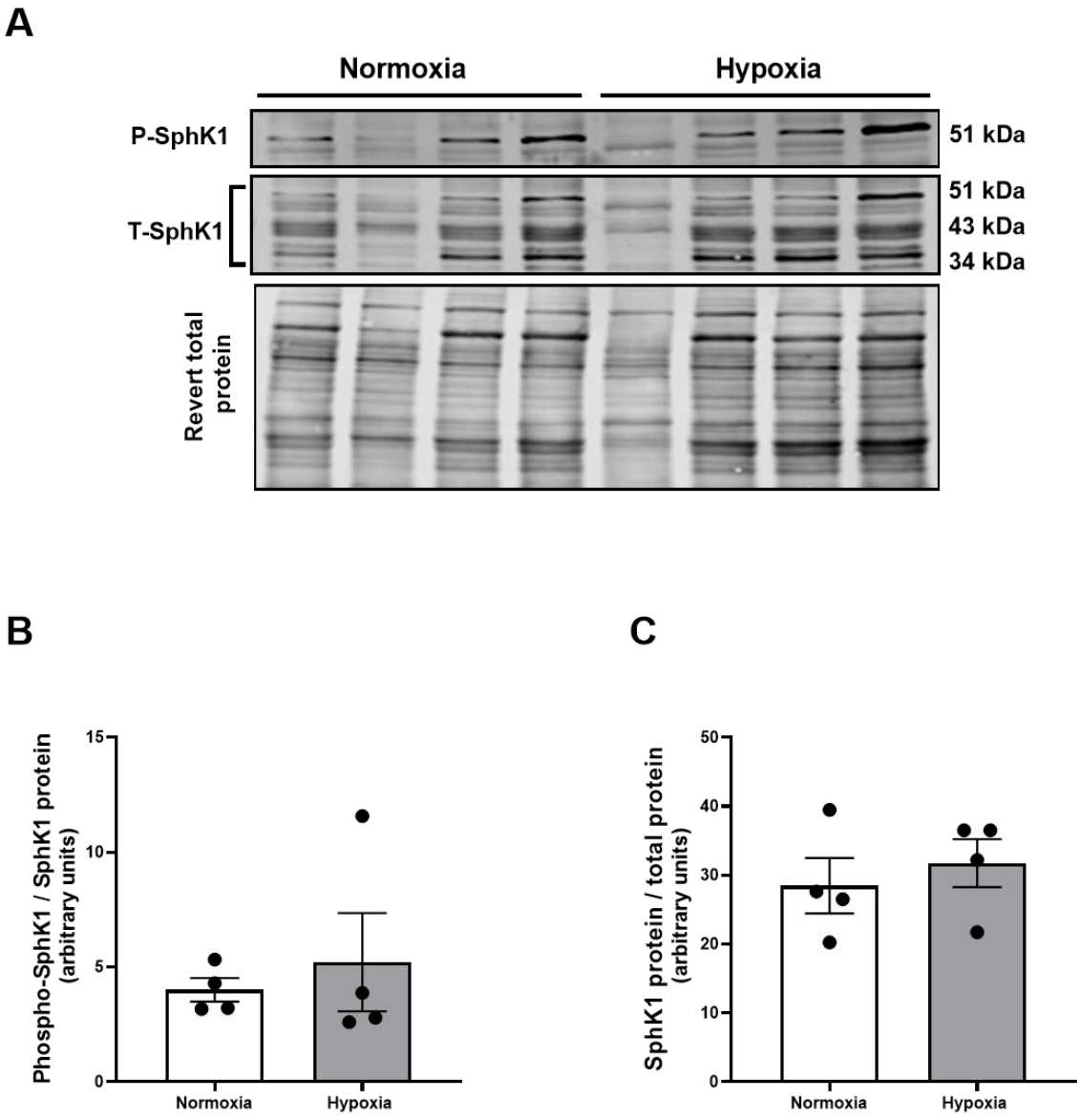

Figure 5-8 Phosphorylated and total SphK1 expression in thoracic PVAT under normoxic and hypoxic conditions.
PVAT samples were initially incubated under normoxic conditions (95% O_2 and 5% CO_2) for 30 minutes, followed by continued normoxia or exposure to hypoxia (95% N_2 and 5% CO_2) for an additional 30 minutes. **(A)** Immunoblot images show the expression of phosphorylated SphK1 (P-SphK1) and total SphK1 (T-SphK1) proteins in thoracic PVAT (lanes 1–4, normoxia; lanes 5–8, hypoxia). The quantified P-SphK1 band was located at ~51 kDa, and the quantified T-SphK1 band was located within the ~34–51 kDa. **(B)** Quantification of P-SphK1 levels normalised to total SphK1. **(C)** Quantification of T-SphK1 levels normalised to total protein stain. Data are presented as mean ± SEM from four independent experiments (n=4) and expressed in arbitrary units. Statistical analysis was performed using the Mann–Whitney U test.

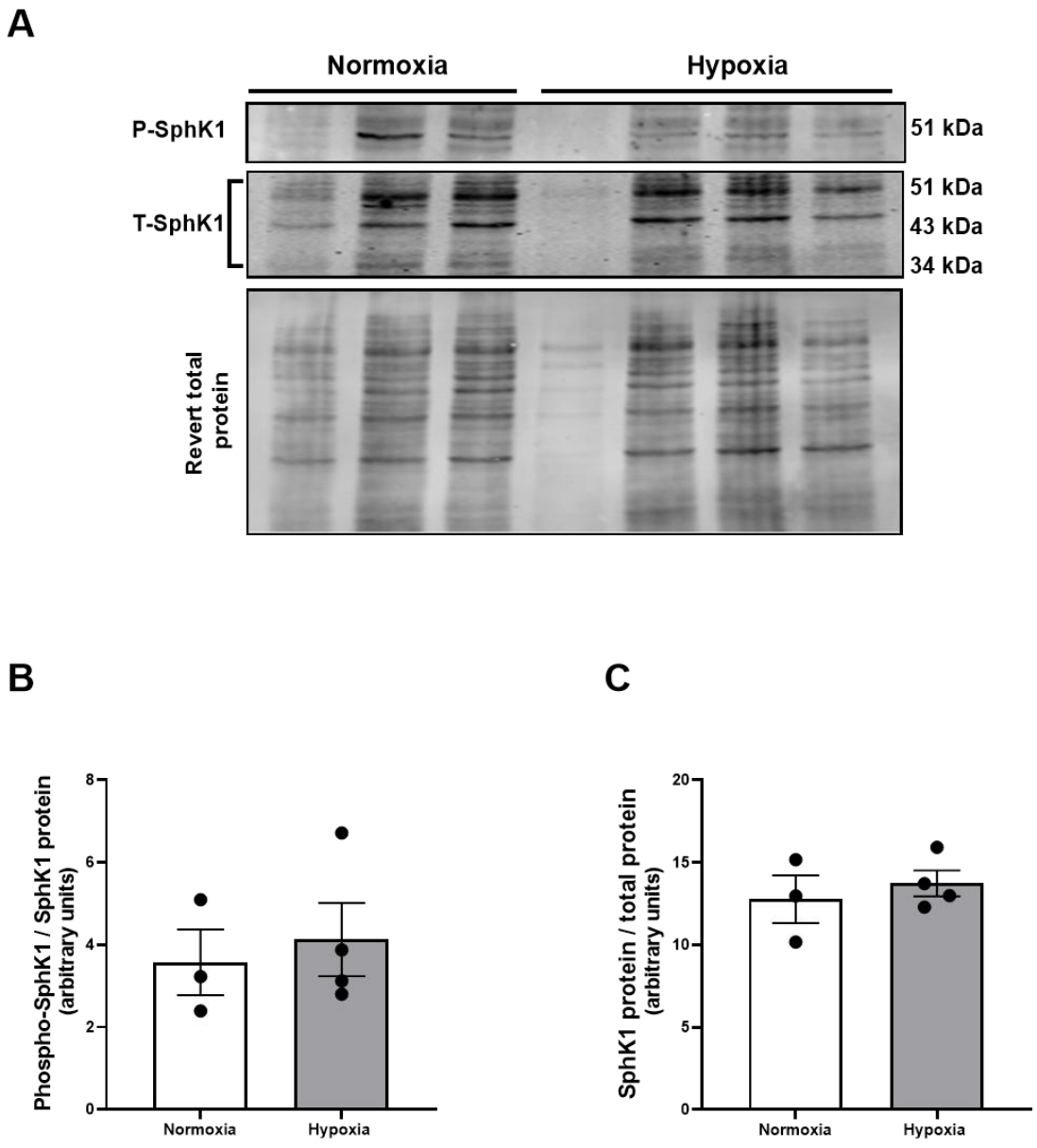

Figure 5-9 Expression of phosphorylated and total SphK1 in mesenteric PVAT under normoxic and hypoxic conditions.
PVAT samples were initially incubated under normoxic conditions (95% O_2 and 5% CO_2) for 30 minutes, followed by continued normoxia or exposure to hypoxia (95% N_2 and 5% CO_2) for an additional 30 minutes. **(A)** Immunoblot images show the expression of phosphorylated SphK1 (P-SphK1) and total SphK1 (T-SphK1) proteins in mesenteric PVAT (lanes 1–3, normoxia; lanes 4–7, hypoxia). The quantified P-SphK1 band was located at ~51 kDa, and the quantified T-SphK1 band was located within the ~34–51 kDa. **(B)** Quantification of P-SphK1 levels normalised to total SphK1. **(C)** Quantification of T-SphK1 levels normalised to total protein stain. Data are presented as mean ± SEM from three independent experiments for normoxia and four for hypoxia (n=3 normoxia, n=4 hypoxia) and expressed in arbitrary units. Statistical analysis was performed using an unpaired Student's t-test.

5.3.8 SphK1 protein accumulation via inhibition of protein degradation

5.3.8.1 SphK1 expression in the presence of protein synthesis and degradation inhibitors in thoracic and mesenteric PVAT under normoxia and hypoxia

Following the observation that SphK1 mRNA expression was not significantly altered in thoracic or mesenteric PVAT under hypoxia, and that neither SphK1 phosphorylation nor total protein levels were significantly affected, I next explored whether hypoxia might regulate SphK1 at the post-translational level. In my earlier work using 3T3-L1 adipocytes, I found that $CoCl_2$-induced hypoxia increased SphK1 mRNA expression without significantly altering total SphK1 protein levels, whereas gas-induced hypoxia led to a transient increase in SphK1 phosphorylation at 1 hour. Furthermore, pharmacological inhibition of proteasomal and lysosomal pathways did not lead to a significant increase in total SphK1 protein levels. To determine whether similar mechanisms operate in PVAT, thoracic and mesenteric PVAT samples were preincubated with the protein synthesis inhibitor cycloheximide (10 μM), the proteasome inhibitors lactacystin and MG132 (10 μM each), the cathepsin B inhibitor CA-074ME (10 μM), or a combination of MG132 and CA-074ME, and subsequently maintained under normoxic conditions or exposed to hypoxia. In thoracic PVAT, none of the inhibitors significantly affected SphK1 expression under normoxia (Figure 5-10A) but under hypoxic conditions, the combination of CA-074ME with MG132 significantly increased SphK1 protein levels ($p < 0.01$) (Figure 5-10B). In contrast, no significant effects were observed in mesenteric PVAT under either normoxic or hypoxic conditions following treatment with any of the inhibitors (Figure 5-11A and B).

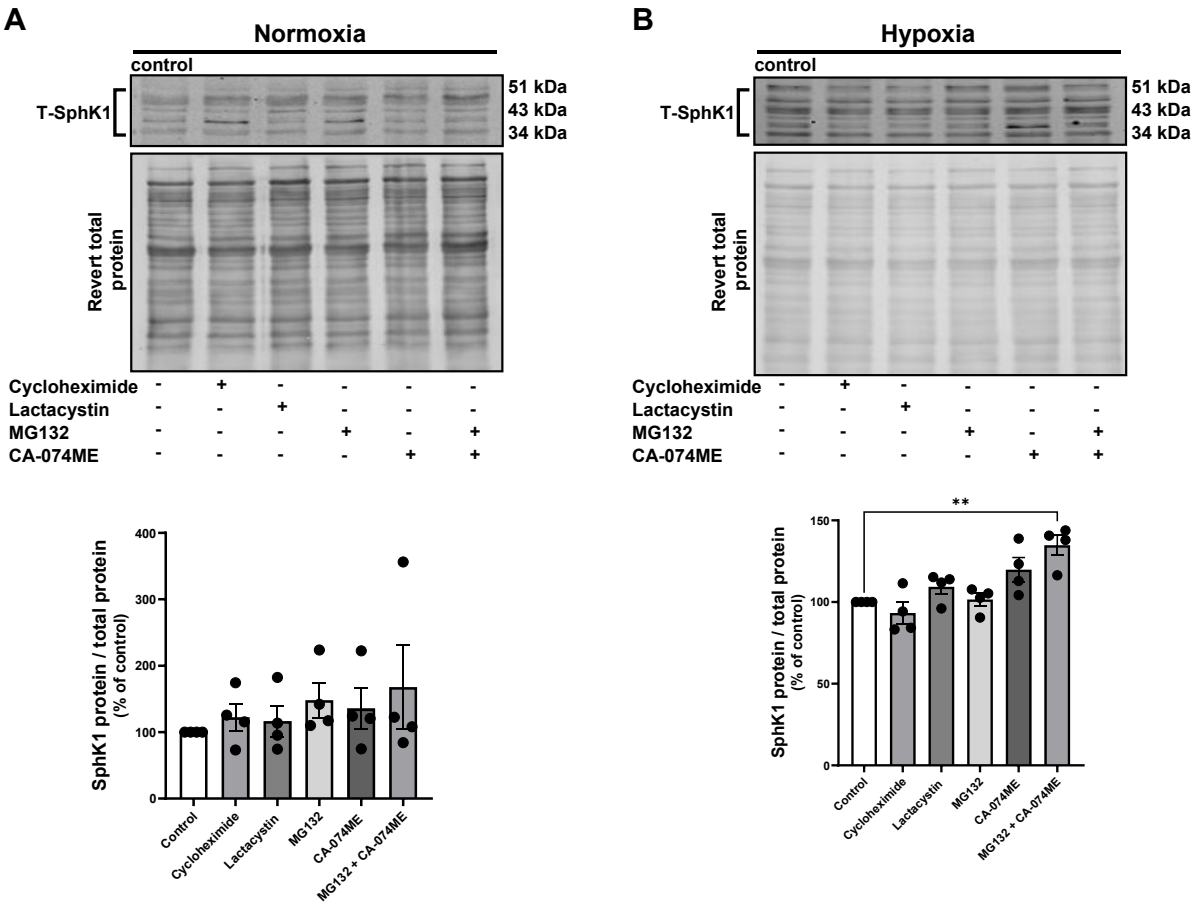

Figure 5-10 Effect of protein synthesis and degradation inhibitors on SphK1 expression in thoracic PVAT under normoxia and hypoxia.

Representative immunoblot and quantification showing the effect of pre-treatment with cycloheximide (10 μM, 30 min), lactacystin (10 μM, 30 min), MG132 (10 μM, 30 min), CA-074ME (10 μM, 30 min), or a combination of MG132 and CA-074ME on SphK1 protein expression in rat thoracic PVAT under **(A)** normoxia and **(B)** hypoxia. Total SphK1 (T-SphK1) levels were normalised to total protein stain. The quantified T-SphK1 band was located within the ~34–51 kDa. Data are expressed as percent fold-change relative to untreated control and presented as mean ± SEM from four independent experiments (n = 4). As data in panel A were not normally distributed, panel A and B was analysed using the Kruskal–Wallis test followed by Dunn's multiple comparisons test. Asterisks indicate statistical significance (*p < 0.05, ***p < 0.001).

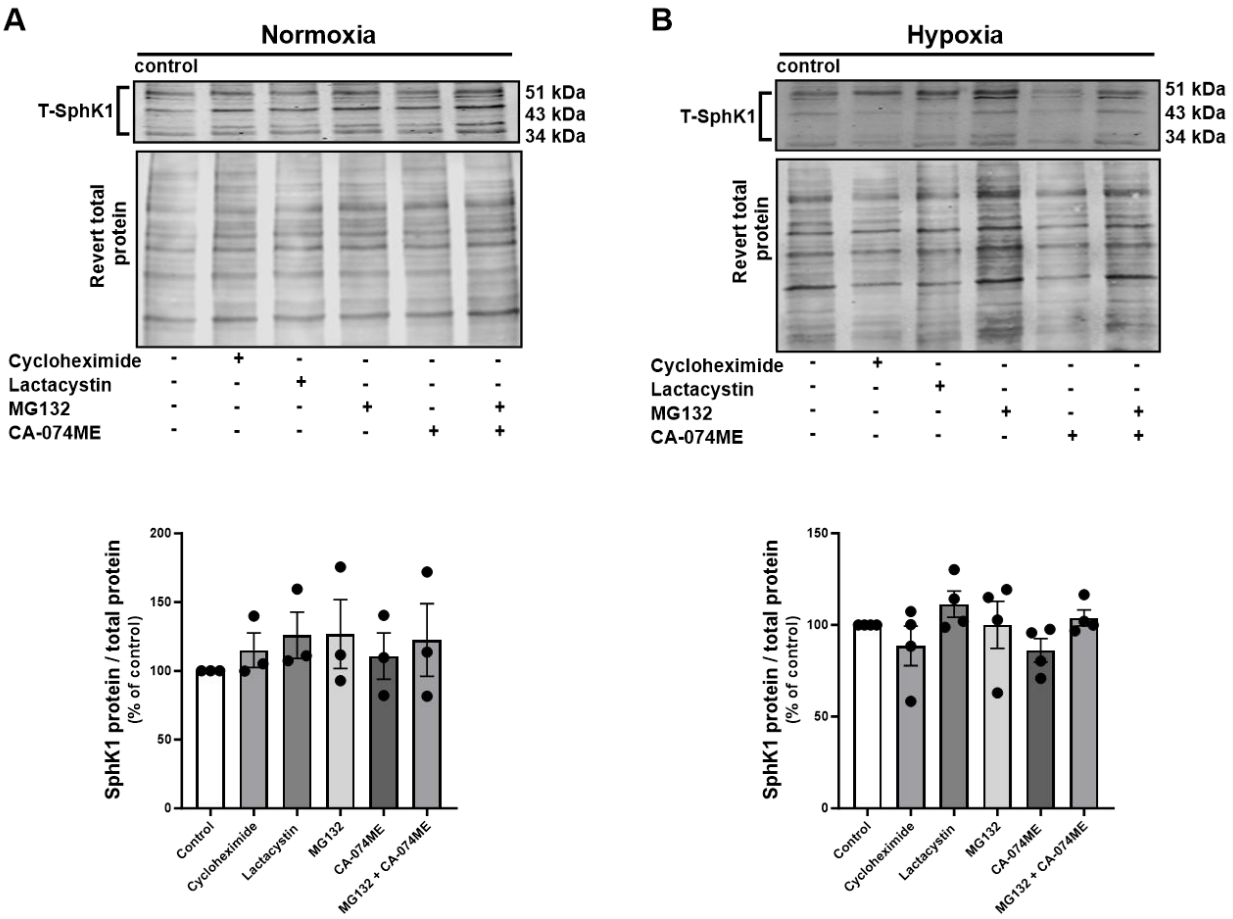

Figure 5-11 Effect of protein synthesis and degradation inhibitors on SphK1 expression in mesenteric PVAT under normoxic and hypoxic conditions.
Representative immunoblot and quantification showing the effect of pre-treatment with cycloheximide (10 μM, 30 min), lactacystin (10 μM, 30 min), MG132 (10 μM, 30 min), CA-074ME (10 μM, 30 min), or a combination of MG132 and CA-074ME on SphK1 protein expression in rat mesenteric PVAT under **(A)** normoxia and **(B)** hypoxia. Total SphK1 (T-SphK1) levels were normalised to total protein stain. The quantified T-SphK1 band was located within the ~34–51 kDa. Data are expressed as percent fold-change relative to untreated control and presented as mean ± SEM from three independent experiments for normoxia and four for hypoxia (n=3 normoxia, n=4 hypoxia). Statistical analysis was performed using one-way ANOVA followed by Dunnett's post-hoc test.

5.3.9 S1P content in thoracic and mesenteric PVAT lysate under normoxia and hypoxia

Following the modulation of SphK1 protein stability under hypoxic conditions, I next measured S1P content within PVAT lysates to determine whether these molecular changes were associated with alterations in local S1P levels. PVAT samples were maintained under normoxic conditions or exposed to hypoxia (95% N_2, 5% CO_2) for 30 minutes, and S1P content was measured using an ELISA-based assay. No significant differences in S1P levels were observed between normoxic and hypoxic conditions in either thoracic or mesenteric PVAT (Figure 5-12). However, baseline S1P content in thoracic PVAT was significantly lower than that in mesenteric PVAT under both normoxia ($p < 0.01$) and hypoxia ($p < 0.05$), consistent with regional differences in PVAT metabolic profiles.

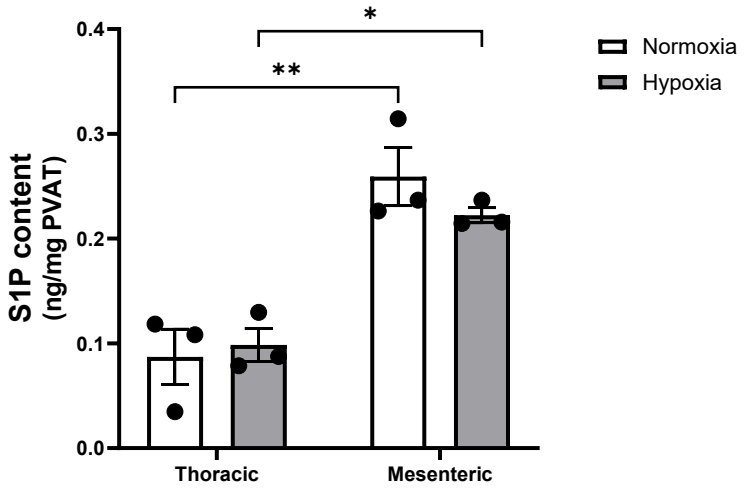

Figure 5-12 S1P levels in thoracic and mesenteric PVAT lysates under normoxic and hypoxic conditions.
S1P levels were quantified by ELISA in lysates of thoracic and mesenteric PVAT from rats exposed to normoxic or hypoxic conditions. PVAT samples were initially incubated under normoxic conditions (95% O_2 and 5% CO_2) for 30 minutes, followed by continued normoxia or exposure to hypoxia (95% N_2 and 5% CO_2) for an additional 30 minutes. S1P concentrations are expressed as ng S1P per mg tissue. Data are presented as mean ± SEM from three independent experiments (n=3). Statistical analysis was performed using two-way ANOVA followed by Tukey's post-hoc test. Asterisks indicate statistical significance (*$p < 0.05$, **$p < 0.01$).

5.3.10 Effect of hypoxia and SphK1 inhibition on S1P content in thoracic PVAT Conditioned Media

To further explore S1P regulation in thoracic PVAT, I measured S1P release into conditioned media collected under normoxic and hypoxic conditions. S1P levels were quantified by ELISA following 30 minutes of incubation. Under hypoxia, S1P release was significantly decreased compared to normoxia ($p < 0.01$) (Figure 5-13A). To determine the contribution of SphK1 activity under normoxic conditions, thoracic PVAT samples were pre-treated with the SphK1 inhibitor PF543 (100 nM) for 30 minutes. Pre-treatment with PF543 under normoxia resulted in a significant decrease in S1P release compared to untreated normoxic controls ($p < 0.01$) (Figure 5-13B). Furthermore, when comparing PF543-treated samples under normoxic and hypoxic conditions, hypoxia induced a further significant decrease in S1P release ($p < 0.05$) (Figure 5-13C).

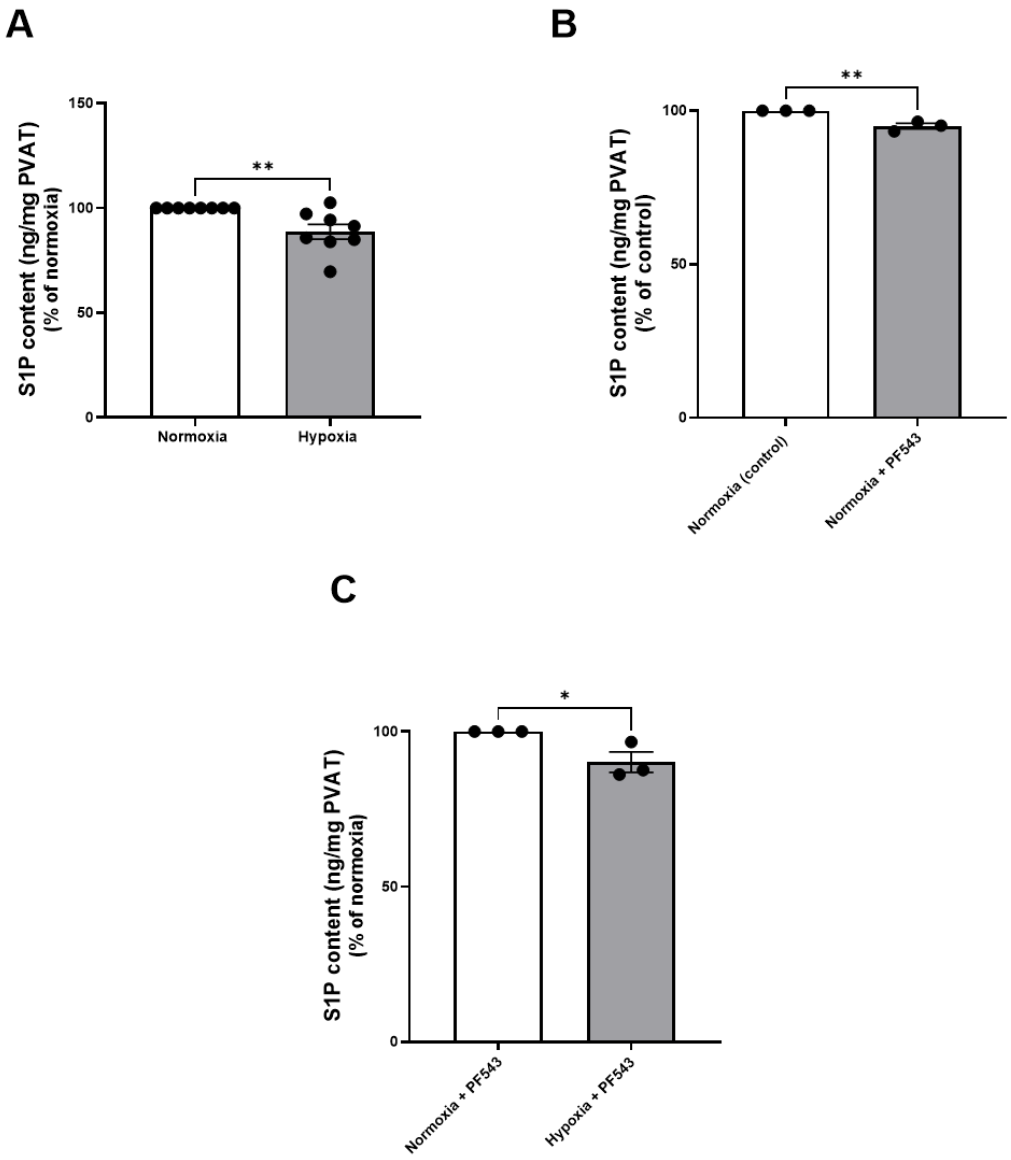

Figure 5-13 Impact of hypoxia and PF543 on S1P content in thoracic PVAT.
S1P levels were measured by ELISA in conditioned media collected from thoracic PVAT samples maintained under normoxic or hypoxic conditions. PVAT samples were initially incubated under normoxic conditions (95% O_2 and 5% CO_2) for 30 minutes, followed by continued normoxia or exposure to hypoxia (95% N_2 and 5% CO_2) for an additional 30 minutes. **(A)** S1P release under normoxia and hypoxia (n = 8). **(B)** Comparison between untreated and PF543 pre-treatment under normoxia (n = 3). **(C)** Comparison between PF543-treated samples under hypoxia versus PF543 normoxia (n = 3). S1P concentrations are expressed as ng S1P per mg PVAT. Data are presented as mean ± SEM. Statistical analysis was performed using unpaired Student's t-test. Asterisks indicate statistical significance (*p < 0.05, **p < 0.01).

5.3.11 S1P release in mesenteric PVAT conditioned media

To determine whether similar regulatory patterns occurred in mesenteric PVAT, I next assessed S1P release into conditioned media collected from mesenteric PVAT samples maintained under normoxic and hypoxic conditions. In contrast to the findings in thoracic PVAT, no significant differences in S1P release were observed

between normoxia and hypoxia, or following pre-treatment with the SphK1 inhibitor PF543 (Figure 5-14)

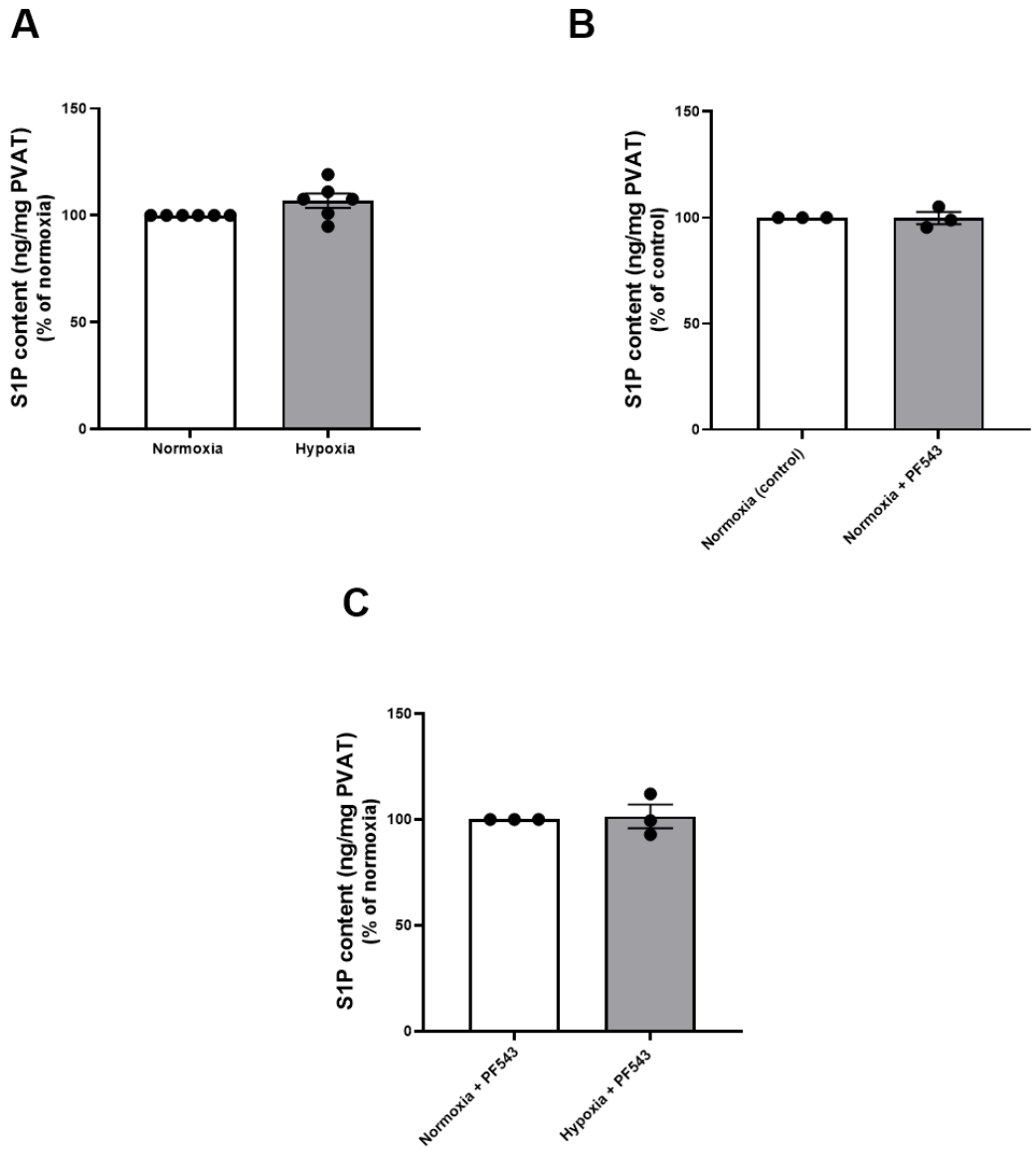

Figure 5-14 Effect of hypoxia and SphK1 inhibition on S1P content in mesenteric PVAT Conditioned Media.
S1P levels were measured by ELISA in conditioned media collected from mesenteric PVAT samples maintained under normoxic or hypoxic conditions. PVAT samples were initially incubated under normoxic conditions (95% O_2 and 5% CO_2) for 30 minutes, followed by continued normoxia or exposure to hypoxia (95% N_2 and 5% CO_2) for an additional 30 minutes. **(A)** S1P release under normoxia and hypoxia (n=6). **(B)** Comparison between untreated and PF543 pre-treatment under normoxia (n=3). **(C)** Comparison between PF543-treated samples under hypoxia versus PF543 normoxia (n=3). S1P concentrations are expressed as ng S1P per mg PVAT. Data are presented as mean ± SEM. Statistical analysis was performed using unpaired Student's t-test.

5.3.12 Effect of S1P and $S1P_2$ receptor activation on hypoxia-induced relaxation in PE-precontracted thoracic aorta

To investigate whether S1P signalling contributes to the acute hypoxia-induced vascular relaxation observed in Chapter 3, thoracic aortic rings were pretreated

with either S1P (10 μM) or the selective $S1P_2$ agonist CYM 5478 (10 μM) before exposure to hypoxia.

In PVAT(+)/E+ and PVAT(+)/E– rings, there were no significant differences in hypoxia-induced relaxation between hypoxia-only rings (control), S1P-, and CYM 5478-treated groups (Figure 5-15A, B). In contrast, in PVAT(–)/E+ rings, both S1P and CYM 5478 significantly reduced relaxation compared to hypoxia-only rings (controls) ($p < 0.05$) (Figure 5-15C). In PVAT(–)/E– rings, treatment with CYM 5478 abolished hypoxia-induced relaxation ($p < 0.01$), whereas S1P had no significant effect (Figure 5-15D). A representative control recording from a PVAT(+) ring is provided in Figure 5-15E to illustrate hypoxia-induced relaxation. **In summary, S1P and $S1P_2$ activation had no effect on hypoxia-induced relaxation in PVAT(+) rings, but significantly reduced relaxation in PVAT(–) rings.**

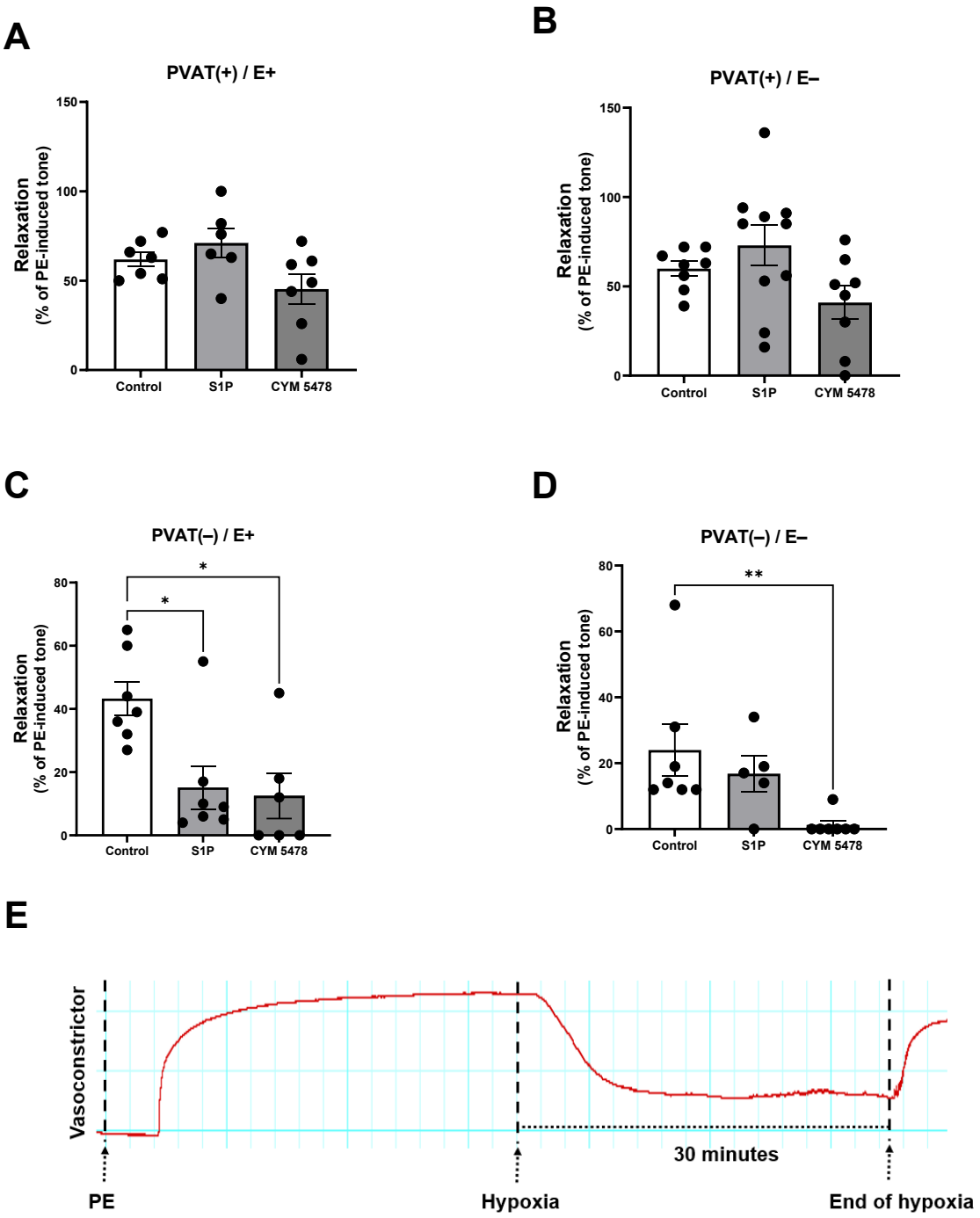

Figure 5-15 Hypoxia-induced relaxation in S1P- and CYM-treated thoracic aorta with and without PVAT and endothelium.

Thoracic aortic rings were precontracted with PE (1 μM), then treated with either S1P (10 μM) or the selective $S1P_2$ agonist CYM 5478 (10 μM) or left untreated as hypoxia-only control rings prior to hypoxic exposure (95% N_2 and 5% CO_2 for 30 minutes). Relaxation is expressed as a percentage of the precontracted tone induced by PE and presented as mean ± SEM from arteries obtained from different animals. **(A)** PVAT(+) /E+ rings (n = 7 control, 6 for S1P and 7 for CYM 5478). **(B)** PVAT(+) /E– rings (n = 8 control, 10 for S1P and 8 for CYM 5478). **(C)** PVAT(–)/E+ rings (n = 7 control, 7 for S1P and 6 for CYM 5478). **(D)** PVAT(–)/E– rings (n = 7 control, 5 for S1P and 7 for CYM 5478). (E) Representative myograph recording from a PVAT(+) control ring showing PE pre-contraction, the onset of hypoxia and the subsequent relaxation. Statistical analysis was performed using the Kruskal–Wallis test followed by Dunn's multiple comparisons test. Asterisks indicate statistical significance (*$p < 0.05$, **$p < 0.01$).

5.3.13 Modulatory effect of CYM 5478 on PE-precontracted thoracic aorta under normoxia

A relaxation in response to CYM 5478 was noted before hypoxic exposure. As this was not observed with S1P, the direct effect of CYM 5478 on vascular tone was further investigated under normoxic conditions. Thoracic aortic rings were precontracted with PE (1 μM) and subsequently treated with CYM 5478 (10 μM). CYM 5478 induced significant relaxation in PVAT(+)/E+ and PVAT(+)/E– rings ($p < 0.01$), as well as in PVAT(–)/E+ and PVAT(–)/E– rings ($p < 0.05$), compared with untreated controls (Figure 5-16).

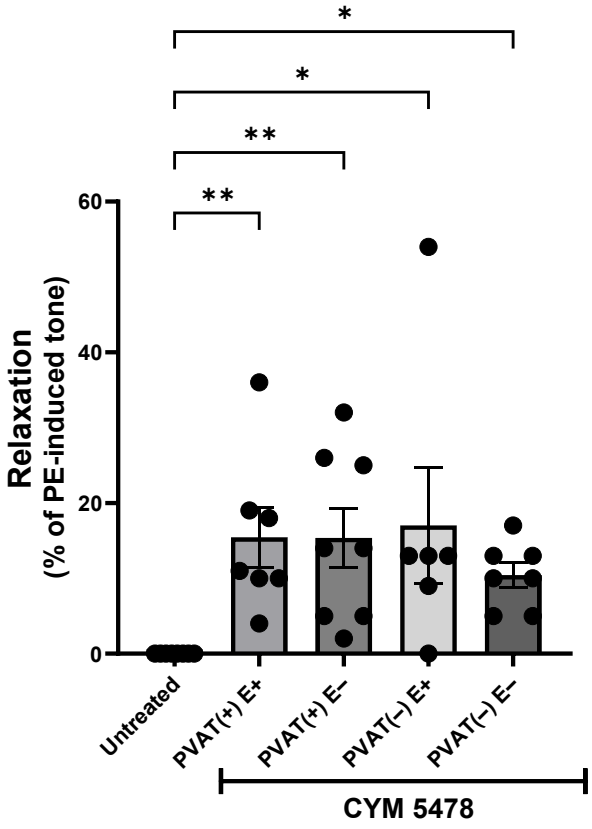

Figure 5-16 Effect of CYM 5478 on relaxation in thoracic aorta with and without PVAT under normoxia.
Thoracic aortic rings were precontracted with PE (1 μM) and subsequently treated with CYM 5478 (10 μM) under normoxic conditions. Relaxation is expressed as a percentage of the precontracted tone induced by PE and presented as mean ± SEM from arteries obtained from different animals. Data are presented as mean ± SEM from seven independent experiments for control (untreated), seven for PVAT(+) /E+, eight for PVAT(+) /E–, six for PVAT(–)/E+, and seven for PVAT(–)/E–. Statistical analysis was performed using the Kruskal–Wallis test followed by Dunn's multiple comparisons test. Asterisks indicate statistical significance (*$p < 0.05$, **$p < 0.01$).

5.4 Discussion

This chapter aimed to define how acute hypoxia affects the SphK/S1P axis in adipocytes and PVAT from different anatomical locations and to test whether S1P signalling contributes to the PVAT-dependent hypoxic relaxation observed previously (Chapter 3). In differentiated 3T3-L1 adipocytes, both chemical ($CoCl_2$) and gas hypoxia selectively increased SphK1 mRNA, but only gas hypoxia transiently increased SphK1 phosphorylation and total SphK1 protein was unchanged. Despite this shared transcriptional response, extracellular S1P release differed, increasing with $CoCl_2$ (4 h) and decreasing with gas hypoxia (1 h). A short period of gas hypoxia (30 min) did not significantly alter SphK1 mRNA, SphK1 phosphorylation, total SphK1, or tissue S1P content in thoracic or mesenteric PVAT. However, thoracic PVAT released less S1P into conditioned medium during hypoxia, and basal S1P release was sensitive to SphK1 inhibition (PF543), whereas mesenteric PVAT showed effect of hypoxia on S1P release. In thoracic aorta, exogenous S1P or the $S1P_2$ agonist CYM 5478 did not modify hypoxic relaxation when PVAT was present but reduced relaxation when PVAT was removed, and under normoxia CYM 5478 produced a modest relaxation in most ring preparations. Taken together, these findings indicate that (i) acute gas hypoxia suppresses S1P release from thoracic PVAT despite preserved SphK1 protein, (ii) $S1P/S1P_2$ signalling can oppose hypoxic relaxation at the vessel wall when PVAT is absent, and (iii) PVAT-derived factors predominate over $S1P/S1P_2$ under PVAT-replete conditions, consistent with Chapter 3 where the presence of PVAT enables robust hypoxic relaxation.

My results from 3T3-L1 adipocytes demonstrate that chemical ($CoCl_2$) and gas-induced hypoxia had differential effects on the SphK/S1P signalling. Both increased SphK1 mRNA; however, only gas hypoxia increased SphK1 phosphorylation at 1 h, and only $CoCl_2$ increased extracellular S1P at 4 h, whereas gas hypoxia actually decreased it. These differences likely reflect the mechanism of action of $CoCl_2$, which functions as a prolyl-hydroxylase (PHD) inhibitor and transition metal that stabilises HIF-α by substituting for Fe^{2+} in the catalytic centre of PHD enzymes. This disrupts recognition of hydroxylated HIF-α by the von Hippel–Lindau (pVHL) E3 ubiquitin ligase complex, thereby preventing ubiquitination and proteasomal degradation (Muñoz-Sánchez and Chánez-Cárdenas, 2019, Srinivasan and Dunn, 2011). $CoCl_2$ has also been reported to

display HIF-isoform bias, with a tendency to favour induction of HIF-1α over HIF-2α in certain cellular contexts, and to trigger additional redox -metallic effects unrelated to physiological oxygen sensing (Leonard et al., 2004, Tripathi et al., 2019, Befani et al., 2013). In contrast, gas hypoxia engages oxygen-sensing pathways more broadly, including HIF-2α–dependent SphK1 programmes (Anelli et al., 2008) and the wider hypoxia stress response.

Functionally, effective concentrations of S1P depend not only on synthesis by SphK1/2 but also on degradation by sphingosine-1-phosphate phosphatase 1 (SGPP1) and S1P lyase (SPL), and on export by transporters such as SPNS2, MFSD2B and ABCC1. In RA synoviocytes, chemical hypoxia decreases intracellular S1P by upregulating SGPP1 and SPL and blocking SPL restores S1P-receptor signalling (Zhao et al., 2015a, Zhao et al., 2019). Moreover, SPNS2-dependent export is required for extracellular S1P–HIF coupling in cancer cells; neutralising S1P or knocking down SPNS2 blunts hypoxia–HIF signalling (Bouquerel et al., 2016, Ader et al., 2015). My data are most consistent with a scenario in which gas hypoxia transiently activates SphK1 phosphorylation but simultaneously suppresses S1P export and/or enhances degradation, producing lower extracellular S1P at 1 h. $CoCl_2$, by contrast, may permit or even augment export while stabilising HIF-1α, thereby allowing extracellular S1P accumulation at 4 h, aligning with findings from Ito et al. (2013). Overall, these differences emphasise that $CoCl_2$ and gas hypoxia should not be treated as equivalent, and that gas hypoxia provides the more physiologically relevant stimulus, even though it is technically more demanding.

Hypoxia affects the SphK1/S1P axis differently across cells and conditions. For example, human and rat endothelial cells display increased SphK1 expression and activity during hypoxia, whereas SphK2 expression is not changed (Schwalm et al., 2008, Alganga et al., 2019). Moreover, human pulmonary artery smooth muscle cells exhibit SphK1/2 upregulation after short-term hypoxia and selective SphK1 induction with chronic hypoxia (Ahmad et al., 2006). Additionally, glioma cells show rapid SphK1 mRNA induction peaking at approximately 4 h (Anelli et al., 2008). Furthermore, rat amoeboid microglia demonstrate a quick rise in SphK1 immunoreactivity within 15–60 min (Lin et al., 2011) and osteosarcoma cells display a transient twofold increase in S1P production at 2–4 h that returns to baseline by about 16 h (Gomez-Brouchet et al., 2022). Ader et al. (2008) further demonstrated that SphK1 activation stabilises HIF-1α via Akt/GSK-3β-dependent

inhibition of VHL-mediated proteasomal degradation. In disease conditions with constitutive HIF stabilisation, SphK1 overexpression is likewise evident, for example in clear cell renal carcinoma (Salama et al., 2015). Conversely, in primary HUVECs and rat heart tissue from our lab, short-term hypoxia did not alter SphK1 (Alganga, 2017). In rheumatoid arthritis research, $CoCl_2$ increased SphK1 in fibroblast-like synoviocytes (FLS) from healthy donors (normal FLS) but not in FLS derived from rheumatoid arthritis patients (RA-FLS) (Zhao et al., 2019), and chemical hypoxia lowered intracellular S1P through upregulated SGPP1 and SPL despite potential increases in synthesis (Zhao et al., 2015a). Taken together, these reports indicate that hypoxic regulation of SphK1 is highly context dependent, varying with cell type, the hypoxic stimulus (gas versus $CoCl_2$) and duration, and with the relative effects on synthesis, degradation and export.

Across adipocytes and PVAT, total SphK1 remained stable despite hypoxia-induced transcriptional and/or phospho-activation, indicating that acute regulation is determined by activity and localisation rather than abundance. In 3T3-L1 cells, inhibiting the proteasome (MG132, lactacystin) or cathepsin B/lysosome (CA-074ME) did not elevate SphK1, consistent with protein turnover not being rate-limiting at the sampled times. In contrast, in thoracic PVAT, the combination of CA-074ME with MG132 increased SphK1 under hypoxia, suggesting involvement of both lysosomal and proteasomal pathways in SphK1 turnover in this depot. This is consistent with evidence that SphK1 can be directed to proteasomal or lysosomal degradation in a cell- and stimulus-dependent manner, and with observations in rat coronary endothelium where, under short hypoxia, the non-specific SphK1 inhibitor Ski-induced loss of SphK1 was rescued by either MG132 or CA-074ME alone; implicating both proteasome and lysosome in SphK1 turnover during hypoxia (Taha et al., 2006b, Loveridge et al., 2010, Alganga et al., 2019). Mechanistically, SphK1 can be rapidly activated without a change in total protein through ERK1/2-dependent phosphorylation at Ser225 that drives plasma-membrane recruitment (Pitson et al., 2003), through phosphorylation-independent Gq-coupled receptor signalling that relocalises/activates the enzyme (ter Braak et al., 2009, Gault et al., 2012), and via regulatory interactions (e.g., CIB1 and binding to anionic phospholipids such as phosphatidic acid and phosphatidylserine) that stabilise a high-activity, membrane-proximal conformation (Jarman et al., 2010, Delon et al., 2004, Stahelin et al., 2005).

Beyond these acute changes, SphK1 abundance is regulated more slowly by transcriptional inputs (e.g., Sp1, AP-1/AP-2, E2F family, HIF-2α, LMO2) and microRNA-mediated post-transcriptional downregulation (e.g., miR-124, miR-506, miR-3677, miR-6862) (Hazar-Rethinam et al., 2015, Bonica et al., 2020, Wang et al., 2020d, Zhang et al., 2013b, Lu et al., 2015, Yao et al., 2020, Xue et al., 2020), processes unlikely to shift total protein within the time-frame of 6 h (adipocytes) and 30 min (PVAT) examined here. Finally, the depot-specific behaviour, observed in thoracic but not mesenteric PVAT, likely reflects intrinsic BAT-like versus WAT-like phenotypes and differences in synthesis and release profiles that influence SphK1 localisation and degradation. Collectively, these observations indicate that hypoxia regulates SphK1 mainly via rapid localisation/activation and lysosomal turnover, resulting in reduced extracellular S1P release rather than changes in total protein. A schematic summary of the depot-specific effects in thoracic versus mesenteric PVAT is provided in Figure 5-17.

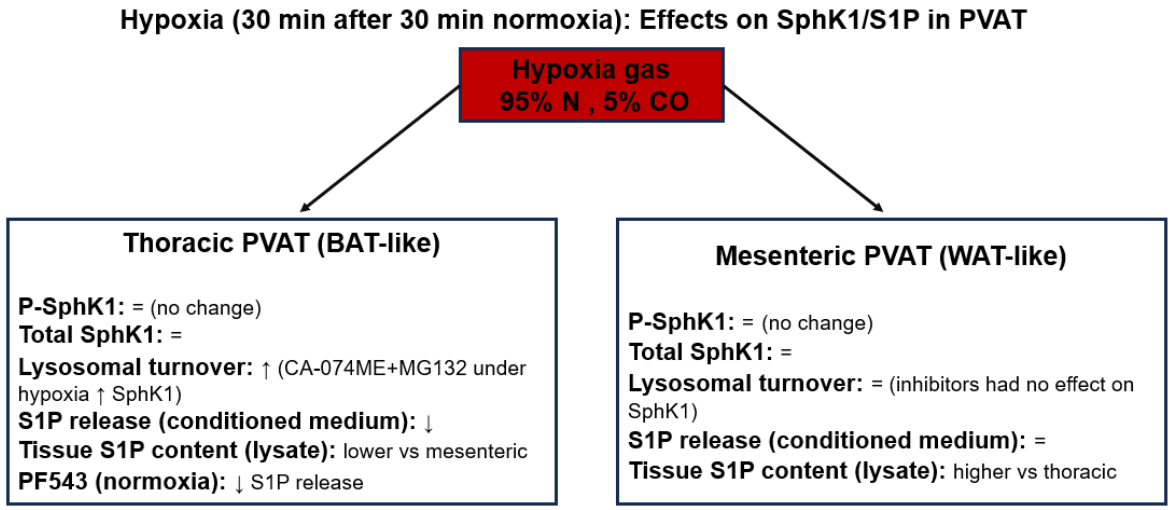

Figure 5-17 Schematic of hypoxia effects on SphK1 and S1P in thoracic and mesenteric PVAT
Thoracic PVAT (BAT-like): Acute gas hypoxia (30 min) does not significantly change P-SphK1 or total SphK1, but the combination of CA-074ME with MG132 under hypoxia increased SphK1, consistent with lysosomal and proteasomal turnover. Hypoxia reduces S1P release into conditioned media; basal S1P release is sensitive to SphK1 inhibition (PF543). Tissue S1P content is lower than in mesenteric PVAT. Mesenteric PVAT (WAT-like): No significant change in P-SphK1 or total SphK1; inhibitors have no effect on SphK1 abundance; S1P release is unchanged by hypoxia; tissue S1P content is higher than in thoracic PVAT. ↑ increase; ↓ decrease; = no detectable change.

Across assays, thoracic PVAT responded differently from mesenteric PVAT. Baseline S1P content in thoracic PVAT lysate was lower than in mesenteric PVAT, hypoxia reduced S1P release from thoracic but not mesenteric PVAT, and SphK1 inhibition with PF543 decreased S1P release from thoracic PVAT under normoxia whereas mesenteric PVAT was relatively unaffected. These depot-specific effects are consistent with the BAT-like phenotype and higher sympathetic tone of

thoracic PVAT (Ahmad et al., 2019, Jeong et al., 2018, Hanscom et al., 2024) and with the established observation that BAT-like and WAT-like PVAT exhibit distinct metabolic and secretory features (Gálvez-Prieto et al., 2008, Padilla et al., 2013, Victorio et al., 2016, Hwej et al., 2024). They also align with Chapter 4, where acute hypoxia selectively suppressed adiponectin in 3T3-L1 adipocytes and thoracic PVAT but not mesenteric PVAT, and where thoracic PVAT showed higher basal adiponectin than mesenteric PVAT, whereas tissue S1P content was higher in mesenteric than thoracic PVAT; moreover, hypoxia reduced S1P release from thoracic but not mesenteric PVAT, reinforcing a depot-specific hypoxic response of the PVAT secretome. A mechanistic basis likely includes differences in expression or activity of S1P exporters such as SPNS2, MFSD2B and ABCC1 and degradative enzymes such as SGPP1 and SPL, which warrant direct measurement. The PF543 sensitivity of thoracic PVAT also aligns with vascular work in which PF543 diminished hypoxia-driven increases in SphK1 and reduced S1P-induced vasorelaxation in rat arteries, supporting SphK1 as a regulatory node for local S1P availability in hypoxic vascular tissues (Alganga et al., 2019).

My wire-myography data indicate no supportive role for exogenous S1P or $S1P_2$ activation in enhancing hypoxic relaxation when PVAT is present, and $S1P/S1P_2$ signalling attenuates relaxation when PVAT is absent. This is consistent with the reduced S1P release from hypoxic thoracic PVAT and suggests S1P is not the PVAT-derived pro-relaxant in acute hypoxia. Instead, PVAT likely releases other vasodilators that counteract any $S1P_2$-mediated anti-relaxant influence on smooth muscle, consistent with Chapter 3 where PVAT enabled robust hypoxic relaxation. Consistent with this interpretation, VSMCs predominantly express $S1P_2$ with lower $S1P_{1/3}$, and S1P binding induces calcium influx and RhoA/ROCK-dependent contraction, providing a likely mechanism by which $S1P/S1P_2$ signalling reduces hypoxic relaxation in PVAT(–) rings (Alewijnse et al., 2004, Bischoff et al., 2000, Hemmings et al., 2006, Coussin et al., 2002). Additionally, PVAT can facilitate hypoxia-induced vasorelaxation via adipocyte-derived relaxing factors, including H_2S, and through activation of ATP-sensitive potassium channels, independently of the endothelium and NO (Donovan et al., 2018, Maenhaut et al., 2010). The normoxic relaxation observed with CYM 5478 is notable and may reflect off-target effects, endothelial crosstalk that secondarily engages $S1P_{1/3}$–eNOS signalling, or differences in baseline tone, as the rings were precontracted with PE.

Nevertheless, its inhibitory effect on hypoxic relaxation in PVAT(–) rings supports the interpretation that $S1P_2$ acts as an inhibitory regulator of hypoxic vasodilation when PVAT-derived relaxants are absent. Notably, independent work from our laboratory showed that activating $S1P_2$ with CYM 5478 increases iNOS expression and NO production in IL-1ß–stimulated 3T3-L1 adipocytes (Aljaezi, 2024), consistent with reports that $S1P_2$ inhibition reduces iNOS in a rat glomerular mesangial cell line (Gong et al., 2020) and lowers iNOS and NO in rat placenta in a preeclampsia model (Zhang et al., 2021).Together, these findings suggest a context-dependent role for $S1P_2$, pro-contractile via RhoA/ROCK in vascular smooth muscle while pro-NO in adipocytes. Overall, PVAT-dependent hypoxic relaxation (Chapter 3) is unlikely to be driven by S1P export from PVAT. Rather, S1P/$S1P_2$ may counter-regulate hypoxic dilation in PVAT(–) vessels while PVAT-derived mediators dominate in PVAT(+) rings.

5.5 Conclusion

In summary, acute gas hypoxia rapidly reduces S1P release from 3T3-L1 adipocytes and thoracic PVAT despite transient SphK1 activation and unchanged total SphK1. Functionally, S1P/$S1P_2$ acts as a negative regulator of hypoxic dilation when PVAT is absent, whereas PVAT-derived mediators dominate in PVAT(+) rings and enable the robust relaxation seen in Chapter 3, arguing against S1P as the PVAT-derived pro-relaxant in acute hypoxia. Depot-specific differences were clear, with thoracic (BAT-like) PVAT showing hypoxia-induced suppression of S1P release and PF543 sensitivity, whereas mesenteric PVAT was comparatively insensitive and had higher S1P content in tissue lysates irrespective of oxygenation. Because they produce distinct S1P responses, $CoCl_2$ and gas hypoxia should not be treated as equivalent models. Future work should focus on S1P exporters, degradative control, receptor-selective pharmacology, and comprehensive proteomics of secreted factors (secretomics) coupled to reconstitution/neutralisation experiments to define how PVAT contributes to hypoxia-induced vasorelaxation.

Chapter 6 General discussion

6.1 Summary and General discussion

The present thesis combined in vitro and ex vivo approaches to determine how acute hypoxia affects adiponectin and SphK1/S1P pathways in adipocytes and PVAT, and how PVAT shapes hypoxic vasoreactivity. The central hypothesis was that PVAT modulates hypoxia-induced vasoreactivity in a vessel- and depot-specific manner, reflecting the differential effects on contractility reported across vascular beds, and that this modulation is conditioned by endothelial integrity and specific receptor pathways (e.g., AdipoR1 and $S1P_2$). In line with this, Chapter 3 analysed functional vascular responses to hypoxia with controlled manipulation of PVAT and endothelium; Chapter 4 examined adiponectin gene expression, protein and secretion in adipocytes and PVAT and tested pathway involvement in hypoxic relaxation; and Chapter 5 investigated SphK1/S1P pathway in adipocytes and PVAT and assessed whether S1P/$S1P_2$ contributes to hypoxia-induced vasorelaxation.

Three broad conclusions emerge from these chapters. First, PVAT augments acute hypoxic vasorelaxation via mechanisms that can function independently of the endothelium. In the acute hypoxia protocol (hypoxia applied during phenylephrine tone), hypoxic relaxation was statistically significant and PVAT-dependent, and it was also observed in endothelium-denuded rings, consistent with PVAT-derived H_2S/CBS pathways and K^+-channel opening observed in other studies (Donovan et al., 2018, Maenhaut et al., 2010, Fang et al., 2009, Daut et al., 1990). This vasodilation primarily augments oxygen delivery to tissues when oxygen availability is reduced. By contrast, when vessels were pre-exposed to hypoxia and then re-oxygenated before testing, phenylephrine contractions increased and cromakalim (K_{ATP} opener) relaxation was also enhanced, highlighting how timing (pre-exposure versus real-time hypoxia) and redox transitions during re-oxygenation remodel PVAT, endothelium and VSMC cross-talk (Granger and Kvietys, 2015, Ku, 1982, VanBenthuysen et al., 1987, Tsao et al., 1990, Pearson et al., 1990, Kaeffer et al., 1996). Mechanistically, previous studies have shown that re-oxygenation elevates reactive oxygen species from mitochondria, xanthine oxidase and NADPH oxidases and activates inflammatory signalling, while adipocytes up-regulate IL-1β, IL-8 and TNF-α during hypoxia/re-oxygenation with peaks on re-oxygenation (He et al., 2014, Hong et al., 2014, Granger and Kvietys, 2015, Ku, 1982, Tsao et al., 1990). Although the present study did not directly quantify reactive oxygen species or cytokines, these literature-supported changes

provide a plausible explanation for the increased phenylephrine contractions and the enhancement of K_{ATP}-dependent relaxation after pre-exposure/re-oxygenation, via impairment of endothelial NO-dependent pathways and a shift in PVAT/VSMC signalling towards greater α_1-adrenergic responsiveness and K_{ATP}-sensitive relaxation.

Secondly, while adiponectin is a widely recognised PVAT-derived relaxing factor (Sena et al., 2017, Chen et al., 2003), acute hypoxic vasorelaxation in the thoracic aorta was largely adiponectin-independent. Acute hypoxia reduced adiponectin expression in 3T3-L1 adipocytes and in thoracic PVAT without detectable cytotoxicity, whereas mesenteric PVAT was relatively resistant over the same brief exposure, consistent with depot heterogeneity (Gil-Ortega et al., 2015, Hwej et al., 2024). Notably, this reduction was statistically significant after 1–4 h in adipocytes and after 30 min in PVAT, earlier than the 6–24 h period commonly examined in studies of adipocyte/adipose hypoxia, including chronic and intermittent hypoxia models of obstructive sleep apnoea, in which reductions in adiponectin expression and/or secretion are frequently reported (Tsuchida et al., 2004, Hosogai et al., 2007, Ye et al., 2007, Wang et al., 2007, Chen et al., 2006, Magalang et al., 2009). Pharmacological modulation showed that neither AdipoR1 blockade nor β_3-adrenoceptor agonists altered hypoxic relaxation when PVAT was present; in PVAT-removed, endothelium-intact rings, β_3-adrenoceptor agonism attenuated relaxation, implying a β_3-linked endothelial inhibitory pathway that is normally buffered by PVAT. This contrasts with report that endothelial β_3-adrenoceptors promote vasorelaxation via NO/EDH in other vascular beds (Dessy et al., 2004, Filippi et al., 2022). This is compatible with reports that β_3-adrenoceptor stimulation of PVAT is associated with endothelium-independent, adiponectin-dependent anticontractile (vasodilatory) effects, suggesting that β_3 activation may promote adiponectin release (Saxton et al., 2018, Weston et al., 2013). Moreover, PVAT provides a range of mediators that can support relaxation under oxygen stress, including hydrogen peroxide (H_2O_2), H_2S and nitric oxide (NO), omentin, methyl palmitate, prostacyclin and angiotensin 1–7 (Tong et al., 2023, Victorio et al., 2016, Lee et al., 2011, Gao et al., 2007, Fang et al., 2009, Gil-Ortega et al., 2014). This diversity of mediators likely preserves the immediate hypoxic response in the thoracic aorta despite a decrease in adiponectin. Generally, systemic arteries dilate under hypoxia to enhance tissue perfusion via

metabolites like adenosine, NO, and HIF activation (Böger and Hannemann, 2020, Hannemann and Böger, 2022).

Thirdly, although brief hypoxic exposure altered S1P release in a depot-specific manner, S1P did not modify PVAT-dependent hypoxic relaxation. In thoracic PVAT, 30 min of gas hypoxia lowered S1P release into conditioned media, an effect reproduced under normoxia by SphK1 inhibition (PF543), whereas mesenteric PVAT was unchanged, consistent with known phenotypic differences between these depots (Gálvez-Prieto et al., 2008, Padilla et al., 2013, Victorio et al., 2016, Hwej et al., 2024). In adipocytes, acute hypoxia selectively engaged SphK1 signalling. Similarly, hypoxia increases SphK1, without affecting SphK2, in human and rat endothelial cells (Schwalm et al., 2008, Alganga et al., 2019). It also produced stimulus-dependent changes in extracellular S1P, increasing with $CoCl_2$ and decreasing with gas hypoxia; this was a clear instance in which the hypoxia model altered the direction of effect in my experiments. The decrease in extracellular S1P with gas hypoxia is most consistent with reduced export and/or enhanced degradation. Consistent with this interpretation, SphK1 inhibition (PF543) mimicked the hypoxia-induced decrease under normoxia and further lowered extracellular S1P during hypoxia, indicating that some SphK1-dependent S1P production continues under low O_2. The net extracellular pool nevertheless declines, plausibly because hypoxia limits export (SPNS2-dependent) and/or accelerates degradation (SGPP1/SPL), as reported in previous studies linking S1P export to HIF signalling and hypoxia-dependent remodelling of S1P turnover (Ader et al., 2015, Bouquerel et al., 2016, Zhao et al., 2015a, Zhao et al., 2019). Functionally, exogenous S1P or the selective $S1P_2$ agonist CYM 5478 reduced hypoxia-induced relaxation in PVAT(–) thoracic aorta, with stronger effects via $S1P_2$. This pattern is in line with previous reports that $S1P_2$ signalling activates RhoA/ROCK in vascular smooth muscle to oppose dilation (Alewijnse et al., 2004, Hemmings et al., 2006, Coussin et al., 2002). By contrast, neither S1P nor CYM 5478 altered hypoxic relaxation when PVAT was present, in keeping with evidence that PVAT-derived mediators such as H_2S and K^+-channel mechanisms dominate under PVAT(+) conditions (Donovan et al., 2018, Maenhaut et al., 2010). Overall, acute hypoxia suppresses S1P release from thoracic PVAT and reveals an S1P/$S1P_2$-mediated inhibitory influence on hypoxic dilation in PVAT-depleted vessels,

indicating that mediators other than S1P likely underlie the acute PVAT-dependent vasorelaxant response.

Integrating across chapters, timing and the hypoxia stimulus are key determinants of outcome, which helps explain why some studies report hypoxia-induced relaxation (Donovan et al., 2018, Maenhaut et al., 2010) while others find impaired PVAT anti-contractility or greater acetylcholine dysfunction in PVAT-intact vessels (Greenstein et al., 2009, Zaborska et al., 2016, Sousa et al., 2019). Acute hypoxia applied during established contraction consistently revealed PVAT's ability to augment endothelium-independent relaxation, whereas pre-exposure to hypoxia followed by re-oxygenation increased phenylephrine contractility and, in some conditions, enhanced K_{ATP}-dependent relaxation under normoxia. As noted above, re-oxygenation can generate reactive oxygen species and inflammatory signalling that reduce endothelial NO and alter PVAT–VSMC cross-talk; these processes may underlie the increased phenylephrine contractions and K_{ATP}-related changes observed here, although I did not measure these mediators in this study (He et al., 2014, Hong et al., 2014, Granger and Kvietys, 2015, Ku, 1982, Tsao et al., 1990, VanBenthuysen et al., 1987, Pearson et al., 1990). The choice of hypoxic stimulus also influences interpretation: as reported in previous studies, $CoCl_2$ acts as an Fe^{2+}-mimetic prolyl-hydroxylase inhibitor that preferentially stabilises HIF-1α and introduces redox-metal effects, whereas gas hypoxia engages physiological O_2-sensing pathways, including HIF-2α-linked transcriptional responses such as SphK1 regulation (Muñoz-Sánchez and Chánez-Cárdenas, 2019, Befani et al., 2013, Anelli et al., 2008, Tripathi et al., 2019, Leonard et al., 2004). Taken together, the timing of oxygen exposure, endothelial integrity, PVAT status and the hypoxia model explain much of the apparent variation across studies and underline the importance of experimental design when deciding which pathways are responsible.

Moreover, depot phenotype plays an important role in regulating the molecular response to hypoxia. Thoracic PVAT displays BAT-like features, with multilocular adipocytes and UCP-1 expression, whereas mesenteric/abdominal PVAT is WAT-like, less vascularised, lower in thermogenic capacity, and more pro-inflammatory (Padilla et al., 2013, Gálvez-Prieto et al., 2008, Cinti, 2011). In line with this background, thoracic depots exhibit higher eNOS/NO bioavailability and greater

sympathetic tone/noradrenaline content than mesenteric depots; in the present data, thoracic PVAT also showed higher basal adiponectin (Victorio et al., 2016, Jeong et al., 2018, Ahmad et al., 2019, Leloup et al., 2015). In this study, brief gas hypoxia reduced adiponectin in 3T3-L1 adipocytes and in thoracic PVAT and lowered S1P release from thoracic PVAT, whereas mesenteric PVAT was less affected over the same interval. These molecular features are consistent with broader BAT biology, including roles in lipid clearance, BATokine signalling and improved insulin sensitivity, although BAT activity declines with obesity (Hildebrand et al., 2018, van Marken Lichtenbelt et al., 2009, Gil-Ortega et al., 2015). Taken together, the thoracic–mesenteric contrast in adipokine pathways (adiponectin) and sphingolipid pathways (S1P/SphK1) provides the mechanistic context for PVAT biology during hypoxia. Additionally, thoracic aorta (elastic conduit) and mesenteric arteries (muscular resistance) differ in wall composition and haemodynamic role (pressure buffering vs control of regional perfusion/systemic resistance); these distinctions shape how PVAT influences reactivity under hypoxia (Leloup et al., 2015). They also align with the distinct disease contexts of each bed, with atherosclerosis in conduit arteries and dysregulated tone and hypertension in resistance arteries. Therefore, interpretation and experimental design should give due consideration to depot identity and, where possible, use depot-derived adipocytes or intact PVAT tissue preparations, rather than generalising from a single differentiated cell line.

During the immediate hypoxic phase, PVAT-derived dilator pathways and K^+-channel mechanisms, notably H_2S and K_{ATP}, set the tone. Acute hypoxia produced clear PVAT-dependent relaxation in both endothelium-intact and endothelium-denuded rings, consistent with published H_2S/CBS and K^+-channel mechanisms (Donovan et al., 2018, Maenhaut et al., 2010). By contrast, adiponectin may be more relevant to basal anticontractility and longer-term homeostasis, consistent with literature showing reduced adiponectin in chronic hypoxia or obesity-associated conditions, and that restoring adiponectin can rescue function (Badran et al., 2019, Almabrouk et al., 2018, Ye et al., 2007). Consistent with this hierarchy, acute hypoxic relaxation in the present study was maintained when AdipoR1 was blocked or when S1P or an $S1P_2$ agonist was applied in PVAT(+) rings, whereas in PVAT-removed vessels exogenous S1P or $S1P_2$ activation limited hypoxic relaxation, consistent with smooth-muscle RhoA/ROCK signalling

(Alewijnse et al., 2004, Hemmings et al., 2006, Coussin et al., 2002). In the systemic circulation and in the absence of PVAT, hypoxia can relax pre-constricted vessels in several species and beds, with proposed mechanisms involving O_2-sensing that lowers intracellular Ca^{2+} in vascular smooth muscle (Totzeck et al., 2014, Kerkhof et al., 2002, Lynch et al., 2006, Herrera and Walker, 1998, Gasser et al., 1993, Pearce et al., 1992). The β_3-adrenoceptor context is also important. In intact PVAT, β_3-adrenoceptor stimulation induces adiponectin-dependent anticontractile effects, indicating that β_3 activation likely promotes adiponectin release (Saxton et al., 2018, Weston et al., 2013), whereas in PVAT(–), endothelium-intact rings β_3 agonism attenuated hypoxic relaxation in this study, pointing to an endothelial β_3-linked inhibitory pathway when PVAT buffering is absent. Taken together, acute hypoxic relaxation in the thoracic aorta is PVAT-supported and largely independent of endothelial status, adiponectin, or sphingosine signalling over this time interval. β_3-adrenoceptor and S1P/$S1P_2$ pathways appear primarily as inhibitory or counter-regulatory influences when PVAT's rapid dilator support is removed.

Link to adiponectin–sphingolipid interplay. Prior work indicates bidirectional crosstalk: adiponectin, through its receptors AdipoR1 and AdipoR2, exhibits intrinsic ceramidase activity that hydrolyses ceramide to sphingosine, which is then phosphorylated by sphingosine kinases to generate S1P, with increased extracellular S1P release also observed (Holland et al., 2010, Bikman and Summers, 2011, Bernacchioni et al., 2022, Botta et al., 2020). Conversely, S1P signalling, particularly via $S1P_2$, can inhibit adipogenesis and reduce adiponectin expression, and genetic or pharmacological suppression of the SphK/S1P pathway increases adiponectin and an anti-inflammatory profile in adipose depots (Moon et al., 2015, Jeong et al., 2015, Moon et al., 2014, Wang et al., 2014). In this thesis, brief gas hypoxia lowered adiponectin in 3T3-L1 adipocytes and thoracic PVAT and reduced S1P release from thoracic PVAT, yet PVAT-dependent hypoxic relaxation remained intact and was unaffected by AdipoR1 blockade and by S1P or $S1P_2$ activation when PVAT was present. These observations are consistent with, but do not establish, a reduction in AdipoR-associated ceramidase activity and ceramide-to-sphingosine flux under acute hypoxia, which could lower S1P generation. Additionally, although S1P/$S1P_2$ signalling has been reported to lower adiponectin (Moon et al., 2015, Jeong et al., 2015, Moon et al., 2014), exogenous

S1P and $S1P_2$ agonism did not diminish hypoxic relaxation in PVAT-intact aorta in this study, with inhibitory effects obvious only in PVAT-removed rings. Adiponectin is therefore unlikely to be a major contributor to PVAT-dependent hypoxic relaxation when the hypoxia is applied acutely.

6.2 Limitation and future direction

6.2.1 limitations

Experimental context. Most vascular experiments used isolated aortic rings and ex vivo PVAT, which allowed tight control of O_2 and pharmacology but removed neural, humoral and haemodynamic inputs present in vivo. Consequently, PVAT–endothelium–VSMC crosstalk was studied without systemic feedback, so effect sizes and mediator hierarchies may differ in the intact circulation.

Euthanasia method. A further limitation is that pentobarbital was used only in the initial thoracic aorta experiment (Section 3.3.2), which involved a small number of vessels (n = 1–2 per condition), whereas all other vascular experiments used CO_2 overdose. Pentobarbital can modulate several ion channels, including $GABA_A$ receptors and certain voltage-gated Ca^{2+} and K^+ channels (Löscher and Rogawski, 2012, Barker and Rogawski, 1993, Joksovic et al., 2004, O'beirne et al., 1987, Gibbons et al., 1996), raising the possibility that euthanasia method might influence vascular tone. Although qualitative inspection of the recordings did not reveal obvious differences between vessels from pentobarbital- and CO_2-euthanised animals, the sample size was too small for statistical comparison. Moreover, all vessels were extensively washed in PSS and required robust KPSS (more than 4.90 mN) and PE responses to be included. However, a minor confounding effect of euthanasia method cannot be formally excluded.

Time-matched controls during prolonged preconstriction. In the hypoxia-induced relaxation experiments (e.g., Figure 3.10), thoracic aortic rings were precontracted with PE and maintained under tension during the 30-minute hypoxic exposure. A time-matched normoxic control in which vessels remain under sustained PE-induced contraction for an equivalent duration was not included. Because vascular tone may slowly decline over time, part of the relaxation could reflect time-dependent changes rather than hypoxia alone. However, the marked and rapid fall in tension immediately following hypoxic gas introduction, together with the clear recontraction upon reoxygenation, strongly suggests that the response was primarily due to hypoxia rather than by time-related changes. Although the absence of a formal time-matched normoxic control introduces some

uncertainty, the overall pattern of relaxation and recovery supports a hypoxia-dependent effect.

Species and depot scope. Work was performed in male Sprague–Dawley rat thoracic aorta and mesenteric beds and in mouse 3T3-L1 adipocytes. Translatability across species, sexes and PVAT depots therefore remains uncertain. Depot heterogeneity was obvious. For example, acute gas hypoxia suppressed adiponectin in thoracic but not mesenteric PVAT, and reduced S1P release from thoracic PVAT but not mesenteric PVAT, underscoring the need to extend beyond the studied beds.

Exposure conditions. Tissues were maintained under 95% O_2/5% CO_2 (normoxia) for viability and challenged with 95% N_2/5% CO_2 (open bath) ex vivo, or 1% O_2 in sealed chambers for cells. Baseline hyperoxia can condition vascular redox tone and increase reactive oxygen species (Singer et al., 2021), which, as reported in the literature, alters endothelium-dependent responses in organ-bath experiments (Wong et al., 2015). Moreover, oxidation of protein sulfhydryl groups and accumulation of oxidized glutathione (GSSG) are established markers of oxidative stress after ischaemia–reperfusion (I/R), illustrating how extremes of O_2 can disrupt redox signalling (Granger and Kvietys, 2015). For physiological context, in healthy humans at sea level, arterial blood is ~95–100 mmHg pO_2 (~12–13% O_2) and mixed venous blood ~40 mmHg (~5% O_2); most tissues work at (physioxia) around ~5% O_2 (typical ~3–7%), far below atmospheric 21% O_2 and well below organ-bath (95% O_2/5% CO_2) (Ortiz-Prado et al., 2019, McKeown, 2014). Within the arterial wall, microelectrode studies show an adventitia-to-media gradient of roughly 30 to 20–25 mmHg (≈4–3% O_2), with further reductions in atherosclerosis (Hajjar et al., 1988). In adipose depots, interstitial pO_2 is usually in the low % O_2 range; obesity can lower adipose pO_2 (Pasarica et al., 2009). Hypoxic exposures here were short (30 min ex vivo; 1–6 h in vitro), examining only early-phase adaptations rather than chronic or intermittent models relevant to conditions like obstructive sleep apnoea, where recurrent hypoxia–reoxygenation contributes to cardiovascular risk (Tietjens et al., 2019, Magalang et al., 2009). Furthermore, chemical ($CoCl_2$) and gas hypoxia were not equivalent: $CoCl_2$ increased extracellular S1P from adipocytes, whereas gas hypoxia reduced it acutely, highlighting stimulus-dependent biology.

Measurement strategy and analytical resolution. S1P was measured by ELISA, which is convenient and relatively rapid but does not resolve molecular species. It cannot distinguish S1P long-chain-base variants, and antibody cross-reactivity with structurally similar lipids can inflate results when analogues are present. This limitation is noted in literature comparing ELISA with LC–MS/MS for S1P (Sun et al., 2022). By contrast, LC–MS/MS provides species-level resolution and validated sensitivity/specificity for S1P and related sphingolipids, so the exact molecule being measured can be confirmed (Tang et al., 2020). Transporters /degradation components (SPNS2, MFSD2B, ABCC1, SGPP1, SPL) were not measured here, limiting mechanistic explanation for the hypoxia-induced drop in S1P release from thoracic PVAT.

Pharmacology and stimulus scope. Functional assays relied on phenylephrine (PE) for constriction and cromakalim (CK) for relaxation. This narrow focus may limit applicability to other stimuli. Likewise, exogenous S1P and the $S1P_2$ agonist CYM 5478 were tested at a single concentration (10 μM) and although used in prior studies (Herr et al., 2016, Moon et al., 2014), a greater range of concentrations may have revealed different effects. For S1P and CYM 5478, full concentration–response curves in the sub-micromolar range and receptor-selective ligands (including $S1P_{1/3}$ agonists and $S1P_2$ antagonists) were not applied.

Mechanistic testing of candidate mediators. While PVAT augmented hypoxic relaxation and adiponectin declined acutely in thoracic PVAT and 3T3-L1 adipocytes, I did not establish adiponectin causality. The study used $ß_3$-adrenoceptor agonism and an AdipoR-blocking peptide during hypoxia; however, recombinant adiponectin add-back, receptor-selective ligands to distinguish AdipoR1 from AdipoR2, and genetic loss-of-function approaches (e.g., PVAT from Adipoq-deficient donors) were not performed. Other candidate dilator pathways, including H_2S signalling and specific K^+ channels, implicated by prior studies, were not tested here(Donovan et al., 2018, Maenhaut et al., 2010).

$ß_3$-adrenoceptor localisation. $ß_3$-AR agonism reduced hypoxic relaxation only in PVAT(–)/E+ rings, indicating an endothelium-dependent inhibitory mechanism that is prevented by PVAT. However, endothelial versus adipocyte $ß_3$-AR contributions were not distinguished.

Group sizes and statistical power. The adipokine array performed on thoracic PVAT conditioned medium indicated early reductions in LIF, IGFBP-1, IL-10 and resistin under hypoxia; however, the small sample size (n = 2) prevented statistical testing, and these findings should therefore be considered exploratory and used only to guide future work. Across several experiments in this thesis, some groups also had modest sample sizes, which reduces statistical power and may limit the ability to detect subtle but biologically relevant differences. This is particularly obvious in datasets that show directional trends without achieving statistical significance (e.g., Figures 3-2B and 4-6B). Although care was taken to apply consistent methodologies and to confirm vessel or cell viability before analysis, smaller group sizes mean that some comparisons may remain underpowered. Moreover, trend-level effects should be interpreted cautiously.

Housekeeping gene selection. Only one housekeeping gene (TBP) was used for qPCR normalisation. Although raw Ct values confirmed that TBP was stable across normoxic and hypoxic conditions, the use of additional stable reference genes is recommended for maximal accuracy and strengthen the reliability of gene expression analyses.

Use of 3T3-L1 adipocytes as a model of PVAT adipocytes. Differentiated 3T3-L1 adipocytes are widely used as an in vitro model of white adipocytes; however, they do not fully reproduce the phenotype of native PVAT. PVAT is heterogeneous, containing white, beige and brown-like adipocytes alongside stromal and immune cells, whereas 3T3-L1 cultures are a homogeneous, fibroblast-derived lineage. Importantly, previous work has shown that 3T3-L1 adipocytes express features of multiple adipocyte lineages. Although their basal gene expression and bioenergetics resemble white adipocytes, they can undergo UCP1-dependent increases in oxygen consumption and upregulate brown-adipocyte-enriched genes in response to catecholamines, while failing to adopt a beige phenotype under beige-inducing protocols (Morrison and McGee, 2015). These mixed-lineage characteristics highlight that 3T3-L1 adipocytes may not accurately reflect the receptor profile, metabolic properties or hypoxia responses of native PVAT adipocytes. Consequently, molecular findings obtained in 3T3-L1 cells should be interpreted with caution when generalising to thoracic or mesenteric PVAT and their functional contributions to vascular tone or to human adipose tissue.

RNA quality and integrity. A further limitation is that RNA integrity was not formally assessed prior to qPCR analysis. The quality of total RNA is a critical determinant of reliable gene expression measurement, as degraded RNA can compromise downstream applications such as qRT-PCR by increasing variability and reducing the consistency of amplification across samples (Fleige and Pfaffl, 2006). This is particularly relevant for experiments where group sizes were modest or where only trend-level differences were observed, as reduced RNA integrity could increase data variability and further limit statistical power. Although RNA was prepared according to standard procedures and samples showed appropriate 260/280 ratios, the absence of a direct integrity measure (e.g., RIN) introduces uncertainty regarding the contribution of RNA quality to the variability observed in some datasets.

Sex differences in adipose tissue biology. Another limitation of the present study is the use of only male rats, which prevents assessment of potential sex-specific differences in PVAT function and responses to hypoxia. Sex is known to influence adipose tissue distribution, endocrine function, and thermogenic capacity. Visceral adipose tissue represents a greater proportion of total fat mass in men (10–20%) compared with women (5–8%) (Ibrahim, 2010, Wajchenberg, 2000), whereas women accumulate more subcutaneous and overall body fat (Palmer and Clegg, 2015, Berryman and List, 2017). Dorsocervical BAT activity is also greater in young adult women than in men (Martinez-Tellez et al., 2019, Gómez-García et al., 2022), and females show an increased propensity for WAT browning and beige adipocyte recruitment (Gómez-García et al., 2022, Herz et al., 2021). These established sex differences may influence adipokine secretion, adipose oxygenation, vascular regulation, and S1P signalling. The absence of female animals therefore limits generalisability, and future studies incorporating both sexes will be needed to determine whether the hypoxia-induced PVAT responses observed here are sex-specific (sexual dimorphism).

6.2.2 Future directions

Expand vascular function experiments. Extend wire-myography to additional constrictors (e.g., U46619, KCl, Ang II, endothelin-1, serotonin) and dilators

(acetylcholine, sodium nitroprusside [SNP], isoprenaline, bradykinin [BK], adenosine). This will test whether PVAT-dependent hypoxic support and S1P/$S1P_2$-mediated inhibition persist across distinct signalling pathways, including α1-AR/Gq (PE), TP/ETA with prominent ROCK activation (U46619/ET-1), and GPCR-independent depolarisation (KCl), and whether PVAT-derived hyperpolarising mediators interact differently with endothelium-dependent (ACh/BK/adenosine) versus endothelium-independent (SNP) relaxations.

Human and primary adipocytes. Repeat key cellular experiments in primary PVAT adipocytes isolated enzymatically from thoracic and mesenteric depots, and in human adipocyte models such as Simpson-Golabi-Behmel syndrome (SGBS) cells and primary human preadipocyte/adipocyte cultures (Wang et al., 2007, Thelen et al., 2018, Scott et al., 2019, Montanari and Colitti, 2018). Compare depot-specific hypoxia responses and adiponectin/S1P coupling, because primary PVAT and human adipocytes preserve depot identity and human relevance, enabling validation of native AdipoR/S1PR/exporter expression and direct causal linkage to vascular function.

Mechanistic characterisation of the S1P axis. Quantify exporters (SPNS2, MFSD2B, ABCC1), degradative enzymes (SGPP1, SPL), and HIF-1α/-2α in adipocytes and PVAT under gas hypoxia ± SphK1 inhibition (PF543). Test whether blocking export or inhibiting lyase/phosphatase restores extracellular S1P during hypoxia, particularly in thoracic PVAT where release decreased acutely. Combine $S1P_2$ antagonism (JTE-013) with ROCK inhibition under hypoxia to confirm the $S1P_2$–ROCK inhibitory mechanism observed in PVAT(–) rings.

Adiponectin causality during acute hypoxia. Perform add-back (recombinant adiponectin; multimer-resolved), neutralisation, and AdipoR1/2 agonism/antagonism during hypoxia in PVAT(+/–) rings. Use PVAT from Adipoq-deficient donors when possible. Increased temporal sampling at 5–10 min intervals of tissue and CM can resolve rapid secretion vs content changes noted in thoracic PVAT.

Define compensatory dilators and channels. In PVAT(+/–) rings during hypoxia, inhibit NOS/sGC, H_2S synthesis (CBS/CSE), neutralise H_2O_2, and block candidate K^+ channels (K_{ATP}, BK_{Ca}, Kv) to quantify the relative contributions when

adiponectin/S1P are altered. This will address why PVAT sustains hypoxic relaxation even when adiponectin declines and S1P/$S1P_2$ limits dilation at the vessel wall.

Improve quantitation and scope of lipidomics/secretomics. Replace/augment ELISAs with targeted LC–MS/MS for S1P species and precursors. LC–MS/MS methods have been validated for S1P quantification and routinely differentiate multiple sphingolipid species by chain length and saturation (Frej et al., 2015, Li et al., 2014, Byeon et al., 2024). Run secretome proteomics on PVAT CM across short time-courses (15–180 min) to capture dynamics suggested by the array. Reconstitute PVAT support by add-back/neutralisation in CM-transfer experiments to identify a minimal mediator set.

Chronic exposure and systemic context. Test intermittent and chronic hypoxia (with re-oxygenation cycles) in vivo and ex vivo, include metabolic stress (diet-induced obesity), both sexes, and additional PVAT depots (abdominal, coronary). Add blood-cell components (e.g., erythrocyte-conditioned medium) to mimic circulating S1P sources alongside local PVAT release.

Together, these steps will convert the present findings into a mechanistic foundation: clarifying how hypoxia modulates PVAT secretomes in a depot- and time-dependent manner, determining when S1P/$S1P_2$ limits dilation versus when PVAT-derived dilators dominate, and establishing whether the same rules apply in human PVAT and in vivo.

6.3 Conclusion

Across complementary cellular, molecular, and functional assays, this thesis shows that PVAT is the dominant enabler of acute hypoxic vasorelaxation in the rat thoracic aorta. Over the same time scale, hypoxia downregulates adiponectin in thoracic PVAT and 3T3-L1 adipocytes, but hypoxic relaxation remains intact, pointing to compensatory PVAT dilators and ion-channel mechanisms. In parallel, the SphK1/S1P axis is reprogrammed in a stimulus- and depot-specific manner: gas hypoxia suppresses S1P release from thoracic PVAT, and vessel-wall S1P/$S1P_2$ signalling attenuates hypoxic dilation when PVAT is absent but is overcome when PVAT is present. Together, these findings refine the Chapter 1 hypothesis by identifying PVAT-centric, adiponectin-independent, and S1P-resistant mechanisms of acute hypoxic vasodilation, and by highlighting depot specialisation as a key determinant of outcome.

Future work should identify the PVAT mediators that acutely drive dilation, characterise how S1P transport and degradation regulate its paracrine bioavailability, and test whether targeted modulation of these pathways can restore PVAT support in disease states with chronic hypoxia and PVAT dysfunction.

Appendices

1.1 Appendix A – Full-Length Western Blot Images

Full, uncropped Western blot images with visible molecular weight (MW) ladders are presented in this appendix for all proteins analysed in the main thesis. These images show the entire membrane, including MW ladder positions, sample lane order, and any non-specific bands. The quantified band used in the main figures is specified in each caption.

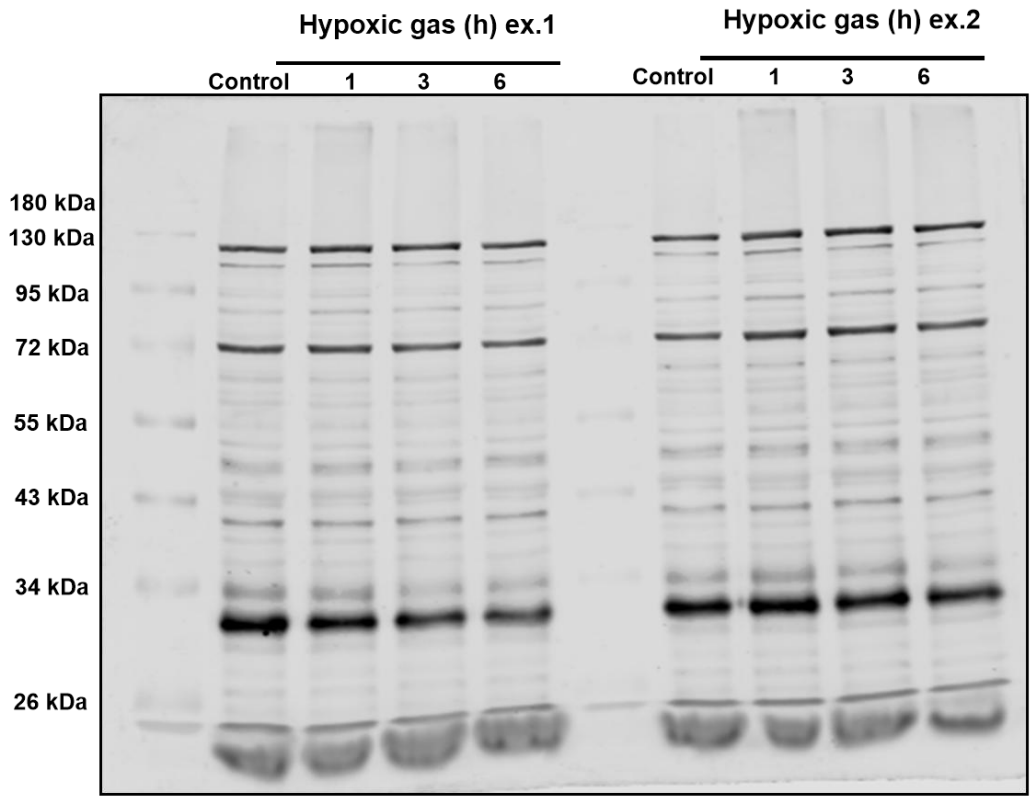

Appendix A 1 Full-length adiponectin Western blot (3T3-L1 adipocytes).
Full, uncropped immunoblot showing adiponectin bands with visible molecular weight ladder. The quantified band in the main figures corresponds to ~30 kDa.

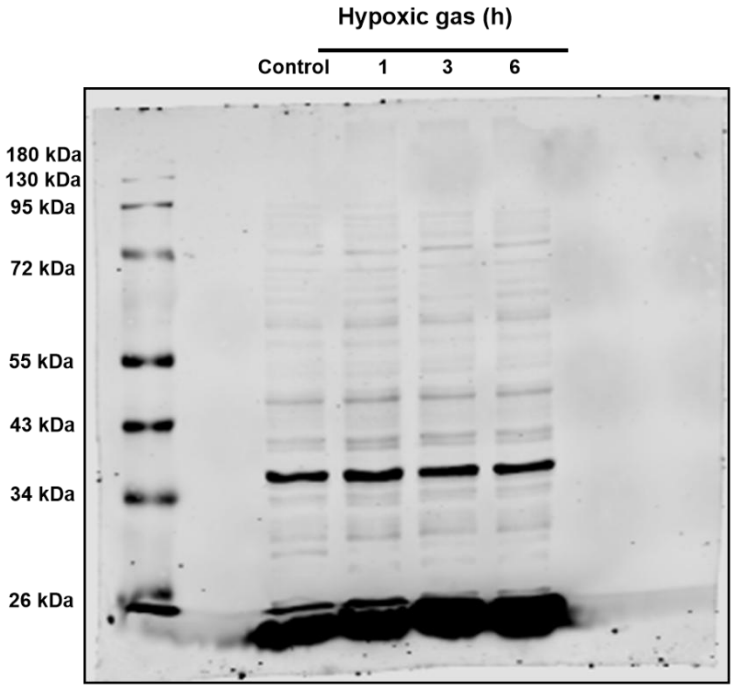

Appendix A 2 Full-length total SphK1 Western blot (3T3-L1 adipocytes).
Complete, uncropped Western blot with MW ladder. Several immunoreactive bands are visible; the band used for quantification in the main figures corresponds to ~34–36 kDa.

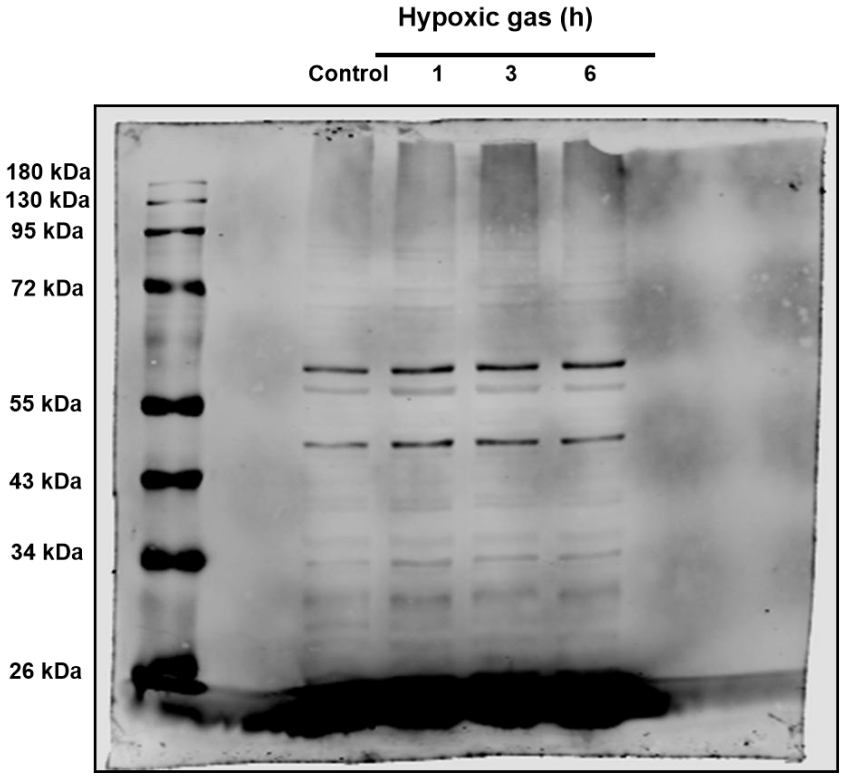

Appendix A 3 Full-length phosphorylated SphK1 (P-SphK1) Western blot (3T3-L1 adipocytes).
Uncropped membrane image with MW ladder visible. The quantified P-SphK1 band in the main figures is located at ~51 kDa.

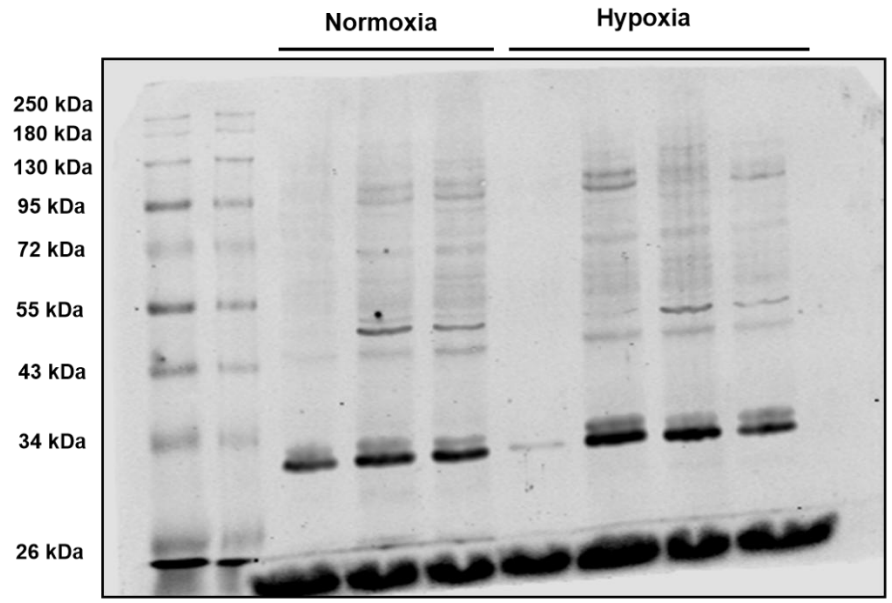

Appendix A 4 Full-length adiponectin Western blot (PVAT).
Full, uncropped immunoblot showing adiponectin bands in mesenteric PVAT with visible molecular weight ladder. The quantified band in the main figures corresponds to ~30 kDa.

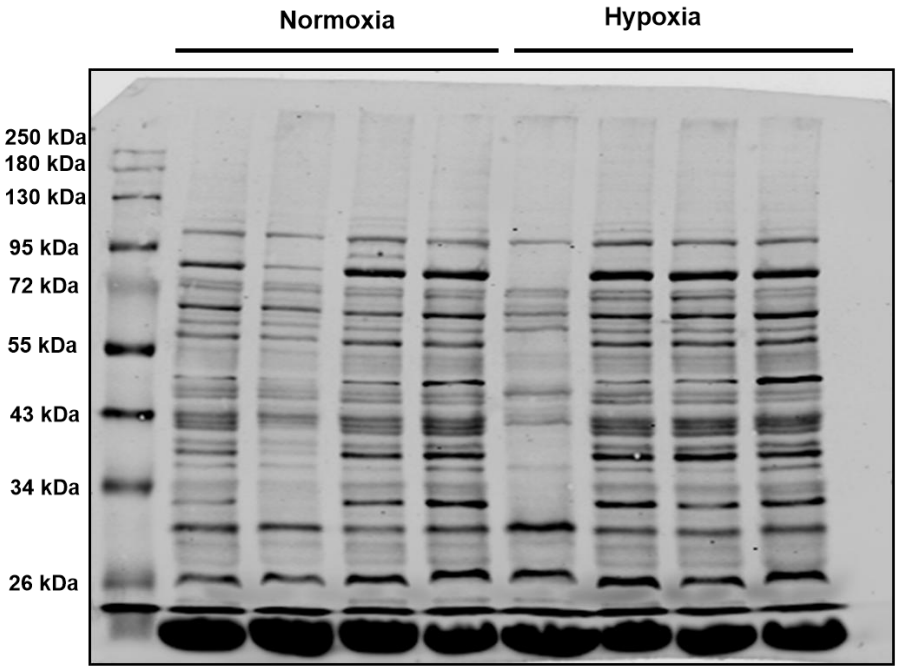

Appendix A 5 Full-length total SphK1 Western blot (PVAT).
Full, uncropped blot showing SphK1 bands in thoracic PVAT alongside the MW ladder. Multiple bands are present; the band used for quantification in the main figures is indicated in that figure and lies between ~34–51 kDa.

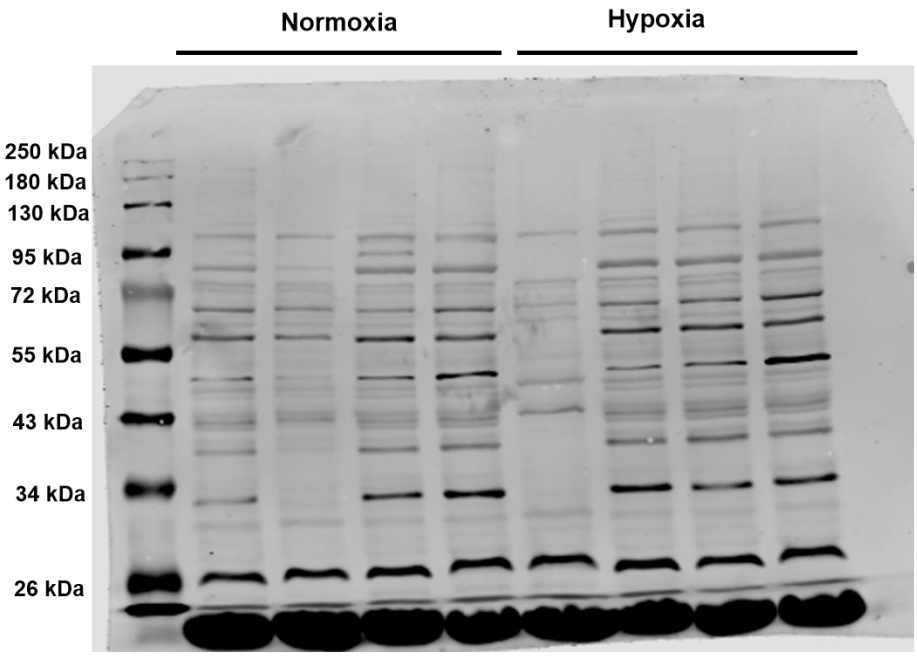

Appendix A 6 Full-length phosphorylated SphK1 Western blot (PVAT).
Uncropped membrane with MW ladder. The quantified P-SphK1 band shown in the main figures corresponds to ~51 kDa.

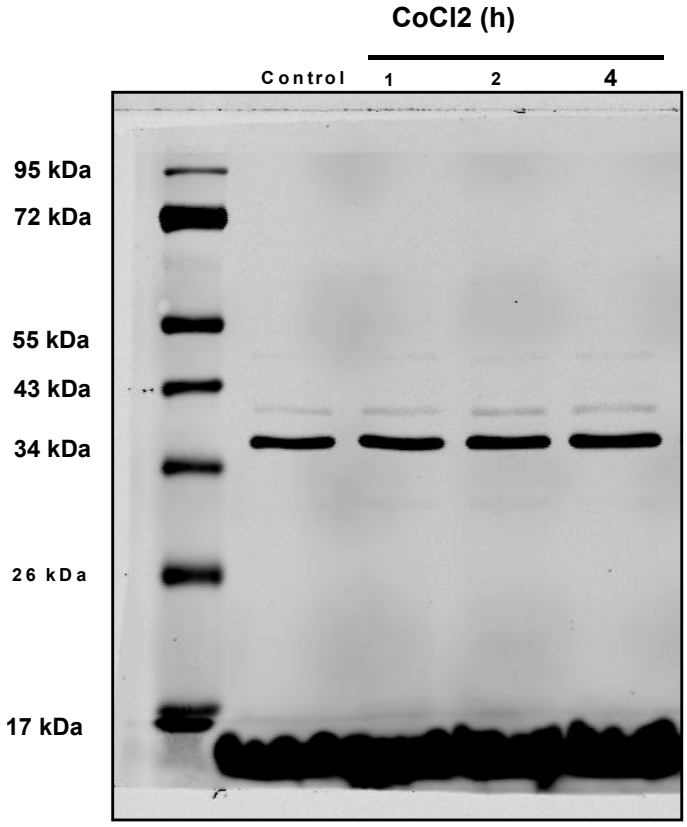

Appendix A 7 Full-length GAPDH Western blot (3T3-L1 adipocytes).
Uncropped Western blot with MW ladder; the quantified GAPDH band was located at ~37 kDa.

List of References

AARONSON, P. I., WARD, J. P. & CONNOLLY, M. J. 2020. *The cardiovascular system at a glance*, John Wiley & Sons.

ABOY-PARDAL, M. C., GUADAMILLAS, M. C., GUERRERO, C. R., CATALÀ-MONTORO, M., TOLEDANO-DONADO, M., TERRÉS-DOMÍNGUEZ, S., PAVÓN, D. M., JIMÉNEZ-JIMÉNEZ, V., JIMENEZ-CARRETERO, D. & ZAMAI, M. 2024. Plasma membrane remodeling determines adipocyte expansion and mechanical adaptability. *Nature Communications,* 15**,** 10102.

ABRASS, C. K., O'CONNOR, S., SCARPACE, P. & ABRASS, I. 1985. Characterization of the beta-adrenergic receptor of the rat peritoneal macrophage. *Journal of immunology (Baltimore, Md.: 1950),* 135**,** 1338-1341.

ADACHI, Y., UEDA, K., NOMURA, S., ITO, K., KATOH, M., KATAGIRI, M., YAMADA, S., HASHIMOTO, M., ZHAI, B. & NUMATA, G. 2022. Beiging of perivascular adipose tissue regulates its inflammation and vascular remodeling. *Nature Communications,* 13**,** 5117.

ADER, I., BRIZUELA, L., BOUQUEREL, P., MALAVAUD, B. & CUVILLIER, O. 2008. Sphingosine kinase 1: a new modulator of hypoxia inducible factor 1alpha during hypoxia in human cancer cells. *Cancer Res,* 68**,** 8635-42.

ADER, I., GSTALDER, C., BOUQUEREL, P., GOLZIO, M., ANDRIEU, G., ZALVIDEA, S., RICHARD, S., SABBADINI, R. A., MALAVAUD, B. & CUVILLIER, O. 2015. Neutralizing S1P inhibits intratumoral hypoxia, induces vascular remodelling and sensitizes to chemotherapy in prostate cancer. *Oncotarget,* 6**,** 13803.

ADZIGBLI, L., SOKOLOV, E. P., WIMMERS, K., SOKOLOVA, I. M. & PONSUKSILI, S. 2022. Effects of hypoxia and reoxygenation on mitochondrial functions and transcriptional profiles of isolated brain and muscle porcine cells. *Scientific Reports,* 12**,** 19881.

AGHAMOHAMMADZADEH, R., GREENSTEIN, A. S., YADAV, R., JEZIORSKA, M., HAMA, S., SOLTANI, F., PEMBERTON, P. W., AMMORI, B., MALIK, R. A. & SORAN, H. 2013. Effects of bariatric surgery on human small artery function: evidence for reduction in perivascular adipocyte inflammation, and the restoration of normal anticontractile activity despite persistent obesity. *Journal of the American College of Cardiology,* 62**,** 128-135.

AGHAMOHAMMADZADEH, R., WITHERS, S., LYNCH, F., GREENSTEIN, A., MALIK, R. & HEAGERTY, A. 2012. Perivascular adipose tissue from human systemic and coronary vessels: the emergence of a new pharmacotherapeutic target. *British journal of pharmacology,* 165**,** 670-682.

AGUILERA, K. Y. & BREKKEN, R. A. 2014. Hypoxia Studies with Pimonidazole in vivo. *Bio-protocol,* 4**,** e1254-e1254.

AHMAD, M., LONG, J. S., PYNE, N. J. & PYNE, S. 2006. The effect of hypoxia on lipid phosphate receptor and sphingosine kinase expression and mitogen-activated protein kinase signaling in human pulmonary smooth muscle cells. *Prostaglandins & other lipid mediators,* 79**,** 278-286.

AHMAD, M. F., FERLAND, D., AYALA-LOPEZ, N., CONTRERAS, G. A., DARIOS, E., THOMPSON, J., ISMAIL, A., THELEN, K., MOESER, A. J. & BURNETT, R. 2019. Perivascular adipocytes store norepinephrine by vesicular transport. *Arteriosclerosis, thrombosis, and vascular biology,* 39**,** 188-199.

AHMED, A., BIBI, A., VALOTI, M. & FUSI, F. 2023. Perivascular Adipose Tissue and Vascular Smooth Muscle Tone: Friends or Foes? *Cells,* 12**,** 1196.

AKOUMIANAKIS, I., TARUN, A. & ANTONIADES, C. 2017. Perivascular adipose tissue as a regulator of vascular disease pathogenesis: identifying novel therapeutic targets. *British journal of pharmacology,* 174**,** 3411-3424.

ALEWIJNSE, A. E., PETERS, S. L. & MICHEL, M. C. 2004. Cardiovascular effects of sphingosine-1-phosphate and other sphingomyelin metabolites. *British journal of pharmacology,* 143**,** 666-684.

ALGANGA, H. 2017. *Effect of hypoxia on the cardiovascular sphingolipid system.* University of Glasgow.

ALGANGA, H., ALMABROUK, T. A., KATWAN, O. J., DALY, C. J., PYNE, S., PYNE, N. J. & KENNEDY, S. 2019. Short periods of hypoxia upregulate sphingosine kinase 1 and increase vasodilation of arteries to sphingosine 1-phosphate (S1P) via S1P3. *Journal of Pharmacology and Experimental Therapeutics,* 371**,** 63-74.

ALJAEZI, I. 2024. *Regulation of inducible Nitric Oxide Synthase in adipocytes and perivascular adipose tissue by the Sphingolipid system.* University of Glasgow.

ALMABROUK, T., EWART, M., SALT, I. & KENNEDY, S. 2014. Perivascular fat, AMP-activated protein kinase and vascular diseases. *British Journal of Pharmacology,* 171**,** 595-617.

ALMABROUK, T. A., UGUSMAN, A. B., KATWAN, O. J., SALT, I. P. & KENNEDY, S. 2017. Deletion of AMPKα1 attenuates the anticontractile effect of perivascular adipose tissue (PVAT) and reduces adiponectin release. *British journal of pharmacology,* 174**,** 3398-3410.

ALMABROUK, T. A., WHITE, A. D., UGUSMAN, A. B., SKIBA, D. S., KATWAN, O. J., ALGANGA, H., GUZIK, T. J., TOUYZ, R. M., SALT, I. P. & KENNEDY, S. 2018. High fat diet attenuates the anticontractile activity of aortic PVAT via a mechanism involving AMPK and reduced adiponectin secretion. *Frontiers in physiology,* 9**,** 51.

ALVAREZ, S. E., HARIKUMAR, K. B., HAIT, N. C., ALLEGOOD, J., STRUB, G. M., KIM, E. Y., MACEYKA, M., JIANG, H., LUO, C. & KORDULA, T. 2010. Sphingosine-1-phosphate is a missing cofactor for the E3 ubiquitin ligase TRAF2. *Nature,* 465**,** 1084-1088.

ANELLI, V., GAULT, C. R., CHENG, A. B. & OBEID, L. M. 2008. Sphingosine kinase 1 is up-regulated during hypoxia in U87MG glioma cells: role of hypoxia-inducible factors 1 and 2. *Journal of Biological Chemistry,* 283**,** 3365-3375.

ANTONIADES, C., ANTONOPOULOS, A., TOUSOULIS, D. & STEFANADIS, C. 2009. Adiponectin: from obesity to cardiovascular disease. *obesity reviews,* 10**,** 269-279.

ANTONOPOULOS, A. S., MARGARITIS, M., COUTINHO, P., SHIRODARIA, C., PSARROS, C., HERDMAN, L., SANNA, F., DE SILVA, R., PETROU, M. & SAYEED, R. 2015. Adiponectin as a link between type 2 diabetes and vascular NADPH oxidase activity in the human arterial wall: the regulatory role of perivascular adipose tissue. *Diabetes,* 64**,** 2207-2219.

ARCARO, G., ZAMBONI, M., ROSSI, L., TURCATO, E., COVI, G., ARMELLINI, F., BOSELLO, O. & LECHI, A. 1999. Body fat distribution predicts the degree of endothelial dysfunction in uncomplicated obesity. *International journal of obesity,* 23**,** 936-942.

ARITA, Y., KIHARA, S., OUCHI, N., MAEDA, K., KURIYAMA, H., OKAMOTO, Y., KUMADA, M., HOTTA, K., NISHIDA, M. & TAKAHASHI, M. 2002. Adipocyte-derived plasma protein adiponectin acts as a platelet-derived growth factor-BB–binding protein and regulates growth factor–induced common

postreceptor signal in vascular smooth muscle cell. *Circulation,* 105**,** 2893-2898.

AYALA-LOPEZ, N., MARTINI, M., JACKSON, W. F., DARIOS, E., BURNETT, R., SEITZ, B., FINK, G. D. & WATTS, S. W. 2014. Perivascular adipose tissue contains functional catecholamines. *Pharmacology research & perspectives,* 2**,** e00041.

AYALA-LOPEZ, N. & WATTS, S. W. 2017. New actions of an old friend: perivascular adipose tissue's adrenergic mechanisms. *British Journal of Pharmacology,* 174**,** 3454-3465.

AZUL, L., LEANDRO, A., BOROUMAND, P., KLIP, A., SEIÇA, R. & SENA, C. M. 2020. Increased inflammation, oxidative stress and a reduction in antioxidant defense enzymes in perivascular adipose tissue contribute to vascular dysfunction in type 2 diabetes. *Free Radical Biology and Medicine,* 146**,** 264-274.

BADRAN, M., YASSIN, B. A., LIN, D. T. S., KOBOR, M. S., AYAS, N. & LAHER, I. 2019. Gestational intermittent hypoxia induces endothelial dysfunction, reduces perivascular adiponectin and causes epigenetic changes in adult male offspring. *The Journal of Physiology,* 597**,** 5349-5364.

BAKLEH, M. Z. & AL HAJ ZEN, A. 2025. The Distinct Role of HIF-1α and HIF-2α in Hypoxia and Angiogenesis. *Cells,* 14**,** 673.

BARGUT, T. C. L., SOUZA-MELLO, V., AGUILA, M. B. & MANDARIM-DE-LACERDA, C. A. 2017. Browning of white adipose tissue: lessons from experimental models. *Hormone molecular biology and clinical investigation,* 31.

BARKER, J. & ROGAWSKI, M. 1993. Calcium current block by (-)-pentobarbital, phenobarbital, and CHEB but not (+)-pentobarbital in acutely isolated hippocampal CA1 neurons: comparison with effects on GABA-activated Cl- current. *Journal of Neuroscience,* 13**,** 3211-3221.

BARP, C. G., BENEDET, P. O. & ASSREUY, J. 2020. Perivascular adipose tissue phenotype and sepsis vascular dysfunction: Differential contribution of NO, ROS and beta 3-adrenergic receptor. *Life Sciences,* 254**,** 117819.

BARR, R. K., LYNN, H. E., MORETTI, P. A., KHEW-GOODALL, Y. & PITSON, S. M. 2008. Deactivation of sphingosine kinase 1 by protein phosphatase 2A. *Journal of Biological Chemistry,* 283**,** 34994-35002.

BASATEMUR, G. L., JØRGENSEN, H. F., CLARKE, M. C., BENNETT, M. R. & MALLAT, Z. 2019. Vascular smooth muscle cells in atherosclerosis. *Nature reviews cardiology,* 16**,** 727-744.

BEFANI, C., MYLONIS, I., GKOTINAKOU, I.-M., GEORGOULIAS, P., HU, C.-J., SIMOS, G. & LIAKOS, P. 2013. Cobalt stimulates HIF-1-dependent but inhibits HIF-2-dependent gene expression in liver cancer cells. *The international journal of biochemistry & cell biology,* 45**,** 2359-2368.

BERNACCHIONI, C., SQUECCO, R., GAMBERI, T., GHINI, V., SCHUMACHER, F., MANNELLI, M., GARELLA, R., IDRIZAJ, E., CENCETTI, F. & PULITI, E. 2022. S1P signalling axis is necessary for adiponectin-directed regulation of electrophysiological properties and oxidative metabolism in C2C12 myotubes. *Cells,* 11**,** 713.

BERRYMAN, D. E. & LIST, E. O. 2017. Growth hormone's effect on adipose tissue: quality versus quantity. *International Journal of Molecular Sciences,* 18**,** 1621.

BIKMAN, B. T. & SUMMERS, S. A. 2011. Ceramides as modulators of cellular and whole-body metabolism. *The Journal of clinical investigation,* 121**,** 4222-4230.

BILLAUD, M., MARTHAN, R., SAVINEAU, J.-P. & GUIBERT, C. 2009. Vascular smooth muscle modulates endothelial control of vasoreactivity via

reactive oxygen species production through myoendothelial communications. *PloS one,* 4**,** e6432.
BILLICH, A., BORNANCIN, F., MECHTCHERIAKOVA, D., NATT, F., HUESKEN, D. & BAUMRUKER, T. 2005. Basal and induced sphingosine kinase 1 activity in A549 carcinoma cells: function in cell survival and IL-1β and TNF-α induced production of inflammatory mediators. *Cellular signalling,* 17**,** 1203-1217.
BISCHOFF, A., CZYBORRA, P., FETSCHER, C., MEYER ZU HERINGDORF, D., JAKOBS, K. H. & MICHEL, M. C. 2000. Sphingosine-1-phosphate and sphingosylphosphorylcholine constrict renal and mesenteric microvessels in vitro. *British journal of pharmacology,* 130**,** 1871-1877.
BLACHNIO-ZABIELSKA, A. U., KOUTSARI, C., TCHKONIA, T. & JENSEN, M. D. 2012. Sphingolipid content of human adipose tissue: relationship to adiponectin and insulin resistance. *Obesity,* 20**,** 2341-2347.
BLAHO, V. A. & HLA, T. 2014. An update on the biology of sphingosine 1-phosphate receptors. *Journal of lipid research,* 55**,** 1596-1608.
BÖGER, R. & HANNEMANN, J. 2020. Dual role of the L-arginine–ADMA–NO pathway in systemic hypoxic vasodilation and pulmonary hypoxic vasoconstriction. *Pulmonary Circulation,* 10**,** 23-30.
BOLINDER, J., KERCKHOFFS, D., MOBERG, E., HAGSTRÖM-TOFT, E. & ARNER, P. 2000. Rates of skeletal muscle and adipose tissue glycerol release in nonobese and obese subjects. *Diabetes,* 49**,** 797-802.
BONICA, J., MAO, C., OBEID, L. M. & HANNUN, Y. A. 2020. Transcriptional regulation of sphingosine kinase 1. *Cells,* 9**,** 2437.
BOTTA, A., ELIZBARYAN, K., TASHAKORINIA, P., LAM, N. H. & SWEENEY, G. 2020. An adiponectin-S1P autocrine axis protects skeletal muscle cells from palmitate-induced cell death. *Lipids in Health and Disease,* 19**,** 1-9.
BOUQUEREL, P., GSTALDER, C., MÜLLER, D., LAURENT, J., BRIZUELA, L., SABBADINI, R., MALAVAUD, B., PYRONNET, S., MARTINEAU, Y. & ADER, I. 2016. Essential role for SphK1/S1P signaling to regulate hypoxia-inducible factor 2α expression and activity in cancer. *Oncogenesis,* 5**,** e209-e209.
BRAHIMI-HORN, M. C. & POUYSSÉGUR, J. 2007. Oxygen, a source of life and stress. *FEBS letters,* 581**,** 3582-3591.
BRIDGES, L. E., WILLIAMS, C. L., POINTER, M. A. & AWUMEY, E. M. 2011. Mesenteric artery contraction and relaxation studies using automated wire myography. *Journal of visualized experiments: JoVE*, 3119.
BRINKMANN, V. & BAUMRUKER, T. 2006. Pulmonary and vascular pharmacology of sphingosine 1-phosphate. *Current opinion in pharmacology,* 6**,** 244-250.
BROUET, A., SONVEAUX, P., DESSY, C., BALLIGAND, J.-L. & FERON, O. 2001. Hsp90 ensures the transition from the early Ca2+-dependent to the late phosphorylation-dependent activation of the endothelial nitric-oxide synthase in vascular endothelial growth factor-exposed endothelial cells. *Journal of Biological Chemistry,* 276**,** 32663-32669.
BROWN, N. K., ZHOU, Z., ZHANG, J., ZENG, R., WU, J., EITZMAN, D. T., CHEN, Y. E. & CHANG, L. 2014. Perivascular adipose tissue in vascular function and disease: a review of current research and animal models. *Arteriosclerosis, thrombosis, and vascular biology,* 34**,** 1621-1630.
BROZOVICH, F., NICHOLSON, C., DEGEN, C., GAO, Y. Z., AGGARWAL, M. & MORGAN, K. G. 2016. Mechanisms of vascular smooth muscle contraction and the basis for pharmacologic treatment of smooth muscle disorders. *Pharmacological reviews,* 68**,** 476-532.

BRYAN JR, R. M., YOU, J., GOLDING, E. M. & MARRELLI, S. P. 2005. Endothelium-derived hyperpolarizing factor: a cousin to nitric oxide and prostacyclin. *Anesthesiology,* 102**,** 1261-1277.

BRYAN, L., KORDULA, T., SPIEGEL, S. & MILSTIEN, S. 2008. Regulation and functions of sphingosine kinases in the brain. *Biochim Biophys Acta,* 1781**,** 459-66.

BU, Y., WU, H., DENG, R. & WANG, Y. 2021. Therapeutic potential of SphK1 inhibitors based on abnormal expression of SphK1 in inflammatory immune related-diseases. *Frontiers in Pharmacology,* 12**,** 733387.

BUSSEY, C. E., WITHERS, S. B., ALDOUS, R. G., EDWARDS, G. & HEAGERTY, A. M. 2016. Obesity-related perivascular adipose tissue damage is reversed by sustained weight loss in the rat. *Arteriosclerosis, thrombosis, and vascular biology,* 36**,** 1377-1385.

BYEON, S. K., KIM, J., WEGWERTH, P. J., ZENKA, R., GEORGE, J. P., PINTO E VAIRO, F., OGLESBEE, D., SCHULTZ, M. J., MATERN, D. & PANDEY, A. 2024. Development of a multiplexed sphingolipids method for diagnosis of inborn errors of ceramide metabolism. *Clinical chemistry,* 70**,** 1366-1374.

BYUN, H.-S., PYNE, S., MACRITCHIE, N., PYNE, N. J. & BITTMAN, R. 2013. Novel sphingosine-containing analogues selectively inhibit sphingosine kinase (SK) isozymes, induce SK1 proteasomal degradation and reduce DNA synthesis in human pulmonary arterial smooth muscle cells. *Medchemcomm,* 4**,** 1394-1399.

CACANYIOVA, S., MAJZUNOVA, M., GOLAS, S. & BERENYIOVA, A. 2019. The role of perivascular adipose tissue and endogenous hydrogen sulfide in vasoactive responses of isolated mesenteric arteries in normotensive and spontaneously hypertensive rats. *Journal of Physiology & Pharmacology,* 70.

CAI, M., ZHAO, D., HAN, X., HAN, S., ZHANG, W., ZANG, Z., GAI, C., RONG, R. & GAO, T. 2023. The role of perivascular adipose tissue-secreted adipocytokines in cardiovascular disease. *Frontiers in immunology,* 14**,** 1271051.

CANNAVO, A., LICCARDO, D., KOMICI, K., CORBI, G., DE LUCIA, C., FEMMINELLA, G. D., ELIA, A., BENCIVENGA, L., FERRARA, N. & KOCH, W. J. 2017. Sphingosine kinases and sphingosine 1-phosphate receptors: signaling and actions in the cardiovascular system. *Frontiers in pharmacology,* 8**,** 556.

CANNON, B. & NEDERGAARD, J. 2004. Brown adipose tissue: function and physiological significance. *Physiological reviews*.

CAO, G., XUAN, X., HU, J., ZHANG, R., JIN, H. & DONG, H. 2022. How vascular smooth muscle cell phenotype switching contributes to vascular disease. *Cell Communication and Signaling,* 20**,** 180.

CARTIER, A. & HLA, T. 2019. Sphingosine 1-phosphate: Lipid signaling in pathology and therapy. *Science,* 366**,** eaar5551.

CATALAN, V., GOMEZ-AMBROSI, J., RODRÍGUEZ, A., RAMÍREZ, B., ROTELLAR, F., VALENTÍ, V., SILVA, C., GIL, M. J., SALVADOR, J. & FRÜHBECK, G. 2012. Increased tenascin C and Toll-like receptor 4 levels in visceral adipose tissue as a link between inflammation and extracellular matrix remodeling in obesity. *The Journal of Clinical Endocrinology & Metabolism,* 97**,** E1880-E1889.

CEDERBERG, A., GRØNNING, L. M., AHRÉN, B., TASKÉN, K., CARLSSON, P. & ENERBÄCK, S. 2001. FOXC2 is a winged helix gene that counteracts obesity, hypertriglyceridemia, and diet-induced insulin resistance. *Cell,* 106**,** 563-573.

CHAIT, A. & DEN HARTIGH, L. J. 2020. Adipose tissue distribution, inflammation and its metabolic consequences, including diabetes and cardiovascular disease. *Frontiers in cardiovascular medicine,* 7**,** 522637.

CHAKRABARTY, S., BUI, Q., BADEANLOU, L., HESTER, K., CHUN, J., RUF, W., CIARALDI, T. P. & SAMAD, F. 2022. S1P/S1PR3 signalling axis protects against obesity-induced metabolic dysfunction. *Adipocyte,* 11**,** 69-83.

CHANG, H.-H., SHEI-DEI YANG, S. & CHANG, S.-J. 2020a. Perivascular adipose tissue modulation of neurogenic vasorelaxation of rat mesenteric arteries. *Journal of Cardiovascular Pharmacology,* 75**,** 21-30.

CHANG, L., GARCIA-BARRIO, M. T. & CHEN, Y. E. 2020b. Perivascular adipose tissue regulates vascular function by targeting vascular smooth muscle cells. *Arteriosclerosis, thrombosis, and vascular biology,* 40**,** 1094-1109.

CHATTERJEE, T. K., STOLL, L. L., DENNING, G. M., HARRELSON, A., BLOMKALNS, A. L., IDELMAN, G., ROTHENBERG, F. G., NELTNER, B., ROMIG-MARTIN, S. A. & DICKSON, E. W. 2009. Proinflammatory phenotype of perivascular adipocytes: influence of high-fat feeding. *Circulation research,* 104**,** 541-549.

CHAUDHRY, R., MIAO, J. H. & REHMAN, A. 2025. Physiology, Cardiovascular. *StatPearls*. Treasure Island (FL): StatPearls Publishing

CHAYTOR, A. T., BAKKER, L. M., EDWARDS, D. H. & GRIFFITH, T. M. 2005. Connexin-mimetic peptides dissociate electrotonic EDHF-type signalling via myoendothelial and smooth muscle gap junctions in the rabbit iliac artery. *British journal of pharmacology,* 144**,** 108-114.

CHEN, B., LAM, K. S., WANG, Y., WU, D., LAM, M. C., SHEN, J., WONG, L., HOO, R. L., ZHANG, J. & XU, A. 2006. Hypoxia dysregulates the production of adiponectin and plasminogen activator inhibitor-1 independent of reactive oxygen species in adipocytes. *Biochemical and biophysical research communications,* 341**,** 549-556.

CHEN, H., MONTAGNANI, M., FUNAHASHI, T., SHIMOMURA, I. & QUON, M. J. 2003. Adiponectin stimulates production of nitric oxide in vascular endothelial cells. *Journal of Biological Chemistry,* 278**,** 45021-45026.

CHEN, J.-Y., WU, Y.-P., LI, C.-Y., JHENG, H.-F., KAO, L.-Z., YANG, C.-C., LEU, S.-Y., LIEN, I.-C., WENG, W.-T. & TAI, H.-C. 2021. PPARγ activation improves the microenvironment of perivascular adipose tissue and attenuates aortic stiffening in obesity. *Journal of biomedical science,* 28**,** 1-19.

CHEN, J., TANG, H., SYSOL, J. R., MORENO-VINASCO, L., SHIOURA, K. M., CHEN, T., GORSHKOVA, I., WANG, L., HUANG, L. S. & USATYUK, P. V. 2014. The sphingosine kinase 1/sphingosine-1-phosphate pathway in pulmonary arterial hypertension. *American journal of respiratory and critical care medicine,* 190**,** 1032-1043.

CHEN, R., MCVEY, D. G., SHEN, D., HUANG, X. & YE, S. 2023a. Phenotypic switching of vascular smooth muscle cells in atherosclerosis. *Journal of the American Heart Association,* 12**,** e031121.

CHEN, X., SHI, C., HE, M., XIONG, S. & XIA, X. 2023b. Endoplasmic reticulum stress: molecular mechanism and therapeutic targets. *Signal transduction and targeted therapy,* 8**,** 352.

CHENG, C. K., BAKAR, H. A., GOLLASCH, M. & HUANG, Y. 2018. Perivascular adipose tissue: the sixth man of the cardiovascular system. *Cardiovascular drugs and therapy,* 32**,** 481-502.

CHEVILLOTTE, E., GIRALT, M., MIROUX, B., RICQUIER, D. & VILLARROYA, F. 2007. Uncoupling protein-2 controls adiponectin gene expression in adipose tissue through the modulation of reactive oxygen species production. *Diabetes,* 56**,** 1042-1050.

CHI, D. S., QUI, M., KRISHNASWAMY, G., LI, C. & STONE, W. 2003. Regulation of nitric oxide production from macrophages by lipopolysaccharide and catecholamines. *Nitric oxide,* 8**,** 127-132.

CHOE, S. S., HUH, J. Y., HWANG, I. J., KIM, J. I. & KIM, J. B. 2016. Adipose tissue remodeling: its role in energy metabolism and metabolic disorders. *Frontiers in endocrinology,* 7**,** 30.

CHOI, J. W. & CHUN, J. 2013. Lysophospholipids and their receptors in the central nervous system. *Biochimica et Biophysica Acta (BBA)-Molecular and Cell Biology of Lipids,* 1831**,** 20-32.

CHOW, W.-S., CHEUNG, B. M., TSO, A. W., XU, A., WAT, N. M., FONG, C. H., ONG, L. H., TAM, S., TAN, K. C. & JANUS, E. D. 2007. Hypoadiponectinemia as a predictor for the development of hypertension: a 5-year prospective study. *Hypertension,* 49**,** 1455-1461.

CHUNG, Y. C. & HYUN, C.-G. 2021. Inhibitory effects of pinostilbene on adipogenesis in 3T3-L1 adipocytes: a study of possible mechanisms. *International Journal of Molecular Sciences,* 22**,** 13446.

CHUSYD, D. E., WANG, D., HUFFMAN, D. M. & NAGY, T. R. 2016. Relationships between rodent white adipose fat pads and human white adipose fat depots. *Frontiers in nutrition,* 3**,** 10.

CIFARELLI, V., BEEMAN, S. C., SMITH, G. I., YOSHINO, J., MOROZOV, D., BEALS, J. W., KAYSER, B. D., WATROUS, J. D., JAIN, M. & PATTERSON, B. W. 2020. Decreased adipose tissue oxygenation associates with insulin resistance in individuals with obesity. *The Journal of clinical investigation,* 130**,** 6688-6699.

CINTI, S. 2011. Between brown and white: novel aspects of adipocyte differentiation. *Annals of medicine,* 43**,** 104-115.

CLEMENT, J. P., KUNJILWAR, K., GONZALEZ, G., SCHWANSTECHER, M., PANTEN, U., AGUILAR-BRYAN, L. & BRYAN, J. 1997. Association and stoichiometry of KATP channel subunits. *Neuron,* 18**,** 827-838.

COELHO, M., OLIVEIRA, T. & FERNANDES, R. 2013. State of the art paper Biochemistry of adipose tissue: an endocrine organ. *Archives of medical science,* 9**,** 191-200.

COMBS, T. P., BERG, A. H., RAJALA, M. W., KLEBANOV, S., IYENGAR, P., JIMENEZ-CHILLARON, J. C., PATTI, M. E., KLEIN, S. L., WEINSTEIN, R. S. & SCHERER, P. E. 2003. Sexual differentiation, pregnancy, calorie restriction, and aging affect the adipocyte-specific secretory protein adiponectin. *Diabetes,* 52**,** 268-276.

COMBS, T. P. & MARLISS, E. B. 2014. Adiponectin signaling in the liver. *Reviews in Endocrine and Metabolic Disorders,* 15**,** 137-147.

CONTOS, J. J., ISHII, I. & CHUN, J. 2000. Lysophosphatidic acid receptors. *Molecular pharmacology,* 58**,** 1188-1196.

COUSSIN, F., SCOTT, R. H., WISE, A. & NIXON, G. F. 2002. Comparison of sphingosine 1-phosphate–induced intracellular signaling pathways in vascular smooth muscles: differential role in vasoconstriction. *Circulation research,* 91**,** 151-157.

CRUZ-LÓPEZ, E. O., TAN, L., STOLK, D. G., VAN DEN BOGAERDT, A. J., VERDONK, K. & DANSER, A. J. 2024. Endothelin-1-and acetylcholine-mediated effects in human and rat vessels: impact of perivascular adipose

tissue, diabetes, angiotensin II, and chemerin. *Blood Pressure,* 33**,** 2414072.

CUEVAS-RAMOS, D., MEHTA, R. & AGUILAR-SALINAS, C. A. 2019. Fibroblast growth factor 21 and browning of white adipose tissue. *Frontiers in physiology,* 10**,** 37.

CUI, F., MI, H., GUAN, Y., ZHU, Y., WANG, R., TIAN, Y., YANG, K. & ZHANG, Y. 2023. Chronic intermittent hypobaric hypoxia ameliorates vascular reactivity through upregulating adiponectin expression of PVAT in metabolic syndrome rats. *Canadian Journal of Physiology and Pharmacology,* 101**,** 160-170.

CUVILLIER, O., PIRIANOV, G., KLEUSER, B., VANEK, P. G., COSO, O. A., GUTKIND, J. S. & SPIEGEL, S. 1996. Suppression of ceramide-mediated programmed cell death by sphingosine-1-phosphate. *Nature,* 381**,** 800-803.

DALLAIRE, P., BELLMANN, K., LAPLANTE, M., GÉLINAS, S., CENTENO-BAEZ, C., PENFORNIS, P., PEYOT, M.-L., LATOUR, M. G., LAMONTAGNE, J. & TRUJILLO, M. E. 2008. Obese mice lacking inducible nitric oxide synthase are sensitized to the metabolic actions of peroxisome proliferator–activated receptor-γ agonism. *Diabetes,* 57**,** 1999-2011.

DALY, C. J. 2019. Examining vascular structure and function using confocal microscopy and 3D imaging techniques. *Biomedical Visualisation: Volume 1***,** 97-106.

DALY, C. J., DEIGHAN, C., MCGEE, A., MENNIE, D., ALI, Z., MCBRIDE, M. & MCGRATH, J. C. 2002. A knockout approach indicates a minor vasoconstrictor role for vascular α 1B-adrenoceptors in mouse. *Physiological genomics,* 9**,** 85-91.

DANTAS, A. P. V., IGARASHI, J. & MICHEL, T. 2003. Sphingosine 1-phosphate and control of vascular tone. *American Journal of Physiology-Heart and Circulatory Physiology,* 284**,** H2045-H2052.

DAUT, J., MAIER-RUDOLPH, W., VON BECKERATH, N., MEHRKE, G., GÜNTHER, K. & GOEDEL-MEINEN, L. 1990. Hypoxic dilation of coronary arteries is mediated by ATP-sensitive potassium channels. *Science,* 247**,** 1341-1344.

DE JONGH, R. T., SERNÉ, E. H., IJZERMAN, R. G., DE VRIES, G. & STEHOUWER, C. D. 2004. Impaired microvascular function in obesity: implications for obesity-associated microangiopathy, hypertension, and insulin resistance. *Circulation,* 109**,** 2529-2535.

DEANFIELD, J. E., HALCOX, J. P. & RABELINK, T. J. 2007. Endothelial function and dysfunction: testing and clinical relevance. *Circulation,* 115**,** 1285-1295.

DELON, C., MANIFAVA, M., WOOD, E., THOMPSON, D., KRUGMANN, S., PYNE, S. & KTISTAKIS, N. T. 2004. Sphingosine kinase 1 is an intracellular effector of phosphatidic acid. *Journal of Biological Chemistry,* 279**,** 44763-44774.

DENG, C., PAOLONI-GIACOBINO, A., KUEHNE, F., BOSS, O., REVELLI, J. P., MOINAT, M., CAWTHORNE, M. A., MUZZIN, P. & GIACOBINO, J. P. 1996. Respective degree of expression of ß1, ß2-and ß3-adrenoceptors in human brown and white adipose tissues. *British journal of pharmacology,* 118**,** 929-934.

DENZEL, M. S., SCIMIA, M.-C., ZUMSTEIN, P. M., WALSH, K., RUIZ-LOZANO, P. & RANSCHT, B. 2010. T-cadherin is critical for adiponectin-mediated cardioprotection in mice. *The Journal of clinical investigation,* 120**,** 4342-4352.

DESSY, C., MONIOTTE, S., GHISDAL, P., HAVAUX, X., NOIRHOMME, P. & BALLIGAND, J.-L. 2004. Endothelial ß3-adrenoceptors mediate

vasorelaxation of human coronary microarteries through nitric oxide and endothelium-dependent hyperpolarization. *Circulation,* 110**,** 948-954.

DI VILLA BIANCA, R. D. E., SORRENTINO, R., SORRENTINO, R., IMBIMBO, C., PALMIERI, A., FUSCO, F., MAGGI, M., DE PALMA, R., CIRINO, G. & MIRONE, V. 2006. Sphingosine 1-phosphate induces endothelial nitric-oxide synthase activation through phosphorylation in human corpus cavernosum. *The Journal of pharmacology and experimental therapeutics,* 316**,** 703-708.

DÍAZ-BULNES, P., SAIZ, M. L., LÓPEZ-LARREA, C. & RODRÍGUEZ, R. M. 2020. Crosstalk between hypoxia and ER stress response: a key regulator of macrophage polarization. *Frontiers in immunology,* 10**,** 2951.

DOCHERTY, J. & MCGRATH, J. 1980. A comparison of pre-and post-junctional potencies of several alpha-adrenoceptor agonists in the cardiovascular system and anococcygeus muscle of the rat: Evidence for two types of post-junctional alpha-adrenoceptor. *Naunyn-Schmiedeberg's Archives of Pharmacology,* 312**,** 107-116.

DONOVAN, J., WONG, P., GARLE, M., ALEXANDER, S. P., DUNN, W. R. & RALEVIC, V. 2018. Coronary artery hypoxic vasorelaxation is augmented by perivascular adipose tissue through a mechanism involving hydrogen sulphide and cystathionine-ß-synthase. *Acta Physiologica,* 224**,** e13126.

DONOVAN, J., WONG, P., ROBERTS, R. E., GARLE, M., ALEXANDER, S. P., DUNN, W. R. & RALEVIC, V. 2017. A critical role for cystathionine-ß-synthase in hydrogen sulfide-mediated hypoxic relaxation of the coronary artery. *Vascular pharmacology,* 93**,** 20-32.

DOS SANTOS GOLDENBERG, R. C. & DE CARVALHO, A. C. C. 2023. *Resident Stem Cells and Regenerative Therapy: Sources and Clinical Applications*, Elsevier.

EBRAHIMI-MAMAEGHANI, M., MOHAMMADI, S., AREFHOSSEINI, S. R., FALLAH, P. & BAZI, Z. 2015. Adiponectin as a potential biomarker of vascular disease. *Vascular health and risk management***,** 55-70.

EL-SHEWY, H. M., PARNHAM, S., FEDAROVICH, D., BULLESBACH, E. & LUTTRELL, L. M. 2018. Sphingosine 1 Phosphate Regulates Store-Operated Calcium Entry through binding to STIM1. *The FASEB Journal,* 32**,** 815.10-815.10.

EMANUEL, A. L., MEIJER, R. I., WOERDEMAN, J., VAN RAALTE, D. H., DIAMANT, M., KRAMER, M. H., SERLIE, M. J., ERINGA, E. C. & SERNÉ, E. H. 2020. Effects of a hypercaloric and hypocaloric diet on insulin-induced microvascular recruitment, glucose uptake, and lipolysis in healthy lean men. *Arteriosclerosis, Thrombosis, and Vascular Biology,* 40**,** 1695-1704.

ENGELI, S., JANKE, J., GORZELNIAK, K., BÖHNKE, J., GHOSE, N., LINDSCHAU, C., LUFT, F. C. & SHARMA, A. M. 2004. Regulation of the nitric oxide system in human adipose tissue. *Journal of lipid research,* 45**,** 1640-1648.

ENGIN, A. 2024. Adipose Tissue Hypoxia in Obesity: Clinical Reappraisal of Hypoxia Hypothesis. *Adv Exp Med Biol,* 1460**,** 329-356.

ESPOSITO, K., PONTILLO, A., GIUGLIANO, F., GIUGLIANO, G., MARFELLA, R., NICOLETTI, G. & GIUGLIANO, D. 2003. Association of low interleukin-10 levels with the metabolic syndrome in obese women. *The Journal of Clinical Endocrinology & Metabolism,* 88**,** 1055-1058.

FANG, L., ZHAO, J., CHEN, Y., MA, T., XU, G., TANG, C., LIU, X. & GENG, B. 2009. Hydrogen sulfide derived from periadventitial adipose tissue is a vasodilator. *Journal of hypertension,* 27**,** 2174-2185.

FAYYAZ, S., HENKEL, J., JAPTOK, L., KRÄMER, S., DAMM, G., SEEHOFER, D., PÜSCHEL, G. P. & KLEUSER, B. 2014. Involvement of sphingosine 1-

phosphate in palmitate-induced insulin resistance of hepatocytes via the S1P2 receptor subtype. *Diabetologia,* 57**,** 373-382.

FERLAND, D. J., DARIOS, E. S., NEUBIG, R. R., SJÖGREN, B., TRUONG, N., TORRES, R., DEXHEIMER, T. S., THOMPSON, J. M. & WATTS, S. W. 2017. Chemerin-induced arterial contraction is Gi-and calcium-dependent. *Vascular pharmacology,* 88**,** 30-41.

FERNÁNDEZ-ALFONSO, M. S., GIL-ORTEGA, M., GARCÍA-PRIETO, C. F., ARANGUEZ, I., RUIZ-GAYO, M. & SOMOZA, B. 2013. Mechanisms of perivascular adipose tissue dysfunction in obesity. *International journal of endocrinology,* 2013.

FÉSÜS, G., DUBROVSKA, G., GORZELNIAK, K., KLUGE, R., HUANG, Y., LUFT, F. C. & GOLLASCH, M. 2007. Adiponectin is a novel humoral vasodilator. *Cardiovascular research,* 75**,** 719-727.

FILIPPI, L., PINI, A., CAMMALLERI, M., BAGNOLI, P. & DAL MONTE, M. 2022. β3-Adrenoceptor, a novel player in the round-trip from neonatal diseases to cancer: Suggestive clues from embryo. *Medicinal Research Reviews,* 42**,** 1179-1201.

FITE, A., ABOU-SAMRA, A. B. & SEYOUM, B. 2015. Macrophages inhibit insulin signalling in adipocytes: role of inducible nitric oxide synthase and nitric oxide. *Canadian Journal of Diabetes,* 39**,** 36-43.

FITZGIBBONS, T. P., KOGAN, S., AOUADI, M., HENDRICKS, G. M., STRAUBHAAR, J. & CZECH, M. P. 2011. Similarity of mouse perivascular and brown adipose tissues and their resistance to diet-induced inflammation. *American Journal of Physiology-Heart and Circulatory Physiology,* 301**,** H1425-H1437.

FLACCO, N., SEGURA, V., PEREZ-ASO, M., ESTRADA, S., SELLER, J., JIMÉNEZ-ALTAYÓ, F., NOGUERA, M., D'OCON, P., VILA, E. & IVORRA, M. 2013. Different β-adrenoceptor subtypes coupling to cAMP or NO/cGMP pathways: implications in the relaxant response of rat conductance and resistance vessels. *British Journal of Pharmacology,* 169**,** 413-425.

FLEIGE, S. & PFAFFL, M. W. 2006. RNA integrity and the effect on the real-time qRT-PCR performance. *Molecular aspects of medicine,* 27**,** 126-139.

FOLKMAN, J., HAHNFELDT, P. & HLATKY, L. 2000. Cancer: looking outside the genome. *Nature Reviews Molecular Cell Biology,* 1**,** 76-79.

FRANCIS, S. H., BUSCH, J. L. & CORBIN, J. D. 2010. cGMP-dependent protein kinases and cGMP phosphodiesterases in nitric oxide and cGMP action. *Pharmacological reviews,* 62**,** 525-563.

FREJ, C., ANDERSSON, A., LARSSON, B., GUO, L. J., NORSTRÖM, E., HAPPONEN, K. E. & DAHLBÄCK, B. 2015. Quantification of sphingosine 1-phosphate by validated LC-MS/MS method revealing strong correlation with apolipoprotein M in plasma but not in serum due to platelet activation during blood coagulation. *Analytical and bioanalytical chemistry,* 407**,** 8533-8542.

FRY, M., SMITH, P. M., HOYDA, T. D., DUNCAN, M., AHIMA, R. S., SHARKEY, K. A. & FERGUSON, A. V. 2006. Area postrema neurons are modulated by the adipocyte hormone adiponectin. *Journal of Neuroscience,* 26**,** 9695-9702.

FUJIMOTO, M., SHIMIZU, N., KUNII, K., MARTYN, J. J., UEKI, K. & KANEKI, M. 2005. A role for iNOS in fasting hyperglycemia and impaired insulin signaling in the liver of obese diabetic mice. *Diabetes,* 54**,** 1340-1348.

FUJITA, T., OKADA, T., HAYASHI, S., JAHANGEER, S., MIWA, N. & NAKAMURA, S.-I. 2004. δ-Catenin/NPRAP (neural plakophilin-related armadillo repeat protein) interacts with and activates sphingosine kinase 1. *Biochemical Journal,* 382**,** 717-723.

FUKUDA, Y., AOYAMA, Y., WADA, A. & IGARASHI, Y. 2004. Identification of PECAM-1 association with sphingosine kinase 1 and its regulation by agonist-induced phosphorylation. *Biochimica et Biophysica Acta (BBA)-Molecular and Cell Biology of Lipids,* 1636**,** 12-21.

FUNCKE, J.-B. & SCHERER, P. E. 2019. Beyond adiponectin and leptin: adipose tissue-derived mediators of inter-organ communication. *Journal of lipid research,* 60**,** 1648-1697.

FURCHGOTT, R. F. & ZAWADZKI, J. V. 1980. The obligatory role of endothelial cells in the relaxation of arterial smooth muscle by acetylcholine. *nature,* 288**,** 373-376.

GALLEY, H. F. & WEBSTER, N. R. 2004. Physiology of the endothelium. *British journal of anaesthesia,* 93**,** 105-113.

GALLO, G., VOLPE, M. & SAVOIA, C. 2022. Endothelial dysfunction in hypertension: current concepts and clinical implications. *Frontiers in medicine,* 8**,** 798958.

GÁLVEZ-PRIETO, B., BOLBRINKER, J., STUCCHI, P., DE LAS HERAS, A., MERINO, B., ARRIBAS, S., RUIZ-GAYO, M., HUBER, M., WEHLAND, M. & KREUTZ, R. 2008. Comparative expression analysis of the renin-angiotensin system components between white and brown perivascular adipose tissue. *Journal of Endocrinology,* 197**,** 55-64.

GÁLVEZ-PRIETO, B., SOMOZA, B., GIL-ORTEGA, M., GARCÍA-PRIETO, C. F., DE LAS HERAS, A. I., GONZÁLEZ, M. C., ARRIBAS, S., ARANGUEZ, I., BOLBRINKER, J. & KREUTZ, R. 2012. Anticontractile effect of perivascular adipose tissue and leptin are reduced in hypertension. *Frontiers in pharmacology,* 3**,** 103.

GAMBARDELLA, J., FIORDELISI, A., AVVISATO, R., BUONAIUTO, A., CERASUOLO, F. A., SORRIENTO, D. & IACCARINO, G. 2023. Adrenergic receptors in endothelial and vascular smooth muscle cells. *Current Opinion in Physiology,* 36**,** 100721.

GAO, Y.-J., ZENG, Z.-H., TEOH, K., SHARMA, A. M., ABOUZAHR, L., CYBULSKY, I., LAMY, A., SEMELHAGO, L. & LEE, R. M. 2005. Perivascular adipose tissue modulates vascular function in the human internal thoracic artery. *The Journal of thoracic and cardiovascular surgery,* 130**,** 1130-1136.

GAO, Y. J., LU, C., SU, L. Y., SHARMA, A. & LEE, R. 2007. Modulation of vascular function by perivascular adipose tissue: the role of endothelium and hydrogen peroxide. *British journal of pharmacology,* 151**,** 323-331.

GASSER, R., KLEIN, W. & KICKENWEIZ, E. 1993. Vasodilative response to hypoxia and simulated ischemia is mediated by ATP-sensitive K+ channels in guinea pig thoracic aorta. *Angiology,* 44**,** 228-243.

GAULT, C. R., EBLEN, S. T., NEUMANN, C. A., HANNUN, Y. A. & OBEID, L. M. 2012. Oncogenic K-Ras regulates bioactive sphingolipids in a sphingosine kinase 1-dependent manner. *Journal of Biological Chemistry,* 287**,** 31794-31803.

GESTA, S., TSENG, Y.-H. & KAHN, C. R. 2007. Developmental origin of fat: tracking obesity to its source. *Cell,* 131**,** 242-256.

GIBBONS, S. J., NUNEZ-HERNANDEZ, R., MAZE, G. & HARRISON, N. L. 1996. Inhibition of a fast inwardly rectifying potassium conductance by barbiturates. *Anesthesia & Analgesia,* 82**,** 1242-1246.

GIL-ORTEGA, M., CONDEZO-HOYOS, L., GARCÍA-PRIETO, C. F., ARRIBAS, S. M., GONZÁLEZ, M. C., ARANGUEZ, I., RUIZ-GAYO, M., SOMOZA, B. & FERNANDEZ-ALFONSO, M. S. 2014. Imbalance between pro and anti-oxidant mechanisms in perivascular adipose tissue aggravates long-term high-fat diet-derived endothelial dysfunction. *PloS one,* 9**,** e95312.

GIL-ORTEGA, M., SOMOZA, B., HUANG, Y., GOLLASCH, M. & FERNÁNDEZ-ALFONSO, M. S. 2015. Regional differences in perivascular adipose tissue impacting vascular homeostasis. *Trends in Endocrinology & Metabolism,* 26, 367-375.

GIL-ORTEGA, M., STUCCHI, P., GUZMAN-RUIZ, R., CANO, V., ARRIBAS, S., GONZÁLEZ, M. C., RUIZ-GAYO, M., FERNANDEZ-ALFONSO, M. S. & SOMOZA, B. 2010. Adaptative nitric oxide overproduction in perivascular adipose tissue during early diet-induced obesity. *Endocrinology,* 151, 3299-3306.

GIORDANO, A., SONG, C. K., BOWERS, R. R., EHLEN, J. C., FRONTINI, A., CINTI, S. & BARTNESS, T. J. 2006. White adipose tissue lacks significant vagal innervation and immunohistochemical evidence of parasympathetic innervation. *American Journal of Physiology-Regulatory, Integrative and Comparative Physiology,* 291, R1243-R1255.

GOMEZ-BROUCHET, A., ILLAC, C., LEDOUX, A., FORTIN, P.-Y., DE BARROS, S., VABRE, C., DESPAS, F., PERIES, S., CASAROLI, C. & BOUVIER, C. 2022. Sphingosine kinase-1 is overexpressed and correlates with hypoxia in osteosarcoma: relationship with clinicopathological parameters. *Cancers,* 14, 499.

GÓMEZ-GARCÍA, I., TREPIANA, J., FERNÁNDEZ-QUINTELA, A., GIRALT, M. & PORTILLO, M. P. 2022. Sexual dimorphism in brown adipose tissue activation and white adipose tissue browning. *International journal of molecular sciences,* 23, 8250.

GONDA, K., OKAMOTO, H., TAKUWA, N., YATOMI, Y., OKAZAKI, H., SAKURAI, T., KIMURA, S., SILLARD, R., HARII, K. & TAKUWA, Y. 1999. The novel sphingosine 1-phosphate receptor AGR16 is coupled via pertussis toxin-sensitive and-insensitive G-proteins to multiple signalling pathways. *Biochemical Journal,* 337, 67-75.

GONG, W., LI, J., CHEN, W., FENG, F. & DENG, Y. 2020. Resveratrol inhibits lipopolysaccharide-induced extracellular matrix accumulation and inflammation in rat glomerular mesangial cells by SphK1/S1P2/NF-κB pathway. *Diabetes, Metabolic Syndrome and Obesity*, 4495-4505.

GOOSSENS, G. H., BIZZARRI, A., VENTECLEF, N., ESSERS, Y., CLEUTJENS, J. P., KONINGS, E., JOCKEN, J. W., ČAJLAKOVIĆ, M., RIBITSCH, V. & CLÉMENT, K. 2011. Increased adipose tissue oxygen tension in obese compared with lean men is accompanied by insulin resistance, impaired adipose tissue capillarization, and inflammation. *Circulation,* 124, 67-76.

GRANGER, D. N. & KVIETYS, P. R. 2015. Reperfusion injury and reactive oxygen species: The evolution of a concept. *Redox biology,* 6, 524-551.

GREENSTEIN, A. S., KHAVANDI, K., WITHERS, S. B., SONOYAMA, K., CLANCY, O., JEZIORSKA, M., LAING, I., YATES, A. P., PEMBERTON, P. W. & MALIK, R. A. 2009. Local inflammation and hypoxia abolish the protective anticontractile properties of perivascular fat in obese patients. *Circulation,* 119, 1661-1670.

GUO, Q., JIN, S., HU, H., ZHOU, Y., YAN, Y., ZONG, H., WANG, Y., HE, H., OH, Y. & LIU, C. 2017. Hypoxia in 3T3-L1 adipocytes suppresses adiponectin expression via the PERK and IRE1 unfolded protein response. *Biochemical and Biophysical Research Communications,* 493, 346-351.

HAIT, N. C., ALLEGOOD, J., MACEYKA, M., STRUB, G. M., HARIKUMAR, K. B., SINGH, S. K., LUO, C., MARMORSTEIN, R., KORDULA, T. & MILSTIEN, S. 2009. Regulation of histone acetylation in the nucleus by sphingosine-1-phosphate. *Science,* 325, 1254-1257.

HAIT, N. C., BELLAMY, A., MILSTIEN, S., KORDULA, T. & SPIEGEL, S. 2007. Sphingosine kinase type 2 activation by ERK-mediated phosphorylation. *Journal of Biological Chemistry,* 282**,** 12058-12065.

HAIT, N. C., SARKAR, S., LE STUNFF, H., MIKAMI, A., MACEYKA, M., MILSTIEN, S. & SPIEGEL, S. 2005. Role of sphingosine kinase 2 in cell migration toward epidermal growth factor. *Journal of Biological Chemistry,* 280**,** 29462-29469.

HAJJAR, D. P., FARBER, I. C. & SMITH, S. C. 1988. Oxygen tension within the arterial wall: relationship to altered bioenergetic metabolism and lipid accumulation. *Archives of biochemistry and biophysics,* 262**,** 375-380.

HALBERG, N., KHAN, T., TRUJILLO, M. E., WERNSTEDT-ASTERHOLM, I., ATTIE, A. D., SHERWANI, S., WANG, Z. V., LANDSKRONER-EIGER, S., DINEEN, S. & MAGALANG, U. J. 2009a. Hypoxia-inducible factor 1α induces fibrosis and insulin resistance in white adipose tissue. *Molecular and cellular biology,* 29**,** 4467-4483.

HALBERG, N., SCHRAW, T. D., WANG, Z. V., KIM, J.-Y., YI, J., HAMILTON, M. P., LUBY-PHELPS, K. & SCHERER, P. E. 2009b. Systemic fate of the adipocyte-derived factor adiponectin. *Diabetes,* 58**,** 1961-1970.

HAN, F., LI, K., PAN, R., XU, W., HAN, X., HOU, N. & SUN, X. 2018. Calycosin directly improves perivascular adipose tissue dysfunction by upregulating the adiponectin/AMPK/eNOS pathway in obese mice. *Food & Function,* 9**,** 2409-2415.

HANNEMANN, J. & BÖGER, R. 2022. Dysregulation of the nitric oxide/Dimethylarginine pathway in hypoxic pulmonary vasoconstriction—molecular mechanisms and clinical significance. *Frontiers in Medicine,* 9**,** 835481.

HANNUN, Y. A. & OBEID, L. M. 2008. Principles of bioactive lipid signalling: lessons from sphingolipids. *Nature reviews Molecular cell biology,* 9**,** 139-150.

HANSCOM, M., MORALES-SOTO, W., WATTS, S. W., JACKSON, W. F. & GULBRANSEN, B. D. 2024. Innervation of adipocytes is limited in mouse perivascular adipose tissue. *American Journal of Physiology-Heart and Circulatory Physiology,* 327**,** H155-H181.

HARMS, M. & SEALE, P. 2013. Brown and beige fat: development, function and therapeutic potential. *Nature medicine,* 19**,** 1252-1263.

HASHIMOTO, T., IGARASHI, J. & KOSAKA, H. 2009. Sphingosine kinase is induced in mouse 3T3-L1 cells and promotes adipogenesis [S]. *Journal of lipid research,* 50**,** 602-610.

HATOUM, D., HADDADI, N., LIN, Y., NASSIF, N. T. & MCGOWAN, E. M. 2017. Mammalian sphingosine kinase (SphK) isoenzymes and isoform expression: challenges for SphK as an oncotarget. *Oncotarget,* 8**,** 36898.

HAZAR-RETHINAM, M., DE LONG, L. M., GANNON, O. M., TOPKAS, E., BOROS, S., VARGAS, A. C., DZIENIS, M., MUKHOPADHYAY, P., SIMPSON, F. & ENDO-MUNOZ, L. 2015. A novel E2F/sphingosine kinase 1 axis regulates anthracycline response in squamous cell carcinoma. *Clinical Cancer Research,* 21**,** 417-427.

HE, Q., GAO, Z., YIN, J., ZHANG, J., YUN, Z. & YE, J. 2011. Regulation of HIF-1α activity in adipose tissue by obesity-associated factors: adipogenesis, insulin, and hypoxia. *American Journal of Physiology-Endocrinology and Metabolism,* 300**,** E877-E885.

HE, Q., YANG, Q.-C., ZHOU, Q., ZHU, H., NIU, W.-Y., FENG, J., WANG, Y., CAO, J. & CHEN, B.-Y. 2014. Effects of varying degrees of intermittent hypoxia

on proinflammatory cytokines and adipokines in rats and 3T3-L1 adipocytes. *PloS one,* 9**,** e86326.

HEDEGAARD, E., NIELSEN, B., KUN, A., HUGHES, A., KRØIGAARD, C., MOGENSEN, S., MATCHKOV, V., FRÖBERT, O. & SIMONSEN, U. 2014. K V7 channels are involved in hypoxia-induced vasodilatation of porcine coronary arteries. *British journal of pharmacology,* 171**,** 69-82.

HEDEGAARD, E. R., STANKEVICIUS, E., SIMONSEN, U. & FRÖBERT, O. 2011. Non-endothelial endothelin counteracts hypoxic vasodilation in porcine large coronary arteries. *BMC physiology,* 11**,** 8.

HEDEMANN, J., FETSCHER, C. & MICHEL, M. 2004. Comparison of noradrenaline and lysosphingolipid-induced vasoconstriction in mouse and rat small mesenteric arteries. *Autonomic and Autacoid Pharmacology,* 24**,** 77-85.

HEFFERNAN-STROUD, L. A., HELKE, K. L., JENKINS, R. W., DE COSTA, A.-M., HANNUN, Y. A. & OBEID, L. M. 2012. Defining a role for sphingosine kinase 1 in p53-dependent tumors. *Oncogene,* 31**,** 1166-1175.

HEMMINGS, D. G., HUDSON, N. K., HALLIDAY, D., O'HARA, M., BAKER, P. N., DAVIDGE, S. T. & TAGGART, M. J. 2006. Sphingosine-1-phosphate acts via rho-associated kinase and nitric oxide to regulate human placental vascular tone. *Biology of reproduction,* 74**,** 88-94.

HENGST, J. A., GUILFORD, J. M., FOX, T. E., WANG, X., CONROY, E. J. & YUN, J. K. 2009. Sphingosine kinase 1 localized to the plasma membrane lipid raft microdomain overcomes serum deprivation induced growth inhibition. *Archives of biochemistry and biophysics,* 492**,** 62-73.

HERR, D. R., REOLO, M. J., PEH, Y. X., WANG, W., LEE, C.-W., RIVERA, R., PATERSON, I. C. & CHUN, J. 2016. Sphingosine 1-phosphate receptor 2 (S1P2) attenuates reactive oxygen species formation and inhibits cell death: implications for otoprotective therapy. *Scientific reports,* 6**,** 24541.

HERRERA, G. M. & WALKER, B. R. 1998. Involvement of L-type calcium channels in hypoxic relaxation of vascular smooth muscle. *Journal of vascular research,* 35**,** 265-273.

HERZ, C. T., KULTERER, O. C., PRAGER, M., MARCULESCU, R., LANGER, F. B., PRAGER, G., KAUTZKY-WILLER, A., HAUG, A. R. & KIEFER, F. W. 2021. Sex differences in brown adipose tissue activity and cold-induced thermogenesis. *Molecular and Cellular Endocrinology,* 534**,** 111365.

HILDEBRAND, S., STÜMER, J. & PFEIFER, A. 2018. PVAT and its relation to brown, beige, and white adipose tissue in development and function. *Frontiers in Physiology,* 9**,** 70.

HILLOCK-WATLING, C. & GOTLIEB, A. I. 2022. The pathobiology of perivascular adipose tissue (PVAT), the fourth layer of the blood vessel wall. *Cardiovascular Pathology,* 61**,** 107459.

HOLLAND, W. L., MILLER, R. A., WANG, Z. V., SUN, K., BARTH, B. M., BUI, H. H., DAVIS, K. E., BIKMAN, B. T., HALBERG, N. & RUTKOWSKI, J. M. 2010. The pleiotropic actions of adiponectin are initiated via receptor-mediated activation of ceramidase activity. *Nature medicine,* 17**,** 55.

HONDARES, E., ROSELL, M., DıAZ-DELFıN, J., OLMOS, Y., MONSALVE, M., IGLESIAS, R., VILLARROYA, F. & GIRALT, M. 2011. Peroxisome proliferator-activated receptor a (PPARa) induces PPARg coactivator 1a (PGC-1a) gene expression and contributes to thermogenic activation of brown fat: involvement of PRDM16. *J. Biol. Chem,* 286**,** 43112-22.

HONG, S. J., PARK, E., XU, W., JIA, S., GALIANO, R. D. & MUSTOE, T. A. 2014. Response of human mature adipocytes to hypoxia-reoxygenation. *Cytotherapy,* 16**,** 1656-1665.

HOSOGAI, N., FUKUHARA, A., OSHIMA, K., MIYATA, Y., TANAKA, S., SEGAWA, K., FURUKAWA, S., TOCHINO, Y., KOMURO, R. & MATSUDA, M. 2007. Adipose tissue hypoxia in obesity and its impact on adipocytokine dysregulation. *Diabetes,* 56**,** 901-911.

HSIAO, S.-H., CONSTABLE, P. D., SMITH, G. W. & HASCHEK, W. M. 2005. Effects of exogenous sphinganine, sphingosine, and sphingosine-1-phosphate on relaxation and contraction of porcine thoracic aortic and pulmonary arterial rings. *Toxicological Sciences,* 86**,** 194-199.

HU, C.-J., SATAUR, A., WANG, L., CHEN, H. & SIMON, M. C. 2007. The N-terminal transactivation domain confers target gene specificity of hypoxia-inducible factors HIF-1α and HIF-2α. *Molecular biology of the cell,* 18**,** 4528-4542.

HU, D., YIN, C., LUO, S., HABENICHT, A. J. & MOHANTA, S. K. 2019. Vascular smooth muscle cells contribute to atherosclerosis immunity. *Frontiers in immunology,* 10**,** 1101.

HU, E., LIANG, P. & SPIEGELMAN, B. M. 1996. AdipoQ is a novel adipose-specific gene dysregulated in obesity (∗). *Journal of biological chemistry,* 271**,** 10697-10703.

HU, H., GARCIA-BARRIO, M., JIANG, Z.-S., CHEN, Y. E. & CHANG, L. 2021. Roles of perivascular adipose tissue in hypertension and atherosclerosis. *Antioxidants & Redox Signaling,* 34**,** 736-749.

HUANG, H., PARK, P. H., MCMULLEN, M. R. & NAGY, L. E. 2008. Mechanisms for the anti-inflammatory effects of adiponectin in macrophages. *Journal of gastroenterology and hepatology,* 23**,** S50-S53.

HUG, C., WANG, J., AHMAD, N. S., BOGAN, J. S., TSAO, T.-S. & LODISH, H. F. 2004. T-cadherin is a receptor for hexameric and high-molecular-weight forms of Acrp30/adiponectin. *Proceedings of the National Academy of Sciences,* 101**,** 10308-10313.

HUSSAIN, M. B. & MARSHALL, I. 1997. Characterization of α1-adrenoceptor subtypes mediating contractions to phenylephrine in rat thoracic aorta, mesenteric artery and pulmonary artery. *British journal of pharmacology,* 122**,** 849-858.

HUYNH, P. M., WANG, F. & AN, Y. A. 2025. Hypoxia signaling in the adipose tissue. *J Mol Cell Biol,* 16.

HWEJ, A., AL-FERJANI, A., ALSHUWEISHI, Y., NAJI, A., KENNEDY, S. & SALT, I. P. 2024. Lack of AMP-activated protein kinase-α1 reduces nitric oxide synthesis in thoracic aorta perivascular adipose tissue. *Vascular Pharmacology,* 157**,** 107437.

IBRAHIM, M. M. 2010. Subcutaneous and visceral adipose tissue: structural and functional differences. *Obesity reviews,* 11**,** 11-18.

IGARASHI, J. & MICHEL, T. 2009. Sphingosine-1-phosphate and modulation of vascular tone. *Cardiovascular research,* 82**,** 212-220.

IGARASHI, N., OKADA, T., HAYASHI, S., FUJITA, T., JAHANGEER, S. & NAKAMURA, S.-I. 2003. Sphingosine kinase 2 is a nuclear protein and inhibits DNA synthesis. *Journal of Biological Chemistry,* 278**,** 46832-46839.

ISLAM, A. S., SULTANA, H., REFAT, M. N. H., FARHANA, Z., KAMIL, A. A. & RAHMAN, M. M. 2024. The global burden of overweight-obesity and its association with economic status, benefiting from STEPs survey of WHO member states: A meta-analysis. *Preventive Medicine Reports,* 46**,** 102882.

ISSLENY, B. M., JAMJOUM, R., MAJUMDER, S. & STIBAN, J. 2023. Sphingolipids: from structural components to signaling hubs. *The enzymes*. Elsevier.

ITO, S., IWAKI, S., KOIKE, K., YUDA, Y., NAGASAKI, A., OHKAWA, R., YATOMI, Y., FURUMOTO, T., TSUTSUI, H. & SOBEL, B. E. 2013. Increased plasma sphingosine-1-phosphate in obese individuals and its capacity to increase the expression of plasminogen activator inhibitor-1 in adipocytes. *Coronary artery disease,* 24**,** 642-650.

JARMAN, K. E., MORETTI, P. A., ZEBOL, J. R. & PITSON, S. M. 2010. Translocation of sphingosine kinase 1 to the plasma membrane is mediated by calcium-and integrin-binding protein 1. *Journal of Biological Chemistry,* 285**,** 483-492.

JAYARATHNE, S., STULL, A. J., MIRANDA, A., SCOGGIN, S., CLAYCOMBE-LARSON, K., KIM, J. H. & MOUSTAID-MOUSSA, N. 2018. Tart cherry reduces inflammation in adipose tissue of zucker fatty rats and cultured 3T3-L1 adipocytes. *Nutrients,* 10**,** 1576.

JEON, M. J., LEEM, J., KO, M. S., JANG, J. E., PARK, H.-S., KIM, H. S., KIM, M., KIM, E. H., YOO, H. J. & LEE, C.-H. 2012. Mitochondrial dysfunction and activation of iNOS are responsible for the palmitate-induced decrease in adiponectin synthesis in 3T3L1 adipocytes. *Experimental & molecular medicine,* 44**,** 562-570.

JEONG, J.-K., MOON, M.-H. & PARK, S.-Y. 2015. Modulation of the expression of sphingosine 1-phosphate 2 receptors regulates the differentiation of pre-adipocytes. *Molecular medicine reports,* 12**,** 7496-7502.

JEONG, J. H., CHANG, J. S. & JO, Y.-H. 2018. Intracellular glycolysis in brown adipose tissue is essential for optogenetically induced nonshivering thermogenesis in mice. *Scientific reports,* 8**,** 6672.

JEREMIC, N., CHATURVEDI, P. & TYAGI, S. C. 2017. Browning of white fat: novel insight into factors, mechanisms, and therapeutics. *Journal of cellular physiology,* 232**,** 61-68.

JO, E., BHHATARAI, B., REPETTO, E., GUERRERO, M., RILEY, S., BROWN, S. J., KOHNO, Y., ROBERTS, E., SCHURER, S. C. & ROSEN, H. 2012. Novel selective allosteric and bitopic ligands for the S1P3 receptor. *ACS chemical biology,* 7**,** 1975-1983.

JO, J., GAVRILOVA, O., PACK, S., JOU, W., MULLEN, S., SUMNER, A. E., CUSHMAN, S. W. & PERIWAL, V. 2009. Hypertrophy and/or hyperplasia: dynamics of adipose tissue growth. *PLoS computational biology,* 5**,** e1000324.

JO, M. G., KIM, M. W., JO, M. H., BIN ABID, N. & KIM, M. O. 2019. Adiponectin homolog osmotin, a potential anti-obesity compound, suppresses abdominal fat accumulation in C57BL/6 mice on high-fat diet and in 3T3-L1 adipocytes. *International Journal of Obesity,* 43**,** 2422-2433.

JOKSOVIC, P. M., BRIMELOW, B. C., MURBARTIÁN, J., PEREZ-REYES, E. & TODOROVIC, S. M. 2004. Contrasting anesthetic sensitivities of T-type Ca2+ channels of reticular thalamic neurons and recombinant Cav3. 3 channels. *British journal of pharmacology,* 144**,** 59.

JONK, A. M., HOUBEN, A. J., DE JONGH, R. T., SERNE, E. H., SCHAPER, N. C. & STEHOUWER, C. D. 2007. Microvascular dysfunction in obesity: a potential mechanism in the pathogenesis of obesity-associated insulin resistance and hypertension. *Physiology,* 22**,** 252-260.

JUN, D.-J., LEE, J.-H., CHOI, B.-H., KOH, T.-K., HA, D.-C., JEONG, M.-W. & KIM, K.-T. 2006. Sphingosine-1-phosphate modulates both lipolysis and leptin production in differentiated rat white adipocytes. *Endocrinology,* 147**,** 5835-5844.

KADOWAKI, T. & YAMAUCHI, T. 2005. Adiponectin and adiponectin receptors. *Endocrine reviews,* 26**,** 439-451.

KADOWAKI, T., YAMAUCHI, T., KUBOTA, N., HARA, K., UEKI, K. & TOBE, K. 2006. Adiponectin and adiponectin receptors in insulin resistance, diabetes, and the metabolic syndrome. *The Journal of clinical investigation,* 116**,** 1784-1792.

KAEFFER, N., RICHARD, V., FRANCOIS, A., LALLEMAND, F., HENRY, J.-P. & THUILLEZ, C. 1996. Preconditioning prevents chronic reperfusion-induced coronary endothelial dysfunction in rats. *American Journal of Physiology-Heart and Circulatory Physiology,* 271**,** H842-H849.

KAELIN JR, W. G. 2002. Molecular basis of the VHL hereditary cancer syndrome. *Nature Reviews Cancer,* 2**,** 673-682.

KAJIKAWA, M. & HIGASHI, Y. 2022. Obesity and endothelial function. *Biomedicines,* 10**,** 1745.

KAJITA, K., ISHII, I., MORI, I., ASANO, M., FUWA, M. & MORITA, H. 2024. Sphingosine 1-phosphate regulates obesity and glucose homeostasis. *International journal of molecular sciences,* 25**,** 932.

KANG, G.-S., JO, H.-J., LEE, Y.-R., OH, T., PARK, H.-J. & AHN, G.-O. 2023. Sensing the oxygen and temperature in the adipose tissues–who's sensing what? *Experimental & Molecular Medicine,* 55**,** 2300-2307.

KARLINER, J. S. 2013. Sphingosine kinase and sphingosine 1-phosphate in the heart: a decade of progress. *Biochimica et Biophysica Acta (BBA)-Molecular and Cell Biology of Lipids,* 1831**,** 203-212.

KARLINER, J. S., HONBO, N., SUMMERS, K., GRAY, M. O. & GOETZL, E. J. 2001. The lysophospholipids sphingosine-1-phosphate and lysophosphatidic acid enhance survival during hypoxia in neonatal rat cardiac myocytes. *Journal of molecular and cellular cardiology,* 33**,** 1713-1717.

KEITH, B., JOHNSON, R. S. & SIMON, M. C. 2012. HIF1α and HIF2α: sibling rivalry in hypoxic tumour growth and progression. *Nature Reviews Cancer,* 12**,** 9-22.

KELLER, M., LIDINGTON, D., VOGEL, L., PETER, B. F., SOHN, H. Y., PAGANO, P. J., PITSON, S., SPIEGEL, S., POHL, U. & BOLZ, S. S. 2006. Sphingosine kinase functionally links elevated transmural pressure and increased reactive oxygen species formation in resistance arteries. *The FASEB journal,* 20**,** 702-704.

KERKHOF, C. J., VAN DER LINDEN, P. J. & SIPKEMA, P. 2002. Role of myocardium and endothelium in coronary vascular smooth muscle responses to hypoxia. *American Journal of Physiology-Heart and Circulatory Physiology,* 282**,** H1296-H1303.

KHALIL, R. A. 2010. Regulation of vascular smooth muscle function.

KIERANS, S. & TAYLOR, C. 2021. Regulation of glycolysis by the hypoxia-inducible factor (HIF): implications for cellular physiology. *The Journal of physiology,* 599**,** 23-37.

KIM, H. W., SHI, H., WINKLER, M. A., LEE, R. & WEINTRAUB, N. L. 2020. Perivascular adipose tissue and vascular perturbation/atherosclerosis. *Arteriosclerosis, thrombosis, and vascular biology,* 40**,** 2569-2576.

KIM, J. K., KIM, H.-J., PARK, S.-Y., CEDERBERG, A., WESTERGREN, R., NILSSON, D., HIGASHIMORI, T., CHO, Y.-R., LIU, Z.-X. & DONG, J. 2005. Adipocyte-specific overexpression of FOXC2 prevents diet-induced increases in intramuscular fatty acyl CoA and insulin resistance. *Diabetes,* 54**,** 1657-1663.

KIM, S., LEE, E.-S., LEE, S.-W., KIM, Y.-H., LEE, C.-H., JO, D.-G. & KIM, S.-H. 2019. Site-specific impairment of perivascular adipose tissue on advanced atherosclerotic plaques using multimodal nonlinear optical imaging. *Proceedings of the National Academy of Sciences,* 116**,** 17765-17774.

KITADA, Y., KAJITA, K., TAGUCHI, K., MORI, I., YAMAUCHI, M., IKEDA, T., KAWASHIMA, M., ASANO, M., KAJITA, T. & ISHIZUKA, T. 2016. Blockade of sphingosine 1-phosphate receptor 2 signaling attenuates high-fat diet-induced adipocyte hypertrophy and systemic glucose intolerance in mice. *Endocrinology,* 157**,** 1839-1851.

KITATANI, K., IDKOWIAK-BALDYS, J. & HANNUN, Y. A. 2008. The sphingolipid salvage pathway in ceramide metabolism and signaling. *Cellular signalling,* 20**,** 1010-1018.

KLUK, M. J. & HLA, T. 2002. Signaling of sphingosine-1-phosphate via the S1P/EDG-family of G-protein-coupled receptors. *Biochimica et Biophysica Acta (BBA)-Molecular and Cell Biology of Lipids,* 1582**,** 72-80.

KOENEN, M., HILL, M. A., COHEN, P. & SOWERS, J. R. 2021. Obesity, adipose tissue and vascular dysfunction. *Circulation research,* 128**,** 951-968.

KOGA, T., TAKATA, Y., KOBAYASHI, K., TAKISHITA, S., YAMASHITA, Y. & FUJISHIMA, M. 1989. Age and hypertension promote endothelium-dependent contractions to acetylcholine in the aorta of the rat. *Hypertension,* 14**,** 542-548.

KOHAMA, T., OLIVERA, A., EDSALL, L., NAGIEC, M. M., DICKSON, R. & SPIEGEL, S. 1998. Molecular cloning and functional characterization of murine sphingosine kinase. *Journal of Biological Chemistry,* 273**,** 23722-23728.

KOTLYAROV, S. & KOTLYAROVA, A. 2021. The role of ABC transporters in lipid metabolism and the comorbid course of chronic obstructive pulmonary disease and atherosclerosis. *International Journal of Molecular Sciences,* 22**,** 6711.

KOWALCZYK, P., SULEJCZAK, D., KLECZKOWSKA, P., BUKOWSKA-OŚKO, I., KUCIA, M., POPIEL, M., WIETRAK, E., KRAMKOWSKI, K., WRZOSEK, K. & KACZYŃSKA, K. 2021. Mitochondrial oxidative stress—a causative factor and therapeutic target in many diseases. *International journal of molecular sciences,* 22**,** 13384.

KOWALSKI, G. M., CAREY, A. L., SELATHURAI, A., KINGWELL, B. A. & BRUCE, C. R. 2013. Plasma sphingosine-1-phosphate is elevated in obesity. *PloS one,* 8**,** e72449.

KRAFT, M. L. 2017. Sphingolipid organization in the plasma membrane and the mechanisms that influence it. *Frontiers in cell and developmental biology,* 4**,** 154.

KRÜGER-GENGE, A., BLOCKI, A., FRANKE, R.-P. & JUNG, F. 2019. Vascular endothelial cell biology: an update. *International journal of molecular sciences,* 20**,** 4411.

KSIĄŻEK, M., CHACIŃSKA, M., CHABOWSKI, A. & BARANOWSKI, M. 2015. Sources, metabolism, and regulation of circulating sphingosine-1-phosphate. *Journal of lipid research,* 56**,** 1271-1281.

KU, D. D. 1982. Coronary vascular reactivity after acute myocardial ischemia. *Science,* 218**,** 576-578.

KUMADA, M., KIHARA, S., SUMITSUJI, S., KAWAMOTO, T., MATSUMOTO, S., OUCHI, N., ARITA, Y., OKAMOTO, Y., SHIMOMURA, I. & HIRAOKA, H. 2003. Association of hypoadiponectinemia with coronary artery disease in men. *Arteriosclerosis, thrombosis, and vascular biology,* 23**,** 85-89.

KUMAR, R. K., DARIOS, E. S., BURNETT, R., THOMPSON, J. M. & WATTS, S. W. 2019. Fenfluramine-induced PVAT-dependent contraction depends on norepinephrine and not serotonin. *Pharmacological research,* 140**,** 43-49.

KUMAR, R. K., YANG, Y., CONTRERAS, A. G., GARVER, H., BHATTACHARYA, S., FINK, G. D., ROCKWELL, C. E. & WATTS, S. W. 2021. Phenotypic changes

in T cell and macrophage subtypes in perivascular adipose tissues precede high-fat diet-induced hypertension. *Frontiers in Physiology,* 12**,** 616055.

KWAIFA, I. K., BAHARI, H., YONG, Y. K. & NOOR, S. M. 2020. Endothelial dysfunction in obesity-induced inflammation: molecular mechanisms and clinical implications. *Biomolecules,* 10**,** 291.

LACANÁ, E., MACEYKA, M., MILSTIEN, S. & SPIEGEL, S. 2002. Cloning and characterization of a protein kinase A anchoring protein (AKAP)-related protein that interacts with and regulates sphingosine kinase 1 activity. *Journal of Biological Chemistry,* 277**,** 32947-32953.

LAFONTAN, M. & BERLAN, M. 1993. Fat cell adrenergic receptors and the control of white and brown fat cell function. *Journal of lipid research,* 34**,** 1057-1091.

LAMBERT, J. M., ANDERSON, A. K. & COWART, L. A. 2018. Sphingolipids in adipose tissue: What's tipping the scale? *Advances in biological regulation,* 70**,** 19-30.

LAU, W. B., OHASHI, K., WANG, Y., OGAWA, H., MUROHARA, T., MA, X.-L. & OUCHI, N. 2017. Role of adipokines in cardiovascular disease. *Circulation Journal,* 81**,** 920-928.

LECLERCQ, T. M., MORETTI, P. A., VADAS, M. A. & PITSON, S. M. 2008. Eukaryotic elongation factor 1A interacts with sphingosine kinase and directly enhances its catalytic activity. *Journal of Biological Chemistry,* 283**,** 9606-9614.

LEE, J. W., KO, J., JU, C. & ELTZSCHIG, H. K. 2019. Hypoxia signaling in human diseases and therapeutic targets. *Experimental & molecular medicine,* 51**,** 1-13.

LEE, M. R., LI, L. & KITAZAWA, T. 1997. Cyclic GMP causes Ca2+ desensitization in vascular smooth muscle by activating the myosin light chain phosphatase. *Journal of Biological Chemistry,* 272**,** 5063-5068.

LEE, S.-Y., LEE, H.-Y., SONG, J.-H., KIM, G.-T., JEON, S., SONG, Y.-J., LEE, J. S., HUR, J.-H., OH, H. H. & PARK, S.-Y. 2017. Adipocyte-specific deficiency of de novo sphingolipid biosynthesis leads to lipodystrophy and insulin resistance. *Diabetes,* 66**,** 2596-2609.

LEE, Y.-C., CHANG, H.-H., CHIANG, C.-L., LIU, C.-H., YEH, J.-I., CHEN, M.-F., CHEN, P.-Y., KUO, J.-S. & LEE, T. J. 2011. Role of perivascular adipose tissue–derived methyl palmitate in vascular tone regulation and pathogenesis of hypertension. *Circulation,* 124**,** 1160-1171.

LEE, Y. S., KIM, J.-W., OSBORNE, O., OH, D. Y., SASIK, R., SCHENK, S., CHEN, A., CHUNG, H., MURPHY, A. & WATKINS, S. M. 2014. Increased adipocyte O2 consumption triggers HIF-1α, causing inflammation and insulin resistance in obesity. *Cell,* 157**,** 1339-1352.

LEFERE, S., VAN STEENKISTE, C., VERHELST, X., VAN VLIERBERGHE, H., DEVISSCHER, L. & GEERTS, A. 2016. Hypoxia-regulated mechanisms in the pathogenesis of obesity and non-alcoholic fatty liver disease. *Cellular and molecular life sciences,* 73**,** 3419-3431.

LEHMAN, S. J., MASSARO, J. M., SCHLETT, C. L., O'DONNELL, C. J., HOFFMANN, U. & FOX, C. S. 2010. Peri-aortic fat, cardiovascular disease risk factors, and aortic calcification: the Framingham Heart Study. *Atherosclerosis,* 210**,** 656-661.

LELOUP, A. J., VAN HOVE, C. E., HEYKERS, A., SCHRIJVERS, D. M., DE MEYER, G. R. & FRANSEN, P. 2015. Elastic and muscular arteries differ in structure, basal NO production and voltage-gated Ca2+-channels. *Frontiers in physiology,* 6**,** 375.

LEONARD, S. S., HARRIS, G. K. & SHI, X. 2004. Metal-induced oxidative stress and signal transduction. *Free Radical Biology and Medicine,* 37**,** 1921-1942.

LEW, M. J., RIVERS, R. J. & DULING, B. R. 1989. Arteriolar smooth muscle responses are modulated by an intramural diffusion barrier. *American Journal of Physiology-Heart and Circulatory Physiology,* 257**,** H10-H16.

LI, H.-F., LIU, H.-T., CHEN, P.-Y., LIN, H. & TSENG, T.-L. 2022. Role of PVAT in obesity-related cardiovascular disease through the buffering activity of ATF3. *Iscience,* 25**,** 105631.

LI, H. F., LIN, H., LIU, H. T., LIN, T. J. & TSENG, T. L. 2025a. Activating transcription factor-3 orchestrates the modulation of vascular anti-contractile activity and relaxation by governing the secretion of HDL-bound sphingosine-1-phosphate in perivascular adipose tissue. *British Journal of Pharmacology,* 182**,** 1763-1782.

LI, H. Z., PIKE, A. C., CHANG, Y.-N., PRAKAASH, D., GELOVA, Z., STANKA, J., MOREAU, C., SCOTT, H. C., WUNDER, F. & WOLF, G. 2025b. Transport and inhibition of the sphingosine-1-phosphate exporter SPNS2. *Nature Communications,* 16**,** 721.

LI, J.-M. & SHAH, A. M. 2004. Endothelial cell superoxide generation: regulation and relevance for cardiovascular pathophysiology. *American Journal of Physiology-Regulatory, Integrative and Comparative Physiology,* 287**,** R1014-R1030.

LI, L., HAN, J., WANG, Z., LIU, J. A., WEI, J., XIONG, S. & ZHAO, Z. 2014. Mass spectrometry methodology in lipid analysis. *International journal of molecular sciences,* 15**,** 10492-10507.

LI, R., ANDERSEN, I., ALEKE, J., GOLUBINSKAYA, V., GUSTAFSSON, H. & NILSSON, H. 2013. Reduced anti-contractile effect of perivascular adipose tissue on mesenteric small arteries from spontaneously hypertensive rats: role of Kv7 channels. *European journal of pharmacology,* 698**,** 310-315.

LI, X., MA, Z. & ZHU, Y. Z. 2021. Regional heterogeneity of perivascular adipose tissue: morphology, origin, and secretome. *Frontiers in Pharmacology,* 12**,** 697720.

LI, Y., TALBOT, C. L. & CHAURASIA, B. 2020. Ceramides in adipose tissue. *Frontiers in Endocrinology,* 11**,** 407.

LIAO, J., YIN, H., HUANG, J. & HU, M. 2021. Dysfunction of perivascular adipose tissue in mesenteric artery is restored by aerobic exercise in high-fat diet induced obesity. *Clinical and Experimental Pharmacology and Physiology,* 48**,** 697-703.

LIDELL, M. E., BETZ, M. J., LEINHARD, O. D., HEGLIND, M., ELANDER, L., SLAWIK, M., MUSSACK, T., NILSSON, D., ROMU, T. & NUUTILA, P. 2013. Evidence for two types of brown adipose tissue in humans. *Nature medicine,* 19**,** 631-634.

LIM, K. G., SUN, C., BITTMAN, R., PYNE, N. J. & PYNE, S. 2011. (R)-FTY720 methyl ether is a specific sphingosine kinase 2 inhibitor: Effect on sphingosine kinase 2 expression in HEK 293 cells and actin rearrangement and survival of MCF-7 breast cancer cells. *Cellular signalling,* 23**,** 1590-1595.

LIN, H., BABY, N., LU, J., KAUR, C., ZHANG, C., XU, J., LING, E.-A. & DHEEN, S. T. 2011. Expression of sphingosine kinase 1 in amoeboid microglial cells in the corpus callosum of postnatal rats. *Journal of neuroinflammation,* 8**,** 13.

LIN, J., NIIMI, Y., CLAUSI, M. G., KANAL, H. D. & LEVISON, S. W. 2020. Neuroregenerative and protective functions of Leukemia Inhibitory Factor

in perinatal hypoxic-ischemic brain injury. *Experimental neurology,* 330, 113324.
LIN, Q., HUANG, Y., BOOTH, C. J., HAASE, V. H., JOHNSON, R. S., CELESTE SIMON, M., GIORDANO, F. J. & YUN, Z. 2013. Activation of hypoxia-inducible factor-2 in adipocytes results in pathological cardiac hypertrophy. *Journal of the American Heart Association,* 2, e000548.
LIU, H., SUGIURA, M., NAVA, V. E., EDSALL, L. C., KONO, K., POULTON, S., MILSTIEN, S., KOHAMA, T. & SPIEGEL, S. 2000. Molecular cloning and functional characterization of a novel mammalian sphingosine kinase type 2 isoform. *Journal of Biological Chemistry,* 275, 19513-19520.
LOBATO, N. D. S., FILGUEIRA, F. P., AKAMINE, E. H., TOSTES, R., CARVALHO, M. H. C. D. & FORTES, Z. B. 2012. Mechanisms of endothelial dysfunction in obesity-associated hypertension. *Brazilian journal of medical and biological research,* 45, 392-400.
LÖHN, M., DUBROVSKA, G., LAUTERBACH, B., LUFT, F. C., GOLLASCH, M. & SHARMA, A. M. 2002. Periadventitial fat releases a vascular relaxing factor. *The FASEB Journal,* 16, 1057-1063.
LOLMEDE, K., DURAND DE SAINT FRONT, V., GALITZKY, J., LAFONTAN, M. & BOULOUMIE, A. 2003. Effects of hypoxia on the expression of proangiogenic factors in differentiated 3T3-F442A adipocytes. *International journal of obesity,* 27, 1187-1195.
LONG, J. Z., SVENSSON, K. J., TSAI, L., ZENG, X., ROH, H. C., KONG, X., RAO, R. R., LOU, J., LOKURKAR, I. & BAUR, W. 2014. A smooth muscle-like origin for beige adipocytes. *Cell metabolism,* 19, 810-820.
LÖSCHER, W. & ROGAWSKI, M. A. 2012. How theories evolved concerning the mechanism of action of barbiturates. *Epilepsia,* 53, 12-25.
LOVERIDGE, C., TONELLI, F., LECLERCQ, T., LIM, K. G., LONG, J. S., BERDYSHEV, E., TATE, R. J., NATARAJAN, V., PITSON, S. M. & PYNE, N. J. 2010. The sphingosine kinase 1 inhibitor 2-(p-hydroxyanilino)-4-(p-chlorophenyl) thiazole induces proteasomal degradation of sphingosine kinase 1 in mammalian cells. *Journal of Biological Chemistry,* 285, 38841-38852.
LU, C., ZHAO, A. X., GAO, Y.-J. & LEE, R. M. 2011. Modulation of vein function by perivascular adipose tissue. *European journal of pharmacology,* 657, 111-116.
LU, Z., ZHANG, W., GAO, S., JIANG, Q., XIAO, Z., YE, L. & ZHANG, X. 2015. MiR-506 suppresses liver cancer angiogenesis through targeting sphingosine kinase 1 (SPHK1) mRNA. *Biochemical and biophysical research communications,* 468, 8-13.
LUO, L. & LIU, M. 2022. Adiponectin: Friend or foe in obesity and inflammation. *Medical Review,* 2, 349-362.
LUSCHER, T. F. & VANHOUTTE, P. M. 2020. *The endothelium: modulator of cardiovascular function*, CRC press.
LUSIS, A. J. 2000. Atherosclerosis. *Nature,* 407, 233-41.
LYNCH, F. M., AUSTIN, C., HEAGERTY, A. M. & IZZARD, A. S. 2006. Adenosine- and hypoxia-induced dilation of human coronary resistance arteries: evidence against the involvement of KATP channels. *British journal of pharmacology,* 147, 455-458.
LYNCH, F. M., WITHERS, S. B., YAO, Z., WERNER, M. E., EDWARDS, G., WESTON, A. H. & HEAGERTY, A. M. 2013. Perivascular adipose tissue-derived adiponectin activates BKCa channels to induce anticontractile responses. *American Journal of Physiology-Heart and Circulatory Physiology,* 304, H786-H795.

MACEYKA, M., ALVAREZ, S. E., MILSTIEN, S. & SPIEGEL, S. 2008. Filamin A links sphingosine kinase 1 and sphingosine-1-phosphate receptor 1 at lamellipodia to orchestrate cell migration. *Molecular and cellular biology,* 28, 5687-5697.

MACEYKA, M., HARIKUMAR, K. B., MILSTIEN, S. & SPIEGEL, S. 2012. Sphingosine-1-phosphate signaling and its role in disease. *Trends in cell biology,* 22, 50-60.

MACEYKA, M., NAVA, V. E., MILSTIEN, S. & SPIEGEL, S. 2004. Aminoacylase 1 is a sphingosine kinase 1-interacting protein. *FEBS letters,* 568, 30-34.

MACEYKA, M. & SPIEGEL, S. 2014. Sphingolipid metabolites in inflammatory disease. *Nature,* 510, 58-67.

MACHADO, S. A., PASQUARELLI-DO-NASCIMENTO, G., DA SILVA, D. S., FARIAS, G. R., DE OLIVEIRA SANTOS, I., BAPTISTA, L. B. & MAGALHÃES, K. G. 2022. Browning of the white adipose tissue regulation: New insights into nutritional and metabolic relevance in health and diseases. *Nutrition & metabolism,* 19, 61.

MACRITCHIE, N., VOLPERT, G., AL WASHIH, M., WATSON, D. G., FUTERMAN, A. H., KENNEDY, S., PYNE, S. & PYNE, N. J. 2016. Effect of the sphingosine kinase 1 selective inhibitor, PF-543 on arterial and cardiac remodelling in a hypoxic model of pulmonary arterial hypertension. *Cellular signalling,* 28, 946-955.

MAEDA, N., SHIMOMURA, I., KISHIDA, K., NISHIZAWA, H., MATSUDA, M., NAGARETANI, H., FURUYAMA, N., KONDO, H., TAKAHASHI, M. & ARITA, Y. 2002. Diet-induced insulin resistance in mice lacking adiponectin/ACRP30. *Nature medicine,* 8, 731-737.

MAENHAUT, N., BOYDENS, C. & VAN DE VOORDE, J. 2010. Hypoxia enhances the relaxing influence of perivascular adipose tissue in isolated mice aorta. *European journal of pharmacology,* 641, 207-212.

MAGALANG, U., CRUFF, J., RAJAPPAN, R., HUNTER, M., PATEL, T., MARSH, C., RAMAN, S. & PARINANDI, N. 2009. Intermittent hypoxia suppresses adiponectin secretion by adipocytes. *Experimental and clinical endocrinology & diabetes,* 117, 129-134.

MAHAJAN-THAKUR, S., BIEN-MÖLLER, S., MARX, S., SCHROEDER, H. & RAUCH, B. H. 2017. Sphingosine 1-phosphate (S1P) signaling in glioblastoma multiforme—A systematic review. *International Journal of Molecular Sciences,* 18, 2448.

MAIR, K., ROBINSON, E., KANE, K., PYNE, S., BRETT, R., PYNE, N. & KENNEDY, S. 2010. Interaction between anandamide and sphingosine-1-phosphate in mediating vasorelaxation in rat coronary artery. *British journal of pharmacology,* 161, 176-192.

MARTINEZ-TELLEZ, B., SANCHEZ-DELGADO, G., ALCANTARA, J. M., ACOSTA, F. M., AMARO-GAHETE, F. J., OSUNA-PRIETO, F. J., PEREZ-BEY, A., JIMENEZ-PAVON, D., LLAMAS-ELVIRA, J. M. & GIL, A. 2019. Evidence of high 18F-fluorodeoxyglucose uptake in the subcutaneous adipose tissue of the dorsocervical area in young adults. *Experimental Physiology,* 104, 168-173.

MASTRANDREA, L. D. 2013. Role of sphingosine kinases and sphingosine 1-phosphate in mediating adipogenesis.

MASTRANDREA, L. D., SESSANNA, S. M. & LAYCHOCK, S. G. 2005. Sphingosine kinase activity and sphingosine-1 phosphate production in rat pancreatic islets and INS-1 cells: response to cytokines. *Diabetes,* 54, 1429-1436.

MATHIEU, P., POIRIER, P., PIBAROT, P., LEMIEUX, I. & DESPRÉS, J.-P. 2009. Visceral obesity: the link among inflammation, hypertension, and cardiovascular disease. *Hypertension,* 53, 577-584.

MATIENZO, D. & BORDONI, B. 2025. Anatomy, Blood Flow. *StatPearls*. Treasure Island (FL): StatPearls Publishing

MATTHIAS, A., OHLSON, K. B., FREDRIKSSON, J. M., JACOBSSON, A., NEDERGAARD, J. & CANNON, B. 2000. Thermogenic responses in brown fat cells are fully UCP1-dependent: UCP2 or UCP3 do not substitute for UCP1 in adrenergically or fatty acid-induced thermogenesis. *Journal of Biological Chemistry,* 275, 25073-25081.

MAZUREK, T., ZHANG, L., ZALEWSKI, A., MANNION, J. D., DIEHL, J. T., ARAFAT, H., SAROV-BLAT, L., O'BRIEN, S., KEIPER, E. A. & JOHNSON, A. G. 2003. Human epicardial adipose tissue is a source of inflammatory mediators. *Circulation,* 108, 2460-2466.

MAZZOTTA, C., BASU, S., GOWER, A. C., KARKI, S., FARB, M. G., SROCZYNSKI, E., ZIZZA, E., SARHAN, A., PANDE, A. N. & WALSH, K. 2021. Perivascular adipose tissue inflammation in ischemic heart disease. *Arteriosclerosis, thrombosis, and vascular biology,* 41, 1239-1250.

MCKEOWN, S. R. 2014. Defining normoxia, physoxia and hypoxia in tumours—implications for treatment response. *The British journal of radiology,* 87, 20130676.

MCNAUGHTON, M., PITMAN, M., PITSON, S. M., PYNE, N. J. & PYNE, S. 2016. Proteasomal degradation of sphingosine kinase 1 and inhibition of dihydroceramide desaturase by the sphingosine kinase inhibitors, SKi or ABC294640, induces growth arrest in androgen-independent LNCaP-Al prostate cancer cells. *Oncotarget,* 7, 16663.

MEANS, C. K. & BROWN, J. H. 2009. Sphingosine-1-phosphate receptor signalling in the heart. *Cardiovascular research,* 82, 193-200.

MEDLIN, M. D., STAUS, D. P., DUBASH, A. D., TAYLOR, J. M. & MACK, C. P. 2010. Sphingosine 1-phosphate receptor 2 signals through leukemia-associated RhoGEF (LARG), to promote smooth muscle cell differentiation. *Arteriosclerosis, thrombosis, and vascular biology,* 30, 1779-1786.

MEIJER, R. I., BAKKER, W., ALTA, C.-L. A., SIPKEMA, P., YUDKIN, J. S., VIOLLET, B., RICHTER, E. A., SMULDERS, Y. M., VAN HINSBERGH, V. W. & SERNÉ, E. H. 2013. Perivascular adipose tissue control of insulin-induced vasoreactivity in muscle is impaired in db/db mice. *Diabetes,* 62, 590-598.

MELENDEZ, A. J., CARLOS-DIAS, E., GOSINK, M., ALLEN, J. M. & TAKACS, L. 2000. Human sphingosine kinase: molecular cloning, functional characterization and tissue distribution. *Gene,* 251, 19-26.

MENDIZÁBAL, Y., LLORENS, S. & NAVA, E. 2013. Vasoactive effects of prostaglandins from the perivascular fat of mesenteric resistance arteries in WKY and SHROB rats. *Life sciences,* 93, 1023-1032.

MENSAH, S. A., CHENG, M. J., HOMAYONI, H., PLOUFFE, B. D., COURY, A. J. & EBONG, E. E. 2017. Regeneration of glycocalyx by heparan sulfate and sphingosine 1-phosphate restores inter-endothelial communication. *PloS one,* 12, e0186116.

MEYER, M. R., FREDETTE, N. C., BARTON, M. & PROSSNITZ, E. R. 2013. Regulation of vascular smooth muscle tone by adipose-derived contracting factor. *PloS one,* 8, e79245.

MICHEL, M. C., MULDERS, A. C., JONGSMA, M., ALEWIJNSE, A. E. & PETERS, S. L. 2007. Vascular effects of sphingolipids. *Acta Paediatrica,* 96, 44-48.

MITIDIERI, E., TURNATURI, C., VANACORE, D., SORRENTINO, R. & D'EMMANUELE DI VILLA BIANCA, R. 2022. The role of perivascular adipose tissue-derived hydrogen sulfide in the control of vascular homeostasis. *Antioxidants & Redox Signaling,* 37**,** 84-97.

MONTANARI, T. & COLITTI, M. 2018. Simpson–Golabi–Behmel syndrome human adipocytes reveal a changing phenotype throughout differentiation. *Histochemistry and Cell Biology,* 149**,** 593-605.

MOON, M.-H., JEONG, J.-K., LEE, Y.-J., SEOL, J.-W. & PARK, S.-Y. 2014. Sphingosine-1-phosphate inhibits the adipogenic differentiation of 3T3-L1 preadipocytes. *International journal of molecular medicine,* 34**,** 1153-1158.

MOON, M. H., JEONG, J. K. & PARK, S. Y. 2015. Activation of S1P2 receptor, a possible mechanism of inhibition of adipogenic differentiation by sphingosine 1-phosphate. *Molecular medicine reports,* 11**,** 1031-1036.

MORISHIGE, J.-I., YOSHIOKA, K., NAKATA, H., ISHIMARU, K., NAGATA, N., TANAKA, T., TAKUWA, Y. & ANDO, H. 2023. Sphingosine kinase 1 is involved in triglyceride breakdown by maintaining lysosomal integrity in brown adipocytes. *Journal of Lipid Research,* 64**,** 100450.

MORRISON, S. & MCGEE, S. L. 2015. 3T3-L1 adipocytes display phenotypic characteristics of multiple adipocyte lineages. *Adipocyte,* 4**,** 295-302.

MUÑOZ-SÁNCHEZ, J. & CHÁNEZ-CÁRDENAS, M. E. 2019. The use of cobalt chloride as a chemical hypoxia model. *Journal of Applied Toxicology,* 39**,** 556-570.

MURAMATSU, I., KIGOSHI, S. & OSHITA, M. 1990. Two distinct α1-adrenoceptor subtypes involved in noradrenaline contraction of the rabbit thoracic aorta. *British journal of pharmacology,* 101**,** 662-666.

NADAR, S., BLANN, A. D. & LIP, G. Y. 2004. Endothelial dysfunction: methods of assessment and application to hypertension. *Current pharmaceutical design,* 10**,** 3591-3605.

NAGAHASHI, M., TAKABE, K., TERRACINA, K. P., SOMA, D., HIROSE, Y., KOBAYASHI, T., MATSUDA, Y. & WAKAI, T. 2014. Sphingosine-1-phosphate transporters as targets for cancer therapy. *BioMed research international,* 2014**,** 651727.

NAKANO, Y., TOBE, T., CHOI-MIURA, N.-H., MAZDA, T. & TOMITA, M. 1996. Isolation and characterization of GBP28, a novel gelatin-binding protein purified from human plasma. *The Journal of Biochemistry,* 120**,** 803-812.

NOSALSKI, R. & GUZIK, T. J. 2017. Perivascular adipose tissue inflammation in vascular disease. *British journal of pharmacology,* 174**,** 3496-3513.

O'BEIRNE, M., GUREVICH, N. & CARLEN, P. 1987. Pentobarbital inhibits hippocampal neurons by increasing potassium conductance. *Canadian journal of physiology and pharmacology,* 65**,** 36-41.

O'ROURKE, R., WHITE, A., METCALF, M., OLIVAS, A., MITRA, P., LARISON, W., CHEANG, E., VARLAMOV, O., CORLESS, C. & ROBERTS JR, C. 2011. Hypoxia-induced inflammatory cytokine secretion in human adipose tissue stromovascular cells. *Diabetologia,* 54**,** 1480-1490.

OBINATA, H. & HLA, T. Sphingosine 1-phosphate in coagulation and inflammation. Seminars in immunopathology, 2012. Springer, 73-91.

OBINATA, H. & HLA, T. 2019. Sphingosine 1-phosphate and inflammation. *International immunology,* 31**,** 617-625.

OKADA, T., DING, G., SONODA, H., KAJIMOTO, T., HAGA, Y., KHOSROWBEYGI, A., GAO, S., MIWA, N., JAHANGEER, S. & NAKAMURA, S.-I. 2005. Involvement of N-terminal-extended form of sphingosine kinase 2 in

serum-dependent regulation of cell proliferation and apoptosis. *Journal of Biological Chemistry,* 280**,** 36318-36325.

OKAMOTO, H., TAKUWA, N., GONDA, K., OKAZAKI, H., CHANG, K., YATOMI, Y., SHIGEMATSU, H. & TAKUWA, Y. 1998. EDG1 is a functional sphingosine-1-phosphate receptor that is linked via a Gi/o to multiple signaling pathways, including phospholipase C activation, Ca2+ mobilization, Ras-mitogen-activated protein kinase activation, and adenylate cyclase inhibition. *Journal of Biological Chemistry,* 273**,** 27104-27110.

ORIOWO, M. A. 2015. Perivascular adipose tissue, vascular reactivity and hypertension. *Medical Principles and Practice,* 24**,** 29-37.

ORLANDO, I. M., LAFLEUR, V. N., STORTI, F., SPIELMANN, P., CROWTHER, L., SANTAMBROGIO, S., SCHÖDEL, J., HOOGEWIJS, D., MOLE, D. R. & WENGER, R. H. 2019. Distal and proximal hypoxia response elements co-operate to regulate organ-specific erythropoietin gene expression. *haematologica,* 105**,** 2774.

ORTIZ-PRADO, E., DUNN, J. F., VASCONEZ, J., CASTILLO, D. & VISCOR, G. 2019. Partial pressure of oxygen in the human body: a general review. *American journal of blood research,* 9**,** 1.

OUCHI, N., OHISHI, M., KIHARA, S., FUNAHASHI, T., NAKAMURA, T., NAGARETANI, H., KUMADA, M., OHASHI, K., OKAMOTO, Y. & NISHIZAWA, H. 2003. Association of hypoadiponectinemia with impaired vasoreactivity. *Hypertension,* 42**,** 231-234.

OUCHI, N., SHIBATA, R. & WALSH, K. 2006. Cardioprotection by adiponectin. *Trends in cardiovascular medicine,* 16**,** 141-146.

OW, C. P., ULLAH, M. M., NGO, J. P., SAYAKKARAGE, A. & EVANS, R. G. 2019. Detection of cellular hypoxia by pimonidazole adduct immunohistochemistry in kidney disease: methodological pitfalls and their solution. *American Journal of Physiology-Renal Physiology,* 317**,** F322-F332.

OWEN, M. K., NOBLET, J. N., SASSOON, D. J., CONTEH, A. M., GOODWILL, A. G. & TUNE, J. D. 2014. Perivascular adipose tissue and coronary vascular disease. *Arteriosclerosis, thrombosis, and vascular biology,* 34**,** 1643-1649.

OWEN, M. K., WITZMANN, F. A., MCKENNEY, M. L., LAI, X., BERWICK, Z. C., MOBERLY, S. P., ALLOOSH, M., STUREK, M. & TUNE, J. D. 2013. Perivascular adipose tissue potentiates contraction of coronary vascular smooth muscle: influence of obesity. *Circulation,* 128**,** 9-18.

OWENS, G. K., KUMAR, M. S. & WAMHOFF, B. R. 2004. Molecular regulation of vascular smooth muscle cell differentiation in development and disease. *Physiological reviews,* 84**,** 767-801.

PADILLA, J., JENKINS, N. T., VIEIRA-POTTER, V. J. & LAUGHLIN, M. H. 2013. Divergent phenotype of rat thoracic and abdominal perivascular adipose tissues. *American Journal of Physiology-Regulatory, Integrative and Comparative Physiology,* 304**,** R543-R552.

PALMER, B. F. & CLEGG, D. J. 2015. The sexual dimorphism of obesity. *Molecular and cellular endocrinology,* 402**,** 113-119.

PAN, S., MI, Y., PALLY, C., BEERLI, C., CHEN, A., GUERINI, D., HINTERDING, K., NUESSLEIN-HILDESHEIM, B., TUNTLAND, T. & LEFEBVRE, S. 2006. A monoselective sphingosine-1-phosphate receptor-1 agonist prevents allograft rejection in a stringent rat heart transplantation model. *Chemistry & biology,* 13**,** 1227-1234.

PANG, T. T. & NARENDRAN, P. 2008. The distribution of adiponectin receptors on human peripheral blood mononuclear cells. *Annals of the New York Academy of Sciences,* 1150**,** 143-145.

PARHAM, K. A., ZEBOL, J. R., TOOLEY, K. L., SUN, W. Y., MOLDENHAUER, L. M., COCKSHELL, M. P., GLIDDON, B. L., MORETTI, P. A., TIGYI, G. & PITSON, S. M. 2015. Sphingosine 1-phosphate is a ligand for peroxisome proliferator-activated receptor-γ that regulates neoangiogenesis. *The FASEB Journal,* 29**,** 3638-3653.

PARK, A., KIM, W. K. & BAE, K.-H. 2014a. Distinction of white, beige and brown adipocytes derived from mesenchymal stem cells. *World journal of stem cells,* 6**,** 33.

PARK, S. Y., KIM, K. H., SEO, K. W., BAE, J. U., KIM, Y. H., LEE, S. J., LEE, W. S. & KIM, C. D. 2014b. Resistin derived from diabetic perivascular adipose tissue up-regulates vascular expression of osteopontin via the AP-1 signalling pathway. *The Journal of Pathology,* 232**,** 87-97.

PARRILL, A. L., SARDAR, V. M. & YUAN, H. Sphingosine 1-phosphate and lysophosphatidic acid receptors: agonist and antagonist binding and progress toward development of receptor-specific ligands. Seminars in cell & developmental biology, 2004. Elsevier, 467-476.

PASARICA, M., SEREDA, O. R., REDMAN, L. M., ALBARADO, D. C., HYMEL, D. T., ROAN, L. E., ROOD, J. C., BURK, D. H. & SMITH, S. R. 2009. Reduced adipose tissue oxygenation in human obesity: evidence for rarefaction, macrophage chemotaxis, and inflammation without an angiogenic response. *Diabetes,* 58**,** 718-725.

PEARCE, W. J., ASHWAL, S., LONG, D. & CUEVAS, J. 1992. Hypoxia inhibits calcium influx in rabbit basilar and carotid arteries. *American Journal of Physiology-Heart and Circulatory Physiology,* 262**,** H106-H113.

PEARSON, P. J., SCHAFF, H. V. & VANHOUTTE, P. M. 1990. Long-term impairment of endothelium-dependent relaxations to aggregating platelets after reperfusion injury in canine coronary arteries. *Circulation,* 81**,** 1921-1927.

PEIXOTO-NEVES, D., WANG, Q., LEAL-CARDOSO, J. H., ROSSONI, L. V. & JAGGAR, J. H. 2015. Eugenol dilates mesenteric arteries and reduces systemic BP by activating endothelial cell TRPV 4 channels. *British Journal of Pharmacology,* 172**,** 3484-3494.

PELHAM, C. J., DREWS, E. M. & AGRAWAL, D. K. 2016. Vitamin D controls resistance artery function through regulation of perivascular adipose tissue hypoxia and inflammation. *Journal of molecular and cellular cardiology,* 98**,** 1-10.

PETERSEN, M. C. & SHULMAN, G. I. 2018. Mechanisms of insulin action and insulin resistance. *Physiological reviews,* 98**,** 2133-2223.

PHAN, F., BOURRON, O., FOUFELLE, F., LE STUNFF, H. & HAJDUCH, E. 2024. Sphingosine-1-phosphate signalling in the heart: exploring emerging perspectives in cardiopathology. *FEBS letters,* 598**,** 2641-2655.

PHELPS, N. H., SINGLETON, R. K., ZHOU, B., HEAP, R. A., MISHRA, A., BENNETT, J. E., PACIOREK, C. J., LHOSTE, V. P., CARRILLO-LARCO, R. M. & STEVENS, G. A. 2024. Worldwide trends in underweight and obesity from 1990 to 2022: a pooled analysis of 3663 population-representative studies with 222 million children, adolescents, and adults. *The Lancet,* 403**,** 1027-1050.

PIASCIK, M. T., GUARINO, R. D., SMITH, M. S., SOLTIS, E. E., SAUSSY, D. & PEREZ, D. M. 1995. The specific contribution of the novel alpha-1D

adrenoceptor to the contraction of vascular smooth muscle. *The Journal of pharmacology and experimental therapeutics,* 275**,** 1583-1589.
PITSON, S. M., MORETTI, P. A., ZEBOL, J. R., LYNN, H. E., XIA, P., VADAS, M. A. & WATTENBERG, B. W. 2003. Activation of sphingosine kinase 1 by ERK1/2-mediated phosphorylation. *The EMBO journal*.
PITSON, S. M., MORETTI, P. A., ZEBOL, J. R., ZAREIE, R., DERIAN, C. K., DARROW, A. L., QI, J., D'ANDREA, R. J., BAGLEY, C. J. & VADAS, M. A. 2002. The nucleotide-binding site of human sphingosine kinase 1. *Journal of Biological Chemistry,* 277**,** 49545-49553.
PITSON, S. M., XIA, P., LECLERCQ, T. M., MORETTI, P. A., ZEBOL, J. R., LYNN, H. E., WATTENBERG, B. W. & VADAS, M. A. 2005. Phosphorylation-dependent translocation of sphingosine kinase to the plasma membrane drives its oncogenic signalling. *The Journal of experimental medicine,* 201**,** 49-54.
PLACE, T. L., DOMANN, F. E. & CASE, A. J. 2017. Limitations of oxygen delivery to cells in culture: An underappreciated problem in basic and translational research. *Free Radical Biology and Medicine,* 113**,** 311-322.
POLZIN, A., DANNENBERG, L., BENKHOFF, M., BARCIK, M., HELTEN, C., MOURIKIS, P., AHLBRECHT, S., WILDEIS, L., ZIESE, J. & ZIKELI, D. 2023. Revealing concealed cardioprotection by platelet Mfsd2b-released S1P in human and murine myocardial infarction. *Nature Communications,* 14**,** 2404.
POWELL-WILEY, T. M., POIRIER, P., BURKE, L. E., DESPRÉS, J.-P., GORDON-LARSEN, P., LAVIE, C. J., LEAR, S. A., NDUMELE, C. E., NEELAND, I. J. & SANDERS, P. 2021. Obesity and cardiovascular disease: a scientific statement from the American Heart Association. *Circulation,* 143**,** e984-e1010.
PRALHADA RAO, R., VAIDYANATHAN, N., RENGASAMY, M., MAMMEN OOMMEN, A., SOMAIYA, N. & JAGANNATH, M. 2013. Sphingolipid metabolic pathway: an overview of major roles played in human diseases. *Journal of lipids,* 2013**,** 178910.
PROIA, R. L. & HLA, T. 2015. Emerging biology of sphingosine-1-phosphate: its role in pathogenesis and therapy. *The Journal of clinical investigation,* 125**,** 1379-1387.
PULKOSKI-GROSS, M. J. & OBEID, L. M. 2018. Molecular mechanisms of regulation of sphingosine kinase 1. *Biochimica et Biophysica Acta (BBA)-Molecular and Cell Biology of Lipids,* 1863**,** 1413-1422.
PYNE, N. J. & PYNE, S. 2010. Sphingosine 1-phosphate and cancer. *Nature Reviews Cancer,* 10**,** 489-503.
PYNE, S., ADAMS, D. R. & PYNE, N. J. 2016. Sphingosine 1-phosphate and sphingosine kinases in health and disease: Recent advances. *Progress in lipid research,* 62**,** 93-106.
PYNE, S., LEE, S. C., LONG, J. & PYNE, N. J. 2009. Role of sphingosine kinases and lipid phosphate phosphatases in regulating spatial sphingosine 1-phosphate signalling in health and disease. *Cellular signalling,* 21**,** 14-21.
PYNE, S. & PYNE, N. J. 2000. Sphingosine 1-phosphate signalling in mammalian cells. *Biochemical Journal,* 349**,** 385-402.
PYNE, S. & PYNE, N. J. 2011. Translational aspects of sphingosine 1-phosphate biology. *Trends in molecular medicine,* 17**,** 463-472.
QI, X.-Y., QU, S.-L., XIONG, W.-H., ROM, O., CHANG, L. & JIANG, Z.-S. 2018. Perivascular adipose tissue (PVAT) in atherosclerosis: a double-edged sword. *Cardiovascular diabetology,* 17**,** 1-20.
QUEHENBERGER, P., EXNER, M., SUNDER-PLASSMANN, R., RUZICKA, K., BIEGLMAYER, C., ENDLER, G., MUELLNER, C., SPEISER, W. & WAGNER, O.

2002. Leptin induces endothelin-1 in endothelial cells in vitro. *Circulation research,* 90, 711-718.

QUEIROZ, M. & SENA, C. M. 2024. Perivascular adipose tissue: a central player in the triad of diabetes, obesity, and cardiovascular health. *Cardiovascular Diabetology,* 23, 455.

QUESADA, I., CEJAS, J., GARCÍA, R., CANNIZZO, B., REDONDO, A. & CASTRO, C. 2018. Vascular dysfunction elicited by a cross talk between periaortic adipose tissue and the vascular wall is reversed by pioglitazone. *Cardiovascular therapeutics,* 36, e12322.

RAJSHEKER, S., MANKA, D., BLOMKALNS, A. L., CHATTERJEE, T. K., STOLL, L. L. & WEINTRAUB, N. L. 2010. Crosstalk between perivascular adipose tissue and blood vessels. *Current opinion in pharmacology,* 10, 191-196.

RAMIREZ-PONCE, M., MATEOS, J. & BELLIDO, J. 2003. Human adipose cells have voltage-dependent potassium currents. *The Journal of membrane biology,* 196, 129-134.

RAMıREZ-PONCE, M., MATEOS, J., CARRION, N. & BELLIDO, J. 1996. Voltage-dependent potassium channels in white adipocytes. *Biochemical and biophysical research communications,* 223, 250-256.

RAMIREZ, J., O'MALLEY, E. & HO, W. 2017. Pro-contractile effects of perivascular fat in health and disease. *British Journal of Pharmacology,* 174, 3482-3495.

RAO, X., HUANG, X., ZHOU, Z. & LIN, X. 2013. An improvement of the 2ˆ (-delta delta CT) method for quantitative real-time polymerase chain reaction data analysis. *Biostatistics, bioinformatics and biomathematics,* 3, 71.

RAPOPORT, R. M. & WILLIAMS, S. P. 1996. Role of prostaglandins in acetylcholine-induced contraction of aorta from spontaneously hypertensive and Wistar-Kyoto rats. *Hypertension,* 28, 64-75.

RAUSCH, M., WEISBERG, S., VARDHANA, P. & TORTORIELLO, D. 2008. Obesity in C57BL/6J mice is characterized by adipose tissue hypoxia and cytotoxic T-cell infiltration. *International journal of obesity,* 32, 451-463.

REILLY, S. M. & SALTIEL, A. R. 2017. Adapting to obesity with adipose tissue inflammation. *Nature Reviews Endocrinology,* 13, 633-643.

REITSEMA, V., BOUMA, H. & KOK, J. 2014. Sphingosine-1-phosphate transport and its role in immunology. *AIMS Molecular Science,* 1, 183-201.

REN, S., XIN, C., PFEILSCHIFTER, J. & HUWILER, A. 2010. A novel mode of action of the putative sphingosine kinase inhibitor 2-(p-hydroxyanilino)-4-(p-chlorophenyl) thiazole (SKI II): induction of lysosomal sphingosine kinase 1 degradation. *Cellular physiology and biochemistry,* 26, 97-104.

REYNÉS, B., VAN SCHOTHORST, E. M., KEIJER, J., CERESI, E., OLIVER, P. & PALOU, A. 2019. Cold induced depot-specific browning in ferret aortic perivascular adipose tissue. *Frontiers in Physiology,* 10, 1171.

RICHARD, A. J., WHITE, U., ELKS, C. M. & STEPHENS, J. M. 2020. Adipose tissue: physiology to metabolic dysfunction. *Endotext [Internet].*

RITTIG, K., DOLDERER, J., BALLETSHOFER, B., MACHANN, J., SCHICK, F., MEILE, T., KÜPER, M., STOCK, U., STAIGER, H. & MACHICAO, F. 2012. The secretion pattern of perivascular fat cells is different from that of subcutaneous and visceral fat cells. *Diabetologia,* 55, 1514-1525.

ROMERO-CORRAL, A., SERT-KUNIYOSHI, F. H., SIERRA-JOHNSON, J., ORBAN, M., GAMI, A., DAVISON, D., SINGH, P., PUSALAVIDYASAGAR, S., HUYBER, C. & VOTRUBA, S. 2010. Modest visceral fat gain causes endothelial dysfunction in healthy humans. *Journal of the American College of Cardiology,* 56, 662-666.

ROSEI, C. A., WITHERS, S. B., BELCAID, L., DE CIUCEIS, C., RIZZONI, D. & HEAGERTY, A. M. 2015. Blockade of the reninâ–“angiotensin system in small arteries and anticontractile function of perivascular adipose tissue. *Journal of hypertension,* 33**,** 1039-1045.

ROSENWALD, M., PERDIKARI, A., RÜLICKE, T. & WOLFRUM, C. 2013. Bi-directional interconversion of brite and white adipocytes. *Nature cell biology,* 15**,** 659-667.

ROVIEZZO, F., BUCCI, M., DELISLE, C., BRANCALEONE, V., LORENZO, A. D., MAYO, I. P., FIORUCCI, S., FONTANA, A., GRATTON, J. P. & CIRINO, G. 2006. Expression of Concern: Essential requirement for sphingosine kinase activity in eNOS-dependent NO release and vasorelaxation. *The FASEB journal,* 20**,** 340-342.

ROYLE, C., LIM, S., XU, B., TOOHER, J., OGLE, R. & HENNESSY, A. 2009. Effect of hypoxia and exogenous IL-10 on the pro-inflammatory cytokine TNF-α and the anti-angiogenic molecule soluble Flt-1 in placental villous explants. *Cytokine,* 47**,** 56-60.

RUEDA-CLAUSEN, C. F., DOLINSKY, V. W., MORTON, J. S., PROCTOR, S. D., DYCK, J. R. & DAVIDGE, S. T. 2011. Hypoxia-Induced Intrauterine Growth Restriction Increases the Susceptibility of Rats to High-Fat Diet–Induced Metabolic Syndrome. *Diabetes,* 60**,** 507-516.

RUIZ, M., DEVKOTA, R., PANAGAKI, D., BERGH, P.-O., KAPER, D., HENRICSSON, M., NIK, A., PETKEVICIUS, K., HÖÖG, J. L. & BOHLOOLY-Y, M. 2022. Sphingosine 1-phosphate mediates adiponectin receptor signaling essential for lipid homeostasis and embryogenesis. *Nature Communications,* 13**,** 7162.

SABERI, M., WOODS, N.-B., DE LUCA, C., SCHENK, S., LU, J. C., BANDYOPADHYAY, G., VERMA, I. M. & OLEFSKY, J. M. 2009. Hematopoietic cell-specific deletion of toll-like receptor 4 ameliorates hepatic and adipose tissue insulin resistance in high-fat-fed mice. *Cell metabolism,* 10**,** 419-429.

SAH, R. K., PATI, S., SAINI, M., BOOPATHI, P. A., KOCHAR, S. K., KOCHAR, D. K., DAS, A. & SINGH, S. 2020. Reduction of sphingosine kinase 1 phosphorylation and activity in plasmodium-infected erythrocytes. *Frontiers in cell and developmental biology,* 8**,** 80.

ŞAHIN, A. S. & BARISKANER, H. 2007. The mechanisms of vasorelaxant effect of leptin on isolated rabbit aorta. *Fundamental & clinical pharmacology,* 21**,** 595-600.

SALAMA, M. F., CARROLL, B., ADADA, M., PULKOSKI-GROSS, M., HANNUN, Y. A. & OBEID, L. M. 2015. A novel role of sphingosine kinase-1 in the invasion and angiogenesis of VHL mutant clear cell renal cell carcinoma. *The FASEB Journal,* 29**,** 2803.

SALCEDO, A., GARIJO, J., MONGE, L., FERNÁNDEZ, N., GARCÍA-VILLALÓN, A. L., TURRIÓN, V. S., CUERVAS-MONS, V. & DIÉGUEZ, G. 2007. Apelin effects in human splanchnic arteries. Role of nitric oxide and prostanoids. *Regulatory peptides,* 144**,** 50-55.

SALMENNIEMI, U., RUOTSALAINEN, E., PIHLAJAMÄKI, J., VAUHKONEN, I., KAINULAINEN, S., PUNNONEN, K., VANNINEN, E. & LAAKSO, M. 2004. Multiple abnormalities in glucose and energy metabolism and coordinated changes in levels of adiponectin, cytokines, and adhesion molecules in subjects with metabolic syndrome. *Circulation,* 110**,** 3842-3848.

SALOMONE, S. & WAEBER, C. 2011. Selectivity and specificity of sphingosine-1-phosphate receptor ligands: caveats and critical thinking in characterizing receptor-mediated effects. *Frontiers in pharmacology,* 2**,** 9.

SAMAD, F., HESTER, K. D., YANG, G., HANNUN, Y. A. & BIELAWSKI, J. 2006. Altered adipose and plasma sphingolipid metabolism in obesity: a potential mechanism for cardiovascular and metabolic risk. *Diabetes,* 55**,** 2579-2587.

SANAGAWA, A., IWAKI, S., ASAI, M., SAKAKIBARA, D., NORIMOTO, H., SOBEL, B. E. & FUJII, S. 2016. Sphingosine 1-phosphate induced by hypoxia increases the expression of PAI-1 in HepG2 cells via HIF-1α. *Molecular Medicine Reports,* 14**,** 1841-1848.

SANDOO, A., VAN ZANTEN, J. J. V., METSIOS, G. S., CARROLL, D. & KITAS, G. D. 2010. The endothelium and its role in regulating vascular tone. *The open cardiovascular medicine journal,* 4**,** 302.

SANDOW, S. L. & HILL, C. E. 2000. Incidence of myoendothelial gap junctions in the proximal and distal mesenteric arteries of the rat is suggestive of a role in endothelium-derived hyperpolarizing factor–mediated responses. *Circulation research,* 86**,** 341-346.

SANDOW, S. L., TARE, M., COLEMAN, H. A., HILL, C. E. & PARKINGTON, H. C. 2002. Involvement of myoendothelial gap junctions in the actions of endothelium-derived hyperpolarizing factor. *Circulation research,* 90**,** 1108-1113.

SANKALA, H. M., HAIT, N. C., PAUGH, S. W., SHIDA, D., LÉPINE, S., ELMORE, L. W., DENT, P., MILSTIEN, S. & SPIEGEL, S. 2007. Involvement of sphingosine kinase 2 in p53-independent induction of p21 by the chemotherapeutic drug doxorubicin. *Cancer research,* 67**,** 10466-10474.

SANNA, M. G., WANG, S.-K., GONZALEZ-CABRERA, P. J., DON, A., MARSOLAIS, D., MATHEU, M. P., WEI, S. H., PARKER, I., JO, E. & CHENG, W.-C. 2006. Enhancement of capillary leakage and restoration of lymphocyte egress by a chiral S1P1 antagonist in vivo. *Nature chemical biology,* 2**,** 434-441.

SANTIAGO, E., MARTÍNEZ, M. P., CLIMENT, B., MUÑOZ, M., BRIONES, A. M., SALAICES, M., GARCÍA-SACRISTÁN, A., RIVERA, L. & PRIETO, D. 2016. Augmented oxidative stress and preserved vasoconstriction induced by hydrogen peroxide in coronary arteries in obesity: role of COX-2. *British journal of pharmacology,* 173**,** 3176-3195.

SAXTON, S. N., CLARK, B. J., WITHERS, S. B., ERINGA, E. C. & HEAGERTY, A. M. 2019a. Mechanistic links between obesity, diabetes, and blood pressure: role of perivascular adipose tissue. *Physiological reviews,* 99**,** 1701-1763.

SAXTON, S. N., RYDING, K. E., ALDOUS, R. G., WITHERS, S. B., OHANIAN, J. & HEAGERTY, A. M. 2018. Role of sympathetic nerves and adipocyte catecholamine uptake in the vasorelaxant function of perivascular adipose tissue. *Arteriosclerosis, thrombosis, and vascular biology,* 38**,** 880-891.

SAXTON, S. N., TOMS, L. K., ALDOUS, R. G., WITHERS, S. B., OHANIAN, J. & HEAGERTY, A. M. 2021. Restoring perivascular adipose tissue function in obesity using exercise. *Cardiovascular Drugs and Therapy***,** 1-14.

SAXTON, S. N., WITHERS, S. B. & HEAGERTY, A. M. 2019b. Emerging roles of sympathetic nerves and inflammation in perivascular adipose tissue. *Cardiovascular drugs and therapy,* 33**,** 245-259.

SAXTON, S. N., WITHERS, S. B. & HEAGERTY, A. M. 2022. Perivascular adipose tissue anticontractile function is mediated by both endothelial and neuronal nitric oxide synthase isoforms. *Journal of Vascular Research,* 59**,** 288-302.

SCHAFFLER, A., MULLER-LADNER, U., SCHOLMERICH, J. & BUCHLER, C. 2006. Role of adipose tissue as an inflammatory organ in human diseases. *Endocrine reviews,* 27**,** 449-467.

SCHERER, P. E., WILLIAMS, S., FOGLIANO, M., BALDINI, G. & LODISH, H. F. 1995. A novel serum protein similar to C1q, produced exclusively in adipocytes. *Journal of Biological chemistry,* 270**,** 26746-26749.

SCHNUTE, M. E., MCREYNOLDS, M. D., KASTEN, T., YATES, M., JEROME, G., RAINS, J. W., HALL, T., CHRENCIK, J., KRAUS, M. & CRONIN, C. N. 2012. Modulation of cellular S1P levels with a novel, potent and specific inhibitor of sphingosine kinase-1. *Biochemical Journal,* 444**,** 79-88.

SCHULZ, M. E., KATUNARIC, B., HOCKENBERRY, J. C., GUTTERMAN, D. D. & FREED, J. K. 2019. Manipulation of the sphingolipid rheostat influences the mediator of flow-induced dilation in the human microvasculature. *Journal of the American Heart Association,* 8**,** e013153.

SCHWALM, S., DÖLL, F., RÖMER, I., BUBNOVA, S., PFEILSCHIFTER, J. & HUWILER, A. 2008. Sphingosine kinase-1 is a hypoxia-regulated gene that stimulates migration of human endothelial cells. *Biochemical and biophysical research communications,* 368**,** 1020-1025.

SCOTT, S. S., YANG, X., ROBICH, M., LIAW, L. & BOUCHER, J. M. 2019. Differentiation capacity of human aortic perivascular adipose progenitor cells. *Journal of visualized experiments: JoVE***,** 10.3791/59337.

SENA, C. M., PEREIRA, A., FERNANDES, R., LETRA, L. & SEIÇA, R. M. 2017. Adiponectin improves endothelial function in mesenteric arteries of rats fed a high-fat diet: role of perivascular adipose tissue. *British journal of pharmacology,* 174**,** 3514-3526.

SHAFIEI, M. S., SHETTY, S., SCHERER, P. E. & ROCKEY, D. C. 2011. Adiponectin regulation of stellate cell activation via PPARγ-dependent and-independent mechanisms. *The American journal of pathology,* 178**,** 2690-2699.

SHARMA, A. X. & HOLLAND, W. L. 2017. Adiponectin and its hydrolase-activated receptors. *Journal of nature and science,* 3**,** e396.

SHENG, L. J., RUAN, C. C., MA, Y., CHEN, D. R., KONG, L. R., ZHU, D. L. & GAO, P. J. 2016. Beta3 adrenergic receptor is involved in vascular injury in deoxycorticosterone acetate-salt hypertensive mice. *FEBS letters,* 590**,** 769-778.

SHI, H., MOUSTAID-MOUSSA, N., WILKISON, W. & ZEMEL, M. B. 1999. Role of the sulfonylurea receptor in regulating human adipocyte metabolism. *The FASEB journal,* 13**,** 1833-1838.

SHIMIZU, I., APRAHAMIAN, T., KIKUCHI, R., SHIMIZU, A., PAPANICOLAOU, K. N., MACLAUCHLAN, S., MARUYAMA, S. & WALSH, K. 2014. Vascular rarefaction mediates whitening of brown fat in obesity. *The Journal of clinical investigation,* 124**,** 2099-2112.

SIEGEL-AXEL, D. I., ULLRICH, S., STEFAN, N., RITTIG, K., GERST, F., KLINGLER, C., SCHMIDT, U., SCHREINER, B., RANDRIANARISOA, E. & SCHALLER, H.-E. 2014. Fetuin-A influences vascular cell growth and production of proinflammatory and angiogenic proteins by human perivascular fat cells. *Diabetologia,* 57**,** 1057-1066.

SIMÕES, M. R., AZEVEDO, B. F., ALONSO, M. J., SALAICES, M. & VASSALLO, D. V. 2021. Chronic low-level lead exposure increases mesenteric vascular reactivity: role of cyclooxygenase-2-derived prostanoids. *Frontiers in physiology,* 11**,** 590308.

SIMONSEN, U. & BOEDTKJER, E. 2016. New roles of factors from perivascular tissue in regulation of vascular tone. Wiley Online Library.

SINGER, M., YOUNG, P. J., LAFFEY, J. G., ASFAR, P., TACCONE, F. S., SKRIFVARS, M. B., MEYHOFF, C. S. & RADERMACHER, P. 2021. Dangers of hyperoxia. *Critical Care,* 25**,** 440.

SINGLETON, P. A., DUDEK, S. M., CHIANG, E. T. & GARCIA, J. G. 2005. Regulation of sphingosine 1-phosphate-induced endothelial cytoskeletal rearrangement and barrier enhancement by S1P1 receptor, PI3 kinase, Tiam1/Rac1, and α-actinin. *The FASEB Journal,* 19**,** 1646-1656.

SKIBA, D., NOSALSKI, R., MIKOLAJCZYK, T., SIEDLINSKI, M., RIOS, F., MONTEZANO, A., JAWIEN, J., OLSZANECKI, R., KORBUT, R. & CZESNIKIEWICZ-GUZIK, M. 2017. Anti-atherosclerotic effect of the angiotensin 1–7 mimetic AVE0991 is mediated by inhibition of perivascular and plaque inflammation in early atherosclerosis. *British Journal of Pharmacology,* 174**,** 4055-4069.

SKOURA, A. & HLA, T. 2009. Regulation of vascular physiology and pathology by the S1P2 receptor subtype. *Cardiovascular research,* 82**,** 221-228.

SKURK, T., ALBERTI-HUBER, C., HERDER, C. & HAUNER, H. 2007. Relationship between adipocyte size and adipokine expression and secretion. *The Journal of Clinical Endocrinology & Metabolism,* 92**,** 1023-1033.

SOLTIS, E. E. & CASSIS, L. A. 1991. Influence of perivascular adipose tissue on rat aortic smooth muscle responsiveness. *Clinical and Experimental Hypertension. Part A: Theory and Practice,* 13**,** 277-296.

SOUSA, A. S., SPONTON, A. C., TRIFONE, C. B. & DELBIN, M. A. 2019. Aerobic exercise training prevents perivascular adipose tissue-induced endothelial dysfunction in thoracic aorta of obese mice. *Frontiers in physiology,* 10**,** 1009.

SOWKA, A. & DOBRZYN, P. 2021. Role of perivascular adipose tissue-derived adiponectin in vascular homeostasis. *Cells,* 10**,** 1485.

SPIEGEL, S., MACZIS, M. A., MACEYKA, M. & MILSTIEN, S. 2019. New insights into functions of the sphingosine-1-phosphate transporter SPNS2. *Journal of lipid research,* 60**,** 484-489.

SPIEGEL, S. & MILSTIEN, S. 2003. Sphingosine-1-phosphate: an enigmatic signalling lipid. *Nature reviews Molecular cell biology,* 4**,** 397-407.

SPIEGEL, S. & MILSTIEN, S. 2011. The outs and the ins of sphingosine-1-phosphate in immunity. *Nature Reviews Immunology,* 11**,** 403-415.

SRINIVASAN, S. & DUNN, J. F. 2011. Stabilization of hypoxia-inducible factor-1α in buffer containing cobalt chloride for Western blot analysis. *Analytical biochemistry,* 416**,** 120-122.

STAHELIN, R. V., HWANG, J. H., KIM, J.-H., PARK, Z.-Y., JOHNSON, K. R., OBEID, L. M. & CHO, W. 2005. The mechanism of membrane targeting of human sphingosine kinase 1. *Journal of Biological Chemistry,* 280**,** 43030-43038.

STANEK, A., BROŻYNA-TKACZYK, K. & MYŚLIŃSKI, W. 2021. The role of obesity-induced perivascular adipose tissue (PVAT) dysfunction in vascular homeostasis. *Nutrients,* 13**,** 3843.

STEINHORN, R., MORIN, F. & RUSSELL, J. A. 1994. The adventitia may be a barrier specific to nitric oxide in rabbit pulmonary artery. *The Journal of clinical investigation,* 94**,** 1883-1888.

STRUB, G. M., MACEYKA, M., HAIT, N. C., MILSTIEN, S. & SPIEGEL, S. 2010. Extracellular and intracellular actions of sphingosine-1-phosphate. *Sphingolipids as signaling and regulatory molecules,* 141-155.

STRUB, G. M., PAILLARD, M., LIANG, J., GOMEZ, L., ALLEGOOD, J. C., HAIT, N. C., MACEYKA, M., PRICE, M. M., CHEN, Q. & SIMPSON, D. C. 2011. Sphingosine-1-phosphate produced by sphingosine kinase 2 in mitochondria interacts with prohibitin 2 to regulate complex IV assembly and respiration. *The FASEB Journal,* 25**,** 600-612.

SUN, J., YAN, G., REN, A., YOU, B. & LIAO, J. K. 2006. FHL2/SLIM3 decreases cardiomyocyte survival by inhibitory interaction with sphingosine kinase-1. *Circulation research,* 99**,** 468-476.

SUN, K., ASTERHOLM, I. W., KUSMINSKI, C. M., BUENO, A. C., WANG, Z. V., POLLARD, J. W., BREKKEN, R. A. & SCHERER, P. E. 2012. Dichotomous effects of VEGF-A on adipose tissue dysfunction. *Proceedings of the national academy of sciences,* 109**,** 5874-5879.

SUN, K., HALBERG, N., KHAN, M., MAGALANG, U. J. & SCHERER, P. E. 2013. Selective inhibition of hypoxia-inducible factor 1α ameliorates adipose tissue dysfunction. *Molecular and cellular biology,* 33**,** 904-917.

SUN, K., KUSMINSKI, C. M. & SCHERER, P. E. 2011. Adipose tissue remodeling and obesity. *The Journal of clinical investigation,* 121**,** 2094-2101.

SUN, M., ZENG, L. & HU, M. 2022. Serum sphingosine-1 phosphate level is increased in patients with hepatitis B and displays a positive association with liver fibrosis. *American Journal of Translational Research,* 14**,** 4964.

SZASZ, T., BOMFIM, G. F. & WEBB, R. C. 2013. The influence of perivascular adipose tissue on vascular homeostasis. *Vascular health and risk management***,** 105-116.

SZASZ, T. & WEBB, R. C. 2012. Perivascular adipose tissue: more than just structural support. *Clinical science,* 122**,** 1-12.

TAHA, T. A., EL-ALWANI, M., HANNUN, Y. A. & OBEID, L. M. 2006a. Sphingosine kinase-1 is cleaved by cathepsin B in vitro: identification of the initial cleavage sites for the protease. *FEBS letters,* 580**,** 6047-6054.

TAHA, T. A., HANNUN, Y. A. & OBEID, L. M. 2006b. Sphingosine kinase: biochemical and cellular regulation and role in disease. *BMB Reports,* 39**,** 113-131.

TAHA, T. A., KITATANI, K., BIELAWSKI, J., CHO, W., HANNUN, Y. A. & OBEID, L. M. 2005. Tumor necrosis factor induces the loss of sphingosine kinase-1 by a cathepsin B-dependent mechanism. *Journal of Biological Chemistry,* 280**,** 17196-17202.

TAHA, T. A., OSTA, W., KOZHAYA, L., BIELAWSKI, J., JOHNSON, K. R., GILLANDERS, W. E., DBAIBO, G. S., HANNUN, Y. A. & OBEID, L. M. 2004. Down-regulation of sphingosine kinase-1 by DNA damage: dependence on proteases and p53. *Journal of Biological Chemistry,* 279**,** 20546-20554.

TAKUWA, Y., DU, W., QI, X., OKAMOTO, Y., TAKUWA, N. & YOSHIOKA, K. 2010. Roles of sphingosine-1-phosphate signaling in angiogenesis. *World journal of biological chemistry,* 1**,** 298.

TAN, K., XU, A., CHOW, W., LAM, M., AI, V., TAM, S. & LAM, K. 2004. Hypoadiponectinemia is associated with impaired endothelium-dependent vasodilation. *The Journal of Clinical Endocrinology & Metabolism,* 89**,** 765-769.

TANG, E. H. & VANHOUTTE, P. M. 2008. Gap junction inhibitors reduce endothelium-dependent contractions in the aorta of spontaneously hypertensive rats. *The Journal of pharmacology and experimental therapeutics,* 327**,** 148-153.

TANG, X., CHEN, H., CHEN, G., DUAN, C., FAN, Q., LI, H., WANG, Y., LI, Z., SHI, W. & LIU, Y. 2020. Validated LC-MS/MS method of Sphingosine 1-phosphate quantification in human serum for evaluation of response to radiotherapy in lung cancer. *Thoracic Cancer,* 11**,** 1443-1452.

TANKÓ, L. B., MIKKELSEN, E. O. & SIMONSEN, U. 1999. A new experimental approach in endothelium-dependent pharmacological investigations on isolated porcine coronary arteries mounted for impedance planimetry. *British journal of pharmacology,* 128**,** 165.

TANO, J.-Y., SCHLEIFENBAUM, J. & GOLLASCH, M. 2014. Perivascular adipose tissue, potassium channels, and vascular dysfunction. *Arteriosclerosis, thrombosis, and vascular biology,* 34**,** 1827-1830.

TAO, C., SIFUENTES, A. & HOLLAND, W. L. 2014. Regulation of glucose and lipid homeostasis by adiponectin: effects on hepatocytes, pancreatic β cells and adipocytes. *Best Practice & Research Clinical Endocrinology & Metabolism,* 28**,** 43-58.

TAO, R., ZHANG, J., VESSEY, D. A., HONBO, N. & KARLINER, J. S. 2007. Deletion of the sphingosine kinase-1 gene influences cell fate during hypoxia and glucose deprivation in adult mouse cardiomyocytes. *Cardiovascular research,* 74**,** 56-63.

TAZUKE, S. I., MAZURE, N. M., SUGAWARA, J., CARLAND, G., FAESSEN, G. H., SUEN, L.-F., IRWIN, J. C., POWELL, D. R., GIACCIA, A. J. & GIUDICE, L. C. 1998. Hypoxia stimulates insulin-like growth factor binding protein 1 (IGFBP-1) gene expression in HepG2 cells: a possible model for IGFBP-1 expression in fetal hypoxia. *Proceedings of the National Academy of Sciences,* 95**,** 10188-10193.

TER BRAAK, M., DANNEBERG, K., LICHTE, K., LIPHARDT, K., KTISTAKIS, N. T., PITSON, S. M., HLA, T., JAKOBS, K. H. & ZU HERINGDORF, D. M. 2009. Gαq-mediated plasma membrane translocation of sphingosine kinase-1 and cross-activation of S1P receptors. *Biochimica et Biophysica Acta (BBA)-Molecular and Cell Biology of Lipids,* 1791**,** 357-370.

THE GLOBAL BURDEN OF DISEASE OBESITY COLLABORATORS 2017. Health effects of overweight and obesity in 195 countries over 25 years. *New England journal of medicine,* 377**,** 13-27.

THELEN, K., WATTS, S. W. & CONTRERAS, G. A. 2018. Adipogenic potential of perivascular adipose tissue preadipocytes is improved by coculture with primary adipocytes. *Cytotechnology,* 70**,** 1435-1445.

TIETJENS, J. R., CLAMAN, D., KEZIRIAN, E. J., DE MARCO, T., MIRZAYAN, A., SADROONRI, B., GOLDBERG, A. N., LONG, C., GERSTENFELD, E. P. & YEGHIAZARIANS, Y. 2019. Obstructive sleep apnea in cardiovascular disease: a review of the literature and proposed multidisciplinary clinical management strategy. *Journal of the American Heart Association,* 8**,** e010440.

TÖLLE, M., LEVKAU, B., KEUL, P., BRINKMANN, V., GIEBING, G. N., SCHÖNFELDER, G., SCHÄFERS, M., LIPINSKI, K. V. W., JANKOWSKI, J. & JANKOWSKI, V. 2005. Immunomodulator FTY720 induces eNOS-dependent arterial vasodilatation via the lysophospholipid receptor S1P3. *Circulation research,* 96**,** 913-920.

TONELLI, F., LIM, K. G., LOVERIDGE, C., LONG, J., PITSON, S. M., TIGYI, G., BITTMAN, R., PYNE, S. & PYNE, N. J. 2010. FTY720 and (S)-FTY720 vinylphosphonate inhibit sphingosine kinase 1 and promote its proteasomal degradation in human pulmonary artery smooth muscle, breast cancer and androgen-independent prostate cancer cells. *Cellular signalling,* 22**,** 1536-1542.

TONG, Y., ZUO, Z., LI, X., LI, M., WANG, Z., GUO, X., WANG, X., SUN, Y., CHEN, D. & ZHANG, Z. 2023. Protective role of perivascular adipose tissue in the cardiovascular system. *Frontiers in Endocrinology,* 14**,** 1296778.

TOTZECK, M., HENDGEN-COTTA, U. B., KELM, M. & RASSAF, T. 2014. Crosstalk between nitrite, myoglobin and reactive oxygen species to regulate vasodilation under hypoxia. *PloS one,* 9**,** e105951.

TOUS, M., FERRER-LORENTE, R. & BADIMON, L. 2014. Selective inhibition of sphingosine kinase-1 protects adipose tissue against LPS-induced

inflammatory response in Zucker diabetic fatty rats. *American Journal of Physiology-Endocrinology and Metabolism,* 307**,** E437-E446.

TOUYZ, R. M., ALVES-LOPES, R., RIOS, F. J., CAMARGO, L. L., ANAGNOSTOPOULOU, A., ARNER, A. & MONTEZANO, A. C. 2018. Vascular smooth muscle contraction in hypertension. *Cardiovascular research,* 114**,** 529-539.

TRAYHURN, P. 2013. Hypoxia and adipose tissue function and dysfunction in obesity. *Physiological reviews,* 93**,** 1-21.

TRAYHURN, P. & WOOD, I. S. 2004. Adipokines: inflammation and the pleiotropic role of white adipose tissue. *British journal of nutrition,* 92**,** 347-355.

TRIPATHI, V. K., SUBRAMANIYAN, S. A. & HWANG, I. 2019. Molecular and cellular response of co-cultured cells toward cobalt chloride (CoCl2)-induced hypoxia. *ACS omega,* 4**,** 20882-20893.

TSAO, P. S., AOKI, N., LEFER, D. J., JOHNSON 3RD, G. & LEFER, A. M. 1990. Time course of endothelial dysfunction and myocardial injury during myocardial ischemia and reperfusion in the cat. *Circulation,* 82**,** 1402-1412.

TSUCHIDA, A., YAMAUCHI, T., ITO, Y., HADA, Y., MAKI, T., TAKEKAWA, S., KAMON, J., KOBAYASHI, M., SUZUKI, R. & HARA, K. 2004. Insulin/Foxo1 pathway regulates expression levels of adiponectin receptors and adiponectin sensitivity. *Journal of Biological Chemistry,* 279**,** 30817-30822.

TSUCHIDA, A., YAMAUCHI, T., TAKEKAWA, S., HADA, Y., ITO, Y., MAKI, T. & KADOWAKI, T. 2005. Peroxisome proliferator–activated receptor (PPAR) α activation increases adiponectin receptors and reduces obesity-related inflammation in adipose tissue: comparison of activation of PPARα, PPARγ, and their combination. *Diabetes,* 54**,** 3358-3370.

TSUCHIYA, K., SAKAI, H., SUZUKI, N., IWASHIMA, F., YOSHIMOTO, T., SHICHIRI, M. & HIRATA, Y. 2007. Chronic blockade of nitric oxide synthesis reduces adiposity and improves insulin resistance in high fat-induced obese mice. *Endocrinology,* 148**,** 4548-4556.

URTZ, N., OLIVERA, A., BOFILL-CARDONA, E., CSONGA, R., BILLICH, A., MECHTCHERIAKOVA, D., BORNANCIN, F., WOISETSCHLÄGER, M., RIVERA, J. & BAUMRUKER, T. 2004. Early activation of sphingosine kinase in mast cells and recruitment to FcεRI are mediated by its interaction with Lyn kinase. *Molecular and cellular biology,* 24**,** 8765-8777.

VALENTINI, A., CARDILLO, C., DELLA MORTE, D. & TESAURO, M. 2023. The role of perivascular adipose tissue in the pathogenesis of endothelial dysfunction in cardiovascular diseases and type 2 diabetes mellitus. *Biomedicines,* 11**,** 3006.

VAN MARKEN LICHTENBELT, W. D., VANHOMMERIG, J. W., SMULDERS, N. M., DROSSAERTS, J. M., KEMERINK, G. J., BOUVY, N. D., SCHRAUWEN, P. & TEULE, G. J. 2009. Cold-activated brown adipose tissue in healthy men. *New England Journal of Medicine,* 360**,** 1500-1508.

VAN MIL, A. H., SPILT, A., VAN BUCHEM, M. A., BOLLEN, E. L., TEPPEMA, L., WESTENDORP, R. G. & BLAUW, G. J. 2002. Nitric oxide mediates hypoxia-induced cerebral vasodilation in humans. *Journal of applied physiology,* 92**,** 962-966.

VANBENTHUYSEN, K., MCMURTRY, I. & HORWITZ, L. 1987. Reperfusion after acute coronary occlusion in dogs impairs endothelium-dependent relaxation to acetylcholine and augments contractile reactivity in vitro. *The Journal of clinical investigation,* 79**,** 265-274.

VENKATARAMAN, K., LEE, Y.-M., MICHAUD, J., THANGADA, S., AI, Y., BONKOVSKY, H. L., PARIKH, N. S., HABRUKOWICH, C. & HLA, T. 2008. Vascular endothelium as a contributor of plasma sphingosine 1-phosphate. *Circulation research,* 102, 669-676.

VENKATARAMAN, K., THANGADA, S., MICHAUD, J., OO, M. L., AI, Y., LEE, Y.-M., WU, M., PARIKH, N. S., KHAN, F. & PROIA, R. L. 2006. Extracellular export of sphingosine kinase-1a contributes to the vascular S1P gradient. *Biochemical Journal,* 397, 461-471.

VERLOHREN, S., DUBROVSKA, G., TSANG, S.-Y., ESSIN, K., LUFT, F. C., HUANG, Y. & GOLLASCH, M. 2004. Visceral periadventitial adipose tissue regulates arterial tone of mesenteric arteries. *Hypertension,* 44, 271-276.

VICTORIO, J. A., FONTES, M. T., ROSSONI, L. V. & DAVEL, A. P. 2016. Different anti-contractile function and nitric oxide production of thoracic and abdominal perivascular adipose tissues. *Frontiers in physiology,* 7, 295.

VIDA, G., PEÑA, G., KANASHIRO, A., DEL ROCIO THOMPSON-BONILLA, M., PALANGE, D., DEITCH, E. A. & ULLOA, L. 2011. β2-Adrenoreceptors of regulatory lymphocytes are essential for vagal neuromodulation of the innate immune system. *The FASEB Journal,* 25, 4476.

VILELA, V. R., SAMSON, N., NACHBAR, R., PERAZZA, L. R., LACHANCE, G., ROKATOARIVELO, V., CENTANO-BAEZ, C., ZANCAN, P., SOLA-PENNA, M. & BELLMANN, K. 2022. Adipocyte-specific Nos2 deletion improves insulin resistance and dyslipidemia through brown fat activation in diet-induced obese mice. *Molecular metabolism,* 57, 101437.

VILLACORTA, L. & CHANG, L. 2015. The role of perivascular adipose tissue in vasoconstriction, arterial stiffness, and aneurysm. *Hormone molecular biology and clinical investigation,* 21, 137-147.

VILLALOBOS-MOLINA, R. & IBARRA, M. 1996. α1-Adrenoceptors mediating contraction in arteries of normotensive and spontaneously hypertensive rats are of the α1D or α1A subtypes. *European journal of pharmacology,* 298, 257-263.

VU, T. M., ISHIZU, A.-N., FOO, J. C., TOH, X. R., ZHANG, F., WHEE, D. M., TORTA, F., CAZENAVE-GASSIOT, A., MATSUMURA, T. & KIM, S. 2017. Mfsd2b is essential for the sphingosine-1-phosphate export in erythrocytes and platelets. *Nature,* 550, 524-528.

WACKER, B. K., PARK, T. S. & GIDDAY, J. M. 2009. Hypoxic preconditioning-induced cerebral ischemic tolerance: role of microvascular sphingosine kinase 2. *Stroke,* 40, 3342-3348.

WAJCHENBERG, B. L. 2000. Subcutaneous and visceral adipose tissue: their relation to the metabolic syndrome. *Endocrine reviews,* 21, 697-738.

WALFORD, G. & LOSCALZO, J. 2003. Nitric oxide in vascular biology. *Journal of Thrombosis and Haemostasis,* 1, 2112-2118.

WANG, B., WOOD, I. S. & TRAYHURN, P. 2007. Dysregulation of the expression and secretion of inflammation-related adipokines by hypoxia in human adipocytes. *Pflügers Archiv-European Journal of Physiology,* 455, 479-492.

WANG, G. L. & SEMENZA, G. L. 1993. Characterization of hypoxia-inducible factor 1 and regulation of DNA binding activity by hypoxia. *Journal of Biological Chemistry,* 268, 21513-21518.

WANG, J., BADEANLOU, L., BIELAWSKI, J., CIARALDI, T. P. & SAMAD, F. 2014. Sphingosine kinase 1 regulates adipose proinflammatory responses and insulin resistance. *American Journal of Physiology-Endocrinology and Metabolism,* 306, E756-E768.

WANG, J., POLAKI, V., CHEN, S. & BIHL, J. C. 2020a. Exercise improves endothelial function associated with alleviated inflammation and

oxidative stress of perivascular adipose tissue in type 2 diabetic mice. *Oxidative Medicine and Cellular Longevity,* 2020, 8830537.
WANG, L., CHENG, C. K., YI, M., LUI, K. O. & HUANG, Y. 2022a. Targeting endothelial dysfunction and inflammation. *Journal of molecular and cellular cardiology,* 168, 58-67.
WANG, L., LUO, Y., LUO, L., WU, D., DING, X., ZHENG, H., WU, H., LIU, B., YANG, X. & SILVA, F. 2020b. Adiponectin restrains ILC2 activation by AMPK-mediated feedback inhibition of IL-33 signaling. *Journal of Experimental Medicine,* 218, e20191054.
WANG, N., LI, J.-Y., ZENG, B. & CHEN, G.-L. 2023. Sphingosine-1-phosphate signaling in cardiovascular diseases. *Biomolecules,* 13, 818.
WANG, P., XU, T.-Y., GUAN, Y.-F., SU, D.-F., FAN, G.-R. & MIAO, C.-Y. 2009. Perivascular adipose tissue-derived visfatin is a vascular smooth muscle cell growth factor: role of nicotinamide mononucleotide. *Cardiovascular research,* 81, 370-380.
WANG, R., SUN, Q., WU, X., ZHANG, Y., XING, X., LIN, K., FENG, Y., WANG, M., WANG, Y. & WANG, R. 2022b. Hypoxia as a double-edged sword to combat obesity and comorbidities. *Cells,* 11, 3735.
WANG, W., XIANG, P., CHEW, W. S., TORTA, F., BANDLA, A., LOPEZ, V., SEOW, W. L., LAM, B. W. S., CHANG, J. K. & WONG, P. 2020c. Activation of sphingosine 1-phosphate receptor 2 attenuates chemotherapy-induced neuropathy. *Journal of Biological Chemistry,* 295, 1143-1152.
WANG, X., SUN, Y., PENG, X., NAQVI, S. M. A. S., YANG, Y., ZHANG, J., CHEN, M., CHEN, Y., CHEN, H. & YAN, H. 2020d. The tumorigenic effect of sphingosine kinase 1 and its potential therapeutic target. *Cancer control,* 27, 1073274820976664.
WANG, Y., YILDIZ, F., STRUVE, A., KASSMANN, M., MARKÓ, L., KÖHLER, M.-B., LUFT, F. C., GOLLASCH, M. & TSVETKOV, D. 2021. Aging affects KV7 channels and perivascular adipose tissue-mediated vascular tone. *Frontiers in Physiology,* 12, 749709.
WATSON, D. G., TONELLI, F., ALOSSAIMI, M., WILLIAMSON, L., CHAN, E., GORSHKOVA, I., BERDYSHEV, E., BITTMAN, R., PYNE, N. J. & PYNE, S. 2013. The roles of sphingosine kinases 1 and 2 in regulating the Warburg effect in prostate cancer cells. *Cellular signalling,* 25, 1011-1017.
WAYPA, G. B. & SCHUMACKER, P. T. 2010. Hypoxia-induced changes in pulmonary and systemic vascular resistance: where is the O2 sensor? *Respiratory physiology & neurobiology,* 174, 201-211.
WEIDEMANN, A. & JOHNSON, R. 2008. Biology of HIF-1α. *Cell Death & Differentiation,* 15, 621-627.
WEIGEL, C., BELLACI, J. & SPIEGEL, S. 2023. Sphingosine-1-phosphate and its receptors in vascular endothelial and lymphatic barrier function. *Journal of Biological Chemistry,* 299.
WEIGERT, A., CREMER, S., SCHMIDT, M. V., VON KNETHEN, A., ANGIONI, C., GEISSLINGER, G. & BRÜNE, B. 2010. Cleavage of sphingosine kinase 2 by caspase-1 provokes its release from apoptotic cells. *Blood, The Journal of the American Society of Hematology,* 115, 3531-3540.
WEIGERT, A., VON KNETHEN, A., THOMAS, D., FARIA, I., NAMGALADZE, D., ZEZINA, E., FUHRMANN, D., PETCHERSKI, A., ZU HERINGDORF, D. M. & RADEKE, H. H. 2019. Sphingosine kinase 2 is a negative regulator of inflammatory macrophage activation. *Biochimica et Biophysica Acta (BBA)-Molecular and Cell Biology of Lipids,* 1864, 1235-1246.
WEISBERG, S. P., MCCANN, D., DESAI, M., ROSENBAUM, M., LEIBEL, R. L. & FERRANTE, A. W. 2003. Obesity is associated with macrophage

accumulation in adipose tissue. *The Journal of clinical investigation,* 112**,** 1796-1808.

WESTON, A., EGNER, I., DONG, Y., PORTER, E., HEAGERTY, A. & EDWARDS, G. 2013. Stimulated release of a hyperpolarizing factor (ADHF) from mesenteric artery perivascular adipose tissue: involvement of myocyte BKCa channels and adiponectin. *British journal of pharmacology,* 169**,** 1500-1509.

WHO 2000. Obesity: preventing and managing the global epidemic.

WILSON, D. 2011. Vascular smooth muscle structure and function. *Mechanisms of Vascular***,** 13.

WITHERS, S. B., AGABITI-ROSEI, C., LIVINGSTONE, D. M., LITTLE, M. C., ASLAM, R., MALIK, R. A. & HEAGERTY, A. M. 2011. Macrophage activation is responsible for loss of anticontractile function in inflamed perivascular fat. *Arteriosclerosis, thrombosis, and vascular biology,* 31**,** 908-913.

WITHERS, S. B., SIMPSON, L., FATTAH, S., WERNER, M. E. & HEAGERTY, A. M. 2014. cGMP-dependent protein kinase (PKG) mediates the anticontractile capacity of perivascular adipose tissue. *Cardiovascular research,* 101**,** 130-137.

WONG, P. S., ROBERTS, R. E. & RANDALL, M. D. 2015. Hyperoxic gassing with Tiron enhances bradykinin-induced endothelium-dependent and EDH-type relaxation through generation of hydrogen peroxide. *Pharmacol Res,* 91**,** 29-35.

XIA, P., GAMBLE, J. R., WANG, L., PITSON, S. M., MORETTI, P. A., WATTENBERG, B. W., D'ANDREA, R. J. & VADAS, M. A. 2000. An oncogenic role of sphingosine kinase. *Current Biology,* 10**,** 1527-1530.

XIA, P., WANG, L., MORETTI, P. A., ALBANESE, N., CHAI, F., PITSON, S. M., D'ANDREA, R. J., GAMBLE, J. R. & VADAS, M. A. 2002. Sphingosine kinase interacts with TRAF2 and dissects tumor necrosis factor-α signaling. *Journal of Biological Chemistry,* 277**,** 7996-8003.

XIAO, S., PENG, K., LI, C., LONG, Y. & YU, Q. 2023. The role of sphingosine-1-phosphate in autophagy and related disorders. *Cell Death Discovery,* 9**,** 380.

XIONG, Y. & HLA, T. 2014. S1P control of endothelial integrity. *Sphingosine-1-phosphate signaling in immunology and infectious diseases***,** 85-105.

XU, A., WANG, Y., KESHAW, H., XU, L. Y., LAM, K. S. & COOPER, G. J. 2003. The fat-derived hormone adiponectin alleviates alcoholic and nonalcoholic fatty liver diseases in mice. *The Journal of clinical investigation,* 112**,** 91-100.

XUE, G., CHEN, J.-P., LI, Y., ZHANG, Z.-Q., ZHU, J.-L. & DONG, W. 2020. MicroRNA-6862 inhibition elevates sphingosine kinase 1 and protects neuronal cells from MPP+-induced apoptosis. *Aging (Albany NY),* 13**,** 1369.

YAMAUCHI, T. & KADOWAKI, T. 2008. Physiological and pathophysiological roles of adiponectin and adiponectin receptors in the integrated regulation of metabolic and cardiovascular diseases. *International journal of obesity,* 32**,** S13-S18.

YAMAUCHI, T., KAMON, J., ITO, Y., TSUCHIDA, A., YOKOMIZO, T., KITA, S., SUGIYAMA, T., MIYAGISHI, M., HARA, K. & TSUNODA, M. 2003. Cloning of adiponectin receptors that mediate antidiabetic metabolic effects. *Nature,* 423**,** 762-769.

YAMAUCHI, T., KAMON, J., WAKI, H., TERAUCHI, Y., KUBOTA, N., HARA, K., MORI, Y., IDE, T., MURAKAMI, K. & TSUBOYAMA-KASAOKA, N. 2001. The fat-derived hormone adiponectin reverses insulin resistance associated with both lipoatrophy and obesity. *Nature medicine,* 7**,** 941-946.

YANAGISAWA, M., KURIHARA, H., KIMURA, S., TOMOBE, Y., KOBAYASHI, M., MITSUI, Y., YAZAKI, Y., GOTO, K. & MASAKI, T. 1988. A novel potent vasoconstrictor peptide produced by vascular endothelial cells. *nature,* 332**,** 411-415.

YAO, C., RUAN, J.-W., ZHU, Y.-R., LIU, F., WU, H.-M., ZHANG, Y. & JIANG, Q. 2020. The therapeutic value of the SphK1-targeting microRNA-3677 in human osteosarcoma cells. *Aging (Albany NY),* 12**,** 5399.

YAP, Z. J., SHARIF, M. & BASHIR, M. 2021. Is there an immunogenomic difference between thoracic and abdominal aortic aneurysms? *Journal of Cardiac Surgery,* 36**,** 1520-1530.

YE, J., GAO, Z., YIN, J. & HE, Q. 2007. Hypoxia is a potential risk factor for chronic inflammation and adiponectin reduction in adipose tissue of ob/ob and dietary obese mice. *American Journal of Physiology-Endocrinology and Metabolism,* 293**,** E1118-E1128.

YE, R., HOLLAND, W. L., GORDILLO, R., WANG, M., WANG, Q. A., SHAO, M., MORLEY, T. S., GUPTA, R. K., STAHL, A. & SCHERER, P. E. 2014. Adiponectin is essential for lipid homeostasis and survival under insulin deficiency and promotes ß-cell regeneration. *Elife,* 3**,** e03851.

YI, X., TANG, X., LI, T., CHEN, L., HE, H., WU, X., XIANG, C., CAO, M., WANG, Z. & WANG, Y. 2023. Therapeutic potential of the sphingosine kinase 1 inhibitor, PF-543. *Biomedicine & Pharmacotherapy,* 163**,** 114401.

YU, H., SHAO, Y., GAO, L., ZHANG, L., GUO, K., WU, C., HU, X. & DUAN, H. 2012. Acetylation of sphingosine kinase 1 regulates cell growth and cell-cycle progression. *Biochemical and biophysical research communications,* 417**,** 1242-1247.

YUAN, Y., JIA, G., WU, C., WANG, W., CHENG, L., LI, Q., LI, Z., LUO, K., YANG, S. & YAN, W. 2021. Structures of signaling complexes of lipid receptors S1PR1 and S1PR5 reveal mechanisms of activation and drug recognition. *Cell research,* 31**,** 1263-1274.

YUN, Z., MAECKER, H. L., JOHNSON, R. S. & GIACCIA, A. J. 2002. Inhibition of PPARγ2 gene expression by the HIF-1-regulated gene DEC1/Stra13: a mechanism for regulation of adipogenesis by hypoxia. *Developmental cell,* 2**,** 331-341.

ZABORSKA, K. E., WAREING, M., EDWARDS, G. & AUSTIN, C. 2016. Loss of anti-contractile effect of perivascular adipose tissue in offspring of obese rats. *International Journal of Obesity,* 40**,** 1205-1214.

ŻELECHOWSKA, P., BRZEZIŃSKA-BŁASZCZYK, E., WIKTORSKA, M., RÓŻALSKA, S., WAWROCKI, S., KOZŁOWSKA, E. & AGIER, J. 2019. Adipocytokines leptin and adiponectin function as mast cell activity modulators. *Immunology,* 158**,** 3-18.

ZEYDA, M. & STULNIG, T. M. 2007. Adipose tissue macrophages. *Immunology letters,* 112**,** 61-67.

ZHANG, G., YANG, L., KIM, G. S., RYAN, K., LU, S., O'DONNELL, R. K., SPOKES, K., SHAPIRO, N., AIRD, W. C. & KLUK, M. J. 2013a. Critical role of sphingosine-1-phosphate receptor 2 (S1PR2) in acute vascular inflammation. *Blood, The Journal of the American Society of Hematology,* 122**,** 443-455.

ZHANG, H., WANG, Q., ZHAO, Q. & DI, W. 2013b. MiR-124 inhibits the migration and invasion of ovarian cancer cells by targeting SphK1. *Journal of ovarian research,* 6**,** 1-9.

ZHANG, R., LI, L., YUAN, L. & ZHAO, M. 2016. Hypoxic preconditioning protects cardiomyocytes against hypoxia/reoxygenation-induced cell apoptosis via

sphingosine kinase 2 and FAK/AKT pathway. *Experimental and Molecular Pathology,* 100**,** 51-58.

ZHANG, T., GUO, D., ZHENG, W. & DAI, Q. 2021. Effects of S1PR2 antagonist on blood pressure and angiogenesis imbalance in preeclampsia rats. *Molecular Medicine Reports,* 23**,** 456.

ZHAO, C., AMIABLE, N., LAFLAMME, M., MARSOLAIS, D., DI BATTISTA, J. A., FERNANDES, M. J. & BOURGOIN, S. G. 2019. Impairment of chemical hypoxia-induced sphingosine kinase-1 expression and activation in rheumatoid arthritis synovial fibroblasts: A signature of exhaustion? *Biochemical pharmacology,* 165**,** 249-262.

ZHAO, C., MORENO-NIEVES, U., DI BATTISTA, J. A., FERNANDES, M. J., TOUAIBIA, M. & BOURGOIN, S. G. 2015a. Chemical Hypoxia Brings to Light Altered Autocrine Sphingosine-1-Phosphate Signalling in Rheumatoid Arthritis Synovial Fibroblasts. *Mediators of Inflammation,* 2015**,** 436525.

ZHAO, Y., VANHOUTTE, P. M. & LEUNG, S. W. 2015b. Vascular nitric oxide: Beyond eNOS. *Journal of pharmacological sciences,* 129**,** 83-94.

ZU HERINGDORF, D. M., LILIOM, K., SCHAEFER, M., DANNEBERG, K., JAGGAR, J. H., TIGYI, G. & JAKOBS, K. H. 2003. Photolysis of intracellular caged sphingosine-1-phosphate causes Ca2+ mobilization independently of G-protein-coupled receptors. *FEBS letters,* 554**,** 443-449.

ZUHRA, K., AUGSBURGER, F., MAJTAN, T. & SZABO, C. 2020. Cystathionine-ß-synthase: molecular regulation and pharmacological inhibition. *Biomolecules,* 10**,** 697.

ZWICK, R. K., GUERRERO-JUAREZ, C. F., HORSLEY, V. & PLIKUS, M. V. 2018. Anatomical, physiological, and functional diversity of adipose tissue. *Cell metabolism,* 27**,** 68-83.